University of Alberta

Sand on Demand: An Approach to Improving Productivity in Horizontal Wells under Heavy Oil Primary Production

By

Brígida Inmaculada Meza Díaz

A thesis submitted to the Faculty of Graduate Studies and Research in partial fulfillment of the requirements for the degree of

Doctor of Philosophy
in
Petroleum Engineering

Department of Civil and Environmental Engineering

Edmonton, Alberta
Fall 2008

Your file Votre référence
ISBN: 978-0-494-55649-8
Our file Notre référence
ISBN: 978-0-494-55649-8

To my father, Victor Manuel Meza Burgos

To Melisa

To Özgür

To my family in Venezuela

ABSTRACT

The cold production recovery process, as practised in Western Canada, is successful in vertical wells. Attempts at cold production in horizontal wells have been less successful.

This dissertation presents the results of research examining the possibility of controlled sand production, "sand on demand" for horizontal wells. Specifically, the effects of slot size, confining stress, fluid velocity and sand grain sorting on sand production under less aggressive production conditions have been investigated.

The results indicate that slot size selection is critical for establishing "sand on demand". For proper slot size selection, it is essential to know the grain size distribution and the sorting (uniformity coefficient) of the sand. The findings from the sand production experiments indicate that the critical pressure gradients required for initiating sand production and for maintaining continuous sand production are much lower for well-sorted sands than for poorly-sorted sands. A correlation between slot size and controlled sand production was found for well-sorted sands that should allow for the specification of appropriate slot sizes.

The critical pressure gradient required for initiating sand production and maintaining continuous sand production decreases as the slot width or confining pressure increases. When flow rates resulted in persistent sand production, channels and/or elliptical dilated zones were created that greatly enhanced the effective permeability near the slot. This observation suggests that producing at low and steady sand cuts for a long period of time might bring two benefits; a way to transport the sand out of the well and the creation of

high permeability channels or zones that can improve the production of the reservoir. Continuing sand production at sand cuts less than 1.5 % was achieved if the initial flow rates were low and were later increased in small increments.

To summarize, it was found that if the appropriate slot size was combined with the right draw down rates, controlled sand production could be achieved with attendant significant increases in permeability. This suggests that radically increased oil rates could be achieved if sand production rates can be maintained at low and consistent levels.

ACKNOWLEDGEMENTS

The author wishes to express her sincere gratitude to her supervisors, Dr. Ronald Sawatzky and Dr. Ergun Kuru, for their guidance, advice and encouragement throughout this study.

The author also would like to thank Dr. Bernard Tremblay who provided technical support and advice in the initial planning of this research work.

The technical assistance and suggestions provided by Kaz Oldakowski, Karen Enders, Shauna Cameron, and Douglas Lillico is greatly appreciated.

Appreciation is extended to my colleagues at ARC in the Heavy Oil and Oil Sands business unit for their support and contributions throughout this research.

The author would like to acknowledge, with appreciation, the useful discussions and suggestions provided by the industry members of the **AERI/ARC C**ore **I**ndustry Research Program (AACI) during the program workshops and annual meetings.

The patience and moral support provided by friends during the research years merits great appreciation. I wish to give particular thanks to Elena Breidenbach, Marlene Huerta, and Shannon Taubner for their understanding, encouragement and irrepressible willingness to help in all situations and under any conditions.

The financial support for my PhD degree provided by the AACI consortium and the Natural Sciences and Engineering Research Council (NSERC) is gratefully acknowledged.

TABLE OF CONTENTS

LIST OF TABLES

LIST OF FIGURES

NOMENCLATURE

A	Specimen cross sectional area
A_c	Cross sectional area in the direction of the flow (cm^2)
A_S	Open area of the slots
ARC	Alberta Research Council
ASTM	American Standards of Testing and Measurement
b	Depth of the slot (thickness of the plate) (mm)
BP	Bottom plate of a stacked set of sieves
BT-3	Commercial name for the coarsest glass bead sand
c	Kozeny constant (m^{-2})
c_F	Compressibility of the fluid (kPa^{-1})
c_g	Gas compressibility (kPa^{-1})
CHOPS	Cold heavy oil production with sand
C_o	Uniaxial compressive strength
CO_2	Carbon dioxide
C_s	Sand concentration or sand cut (fraction or %)
c_T	Total compressibility (kPa^{-1})
c_u	Inherent shear strength of the material (cohesive strength) (kPa, psi)
C_u	Uniformity coefficient (dimensionless)
C_D	Drag coefficient (dimensionless)
CT	Computed tomography
c_w	Water compressibility (kPa^{-1})
dm	Differential mass (g)
dm_{oi}	Differential mass of injected oil (g)
dm_{op}	Differential mass of produced oil (g)
dm_{ot}	Differential mass of oil in the cell (g)
dm_{slurry}	Differential mass of slurry (g)
dm_{sp}	Differential mass of produced sand (g)
dm_{st}	Differential mass of sand in the cell (g)
$\partial p / \partial$	Partial derivative of pressure
(dp/dL)	Pressure gradients
$(dp/dr)_{AH}$	Pressure gradient into a hemisphere (MPa/cm or kPa/cm)
$(dp/dL)_{AS}$	Pressure gradient taking the cross sectional area of the slot (MPa/cm or kPa/cm)
$(dp/dr)_{Ch}$	Pressure gradient at the tip of the channel
$(dp/dr)_{Cr}$	Critical pressure gradient for sand failure
$(dp/dL)_{csp}$	Critical pressure gradient (calculated through the slot) for continuing sand production
$(dp/dL)_{isp}$	Critical pressure gradient (calculated through the slot) for initiation of sand production
$(dp/dL)_{UP}$	Average pressure gradient in the undisturbed part of the pack
$(dp/dL)_{3,4}$	Pressure gradient between ports 3 and 4 (kPa/cm)
$(dp/dL)_{8,9}$	Pressure gradient between ports 8 and 9 (kPa/cm)
$(dp/dL)_{10,9}$	Pressure gradient between ports 10 and 9 (kPa/cm)

$(dp/dL)_{11,slot}$	Pressure gradient between ports 11 and slot (kPa/cm)
$(d\sigma/dr)$	Radial stress profile
dt	Time increment (s or h)
dV	Differential volume (cm^3 or cc)
$\partial V / \partial$	Partial derivative of volume
dV_{ot}	Differential Volume of oil at time t (cm^3 or cc)
dV_{st}	Differential Volume of slurry at time t (cm^3 or cc)
D	Diameter (cm or mm)
D_w	Outer Diameter of the pipe (in or cm)
D_i	Equivalent grain diameter at a given i percentile
D_{10}	Sieve size at which 10 % by weight of the sand will go through (mm)
D_{50}	Sieve size at which 50 % by weight of the sand will go through (mm)
D_{60}	Sieve size at which 60 % by weight of the sand will go through (mm)
D_{90}	Sieve size at which 90 % by weight of the sand will go through (mm)
$D_{99.9}$	Sieve size at which 99.9 % by weight of the sand will go through (mm)
E	Young's modulus (MPa or psi)
e	Void ratio
EPO-THIN®	Epoxy resin trade mark
F	Force (N)
F_f	Friction force (N)
F_h	Hydrodynamic force (N)
F_N	Normal intergranular force (N)
F_h^1	Drag force related to the pressure gradient (N)
F_h^2	Drag force related to the fluid viscosity (N)
G	Mass picnometer + sand + butanol (g)
GBLH	Glass Beads Like Husky
GBLF	Glass Beads Less Fines
$h_{\text{sand in the cylinder}}$	Height of the sand in the cylinder (cm)
K	Mass picnometer + butanol – mass of picnometer = $m_{Butanol}$ (g)
k	Permeability (Darcy or m^2)
k_o	Effective permeabiltity to oil
k_{of}	Final oil effective permeability
k_{oi}	Initial oil effective permeability
k_{op}	Effective permeabiltity to oil in the sand pack (Darcy or m^2)
k_{os}	Effective permeabiltity to oil at the slot (Darcy or m^2)
k_y	Permeability of the yielded region
L	Length of the pack (m, cm or mm)
L_{hs}	Half-length of the slot
L_s	Length of the slot (cm)
LVDT	Linear variable differential transformer
L_w	Length of the horizontal well (m or cm)
M.B.	Material balance
$m_{Butanol}$	Mass of butanol (g)
$m_{Pic+Butanol}$	Mass of picnometer + butanol (g)
m_{Pic}	Mass of picnometer (g)

m_s	Mass of sand (g)
m_{S+P}	Mass of sand + mass of picnometer (g)
n	Number of moles
OOIP	Original oil in place
p	Pressure (kPa, MPa or psi)
P	Axial load (kPa)
P	Mass picnometer + sand (g)
p_{atm}	Atmospheric pressure (kPa or psi)
p_B	Pressure at the end of the slot (kPa)
p_F	Final pressure (kPa)
p_{inj}	Pressure at inlet (kPa)
p_{prod}	Pressure at outlet (kPa)
p_{slot}	pressure at the slot (kPa)
PV	Pore volume (cm^3 or cc)
PVC	Polyvinylchloride
Q	Volumetric fluid flow rate (cm^3/h or cc/h)
Q_{cavity}	Flow rate at which small amount of sand is produced initially forming small cavity
Q_{cr}	Critical flow rate for sand failure
Q_{csp}	Critical flow rate for continuing sand production
Q_{oi}	Volumetric flow rate of oil injected (cm^3/h or cc/h)
Q_{isp}	Critical flow rate for initiation of sand production
Q_o	Volumetric oil flow rate (cm^3/h or cc/h)
Q_{sp}	sand production rate
Q_{slot}	Volumetric flow rate through a slot (l/min, cm^3/h or cc/h)
Q_{well}	Volumetric well flow rate (m^3/day)
R	Universal gas constant
r	Contact radius or just radius (mm or cm)
r_{Ch}	Average radius of the channel
r_{sc}	Radius of spherical cavity form after small amount of sand production
r_9	Distance from port 9 to the center of the slot
r_{10}	Distance from port 10 to the center of the slot
R_c	Radius of the Coulomb zone (mm)
R_I	Radius of the arch (mm)
R_g	Radius of a grain (mm or μm)
S	Mass of picnometer+sand – Mass of picnometer (g)
S_g	Gas saturation (dimensionless)
S_o	Sand pack oil saturation (dimensionless)
S_s	Slot surface area (cm^2)
S_T	Total surface area of the horizontal well (cm^2)
Sil-1	Synthetic silica sand
S_w	Sand pack water saturation (dimensionless)
SW	Slot width
SW_{min}	Probable minimum slot size to initiate sand production.
SW_{max}	Probable maximum slot size for control sand production

SWcsp	Slot size interval where control sand production might be possible
SWEGD	Slot width equivalent grain diameter ratio
T	Temperature (K or °C)
T_α	Parameter dependent on failure angle
T_{cell}	Cell temperature (K or °C)
T_{room}	Room temperature (K or °C)
v_f	Superficial velocity (cm/h)
v_o	Oil velocity (cm/h)
v_s	Sand velocity (cm/h)
V	Volume (l, cc or cm^3)
$V_{@atm}$	Volume at atmospheric pressure (cc or cm^3)
V_{air}	Air volume (cc or cm^3)
V_B	Volume of butanol (cc or cm^3)
V'_B	Volume of butanol in the mix sand +butanol (cc or cm^3)
V_{cell}	Cell volume (cc or cm^3)
$V_{cilynder}$	Volume of the cylinder (cc or cm^3)
V_{cs}	Volume of the circumscribed sphere (cc or cm^3)
V_g	Gas volume (cc or cm^3)
V_o	Oil Volume (cc or cm^3)
V_p	Volume of the particle (cc or cm^3)
V_{pic}	Volume of picnometer (cc or cm^3)
V_s	Sand Volume or solid volume (cc or cm^3)
V_T	Total volume (cc or cm^3)
W	With of the slot divided by two
W_s	Width of the slot
W_{sand}	Mass of sand produced (g)

LIST OF GREEK SYMBOLS

α	Failure angle (degrees)
ΔL	Length increment (cm)
Δp	Pressure drop (kPa or psi)
ΔV	Volume increment (cm^3)
ϕ	Porosity (fraction or %)
ϕ_B	Porosity at the bottom of the pack
ϕ_{Ch}	Porosity inside the channel
ϕ_f	Final porosity (fraction or %)
ϕ_i	Initial porosity (fraction or %)
ϕ_M	Porosity in the middle of the pack (fraction or %)
ϕ_p	Porosity in the sand pack (fraction or %)
ϕ_s	Porosity at the slot (fraction or %)
ϕ_{slurry}	Porosity of produced slurry(fraction or %)
ϕ_T	Porosity at the top of the pack (fraction or %)
ϕ_y	Porosity of the yielded region (fraction or %)
φ	Internal friction angle (Degrees)
μ	Viscosity (cP)
μ_o	Oil viscosity (cP)
μ_r	Relative viscosity (cP)
μ_{Slurry}	Viscosity of the sand-oil slurry (cP)
ν	Poisson's ratio (dimensionless)
ρ	Density (g/cm^3 or g/cc)
ρ_1	Dee Valley oil 1 density (g/cm^3 or g/cc)
ρ_2	Dee Valley oil 2 density (g/cm^3 or g/cc)
$\rho_{Butanol}$	Butanol density (g/cm^3 or g/cc)
ρ_f	Fluid density (g/cm^3 or g/cc)
ρ_{H2O}	Density of water (g/cm^3 or g/cc)
ρ_o	Density of oil (g/cm^3 or g/cc)
ρ_s	Density of sand (g/cm^3 or g/cc)
σ	Total stress (MPa, kPa or psi)
σ'_A	Effective axial stress (MPa, kPa or psi)
σ_s	Standard deviation
σ_c	Confining stress (MPa, kPa or psi)
σ'	Effective stress (MPa, kPa or psi)
σ_n	Normal stress (MPa, kPa or psi)
σ_{pp}	Total radial stress (MPa, kPa or psi)
σ_r	Radial stress (MPa, kPa or psi)
σ'_r	Effective radial stress (MPa, kPa or psi)
σ_T	Tensile stress (MPa, kPa or psi)
σ'_v	Effective vertical stress (MPa, kPa or psi)
$\sigma_{\theta\theta}$	Total hoop stress (MPa, kPa or psi)

$\sigma_{\theta\theta}'$	Effective hoop stress (MPa, kPa or psi)
σ_1	Major principal stress (MPa, kPa or psi)
σ_3	Minor principal stress (MPa, kPa or psi)
τ_f	Maximum shearing resistance (MPa, kPa or psi)

1 Introduction

1.1 Overview

Heavy oil production is becoming more important in Canada, due to the depletion of conventional oil reserves. Western Canadian crude oil production is approximately 370,000 m^3/d. Of this amount, nearly 75% is comprised of heavy crude and bitumen (including bitumen produced at mining plants). In situ heavy oil and bitumen production has nearly tripled from 56,000 m^3/d to over 165,000 m^3/d in the last 25 years [1,2].

Historically, the recovery factor for conventional heavy oil primary production has been between 1-5% of the original oil in place (OOIP). However, the implementation of an enhanced primary production technique in the mid to late 1980s has improved recovery factors to between 5-20%. The new operating technique has been named "cold production" by Canadian producers; it has also been called Cold Heavy Oil Production with Sand, or CHOPS. In the cold production process, sand is produced aggressively along with the heavy oil. This process has been successfully implemented in vertical (or slant or deviated) wells equipped with specialized pumping equipment (progressive cavity pumps). Nearly 50% of western Canadian conventional heavy oil production (~ 37,000 m^3/day) comes from cold production areas in eastern Alberta and western Saskatchewan [3].

Horizontal drilling is a cost effective means of increasing output while unlocking reserves previously considered unrecoverable using conventional drilling technology. Applications of cold production technology in horizontal wells, however, have been much less successful than in vertical wells. Horizontal wells produced under aggressive sanding conditions have required frequent sand cleanouts, which significantly increased the cost of the operations.

A limited amount of sand production into horizontal wells, small enough to avoid plugging of the wells, may help to increase the permeability of the formation around the wells and lead to increased production rates. Therefore, a controlled sand production strategy aimed at enhancing the surrounding permeability of the formation could be an important factor in optimizing cold production in horizontal wells from unconsolidated heavy oil reservoirs.

Many studies have been performed in the past on different aspects of sand production. However, they have mainly concentrated on finding effective methods to avoid sand production due to the high operating costs involved in handling and disposing of produced sand. Recent successes in cold production have rekindled interest in sand production. Rather than avoiding sand production, emphasis is being placed on control and management of the produced sand. This new focus opens a wide area for research, especially in the case of the horizontal well technology for heavy oil recovery.

Only a few studies have been performed to assess the feasibility of using horizontal wells in the cold production process. The results reported in the literature suggest that the process could have promise under certain conditions, but they are not sufficient to draw definitive conclusions. The main challenge is to reduce operating costs while maintaining oil production rates. One way to reduce operating costs is to produce sand from horizontal wells in a controlled manner to avoid the need for frequent sand cleanouts. The idea is to produce sand less aggressively, but still achieve enhanced oil rates. For example, relatively small amounts of sand could be produced temporarily to stimulate oil production, and then sand production could be stopped. When oil production rates decline, sand production could be initiated again. This process of starting and stopping sand production could be continued *ad infinitum.* The concept is to produce "sand on demand".

This study consists of a comprehensive experimental program focused on the investigation of the flow of oil and sand in the vicinity of a heavy oil horizontal well under cold production. The experiments model the flow of oil and sand into a slot in a horizontal well liner. Emphasis has been placed on obtaining measurements of flow-related variables (e.g. pressures) inside the porous medium, including around the slot. The data from these experiments (including pressures and pressure gradients) have been analyzed in an effort to improve the understanding of the mechanisms involved in the flow of oil and sand around, into, and through the slot and of the response of the porous medium to sand production. It is envisioned that the findings from this work will contribute to the development of effective sand management strategies, from the viewpoint of slot size selection for reservoir sands of a given size distribution and morphology.

1.2 Statement of the Problem

The cold production recovery process, as it is practiced in western Canada, has proven to be successful for vertical (or slant or deviated) wells [4,5,6,7,8,9,10]. Research efforts have been dedicated in the last two decades to understand, control and forecast this process in vertical wells [11,12,13,14,15,16,17,18,19,20,21,22,23,24]. However, cold production in horizontal wells has not been undertaken nearly as much as in vertical wells. This has been due mainly to economic issues. Horizontal wells produced under aggressive sanding conditions will require frequent sand cleanouts, as the sand deposits at the bottom of the horizontal well and thus reduces the effective size of the conduit. The cost of sand cleanouts is quite significant, increasing the production costs and affecting the economics of the operations. As a result, the tendency has been to prevent, instead of attempting to optimize, sand production into horizontal wells. This tendency has guided the direction of research efforts on the subject.

Field practices have shown that the cold production technique, as it is practiced in vertical wells, (i.e. with massive sand production), cannot be applied in the same manner in horizontal wells. New strategies have to be found to make cold heavy oil production with sand a technical and economic success in horizontal wells.

Many questions arise associated with horizontal well applications of cold heavy oil production with sand:

- The first and most important one would be: is there any advantage in applying cold production in horizontal wells?

- Is it possible to apply cold heavy oil production with sand (CHOPS) in horizontal wells by producing sand in just enough quantity to improve the oil recovery but maintaining the operational costs low enough to make the project profitable?

- How can the sand production be controlled?

- If the oil recovery is improved, what are the mechanisms? Are horizontal wells capable of allowing the initiation and propagation of high permeability channels similar to vertical wells?

In an earlier study, Meza [25] has shown that it is possible to enhance permeability and porosity around a horizontal well slot when controlled sand production with oil is allowed. Although this study showed promising results, it is important to emphasize that, as a preliminary work on a very complex subject, a simplified system was used. For example, there was no applied stress field, the cohesive strength of the sand was very small, and only a single fluid phase was involved.

In order to find answers to the questions raised above and to determine conditions in favour of optimal sand production rates, (e.g. the minimum sand production rate that will allow improvement in the oil recovery), a comprehensive study of the parameters that affect the initiation and subsequent production rates of sand from horizontal wells needs to be conducted. The consequences of sand production on the oil production rate should also be addressed in the study. As a key component of such a comprehensive study, further experimental investigations involving a better representation of field conditions, including water-wet sands and confining stress, are necessary.

1.3 Objectives

The primary goal of this research is to explore the possibility of applying cold heavy oil production with sand using horizontal wells. To evaluate this possibility it is necessary to determine if a controlled sand production strategy will enhance the oil recovery.

A critical factor affecting the potential for improvements in the oil production rate is the relationship between sand production and changes in the permeability of the formation, specifically in the near wellbore region. Therefore laboratory experiments simulating the flow of oil and sand in the vicinity of a slotted liner under cold production are proposed to investigate this relationship. Emphasis will be placed on obtaining measurements of flow-related variables (e.g. pressure) inside the porous medium, including around the slot. Experiments will be conducted to improve the understanding of the mechanisms involved in the flow of oil and sand around, into, and through the slot and of the response of the porous medium to sand production.

It is envisioned that the findings from this work will contribute to the development of improved strategies for applying the cold production process in horizontal wells.

1.4 Scope of Research

In view of all the considerations mentioned above, including the results of a literature review and a previous experimental study on sand production through slots [25], the following work plan was developed.

A series of laboratory experiments were planned to determine the effect of the following parameters on changes to the permeability and porosity around slots in a horizontal well as a result of sand production:

- Grain size distribution
- Slot size
- Stress field
- Fluid flow rate

These experiments were performed in a cylindrical model in which confining stress can be applied. During these experiments there was also an investigation of conditions that can destabilize existing sand bridges and arches, such as sharp changes in bottom hole pressure, to examine the potential for controlled sand production.

Additional information, such as the porosity distribution and the type of structures formed around the slot, was obtained through another set of experiments utilizing X-ray computed tomography (CT) tests. These experiments were performed in smaller cylindrical vessels but under similar conditions to those carried out in the larger vessel. The X-ray computed tomography tests were conducted to visualize and quantify the effect of sand production on the porosity distribution in the near-wellbore region. In addition, an attempt was made to perform structure visualization tests using thin sections in cylindrical vessels similar to those used for the X-ray computed tomography tests. These tests were attempted for a qualitative investigation of both the structure formed around the slots and preferential channels that could penetrate more deeply along the core. Unfortunately, challenges in preparing the packs for creating thin sections and in preparing thin sections later could not be overcome, so no thin sections were generated.

1.5 Methodology of Research

Figure 1-2 shows a flow chart outlining the proposed methodology for the research. The first step is the selection of the materials to be used. Once the material selection is completed, the next step is the characterization of these materials. Morphology and sieve analyses of the sands will be conducted. The density of the sands will be measured and their geomechanical properties will be determined in triaxial cell tests. The viscosity and density of the fluids will be measured.

Screening experiments with air will initiate the experimental program. From these preliminary tests the slot sizes to be used in the sand production experiments with heavy oil will be chosen.

The majority of the sand production experiments will be conducted by using a larger cylindrical confining cell. The effect of the stress field, oil flow rate, slot size, and sand size distribution on sand production initiation and sand production flow rate will be investigated (see Table 1-1).

The results of the larger cylindrical confining cell tests will be combined with the results of the CT scanner experiments and the visualization tests using thin sections to determine the effect of sand production on the characteristics of the near wellbore region.

The final aim of the project will be to identify a set of sand production strategies that could improve the economics of exploiting heavy oil reservoirs using horizontal wells in the cold production process.

1.6 Impact and Contributions of the Current Research

There is a strong interest in the development of viable and environmentally sustainable bitumen/heavy oil recovery processes that are less energy intensive and use less water than steam-based processes. One way to develop less energy intensive processes is to focus on extending the life of primary recovery processes.

The research presented in this thesis is a pioneering effort aimed at developing improvements to primary production in horizontal wells – enhancing oil production rates and increasing recovery factors through the managed production of sand. This approach has the potential to mitigate the decline in oil production rates in horizontal wells for extended periods of time, in a manner similar to cold production (CHOPS). Productivity in pools exploited by primary production from horizontal wells could increase by up to a factor of three (based on current production of about 65,000 bbls/d) with the successful implementation of this recovery technology, incremental oil recovery could increase by up to 5% (for a heavy oil resource base in the Western Canadian Sedimentary Basin (WCSB) estimated to be on the order of several billion bbls), and additional heavy oil resources could be made accessible in pools for which there are currently no available recovery technologies.

This research was based on an assessment of strategies for enhancing primary production in horizontal wells through managed sand production. A comprehensive research program was executed under experimental conditions closer to field conditions than any previous work on this topic found in the literature by the author.

The results of this work indicate that it is possible to generate significant increases in near-well permeability through managed sand production with low sand cuts. This improvement in permeability includes a reduction of skin effects and the possible formation of high permeability channels. It also highlights that with proper slot size selection and correct handling of production flow rates, sand production could be managed. This opens the possibility that primary heavy oil production with sand in horizontal wells could be developed into a technical and economical success. However, more research has to be performed to support these findings, especially with numerical modelling to forecast the impact of managed sand production on oil production rates.

The results of this project may also be applied in the design of sand control devices (e.g. slotted liners) for horizontal wells in other heavy oil recovery processes, such as steam-based processes or solvent-based processes.

Finally, this research project sets a foundation for the development of a new area of research on the improvement of heavy oil recovery processes through the managed production of sand. With the potential that this approach has for improving the economics of heavy oil recovery processes while reducing their energy intensity, it is a field that should continue to be explored, both broadly and deeply.

1.7 Structure of the Dissertation

This dissertation has been divided into 6 main chapters. Following the introduction contained in chapter 1, a summary of the findings of a literature survey is presented in chapter 2. The literature review was performed to find out what has been published concerning the cold production process in horizontal wells and to gain knowledge from the vast experience accumulated on sand control during the last few decades. Considerable attention is given to the stabilization and destruction of sand arches, as they are influenced by the sand size distribution, grain morphology, effective stress, opening diameter, flow rate and other parameters such as wettability and surface tension between reservoir fluids in the formation. Finally, at the end of the chapter, a summary of the principal findings of the literature review is presented.

Chapter 3 details the materials used, as well as the laboratory apparatus and procedures employed during this research program. Firstly, a description of the fluids and sands as well as the procedures for their characterization is presented. Secondly, the experimental apparatus and procedures are described. Thirdly, a section outlining experimental conditions and parameter selection is presented.

The experimental results and discussion are presented in chapter 4. The presentation of the results was sub-divided into four main sections: screening experiments with air, sand production experiments under confining stress, sand strength experiments, and visualization experiments using a CT scanner. An assessment of the relative significance of the variables that affect sand production studied in this project is given.

The sand production experiments using air as the flowing fluid allowed a rapid scoping of the factors affecting sand production. The analysis of the screening experiments with air yielded a correlation between slot size and grain size distribution. The correlation was used to choose the slot sizes for the experiments with water wet sand packs saturated with dead heavy oil.

The results of the sand production experiments under confining stress are presented and discussed in the second section of chapter 4. Seventeen sand production experiments were performed using water wet sand packs saturated with dead Dee Valley heavy oil and subjected to confining stress to analyze the effect of slot size, fluid flow rate, grain size distribution, and confining stress on the sand production behaviour.

In the third section of chapter 4, a series of triaxial compression (strength) experiments performed to determine the strength parameters (internal friction angle and cohesion) of sand packs saturated with residual water and dead heavy oil is presented. The purpose of measuring the strength of the sands was to establish a relationship between sand strength and sand production behaviour.

The last section of the chapter 4 presents the visualization experiments using a CT scanner. Two types of experiments were performed to obtain information on the changes in the sand pack porosities due to sand production. The first type of experiment, called dynamic experiments, was similar to the set of sand production experiments under confining stress. In these experiments, the pack was periodically scanned to track the porosity changes. The second type of experiment involved scanning of epoxied sand cores obtained from the sand arch visualization experiments.

Conclusions based on the experimental findings are drawn and presented in chapter 5. The final chapter of this thesis presents recommendations for future research. References and appendixes are given at the end of the document.

Table 1-1: Experimental matrix.

Sand	**Slot Size** (4 slot sizes, constant σ_c, variable Q)				**Confining Stress** (5 σ_c, 2 slot sizes, variable Q)					**Grain Size Distribution** (1 slot size, constant σ_c, variable Q)	**Sand Strength** (3 experiments per sand @ different σ’)			**Visualization Tests**	
	1	2	3	4	1	2	3	4	5	1	1	2	3	CT Scanner	Thin sections
Silica Well Sorted	√	√	√	√	√	√	√	√	√	√	√	√	√	--	√
Silica Poorly Sorted	√	√	√	√	--	--	--	--	--	√	√	√	√	--	√
Silica No Large Fractions	--	--	--	--	--	--	--	--	--	√	√	√	√	√	--
Silica No Fine Fractions	--	--	--	--	--	--	--	--	--	√	√	√	√	--	--
Husky Sand	--	--	√	--	--	--	--	--	--	--	√	√	√	√	√

σ_c= confining stress (kPa)
Q = flow rate (cc/h)
σ’ = effective stress

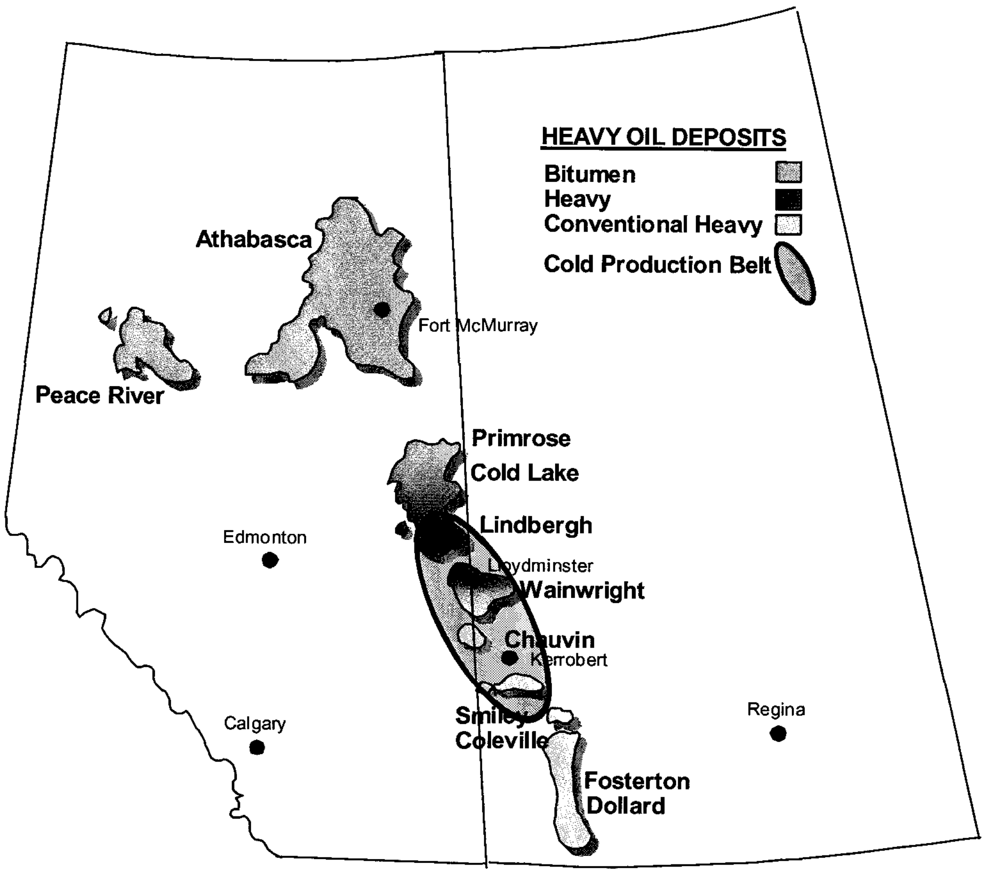

Figure 1-1: Heavy oil deposits in Alberta and Saskatchewan, with an indication of the cold production belt surrounding Lloydminster [3].

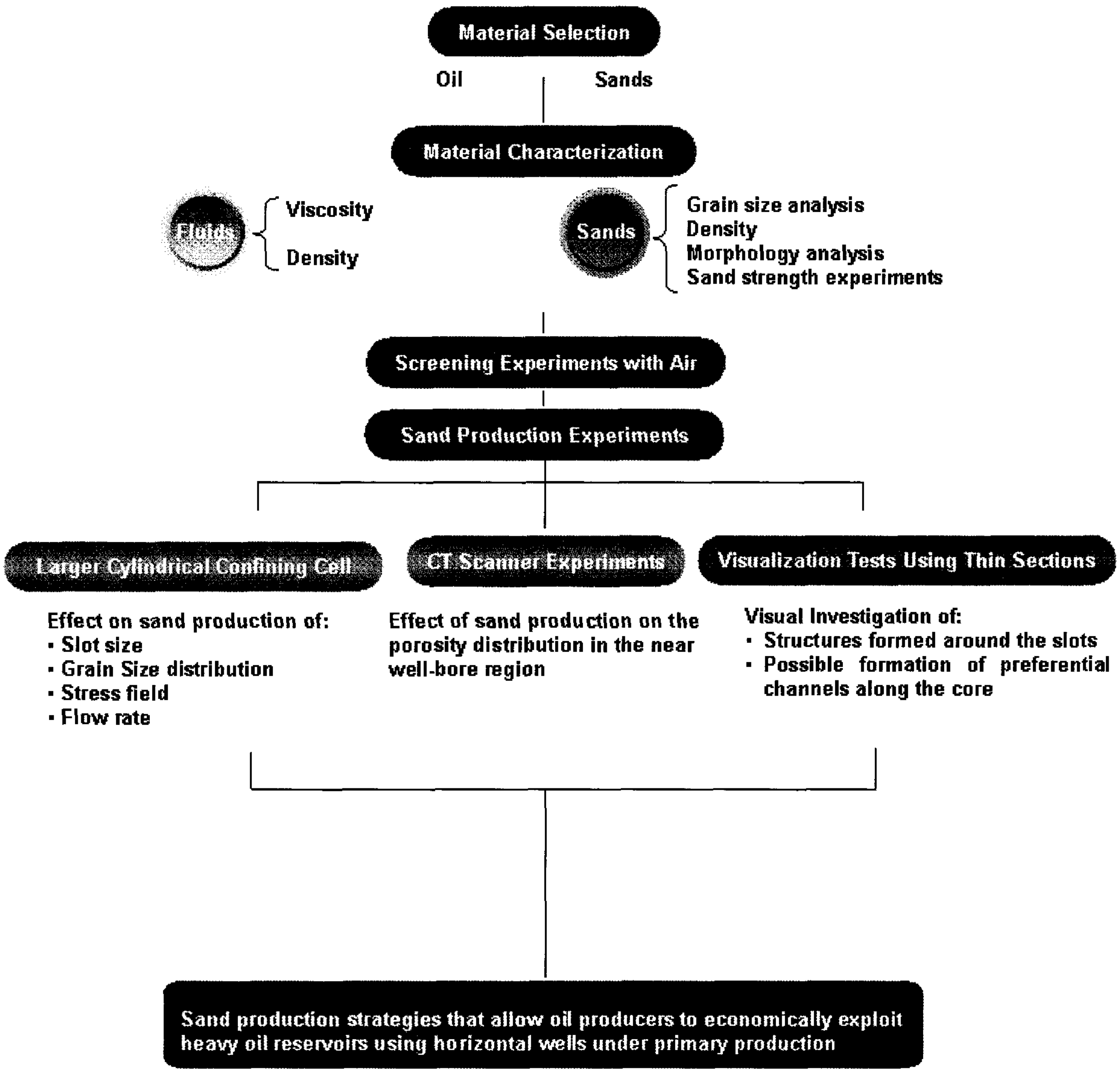

Figure 1-2: Flow diagram for methodology of the research.

2 Literature Review

One of the first activities in this research project was to perform a literature survey to find out what has been published regarding the cold production process in horizontal wells and to gain knowledge from the vast experience accumulated on sand control during the last few decades. The results of this literature survey are presented at length in this chapter.

The literature review was initiated with an online search performed in 1999 using the following databases: Tulsa (Petroleum Abstracts), American Petroleum Institute, Energy Science and Technology, Engineering Index, and Chemical Engineering & Biotechnology Abstracts. The online search was performed from 1965 to 1999 using the following key words: cold production, sand control and/or production, horizontal wells, slotted liner. The online search was first updated in 2002 and more recently in 2007.

The literature review starts with highlights about the cold production process. It continues with information reported on cold production in horizontal wells followed by the information published for vertical wells. Field tests, laboratory results and numerical studies are reported for both cases. This is followed by a detailed description of the mechanisms involved in sand production and the parameters that influence those mechanisms. Considerable attention is given to the influence of sand size distribution, grain morphology, effective stress, opening diameter, flow rate and other parameters such as wettability and surface tension between reservoir fluids in the formation, on the stabilization and destruction of sand arches. Finally, at the end of the chapter, a summary of the principal findings of the literature review is presented.

2.1 Cold Heavy Oil Production with Sand (CHOPS)

Cold heavy oil production with sand (CHOPS) is a primary non-thermal process used in unconsolidated heavy oil reservoirs in Alberta and Saskatchewan, Canada. In this process sand and oil are produced together in order to enhance the oil recovery [1,3,24,26,27,28, 29]. This process has proven to be economically viable when vertical wells are used [24,27,30].

Cold production is characterized by high oil flow rates more than 10 times higher than the flow rates predicted by using Darcy's radial flow equation [4-6,29]. Cumulative oil recovery has also been reported to be significantly higher than predicted by classical flow models [7].

It is believed that two main mechanisms are key factors in the unexpectedly high primary oil recovery observed in these reservoirs. The first one is associated with gas evolution from the heavy oil (foamy oil) and the second one with sand production [7,31]. A comprehensive review of cold production has been presented by Tremblay et al. [26].

The presence of foamy oil in primary production reservoirs has been the subject of numerous studies since Smith [8] postulated its existence based on observations of bubbles in the produced oil. The foamy oil behaviour is considered to be a highly efficient solution gas drive mechanism, more complex than the conventional solution gas drive [32]. The foamy oil phenomenon will not be discussed in detail in the present literature review since the experimental work to be performed in this research is focused on the second mechanism involved in cold production, i.e. sand production. More information about the foamy oil process can be found in references [32,33,34,35,36,37,38].

2.2 Cold Production in Horizontal Wells

Cold production has proven to be successful when vertical wells are used. However, applications of cold production technology to horizontal wells are much less common. The main reason is economics. Sand cleanout costs in horizontal wells are high, around U.S. $4.20/bbl [6], which significantly increases the production costs [6,7,39,40].

2.2.1 Field Tests

The only cold production pilot test using horizontal wells that the literature search uncovered was reported by Texaco Canada Petroleum Inc. The test was conducted at Frog Lake, Alberta. Ten horizontal wells were completed in the Lower Waseca formation and were produced through a co-production of sand and oil from the reservoir at ambient temperatures. The Lower Waseca zone is a relatively thin (12 to 16 ft) zone. The gravity of the heavy oil ranges from 10 to 14°API, and the oil viscosity ranges from 20,000 to 50,000 mPa · s [6].

Huang et al. [6] claimed that the wells were very successful, with most of the wells displaying production capabilities in excess of 100 bbl/d. However, they made clear in their article that some technical challenges related to reduction of operating costs have to be faced before the development plan using horizontal wells under cold production could be extended in that field. The authors pointed out that well servicing (U.S. $4.20/bbl) and sand handling (U.S. $1.20/bbl) are two of the biggest operating expenses.

The first horizontal well in this project yielded initial primary cold production rates of up to 100 bbl/d, which encouraged the drilling of a second horizontal well. This well produced on primary at rates in excess of 100 bbl/d with initial high sand cuts of 30%. The sand cuts decreased very quickly to the 2 to 4% range. In general, the Lower Waseca horizontal well performance exhibited typical fluid and sand production profiles for a cold production vertical well. It was characterized by a short start up period of high sand cuts of greater than 25%, followed by decreasing sand production and rising fluid production. Sand production was relatively high over the first 6 months of production, but later declined to an average cut of less than 5% [6].

In this pilot test, the optimum spacing for horizontal development (40-acre vs. 80-acre patterns) and the effect of different horizontal lengths and casing sizes on production performance were also evaluated. Nine of the wells were equipped with 8.625 inch casing whereas one well was equipped with 9.625 inch casing. Horizontal sections of approximately 1,600 ft and 2,500ft were drilled. All of the wells were completed with

5.5-in. liners slotted with *0.25 inch (6.35 mm) slots*. The results showed that after 20 months of production history, there was no indication of interference between the wells and no significant differences were observed because of the horizontal length. One of the best performing wells, in terms of productivity and minimal downtime, was the well with the larger casing size [6].

Huang et al. [6] also pointed out that the first horizontal well produced four times more than a conventional vertical well in the same area. Except for the higher oil production rate, the oil/water ratio and sand cut responses in the horizontal well were similar to those of a vertical well in the Lower Waseca sand. An important observation made by the authors was that no appreciable decline could be detected from the production data.

From the overview of this pilot test it seems that CHOPS in horizontal wells cannot be applied in the same way as it is applied in vertical wells (i.e. with aggressive sand production). The operating costs associated with a horizontal well represent an economic barrier that has to be overcome. Therefore, reducing sand cleanout costs by controlling sand production into a horizontal well while enhancing oil inflow into the well is an important factor in trying to optimize cold production from unconsolidated heavy oil reservoirs.

2.2.2 Physical Modelling

Meza et al. [25,41,42] have made the first experimental attempt (and only one known to the authors) to study the cold production process in horizontal wells. They performed an experimental investigation of the flow of oil and sand in the vicinity of a horizontal well under cold production. The experiments physically simulated the flow of oil and sand into a slot in a horizontal well liner. The parameters studied included slot width and sand properties (morphology and grain size distribution).

This experimental study used a physical model consisting of a stainless steel vessel with a cylindrical upper section and a converging lower section, with a steel plate at the bottom.

Plates with three different slot widths were used: 0.46 mm (0.018 in), 0.71 mm (0.028 in) and 1.02 mm (0.040 in). The slots were 7.6 cm in length [41,42].

Different types of experiments were conducted. The first set of experiments involved air as the flowing fluid. These experiments allowed rapid scoping of the factors affecting sand production. A second set of experiments on sand production was carried out with a liquid (silicone oil) as the flowing fluid in the same physical model. In these experiments Meza et al. investigated the effects of slot size, sand type and distribution, and oil flow rate on sand production. In addition, analytical models were utilized to provide an estimate of the change in sand rock properties (i.e. porosity and permeability) due to sand production [41,42].

They also performed two types of qualitative sand production experiments. The first one was to visually investigate the structures and rearrangement of the sand grains in the vicinity of the slot when sand production stops [42]. Following each sand production test, the sand pack was impregnated with epoxy resin to immobilize the sand grains. Thin sections of the solidified sand packs were cut perpendicular to the slot length. The prepared thin sections were examined using a microscope to observe the structures and possible porosity changes in the proximity of the slot.

The second type of qualitative experiments was performed using X-ray computed tomography. These experiments were intended to investigate the effect of sand production on the porosity distribution within the sand pack.

The main conclusions of Meza et al. [41,42] were:

- Sand production through horizontal well slots can be controlled, depending more on the sand grain sorting than on the grain morphology or the average diameter.
- Significant changes in the permeability and porosity can occur in the vicinity of the slot. The changes in these parameters were less significant away from the slot.
- The largest fractions of the sand (bigger than 500 μm) have an important role in arch/bridge formation.

- The sand cut behaviour was similar to that of observed in the field; that is, the sand cut had a tendency to be higher at the beginning of the sand production period and to decline with time. In most tests, the decline in sand cuts continued until no more sand was produced.

The work presented by Meza et al. [41,42] was a preliminary investigation in this field. Although this study showed some promising results, it was performed using a simplified test system (i.e. cohesionless sand, no stress field, single fluid system). Therefore, more work needs to be performed for any sustained conclusions to be drawn.

2.2.3 Numerical Modelling

Metwally and Solanki [7] conducted numerical studies to understand the mechanisms of the cold production process applied to the Lindbergh and Frog Lake Fields. Although the studies were focused on cold production in vertical wells, the analysis from vertical well simulation was also extended to horizontal wells.

The authors [7] predicted the production capability of a horizontal well under different conditions. They used a 1000 m long horizontal well located 0.762 m away from the bottom of a 6 m thick reservoir. They performed three series of simulations. In the first series, no sand production and no pressure support mechanism were present. The second series of simulation were performed without sand production, (i.e. without an enhanced permeability zone), but with reservoir pressure support. Finally, in the third series, pressure support and an enhanced permeability zone were specified.

Their results [7] showed that the best-case scenario is when sand production is allowed and pressure support is present. In this case, both oil flow rate and total primary recovery increased. Three-fold increases in the production rate were achieved compared with the case of no sand production and no pressure maintenance. A difference of 20% in production rate was found when comparing the best-case scenario with the case of no sand production but pressure support.

2.3 Cold Production in Vertical Wells

Due to the lack of information on cold production in horizontal wells it was necessary to pursue a literature search on studies of the cold production process in vertical wells. The experience obtained on cold production in vertical wells during the last two decades is valuable since the mechanisms and main factors are similar to those involved in the cold production process in horizontal wells.

2.3.1 Field Experience

The cold production process using vertical wells has been established as one of the principal methods for recovering heavy oil from the Western Canadian Sedimentary Basin (WCSB). It has become an alternative technology for the recovery of heavy oil since the mid to late 1980s, with the adaptation of progressive cavity pumps for heavy oil lift operations. Furthermore, much of the knowledge and expertise on cold production exploitation strategies and operating practices have been accumulated by Canadian heavy oil producers [3].

Although the process has been successfully developed in Western Canada, it was first practised in California [3]. Vonde [43] reported that with the application of specially designed pumping equipment Husky Oil Co. was producing crude oil as low as 4 °API with sand cuts of up to 70%. The wells were located in the Brooks sand, Cat Canyon field, California.

The specialized bottom-hole pumping equipment allowed primary production rates in excess of 150 bbl/d (24 m^3/d) oil from wells that were restricted to less than 10 bbl/d (1.5 m^3/d) when produced with conventional rod pumps and sand control completion methods [43].

The Brooks oil had an average gravity of 6 °API, and a viscosity of 15,000 mPa·s at reservoir conditions. The sand was very fine-grained and well sorted with an average diameter of 0.0065 in (0.165 mm). The net sand thickness was 150 ft (46 m) [43].

Production from the Brooks zone began in 1909. The wells were completed either with 250 mesh (0.25 in or 6.35 mm) slots or 0.5 inch (12.7 mm) holes through the zone, which allowed almost unrestrained sand production from the unconsolidated formation. Initially, the wells produced up to 400 bbl/d (64 m^3/d) of 10° API oil containing about 15% sand cuts. Cumulative recovery from the oldest part of the field reached more than 10% of the oil in place (OOIP). Individual wells have produced over 400,000 bbl (64,000 m^3) of oil and 40,000 bbl (6,400 m^3) of sand over a 40-year life [43].

Steam stimulation was tried in the field in the 1960s. As a result, an exploitation plan was implemented where the wells were completed with gravel-pack liners or 16 mesh (0.016 in or 0.40 mm) liner slots designed to exclude sand. However, the steam process was not economically successful and the wells were re-completed using the same opening dimensions as the early wells: i.e. 250 mesh (0.25 inch or 6.35 mm) slots or 0.5 inch (12.7 mm) holes. They were back into sand production with flow rates around 50 bbl/d (8 m^3/d). However, they faced severe operating problems at that time. The problems decreased with the development of improved downhole pumping equipment in the late 1960s. Vonde [43] reported that the downhole pumps then available were capable of producing extremely low-gravity crude up to 70% of entrained sand.

More recently, McCaffrey and Bowman [4] analysed the performance of Amoco's Elk Point and Lindbergh fields in Canada. They considered that sand production enhanced the productivity of the producing interval allowing greater fluid flow rates to the wells. The presence of high permeability zones was inferred after lost circulation during an infill drilling program occurred. These results were confirmed in a detailed program carried out subsequently by Amoco Canada [9]. The program was planned to investigate the communication between wells. Tracer material (fluorescein dye) was pumped into the casing of a selected well. The results indicated that the tracer flowed through channel systems over 2 km in length that connected up to 12 wells. These results were also supported by Yeung's findings [10] in a published study performed of the Burnt Lake cold production pilot project in the Cold Lake field operated by Suncor. The observed high oil productivity was believed to be a consequence of three main factors: 1) the sand failure and its removal from the wellbore area which provided a larger effective wellbore drainage radius; 2) the viscosity of the bitumen, which allowed the sand to be suspended in the bitumen and carried out of the formation, and improved the solution gas mechanism by retarding the coalescence of bubbles formed below the bubble point; 3) the creation of high permeability channels (wormholes), which improved the overall permeability of the reservoir.

Metwally and Solanki [7] evaluated cold production in the Lindbergh and Frog Lake heavy oil reservoirs in order to investigate the recovery mechanisms that contribute to the improvement of the primary production. They suggested that sand production leads to the creation of a high porosity disturbed zone that supplies slurry of sand and fluid to the wellbore. They also pointed out that sand production reduces in situ stresses around the wellbore. They assumed that near well stress reduction, along with foamy oil behaviour, cause the disturbed zone to grow into channels of unknown geometry. They suggested that these channels provide low resistance drainage paths, supply most of the produced fluids, and function like fractures.

2.3.2 Physical Simulation of Cold Production

A number of laboratory studies have been conducted to determine how sand production enhances oil production in heavy oil fields under cold production [11-17,44]. Two possible explanations have been given: formation of high permeability channels (wormholes) [3,11-15,44] or compact growth of a remolded zone (cavity formation) [16,17, 24].

Tremblay et al. [11-14,44] have published several papers reporting their experimental work on cold production. They simulated the production of oil and sand into a perforation (6.35 mm diameter) in a vertical well using horizontal sand packs. They used reservoir sand obtained from production wells at Suncor's Burnt Lake pilot site. They used both dead oil [11-13] and live oil [14,44] in the experiments. When dead oil was used, it was injected through the sand pack and was produced with sand through the perforation at the other end of the sand pack. Depletion experiments were carried out when live oil was used. In this case, the drive mechanism was provided by solution gas within the live oil.

In the experiments performed by Tremblay et al. [11-14,44], the sand packs were scanned using X-ray computed tomography to determine the spatial variation of the porosity within the sand pack. In all the experiments, the CT images showed that a high porosity channel or "wormhole" formed in the pack when sand was produced. The porosity within the wormhole was much higher (52%) than the average porosity within the undisturbed sand pack (32%). Tremblay et al. also found that the wormhole developed in regions of higher porosity and therefore lower unconfined compressive strength. This implies that in the field, channels are more likely to develop in the higher porosity (richer) oil sand. They concluded that the presence of these high permeability channels increases the drainage of the reservoir, which leads to the higher oil recovery observed in the field.

Other conclusions reached by these researchers were [12,13]: 1) the development of the high permeability channel occurred after the pressure gradient achieved a critical value; 2) the "wormhole" is filled with sand when it develops. The produced sand concentration when the wormhole developed was high (44% by volume). They also postulated [12,13] that the high sand cuts observed initially in the experiments are due to the growth of wormholes while the sudden decrease in sand cuts (1%-3%) indicates that the wormholes stopped growing. They observed that once the wormhole broke through the inlet, the loose sand at the top of the wormhole was slowly scoured away by the flowing oil. The top part of the wormhole had a porosity of 100%, while the loose sand had 53% porosity. As soon as the wormhole broke through at the inlet, the sand cut started to decline. They believed that the formation of a sand free channel at the top of the wormhole would explain the significant increase in oil production observed in the field after the sand cuts start to decline, while the residual sand cuts observed in the field are likely due to the scouring of the sand within the wormholes.

In the experiments performed with live oil, two conditions were recognized under which the channels could grow: 1) the pressure gradient at the tip of the wormhole must be sufficiently large to dislodge the sand grains; and, 2) the pressure gradient along the wormhole must be large enough to carry the sand from the tip to the orifice. It was established that the minimum pressure gradient needed to transport the sand through the channel is important for calculating wormhole growth in the field. They also observed the collapse of a wormhole when the backpressure was suddenly decreased (by 500 psi). They argued that this collapse was due to the low hydraulic diffusivity of the live oil outside the wormhole. They believed that similar behaviour might occur in the field with a sudden decline in the bottom hole pressure [14,44].

An important difference between the dead and live oil experiments performed by Tremblay et al. [11,12,14] was the magnitude of the minimum pressure gradient necessary for the development of a wormhole. The pressure gradient for the live experiments was significantly lower (1 MPa/m) than the one found in the dead oil experiments (800 and 32 MPa/m). This significant difference was attributed to a destabilization of the sand grains at the wormhole tip due to growth of gas bubbles in the pressure depletion experiments.

The rate of advance of the wormhole was found to be proportional to the oil flow rate through the sand pack. Tremblay et al. concluded that the average flux of sand at the tip of the wormhole was proportional to the pressure gradient at the tip [11-14,44].

In a later work, Tremblay and Oldakowski [15] reported on an experimental study where the aim was to investigate the effect of producing large quantities of sand on the permeability of the formation. To achieve their goal they performed a pressure depletion experiment where they simulated the production of sand, oil and gas into perforations in a well during the cold production process. They used a larger model (80.4 cm long and 29.85 cm diameter) than the one used in previous experiments (36.5 cm long and 10.2 cm diameter). Their model also had two production orifices (1.27 cm diameter), rather than the single orifice used in previous experiments.

Tremblay and Oldakowski [15] found similar results as in previous experiments [11-14,44], but in this case they were able to monitor the pressure behaviour along the sand pack more closely. As a consequence, they could gain a better understanding of the wormhole formation. They made direct observations of the physical phenomenon after the depletion experiment finished. They found two craters at the production orifices. The upper crater extended some distance inside the pack while the lower one was short. The hardness of the sand face in and around the upper crater was measured. It was found that the sand outside the crater was significantly harder (115 kN/m) than inside (less than 1 kN/m). This region of loose sand was called a "wormhole". The porosity of the sand in the wormhole was significantly higher (50.5%) than the original porosity (33.8%) of the sand pack. This was similar to the behaviour observed in the earlier experiments [11-14,44].

The authors [15] further investigated the high porosity region (wormhole) by immobilizing the zone with epoxy resin. They observed that the wormhole was composed of a central region of loose sand surrounded by concentric bands. The authors suggested that the concentric bands were likely tensile failure bands since no active confining stress was applied on the sand pack. The dimensions of the wormhole were measured, yielding an average diameter of 17 cm and a length of 36 cm. The wormhole had an elliptical shape. The authors argued that the shape of the wormhole was caused by the direction of the oil flux (pressure gradient). It was largest along the major axis of the wormhole. It was concluded that the sand flux at the surface of the wormhole is proportional to the pressure gradient. The authors also pointed out that wormholes seem to grow by a combination of tensile failure bands and erosion. In addition, the experiment suggested that wormholes do not develop from each perforation in the well. The results found in this test were used in numerical simulations to calculate the drainage into a wormhole and pressure gradients at the tip of the wormhole [15].

Vaziri et al. [16] conducted centrifuge experiments to identify the mode of failure following sand production and to quantify the impact of sand production on flow rate. The authors used water wet sand and canola oil (50 $mPa \cdot s$) as a working fluid. They concluded that sand production under their experimental conditions generated an enlarged cone-shaped cavity, around the opening. They also concluded that the high flow rate observed in the field was due to the formation of this enlarged cavity that could significantly improve the permeability over an appreciable distance around the well. They recognized that the conditions in the experiments were far from field conditions. The sand pack was not as dense as the formation in the field and was not as strong as the formation sand. Also, stress conditions were not modelled and pressure conditions were much smaller than in the field. It seems that when loose sand packs are used, cavities are more likely to occur than wormholes [26]. As well, the fluid used was not as viscous as a typical heavy oil under cold production in Alberta and Saskatchewan fields (1,200 to 55,000 mPa · s) [26]. It was pointed out by Tremblay et al. [26] that the high viscosity of the oil helps to confer a higher transient compressive strength to the sand when it dilates due to higher pore suction and a subsequent increase in local effective stress.

Recently, Wong [17] reported an experimental work that combined the two key factors in the cold production process, sand production and foamy oil. He investigated the effects of the interlocked structure of oil sands, pressure gradient, and gas exsolution on sand production through a perforation. He used a triaxial cell where confining stress could be applied to the sample.

Wong's experiments [17] involved the flow of a single phase fluid (water) or live heavy oil in heavy oil saturated sand cores. Some of the single-phase fluid experiments were performed under constant flow rate and others at constant pressure gradient. The single phase fluid experiments yielded consistent results: negligible sand production with formation of small conical cavity around the perforation. A different tendency was observed when live oil was used. No sand was produced when the outlet pressure was maintained above the bubble point. However, when the pressure dropped slightly (0.1 MPa) below the bubble point sand was flushed out with foamy oil at a high rate. An X-ray of the core revealed that a bulb like cavity was formed and tensile parting was induced in the sand matrix around the cavity. It is important to emphasize that Wong decreased the pressure in the experiments in steps instead of in a steady way. The sudden drop in the pressure could produce a high pressure gradient around the opening which in turn could generate the high sand and oil production rates observed.

Wong [17] concluded that the interlocked structure of natural oil sand provides a high shear resistance against the seepage force generated by the fluid flow. However, he argues that the oil sand is very weak in resisting tensile failure under gas exsolution.

Kantzas and Brook [45] recently published a paper where cold production and post cold production techniques were evaluated. They compared depletion experiments with and without sand production. The recovery during primary production with sand was higher than without sand. They also observed a high permeability channel in their CT scanner experiments.

2.3.3 Numerical Simulation of Cold Production

Some attempts have been made to model the cold production process numerically. However, due to the complexity of the two main mechanisms involved in the process, foamy oil flow and sand production, the tendency has been to focus on one of the mechanisms in the models proposed [18-22,33]. More recently, a few studies have emerged where a coupled reservoir-geomechanics model has been presented [3, 23,46]. Currently, there is not a commercial simulator available that can model the cold production process completely.

Kraus et al. [33] proposed a model based on foamy oil behaviour to explain the unexpected performance of the reservoir under primary production in Western Canada. They introduced the so-called "pseudo-bubble point fluid property model". They developed a methodology that could be used to calculate "foamy oil" fluid properties from conventional PVT data. The performance of the foamy oil reservoir could then be simulated using a conventional simulator and the data generated using their methodology. The pseudo bubble point pressure was an adjustable parameter in this fluid property description. They tested their model using field data. They obtained reasonable matches for three of the anomalous production characteristics observed in the "foamy oil reservoir"; i.e. high oil recovery, low producing GOR, and natural pressure maintenance.

Wan et al. [18] have proposed a coupled geomechanics-hydrodynamic model which emphasizes the geomechanics aspect of the cold production process. In this model oil, fluidized sand, and sand phases interact through mechanical stresses and hydrodynamics. Sand production is generated from the interaction between geomechanics and an erosion process in which sand grains are detached from the solid matrix due to both fluid and stress gradients. The plastic shear deformation of a sand matrix around a well during drilling and pressure drawdown increases the erosion potential. In return, the erosion process also weakens the sand matrix through degradation of its mechanical strength. The volumetric sand production during the cold production process can then be calculated using this self-adjusting mechanism.

Yuan et al. [19] considered that understanding the wormhole development pattern was critical to the modelling of fluid flow behaviour and recovery rates in the cold production process. They proposed that wormhole growth could be described following a probabilistic active walker model (PAW). Following this approach, they used a power law function to calculate the mobility of a slurry of sand and oil through the wormhole network. This mobility was used to calculate oil and sand production rates. They also related the maximum size of the wormhole zone and its expansion rate to the sand production data in a typical cold production operation. Therefore, they believed that the model could be useful in determining well spacing. They also claimed that the tool could be valuable for analysing field data and for the development of field scale simulations of the process.

Denbina et al. [20] attempted to model the cold production process using a modified black oil reservoir simulator. They implemented the main mechanisms of cold production using a wormhole approach and a modified gas relative permeability. To model the wormholes a transmissibility multiplying function (TMF) was introduced. The TMF factor allowed a dynamic and implicit permeability increase due to sand fluidization and production. They adjusted this function in order to history match oil production rate data. Their ultimate goal was to estimate the ultimate recovery for a cold production strategy as well as examine the impact of the cold production depletion scheme on subsequent secondary and tertiary recovery processes.

Wang et al. [21] proposed a wormhole network model that attempted to estimate the cumulative sand production during the cold production process. A classic geomechanics model coupled to a simple foamy oil flow model was used. In the geomechanical part of the model, they simulated the deformation process in the reservoir at the front of the moving wormhole tip. The wormhole tip was considered a moving boundary, which depended on the pressure profile inside the wormhole and the dilatant behaviour of the reservoir formation adjacent to the wormhole. To simulate the foamy oil behaviour, heavy oil with high compressibility was considered. A nonlinear diffusion equation for fluid pressure was developed and coupled to the geomechanical model so that both the effective stresses and the radius of the plastic zone could be calculated. After analyzing a field case using this model, the authors concluded that the sand production and enhanced oil production are a combined result of continuous sand yielding and slurry transport through a wormhole network.

In a subsequent paper, Wang and Chen [22] took a different geomechanical approach. Instead of assuming the formation of high permeability channels as a consequence of sand production, they imposed a zone of high permeability or dilated zone in the reservoir. Solid flow was considered as a continuous moving phase along with the fluid flow. The solid velocity was included in the geomechanics constitutive relationship and the derivation of the material balance equations. They tried to apply their model to field data, but they were unable to generate a good match. They argued that the lack of geomechanical information did not allow them to show more convincing results of the applicability of their model.

More recently, Wang et al. [46] have presented a reservoir-geomechanics model where a three dimensional black oil model is coupled with a simplified slurry transport model. In this model, the formation of high permeability channels was assumed to develop from perforations when pressure gradients exceed the residual cohesion of the sand. It was postulated that wormhole propagation is controlled by a critical velocity or pressure at the tip. Material balance was considered in three different zones: in the slurry, in the wormhole tip propagation zone and in the intact formation. They considered the dissolved gas as a separate component that remains inside the oil after the bubble point is achieved. Under this condition the oil exhibits a higher compressibility than the oil above the bubble point. They assumed that foamy oil flows effectively as a single phase before critical gas saturation is achieved.

Sawatzky et al. [3] reported two cold production models that were developed at the Alberta Research Council (ARC). They pointed out that these numerical models contain modules incorporating the mechanisms representing the influence of foamy oil flow and wormhole network growth. In the first model, wormhole network growth was prescribed from a sand production history. In the second model, a wormhole network growth was predicted by a sand production module fully coupled to a reservoir simulator.

The authors [3] described the first model as a fluid drainage model. In this model, the extent of the wormhole network could be changed dynamically, through a temporal enhancement to the permeability distribution in the reservoir grid (using transmissibility multipliers). The extent of the network was determined from a prescribed sand production history. The permeability distribution within the wormhole network was calculated from variable wormhole properties, such as diameter and porosity. Another important aspect of the model was its treatment of non-equilibrium foamy oil behaviour. The relative permeability of the gas phase was reduced compared to the free gas behaviour, to account for the restricted gas mobility caused by the presence of foamy oil.

They tested this model using field data from a set of Husky cold production wells in the Edam field [3]. Oil production rates were matched successfully for wells with good oil production and wells with poor oil production. From the simulations, they concluded that the wormhole network grows rapidly during the first months of production. The size of the network was estimated to be about 80 to 100 m out from the well. After the initial period of rapid growth the wormhole network continued to grow slowly. From the simulation pressure history, they concluded that the drainage area for a cold production well is approximately the same as the area occupied by the wormhole network.

The second model was called a comprehensive model by the authors [3]. It was a coupling between a fluid drainage model and a sand production module. The sand production module contains a criterion for sand failure at the tip of a wormhole, based on the concept of a critical pressure gradient, and equations for sand transport along a wormhole. This treatment allows wormhole network growth to be predicted, in each horizontal layer of the reservoir grid. The treatment of foamy oil behaviour was also improved in this model. A kinetic model allowing for a dynamic representation of foamy oil flow, replaced the pseudo-equilibrium model of foamy oil behaviour.

The comprehensive field scale model was used to obtain history matches to oil production rates and sand production rates from the same set of Husky Edam cold production wells used with the preliminary model. Reasonable matches were obtained. The simulation results achieved with this model agreed with the preliminary model. The results revealed that the development of a dominant layer of wormhole network growth within the producing zone is critical to the success of the cold production process. In the matches, the drainage area for each cold production well was determined by the extent of the dominant layer [3].

The authors [3] proposed using the modelling results to evaluate cold production behaviour in a pool. They believed the data obtained from the drainage areas and recovery factors from the areas studied could be extrapolated for a complete pool. These parameter estimates could be used to construct drainage footprints for all of the wells in the pool.

Coombe et al. [23] studied the cold production process mechanistically by employing coupled geomechanical-fluid flow simulation models. They proposed that the stress concentration causes mechanical weakening, and fluid flow causes erosional mobilization of sand particles. Further, they considered that porosity change is the primary coupling parameter. As porosity increases, both rock elasticity and strength (cohesion) were assumed to become weaker, while allowing erosional generation of mobilized sand.

These ideas were implemented in coupled simulation models using different coupling strategies and different physical assumptions to study various aspects of the cold production process. The first coupled model was a finite element model for two-dimensional radial plane strain and single-phase fluid flow. Here the geomechanics and fluid flow aspects were fully coupled such that the time dependent (undrained to drained) mechanical stress transfer was preserved. The second coupled model allowed a more complete fluid model (including gas ex-solution and water influx), as well as a time dependent sand mobilization mechanism, but at the expense of a weaker geomechanical-fluid flow coupling [23].

The authors [23] utilized two forms of "sand" in the fluid model. The first is mobilized sand (free sand), which is liberated during the wormhole creation process, and which is assumed to be transported in the oleic phase. The presence of this component can alter the oil phase viscosity, essentially affecting how easily mobile sand can be transported to the production well. The oil phase viscosity with a sand component represents the slurry viscosity. The second form of sand (expressed as the sand component) was considered immobile; however, it represents that portion of the total rock matrix which could be mobilized. This component represents the source of the mobile sand.

When analysing their model, the authors [23] pointed out that the erosion-based mobilization process had hydrodynamic consequences. In addition to the oil viscosity increase due to the presence of mobile sand, there were porosity increases and consequently permeability increases due to the local reduction in the amount of the immobile sand component. A parametric form of the Carmen-Kozeny equation was used to describe this permeability increase. Additionally, the ability to transport sand along the wormhole was limited. Once the (dimensionless) flow velocity fell below a threshold value, the sand stopped moving and the effective permeability dropped dramatically. This was modelled via a capillary number dependence of the oil-sand slurry relative permeability.

2.4 Sand Production

Sand production is defined as the production of small or large amounts of solids together with the reservoir fluids [47]. Traditionally, sand production in oil wells has been seen as a problem that had to be avoided given the negative effects associated with it, such as wear and erosion of the production equipment, problems with the stability of the wellbores, casing collapse, etc. [39,47,48,49].

On the other hand, Dusseault et al. [24] have reported that sanding in cold production is not necessarily a negative factor in oil well management. Some positive aspects mentioned by these authors are: reduction in completion costs, improved production rates, elimination of expensive workovers to remove scale and other sources of near-well blockage.

These positive aspects have been observed in many field case studies of cold production reported recently in the literature. Moreover, field observations have shown that blocking sand production causes a strong decrease in oil production in shallow unconsolidated formations [5,24,30,50].

It is considered that sand production improves the efficiency of the other drive mechanisms by altering the fluid flow characteristics into the wells in heavy oil reservoirs. It is also thought that this might be one of the main reasons for the high production rates observed in the field [4].

2.4.1 Sand Production Mechanisms

Sand production analysis requires coupling of geomechanics (stress, strength, and liquefaction), fluid flow (hydrodynamic drag, pressure, slurry rheology) and solution gas processes (bubble formation, phase behaviour, transport) [24].

Sand failure occurs when the stresses on the formation exceed the strength of the formation. In order for the failed zone to grow the failed sand must be transported. One of the key factors causing formation cohesive strength is due to the cohesive forces between the immobile formation water surrounding the sand grains and the oil [39].

For low cohesion materials, fluid flow can mobilize the grains. The condition for a grain to move under this situation was derived by Charlez [30].

Consider a grain A between two adjacent grains B and C [30] (Figure 2-1). Assuming zero cohesion for the material, the grain is kept in place by contact (friction) through the action of the effective hoop stress:

$$\sigma'_{\theta\theta} = \sigma_{\theta\theta} - p \qquad 2\text{-}1$$

where:
$\sigma_{\theta\theta}'$ = the effective hoop stress
$\sigma_{\theta\theta}$ = the total hoop stress
p = the pore pressure

The effective radial stress is null ($\sigma_r = p$). The condition for a grain to move is written as:

$$F_h \geq F_f = F_N \tan\varphi \qquad 2\text{-}2$$

where:

F_h = Hydrodynamic force related to the fluid velocity
F_f = Friction force
F_N = Normal intergranular force
φ = Internal friction angle

The normal mean contact force is defined to be the product of the mean stress by the contact surface:

$$F_N = \bar{p}\pi r^2 \qquad 2\text{-}3$$

where r is the contact radius. The hydrodynamic force F_h that tends to displace the grain towards the well can be separated in two components: a pressure component connected to the pressure gradient (F_h^1) and a drag force related to the fluid viscosity (F_h^2):

$$F_h^1 = \frac{4}{3}\pi v_f \frac{\mu}{k} R_g^3 \qquad 2\text{-}4$$

where:
R_g = grain radius (sphere in this case)
v_f = fluid velocity
μ = fluid viscosity
k = permeability of the porous media

The drag force of a viscous fluid on any submerged solid is proportional to the kinetic energy of the fluid:

$$F_h^2 = C_D A_c \left(\frac{\rho_f v_f^2}{2} \right) \tag{2-5}$$

where:

A_c = cross sectional area in the direction of flow
ρ_f = fluid density
C_D = drag coefficient depending on the Reynolds number.

In the specific case of laminar flow, Equation 2-5 can be written as:

$$F_h^2 = 6\pi v_f \mu R \tag{2-6}$$

Adding the expressions 2-4 and 2-6, the total drag force F_h is obtained:

$$F_h = 2\pi v_f R\mu \left(\frac{2}{3}\frac{R^2}{k} + 3 \right) \tag{2-7}$$

Using Darcy's law:

$$v_f = -\frac{k}{\mu}\frac{\partial p}{\partial x} \tag{2-8}$$

Equation 2-7 can be rewritten as:

$$F_h = 2\pi k R \left(\frac{2}{3}\frac{R^2}{k} + 3 \right) \left(\frac{\partial p}{\partial x} \right) \tag{2-9}$$

Therefore, the hydrodynamic force acting on a sand grain is directly proportional to the pressure gradient ($\partial p / \partial x$).

It has been stated that there are two main mechanisms involved in sand production [47]

Shear failure is related to a low well pressure. This means that some plane in the near wellbore region is subjected to higher shear stress than it can sustain.

Tensile failure is related to a high production rate. The sand production is then related to fluid drag forces on the grains of the formation. This is the main mechanism for the development of the high permeability channels or “wormholes”.

In practice, the two mechanisms will work together and interact. A formation altered by shear failure may be much more susceptible to fluid drag. Even in the case of shear as a basic failure mechanism, fluid flow is important in bringing the material into the well.

2.4.2 Parameters Influencing Sand Production

The study of sand production control is very complex given the numerous parameters that can influence this process. McCormack [51] has classified the possible parameters that influence sand control as follows:

- *Formation properties*, such as degree of consolidation, grain size distribution, sand morphology, clay content, sand strength, overburden pressure, cohesion, stress concentration.
- *Fluid Flow*, such as fluid saturation, fluid production rates, oil gravity, temperature, flow transients and pressure.
- *Formation Alteration,* such as silica dissolution, clay dissolution and re-precipitation, fines movement.
- *Control techniques,* such as gravel pack sand specifications, wire wrap screen or slotted liner dimensions, consolidation of the wellbore zone by chemical methods, prepack screens, pumping equipment mechanics.

Chalaturnyk et al. [48] claimed that to evaluate the mechanisms controlling sand production it is important to follow the evolution of sand production during the different stages in the life of an oil well. This includes the drilling period, followed by completion, production and workovers. Specifically, the authors divide sand production in two interrelated categories: mechanisms governing sand production initiation and mechanisms governing sustained sand production. Moreover, initiation was defined as being strongly controlled by the disturbance from drilling and completion; it is dominated by near-wellbore effects. Sustained sand production was said to be controlled by global reservoir factors such as geology, in situ stress regimes and multiphase flow. Furthermore, it was stated that as for any other production process, sand production is intimately linked to the pressure behaviour in the well and to the flow processes in the reservoir.

In a recent work Vaziri et al. [52] demonstrated using advanced numerical modelling that while the capillary tension appears to be insignificant (approximately 1 psi), it provides a significant resistance against sand mobilization. They concluded that un-cemented rock around the wellbore is basically held together by capillary tension.

2.5 Sand Arching

Sand arching seems a natural way to control sand production. An arch is a curved structure spanning an opening, serving to support a load by resolving external stresses into tangential and radial stresses [53]. Sand arching in a well completion is different from sand bridging. Sand bridging refers to blockage of an opening to sand movement through the opening by an interlocking of a few grains and stress transfer between grains within or at the mouth of the opening. Arching refers to a structure formed entirely outside the opening [54]. In some instances, bridging and arching may occur simultaneously [40]. Figure 2-2 shows the difference between sand arching and bridging in a schematic form.

A means to visualize the arching phenomenon is through the sketches in Figure 2-3 [30]. A cylindrical vessel with a perforated bottom floor is filled with an unconsolidated sand pack. The overburden stress is simulated by applying a vertical load to the vessel. Fluid is injected into the vessel through the top part at an increasing flow rate. Some sand is produced through the hole and a stable arch is formed. The flow rate can then be increased without any further production of solid until another critical value corresponding to a new arch is reached. The second arch is less stable than the first. The experiment is repeated until eventually the cylinder is almost emptied.

Given the importance of sand production in the petroleum industry, both as a problem and more recently as an advantage in cold production, the phenomenon of sand arching over an opening has been the subject of numerous studies. Factors that influence the formation of arches and their stability have been two of the topics most studied.

2.5.1 Theoretical Development

Bratli and Risnes [55] studied the arching phenomenon occurring in unconsolidated sands due to stresses imposed by a flowing fluid. They proposed a theoretical model, which established a stability criterion for sand arches. The model was validated with experimental work.

The laboratory model used by these authors consisted of a steel cylinder with a central hole at the bottom to simulate a perforation. The cylinder was filled with unconsolidated sand and compressed with a piston vertically to simulate overburden pressure. Fluid was injected into the vessel at the top through an opening beneath the piston, with a wrapped wire screen diffuser. The flow rate Q was increased steadily during the experiments. Air and oil were used as flowing fluids. Two types of sands, 20-40 mesh US and 80-100 mesh US, were used.

From their experimental and theoretical work, Bratli and Risnes [55] distinguished two modes of failure as the flow rate increased:

- *Collapse of a thin inner shell.* A new stable arch radius is formed. The new arch has a larger radius, which leads to a reduction in the stresses imposed by the flowing fluid under controlled flow rate conditions. Usually a series of such collapses occurred in an experiment.

- *Total failure of the sand.* A critical value between the flow rate and the existence of an arch radius was demonstrated. When this critical flow rate was exceeded total failure of the sand resulted, leading to continuous sand production.

The stability criterion developed relates the drag forces and the strength parameters of the sand in the Coulomb failure zone. The criterion is given by:

$$\frac{\mu Q}{4\pi k R_1} \geq \frac{T_\alpha + 1}{T_\alpha} 4S_{co} \tan\alpha \qquad \text{2-10}$$

where:

$T_\alpha = 2(\tan^2\alpha - 1)$

R_1 = radius of the arch

k = permeability of the failure zone

μ = viscosity of the fluid

Q = fluid flow rate

S_{co} = inherent shear strength of the material (cohesive strength)

α = failure angle given by $\frac{\pi}{4} + \frac{\varphi}{2}$

φ = internal friction angle of the material

From the stability criterion, the critical flow rate at which sand production starts can be obtained.

The experimental work of Bratli and Risnes [55] indicated that the arching behaviour was always the same. The flow rate could be increased steadily until a small amount of sand was produced suddenly. Then the flow rate could be increased further without incident until a new amount of sand broke loose. This repeated itself several times until the sand pack broke down completely and came pouring out of the opening.

The arch radius, R_1, was calculated assuming a spherical cavity around the orifice:

$$W_{sand} = \frac{4}{3}\pi R_1^3 (1 - \phi)\rho_S \qquad \text{2-11}$$

where W_{sand} = the mass of sand produced

ρ_S = the sand density

ϕ = porosity

The authors [55] considered that the arches formed were stable if the flow rate could be reduced to zero and increased to its former value several times without sand production. This latter effect was probably caused by using well-sorted sand.

From the theoretical analysis it was observed that the fluid drag forces appear through the term:

$$\frac{\mu Q}{4k\pi R_1} \qquad 2\text{-}12$$

Critical conditions are reached when this flow term exceeds a value given by the strength parameters S_{co}, and α for the sand.

The authors emphasized that the spread in the experimental results and the uncertainties in the parameters involved made it impossible to discuss each experiment and the difference between them in detail. They tested their theories with average values of the calculated radius and flow rates.

Sawatzky et al. [56] provided an assessment of the capability of sand matrix failure models to act as predictive tools for the initiation of sand production, by comparing the critical pressure gradients for sand production predicted by these failure models with the pressure gradients observed under field conditions and in laboratory experiments. They analyzed the Bratli and Risnes analytical model [55] and the Morita et al. [57] numerical approach.

They found that typical pressure gradients necessary for initiation of sand production in the cold production process under field conditions, calculated without including the effects of live oil, are at least two orders of magnitude larger than predicted critical pressure gradients for failure of the sand matrix. Laboratory experiments also support these observations indicating that the pressure gradients required to initiate sand production are also much larger than the predicted critical pressure gradients.

After their assessment they concluded that analytical failure models could not be used as tools for field prediction of cold production. Further, numerical failure models could not be used for field predictions either since they also under-predict the critical pressure gradients required for sand production [56].

They [56] gave suggestions on how to develop methods to predict initiation of sand production. First they considered that the measurement of the material properties of the sand matrix could be improved for use in existing models. As an example they mentioned that the influence of factors such as stress and fluid viscosity on the material properties could be measured. Second, they believed the failure mechanisms incorporated into existing failure models could be improved. They suggested making fewer simplifications in the modes of failure in the sand matrix since the process is intrinsically more complicated than the simple mode of tensile failure in a hemispherical arch proposed by the Bratli and Risnes model. Finally, they considered that a sand transport mechanism should be included in failure models, for those cases where sand transport and not sand matrix failure is the dominant mechanism in the field.

2.5.2 Effect of Grain Morphology, Grain Size Distribution and Opening Diameter

Hall and Harrisberger [53] studied the stability of sand arches and their relation to the maximum sand-free petroleum production rate. They found that arch stability might be rate sensitive at low confining stress but independent of flow rate at high confining stress levels. The difference between round sands and angular sands in regard to the stress level for grain crushing was shown. Arch failure under load occurred at lower stresses for angular sands.

The apparatus used by Hall and Harrisberger [53] consisted of a cylindrical chamber 3.75 in (9.53 cm) in diameter, fitted with a piston loaded vertically by a hydraulic jack. In order to observe arch formation a removable trap door of 7/16 in (1.11 cm) was placed in the centre of the vessel floor. The experiments consisted of removing the trap door and observing the formation of an arch or the production of sand. To evaluate the stability of the arch, the load was increased or fluids were injected through the inlet or outlet of the cell.

They compared the arch stability for round sands to angular sands. They observed that angular sand without compaction did not form an arch. When a moderate compaction was applied, it could lead to a slightly stable arch, easily destroyed by tapping the apparatus. A higher load of 500 psi (3.4 MPa) helped to stabilize the arch. A better interlocking of the surface grains was the explanation for this result. A slow flow of air through the outlet did not disrupt the arch, although a higher flow rate did. When a 2,000 psi load (13.8 MPa) was applied, and the trap door was open, the arch failed.

For the round sand, they found that it would not arch for a loose or dense pack at low loads. Even at 500 psi (3.4 MPa) it seems that the grains did not interlock enough to stabilize the structure. The only way they could form arches with this sand was to inject air from the outlet; in this way they could even go to higher loads without grain crushing. However as soon as the air flow decreased the arch failed.

Yim et al. [58] established the arch stability is strongly dependent on the granulometry of the porous material and the size of the perforation, in addition to the flow rate. Larger perforations required larger grains to form stable arches. Thus the selection of the perforation diameter could also be used in designing a sand control strategy.

McCormack [59] conducted experimental work with spherical particles to determine the arching/bridging mechanism that influences the performance of wire-wrapped sand screens. He cited Coberly's work [60], who also studied the arching/bridging of steel balls and sands using an adjustable gap opening size. McCormack summarized Coberly's findings as follows:

- For both well rounded sands and steel balls of a uniform size, stable arches were observed when the gap opening or slot size was less than 2 times the diameter of the particles. Unstable arches were observed when the slot width to particle diameter ratio was 2.5.

- Particle mixtures of two sizes produce results that are intermediate between those of the individual sizes. When the difference in particle size is small, the mixture behaves like the larger of the two particles except at very low concentrations of the large particles. When the size difference is greater, the smaller particles have a greater influence on the performance of the mixture.

- Two types of arches were observed in the cell: a low three-particle type, and a high, four- or five-particle type. The lower type of arch tended to re-establish more quickly when the cell was disturbed.

- A test with oil flowing through the cell had nearly identical results to a test with dry sand when other conditions were held constant. However, when oil wet sand with no fluid flow was tested, wider stable arches could be formed.

- The stable gap opening size was generally 2 times the tenth percentile size, D_{10}, of the sand. Vertical and horizontal slots gave similar results when sufficient particles covered the openings and oil is flowing. Gap openings with parallel sides were plugged. However, if an undercut, or keystone was used then no plugging occurred. Arch stability was affected by the spacing between adjacent gap openings.

McCormack [59] also mentioned that even though there are several selection criteria for gap size opening cited in the literature, there is limited evidence that supports the selection of these criteria.

McCormack [59] recognized two types of packing used with wire-wrapped screen. The first one is multiple particle arches; in this type of packing, breaking and re-establishment of the arches is observed which allows some resistance to fines plugging. This type of packing was called "partial sand retainment". The second type of packing is total sand retainment, which is usually employed with gravel packs. In this type of sand control an opening is chosen that is smaller than the size of the smallest particles. Therefore, no sand is produced but plugging with fines may occur.

In the study by McCormack [59], a series of 2- and 3-dimensional experiments were performed. The tests were carried out using glass beads that were of nearly uniform size, about 14.2 mm in diameter. No fluids were used in the tests.

The 2D experiments were carried out in a visual model where the packing structure could be seen. Gaps opening that were 1.5 and 2 times the average diameter of the glass beads were used in the experiments.

The most important results were:

- The arches formed in arrangements of 3, 4, or 5 particles.
- The location of the side particles of the arch could drastically affect arch stability and formation. He observed that when side arch particles were not firmly supported by the end walls arch stability was greatly reduced.
- The opening that was 1.5 times the diameter of the uniform particles had a tendency to form faster and more stables arches.

In the 3D experiments, glass beads of 15.4 mm diameter were used. The major results were:

- Stable arches were observed when the opening was 1.8 times the particle diameter. However, for size openings around twice the particle diameter, stable arches would not form after the arch was even slightly disturbed. More glass beads went through the opening when the bed height was low and/or when the size opening was increased.
- As the gap opening size increased, the arches tended to be composed of more particles.

Some of the limitations of the study were mentioned by McCormack [59]. Glass beads of uniform size were used. Different results may be found with sand particles of different shape and with different size distribution. Fluid flow was not considered; therefore the effects of fines and porosity changes in the pack were not taken into account. The applied stress field was due to gravity only. In real systems, the stress field would be multi-dimensional with localized stress concentrations [59].

McCormack concluded that:

1) For multiple particles, (2 to 6), arching occurs when "partial sand retainment" is used.

2) Significant force concentrations can be expected on the arch particles. Breakage of particles is a probable source of arch failure and sand production. A controlled amount of breakage can serve to clean the arch of fines and scale plugging.

More recently, Meza et al. [41] reported an experimental investigation of the flow of oil and sand in the vicinity of a horizontal well under cold production. Specifically, the experiments physically simulated the flow of oil and sand into a slot in a horizontal well liner. The parameters studied included slot width and sand properties (morphology and grain size distribution).

They [41] used three different sands: 1) reservoir sand: (Husky sand), obtained from cold production surface collection tanks in the Lloydminster area; 2) synthetic sand: Sil-1 (crystalline silica) sand; and, 3) glass (soda lime) beads. Two different glass bead sands were prepared. One, which was called Glass Beads Like Husky (GBLH), had a size distribution similar to that of the Husky sand. The other sand, called Glass Beads Less Fines (GBLF), had the same particle size distribution as the Husky sand except the diameters below 170 U.S. mesh (90 microns) were removed. Two fluids were used in the experiments: air and silicone oil. The viscosity (μ) of the oil varied between 13,300 and 12,400 mPa·s for the range of temperatures used in the experiments (23 to 28 °C). Plates with three different slot widths were used: 0.46 mm (0.018 in), 0.71 mm (0.028 in) and 1.02 mm (0.040 in). The stability of the arches formed under this condition was evaluated by changing the fluid flow rate [41].

This study [41] emphasized the importance of the slot width to equivalent sand grain diameter ratio (SW/D_i) as an important parameter in the investigation of sand production through the slots. They calculated the equivalent diameter at different percentiles and determined this ratio (SW/D_i) for each sand. They noticed, in comparing the Sil-1 and Husky sands, that the slot width to grain diameter ratio was smaller for the Sil-1 sand for all diameters except the $D_{99.9}$ diameter.

The results on the effect of the slot width on sand production, for both Sil-1 and Husky sands, showed that neither the Sil-1 sand nor the Husky sand could be produced through the 0.46 mm (0.018 in) slot at all injection pressures [41]. The lack of sand production was attributed to arching/ bridging/plugging at the entrance, and/or within the slot, as was observed in thin sections by the same authors [42], since the slot width to sand grain diameter ratio was, in general, small for both sands at that slot width size. However, sand was produced when the 0.711 mm (0.028 in) and 1.02 mm (0.040 in) slotted plates were used with both sands. They found that: 1) more sand was produced when the slot width increased; and, that 2) Husky sand appeared to arch/bridge more easily than Sil-1 sand since less Husky sand was produced. The increase in sand production with increasing slot width was explained by the decrease in stability of the arches formed over the wider slots. A large arch would require the proper alignment of more sand grains. All the Sil-1 sand was produced under gravity flow with the 1.02 mm (0.040 in) wide slot. Husky sand was able to arch for the same slot. They concluded that the slot width to average equivalent diameter ratio should not be the main criterion to use in determining the correct slot width to control sand production. One possible explanation for these results was that the higher percentiles are important in stopping the sand production because larger grains of this size can plug the slots. The Sil-1 sand had a smaller slot width to equivalent diameter ratio at all diameters except the $D_{99.9}$ diameter. It was also found that not only did the Husky sand arch/bridge more easily than the Sil-1 sand, but the structures formed were also more stable.

A test with glass beads, having the same size distribution as the Husky sand (GBLH), was prepared to investigate the effect of roundness and angularity on sand production. The results show that the roundness of the grains, given the inherent randomness of the process, did not seem to play as critical a role in the sand production behaviour as the role of the sand particle size distribution. The difference in sand production between the Husky and GBLH sands was within the standard deviation observed in this type of experiment.

The difference in sand production behaviour between the Sil-1 sand and Husky sands was thought to be mainly due to differences in grain size distribution. The hypothesis was that either the fine particles or the largest particles were responsible for the difference in sand production between the Husky and Sil-1 sands. Another glass bead sand (GBLF) with the same size distribution as the glass bead like Husky sand (GBLH), except for lower fines content, was prepared. Approximately the same quantity of sand was produced with the GBLF as with the GBLH sands in both air and liquid experiments. A greater production of GBLF sand would be expected if the fines were the key in forming arches/bridges.

The study [41] concluded that it is likely the particles with greater average diameter have a significant influence on the formation of the arches/bridges although they represent a small percentage of the total size distribution.

2.5.3 Effect of Confining Stress

Selby and Farouq Ali [61] performed sand production experiments in a cylindrical model 17.7 cm in height by 20.0 cm in diameter. A perforated tubing 1.3 cm in diameter was fitted into a hole drilled in the centre of the cell bottom. Radial flow was simulated by lining the walls of the cell with a sintered sheet to distribute the flow from two injection ports. They varied the overburden pressure, the flow rate, the sand grain size and shape, and the size and shape of the tubing perforations.

They [61] performed tests to evaluate the effect of grain size on sand production both with and without an overburden load. Ottawa sand (70 to 140 mesh) and Silica sand (40 to 70 mesh) were used in the experiments. In the case where overburden pressure was applied, no arching was observed when the sand with the smaller grain size diameter was used and unstable arches were observed for the sand with the larger grain size diameters. In the other case, without overburden pressure, both sands formed stable arches around the perforation. They reported that sand production was higher for the smaller diameter sand.

No arches were formed when glass beads were used under the same conditions used in the Ottawa sand and Silica sand experiments. Therefore, more sand was produced for the glass beads than for the angular sand [61].

Selby and Farouq Ali [61] also studied the effect of the perforation shape and size. They observed that all wells (slotted and round perforations) produced glass beads. The slotted tubing allowed more bead production than angular sand. Increasing the perforation size from 0.08 to 0.11 cm lead to a slight decrease in the amount of sand produced. Similar runs were performed with Ottawa sand of the same size. No sand production was observed when the wells with the round perforations were used whereas substantial sand was produced when the slotted well was used.

The sand arches formed very slowly at low flow rates in the tests using the slotted tubing. Arching occurred rapidly at higher flow rates when no overburden was applied. However, sand arches were formed instantaneously when tubings with round holes were used, even though the tests were conducted under moderate overburden loads [61].

Hall and Harrisberger [53] examined the load that would cause an arch to fail by sand crushing. They formed the arch with a load of 500 psi (3.4 MPa) and then they increased the load. They found that the arch formed by the rounded sand supported the total load that could be applied with the experimental apparatus (3,450 psi or 23.8 MPa). The angular sand was crushed at 1,950 psi (13.4 MPa).

In conclusion, Hall and Harrisberger [53] identified two conditions required for stability of an arch of sand: 1) Dilatancy; and, 2) Cohesiveness or some other grain restraint.

Toma et al. [40] mentioned that sand arching is directly related to the high confining stress. The failure of arches leads to massive sand inflow. For a given sand and cohesive force, the size of the arch depends on the pressure drop across it. With increasing fluid production rate, an increase in the arch radius is required to maintain the integrity of the arch. At a critical flow rate the arch will collapse. Furthermore, the maximum arch radius and critical flow rate do not depend directly on slot size.

Bratli and Risnes [55,62] stated that a comprehensive study of the stability of sand arches must include a study of the stress distribution in the sand. These stresses will depend on the stress at the boundaries, the fluid pressure and flow rate, the geometry of the arch and on the stress strain relations of the material. They also studied the effect of overburden pressure and surface tension on the stability and formation of arches.

Cleary et al. [63] reported an experimental study of the sand behaviour across casing perforations. Bottom hole production conditions with overburden stresses of 250 psi (1.7 MPa), 750 psi (5.2 MPa), 1,500 psi (10.3 MPa), 2,250 psi (15.5 MPa) and 3,000 psi (20.7 MPa) were used. The sand stabilization mechanism around the wellbore was by the formation of sand arches across the perforations.

Cleary et al. [63] observed that the structure of an arch depends on the stress distribution in a sand pack. They also observed that the shape of the sand arch depended on the direction of the principal stresses with arch size decreasing with increasing confining pressure. It was also found that arch stability increased with increasing horizontal and vertical stresses. More stable arches were formed when the horizontal stress was maximum and the vertical stress minimum. The cohesive force was shown to have an important role in arch stability when different hydrocarbon liquids were used.

Cleary et al. [63] pointed out that sand flow into the wellbore is generally associated with one or more of the following factors:

- Fluid drag associated with high oil viscosities.
- Fluid drag due to high oil velocities.
- Skin build up around the wellbore
- Rate surges
- Changing loading conditions around the wellbore due to pore pressure changes.
- The destruction of cohesive forces between the sand grains due to phase changes or changing saturations around the wellbore.

They [63] used coarse sand (20-40 mesh). The arch size decreased with increased overburden pressure. They [63] visualized cavities (the void space containing unstressed sand downstream of the arch) in all tests after the overburden was applied. The cavities were ellipsoidal with the major axis in the vertical direction. They extended over the perforation. The cavity was observed to grow in the vertical direction when the flow rate was increased.

Cleary et al. [63] stated that the mechanism that governs cavity growth is a combination of fluid effects and stress at the arch. They investigated the influence of cohesive force through the use of two different hydrocarbon liquids: mineral spirit and kerosene. The mineral spirit/water system did not exhibit as much cohesion as did the kerosene/water system. As a result, the arches did not exhibit the same level of stability as observed with the kerosene/water system.

Cleary et al. [63] pointed out that when discussing restructuring of the sand arches, the viscosity of the fluids becomes important. Mineral spirit which has a lower viscosity than kerosene has a higher initial arch restructuring flow rate.

Flow rates through the arch were increased until sand failure occurred. The arch failure was marked by a decrease in inlet and outlet pressures and a corresponding drop in sand stress. In their test with mineral spirit they observed that the stress dropped at initial arch failure at lower applied stress levels. They concluded that the stress drop at arch failure decreased as the initial stress increased [63].

Fines migration during oil flow results in an increase in the skin factor around the perforation. The pressure drop due to skin damage causes a rate surge at arch failure, which results in greater sand production. The increase in sand production results in an increase in stress drop at arch failure. The first test for each sand pack indicated a general decrease in vertical stress drop at arch failure as the initial vertical stress was increased. Likewise, a general decrease in horizontal stress drop at arch failure was observed as the initial horizontal stress was increased [63].

The authors [63] concluded that sand-free producing rates occurred through stable sand arches formed by sand stress around the perforation. The arch size was found to be a function of the confining stress level. Arch size decreased with increasing confining stress. A more stable arch occurred when the horizontal stress was maximum and the vertical stress was minimum. Arch restabilization under reloading conditions was found to occur at the upper confining stress level. Two modes of arch instability were indicated: initial arch restructuring and final arch failure. Only in highly cohesive sand packs did arches exhibit both modes of instability.

Melvan [65] and Cleary et al. [63] mentioned that the arch that forms around a perforation is oriented so that its minimum cross-sectional area faces the direction of maximum principal stress. They concluded that the orientation of the principal stress axes would govern the shape of the initial arch, which forms upon the application of the overburden load.

Melvan [65] found that arch stability increases with increasing stress. He also observed that additional tests with the same sand pack resulted in less stable arches as a result of sand movement around the perforation which implied a decrease in the cohesive force. Water injection prior to each test would increase the cohesive force enough to allow an arch to form but not enough to obtain the same cohesion force as existed during the first test. It can be concluded that the cohesive forces between sand grains, which are necessary for arch formation, are very sensitive to sand movement. It was observed that confining stress (horizontal) is more conducive to forming stable arches than vertical stress.

Miller [64] studied the flow of sand into and through well-casing perforations. The effect of sand particle size, casing perforation diameter, shape and roughness of perforation opening, sand porosity, sand confining stress, flow conditions through perforations and capillary cohesion between two fluids in a sand were examined experimentally.

Miller [64] found that heavy oil formation sand, with only one fluid present, would not arch over or plug field size perforation openings. However, increased confining stress resulted in decreased sand flow rates. The presence of a high enough confining stress was able to prevent sand flow. Capillary cohesion between two fluids in a sand, such as gas and water, gas and oil or oil and water resulted in the formation of sand arches over a perforation. The other variables investigated (i.e. sand particle size, casing perforation diameter, shape and roughness of perforation opening, sand porosity) had no or little effect on sand arching compared to the effect of capillary cohesion and confining stress.

2.5.4 Effect of Flow Rate and Other Parameters

Melvan [65] observed in his experimental work that the flow rate could be increased until sand failure occurred. The arch failure was marked by a decrease in inlet and outlet pressure with a corresponding rate surge. Flow rate surge was controlled in the experiment using a flow control valve located downstream from the perforation. He also observed that sand flow would occur with a corresponding drop in effective stress.

Hall and Harrisberger [53] investigated the effect of wettability and surface tension on the formation of arches with rounded sand. They observed that a wetting fluid like water can give cohesion to the sand and allow it to form stable arches; an opposite result was obtained when kerosene was used.

Melvan [65] observed that in addition to the application of stress, cohesive force is also needed to form an arch. He showed that sand production at arch failure disturbed the two phase saturation around the perforation enough to reduce the cohesive forces. Because of this, a new arch could not be formed upon the application of the overburden load as indicated by the drop in sand stress following a small amount of sand production. To prove the importance of cohesive forces in the formation of arches, he injected water through the perforation prior to the start of each subsequent test where mineral oil or kerosene was used as a flowing fluid. The water injection increased the cohesive force sufficiently to allow the formation of a new arch.

Durrett et al. [66] concluded from their tests on the cohesive strength of the formation that interfacial tension forces could be significant in controlling sand production. They studied: 1) the static forces holding sand in place; 2) the dynamic and static forces tending to counteract these static stabilizing forces; 3) the sand transport phenomenon.

He [66] mentioned that the presence of two fluids in the matrix helped to avoid sand production due to an increase in cohesive strength. This was shown in experiments with either a mixture of oil and water or with just one fluid. In the first case flow rates up to 7 bbl/d per perforation were reached before sand production occurred through the perforation at the downstream end of the cell. When the test was repeated with only one fluid, sand production occurred at a flow rate of 0.5 bbl/d per perforation.

These tests indicated that interfacial tension forces could be significant in controlling sand production. The findings of these tests are in agreement with field observations where an increase in the water cut leads to an increase in sand production. Due to an increase in the water saturation, there is a decrease in the cohesive strength.

Sand grains will be transported to the wellbore when the drag forces of the produced fluid exceed the body forces holding the sand in place. Stein et al. [67] considered that it is possible to produce oil or gas at high flow rates from a friable formation, with potential problems of sand production, without any sand control measures. They considered that stable arches could form around the perforation. They determined the maximum flow rate that can be achieved without sand production using sonic and density log data.

These authors [67] concluded that when the stress at the arch face exceeds the strength of the sand, particle movement would begin. The stress at the arch face is directly related to the fluid pressure gradient, which is a critical factor in maintaining formation stability. Moreover, the maximum stress that may be applied without causing a sand production problem should be proportional to the strength of the sand.

Vaziri [68] showed theoretically that sand production causes changes in permeability and formation properties, which develop around the wellbore. He concluded that the major factor responsible for fluid production under primary conditions is the increase in compressibility of the pore fluid due to gas exsolution. Large movements in the soil mass around the unsupported region resulted in an enlarged cavity surrounded by a plastic zone when the well was on production. The flow rate was shown to be the main parameter that governs the instability around the wellbore. He showed that a critical flow rate for the instability of the system might exist, leading to the development or extension of a liquid and plastic zone.

Tippie and Kohlhaas [54] described an investigation of flow rate effects on arch formation and stability. They used a semi-cylindrical cell which had a semi-cylindrical casing attached to its flat side. They performed experiments where the initial flow rate was gradually increased until sand production occurred. Their results showed that arch size increased with increasing fluid velocity at a controlled flow rate. Small arches were found to be more stable than large arches. When an arch was re-established after an increase in flow rate the new arch was larger than the previous one. A gradual increase in flow rate to a certain value during a test yielded a stable arch. Starting the test at this flow rate resulted in sand failure. They determined that flow rate is a factor determining arch size and stability and that adjusting the flow rate can have marked effects on the producing characteristics of unconsolidated sand reservoirs.

Selby and Farouq Ali [61] also investigated the effect of flow rate on sand production. In their experiments, the flow rate was varied from 2 ml/min to 13.3 ml/min with an intermediate flow rate of 8 ml/min. No overburden pressure was applied. The results were compared to the case when an overburden pressure was applied. In the absence of an overburden load, the sand formed arches regardless of the flow rate employed. The sand arched more rapidly at higher flow rates; however, the initial sand flux values were higher at higher rates. When overburden pressure was applied, arching occurred at a flow rate of 2 ml/min, but not at higher flow rates.

Meza [25] also studied the effect of the initial flow rate on sand production through horizontal well slots. In order to investigate the influence of the initial air flow rate on sand production, she performed a series of tests at different initial injection pressures (flow rates): atmospheric pressure or gravity flow; 20 psi (138 kPa), Q_A= 9.53 l/min; 40 psi (276 kPa), Q_A=13.68 l/min; and 60 psi (414 kPa), Q_A=14.09 l/min. The results shown that, within experimental error, more sand was produced at a given injection pressure if the pressure is increased directly to that pressure rather than in steps.

2.6 Stress Field Around a Slotted Liner

One issue that arises in the investigation of the flow of sand through slots is the effect of the stress field on the production of sand. The collapse of a heavy oil formation around a slotted liner by rapid depressurizing of a horizontal well was modelled numerically by Boone et al. [69]. These simulations were extended by Yuan [70] in order to calculate the stress field around a slotted liner under typical field pressure and stress conditions.

The simulator (ABAQUS) used in the calculations by Yuan assumes single-phase fluid flow with constant compressibility. The oil and gas in the porous media was assumed to flow as a single fluid with a compressibility given by:

$$c_F = S_g / p \qquad \text{2-13}$$

where c_F = compressibility of the fluid

S_g = gas saturation

p = pressure

The live oil compressibility was neglected. The simulations were run at two compressibilities, $2\text{x}10^{-8}$ Pa^{-1} and $1\text{x}10^{-7}$ Pa^{-1}, corresponding to gas saturations of approximately 1% and 5% respectively at a pressure of 500 kPa. The latter compressibility ($1\text{x}10^{-7}$ Pa^{-1}) is most likely higher than in the field since gas does not come immediately out of solution from heavy oil as is assumed in the calculations.

The simulations showed that the stress field around a typical liner is quite low under low gas saturation conditions (1%) but increases with increasing gas saturation. For example, the radial, tangential and axial effective stress distributions around a 140 mm diameter liner due to the sudden collapse of a 219 mm wellbore are shown in Figures 2-4 to 2-6. At the higher compressibility of $1\text{x}10^{-7}$ Pa^{-1} the radial, tangential and axial effective stress at the wellbore were: 1000 kPa, 284.45 kPa and 554.88 kPa respectively.

The radial distribution of the porosity around the well is shown in Figure 2-6. The porosity at the outer surface of the slotted liner was quite high (58 %). This curve shows that the porosity around a slot in a liner is higher than the formation porosity. Only at a distance of 0.3 m from the axis of the 140 mm diameter slotted liner was the porosity the same as in the field. This suggests that in experimental studies of the flow of sand into a slot using a sand pack with a slot at the bottom, the porosity of the sand pack should be higher than the formation porosity.

2.7 Summary

Few studies have been performed to assess the feasibility of using horizontal wells in the cold production process. The results reported in the literature suggest that the process could have promise under certain conditions, but they are not sufficient to draw definitive conclusions. The main challenge is to reduce operating costs while maintaining oil production rates. One way to reduce operating costs is to produce sand from horizontal wells in a controlled manner to avoid the need for sand cleanouts. The idea is to produce sand less aggressively, but still achieve enhanced oil rates. For example, relatively small amounts of sand could be produced temporarily to stimulate oil production, and then sand production could be stopped. When oil production rates decline, sand production could be initiated again. This process of starting and stopping sand production could be continued *ad infinitum.* The concept is to produce "sand on demand".

Any study of the cold production process in horizontal wells should take advantage of the experience gained up to date in vertical wells using this technique. The cold production process using vertical wells has been established as one of the principal methods for recovering heavy oil from the Western Canadian Sedimentary Basin (WCSB). It has become an alternative technology for the recovery of heavy oil since the mid to late 1980s, with the adaptation of progressive cavity pumps for heavy oil lift operations [3]. The experience obtained during the last two decades is valuable in terms of the mechanisms and main factors involved in the process.

Cold production is characterized by higher oil flow rates (up to 10 times) than the flow rates predicted by using Darcy's radial flow equation [1,4-6]. Recovery factors for cold production have also been reported to be significantly higher than what is predicted by classical flow models [7]. It is believed that two main mechanisms might explain the unexpectedly high primary oil recovery observed in these reservoirs. The first one is associated with gas evolution from the heavy oil (foamy oil) and the second one with sand production [7,31].

Laboratory studies have been conducted to determine how sand production enhances oil production in heavy oil fields under cold production. Two possible explanations have been given: formation of high permeability channels (wormholes) or compact growth of a remoulded zone (cavity formation) [11-17,44,45].

Some attempts have been made to model the cold production process numerically. However, due to the complexity of the two main mechanisms involved in the process, foamy oil flow and sand production, the tendency has been to focus on one of the mechanisms in the models proposed [33,18,19,20,21,22]. More recently, a few studies have emerged where a coupled reservoir-geomechanics model has been presented [3,23,46]. Currently, there is not a commercial simulator available that can model the cold production process completely.

Sand production is defined as the production of small or large amounts of solids together with the reservoir fluids [47]. Sand failure occurs when the stresses on the formation exceed the strength of the formation. In order for the failed zone to grow significantly the sand must be transported.

In unconsolidated formations, cohesive strength is due mainly to the cohesive forces between the immobile formation water and the oil surrounding the sand grains [4,52,54].

Traditionally, sand production in oil wells has been seen as a problem that had to be avoided because of the negative effects associated with it, such as wear and erosion of the production equipment, problems with the stability of the wellbores, casing collapse, etc. [39,47-49]. However, sanding in cold production with vertical wells is not a negative factor. A number of important positive aspects are: reduction in completion costs, improved production rates, continued improvements in productivity index through the removal of the skin effect, and elimination of expensive workovers to remove scale and other sources of near-well blockage [24]. Moreover, field observations have shown that blocking sand production causes a strong decrease in oil production in shallow unconsolidated reservoirs [5,24,30,50]. It is considered that sand production improves the efficiency of the other drive mechanisms by altering the fluid flow characteristics into the wells in heavy oil reservoirs during the cold production process. It is also thought that this might be one of the main reasons for the high production rates observed in the field in the cold production process [4].

Sand production analysis requires coupling of geomechanics (stress, strength, and liquefaction), fluid flow (hydrodynamic drag, pressure, slurry rheology) and solution gas processes (bubble formation, phase behaviour) [24].

McCormack et al. [51] and Cleary et al. [63] have classified the possible parameters that influence sand production as follows:

- *Formation properties*, such as degree of consolidation, grain size distribution, sand morphology, clay content, sand strength, overburden pressure, cohesion, stress concentration.

- *Fluid Flow*, such as fluid saturation, fluid production rates, oil gravity, temperature, flow transients and pressure, fluid drag associated with high oil viscosities, fluid drag due to high oil velocities, rate surges.

- *Formation Alteration,* such as silica dissolution, clay dissolution and reprecipitation, fines movement, the destruction of cohesive forces between the sand grains due to phase changes or changing saturations around the wellbore, skin build up around the wellbore, changing loading conditions around the wellbore due to pore pressure changes.

- *Control techniques,* such as slotted liner dimensions.

Sand arching seems a natural way to control sand production. An arch is a curved structure spanning an opening, serving to support a load by resolving external stresses into tangential and radial stresses [53]. Flow rate, sand size distribution, size of the opening, formation stresses and capillary forces are important in the formation and stability of sand arches.

Some authors believed that sand arching is directly related to a high confining stress [40]. It has been observed that the structure of an arch depends on the stress distribution in a sand pack [63]. Further, the shape of the sand arch depends on the direction of the principal stresses, with arch size decreasing with increasing confining pressure. It has also been found that arch stability increased when the stress increased. More stable arches were formed when the horizontal stress was maximum and the vertical stress was minimum [63,65]. Also, increased confining stress resulted in decreased sand flow rates. The presence of a high enough confining stress could be able to prevent sand flow [64].

Stein et al. [67] concluded that when the stress at the arch face exceeds the strength of the sand, particle movement would begin. The stress at the arch face is directly related to the fluid pressure gradient, which is a critical factor in maintaining formation stability. Moreover, the maximum stress that may be applied without causing a sand production problem should be proportional to the strength of the sand.

Durrett et al. [66] concluded from their tests on cohesive strength that interfacial tension forces could be significant in controlling sand production. He mentioned that the presence of two fluids in the matrix helped to avoid sand production due to an increase in cohesive strength.

The cohesive force has shown to have an important role in arch stability when different hydrocarbon liquids were used. Melvan [65] observed that in addition to the application of stress, cohesive force is also needed to form an arch. Capillary cohesion between two fluids in a sand, such as gas and water, gas and oil or oil and water resulted in the formation of sand arches over a perforation [64]. The other variables investigated (i.e. sand particle size, casing perforation diameter, shape and roughness of perforation opening, sand porosity) had little or no effects on sand arching compared to the effect of capillary cohesion and confining stress [64].

Hall and Harrisberger [53] investigated the effect of wettability and surface tension on the formation of arches with rounded sand. They observed that a wetting fluid like water can give cohesion to the sand and allow it to form stable arches; an opposite result was obtained when kerosene was used.

Cleary et al. [63] pointed out that when discussing restructuring of the sand arches, the viscosity of the fluids becomes important. Thus, a mineral spirit with a lower viscosity has a higher initial arch restructuring flow rate than kerosene with a higher viscosity.

Sand production is known to be rate sensitive. For low cohesion materials, fluid flow can mobilize the grains. Melvan [65] observed in his experimental work that the flow rate could be increased until sand failure occurred.

For a given sand and cohesive force, the size of the arch depends on the pressure drop across it. With increasing fluid production rate, an increase in the arch radius is required to maintain the integrity of the arch. At a critical flow rate the arch will collapse. Furthermore, the maximum arch radius and critical flow rate do not depend directly on slot size. More specifically, some researchers believed that arch stability might be rate sensitive at low confining stress but independent of flow rate at high confining stress levels [40].

Tippie et al. [54] showed that arch size increased with increasing fluid velocity at a controlled flow rate. Small arches were found to be more stable than large arches. When an arch was re-established after an increase in flow rate the new arch was larger than the previous one. A gradual increase in flow rate to a certain value during a test yielded a stable arch. Starting the test at this flow rate resulted in sand failure. They determined that flow rate is a factor determining arch size and stability and that adjusting the flow rate can have marked effects on the producing characteristics of unconsolidated sand reservoirs.

In the absence of an overburden load, the sand formed arches regardless of the flow rate employed. The sand arched more rapidly at higher flow rates; however, the initial sand flux values were higher at higher rates. When overburden pressure is applied, arching occurred at a relatively low flow rate, but not at higher flow rates [61].

The influence of the roundness and sphericity on sand production has been studied. Yim et al. [58] and Hall and Harrisberger [53] established that besides the flow rate, the arch stability is strongly dependent on the granulometry of the porous material and the size of the perforation. Larger perforations required larger grains to form stable arches [58]. However, Meza et al. [41,42] found that the roundness of the grains, given the inherent randomness of the sand production process, did not seem to play as critical a role in the sand production behaviour as the role of the sand particle size distribution when slots are used in a horizontal well. Similar results were found by Miller [64] when he studied sand production through perforations.

The slot width to equivalent sand grain diameter ratio (SW/D_i) is an important parameter in the investigation of sand production through slots. Slot width to average equivalent diameter ratio should not be the main criterion to use in determining the correct slot width to control sand production. The particles with greater average diameter have a significant influence on the formation of the arches/bridges although they represent a small percentage of the total size distribution. Therefore, the larger sand percentiles should be taken into consideration when designing the slot size to control sand production [41].

One issue that arises in the investigation of the flow of sand through slots is the effect of the stress field on the production of sand. Yuan [70] calculated the stress field around a slotted liner under typical field pressure and stress conditions. The simulations showed that the stress field around a typical liner is quite low under low gas saturation conditions (1%) but increases with increasing gas saturation. The same simulation showed that the porosity at the outer surface of the slotted liner was higher than the formation porosity (34% vs. 58%). This suggests that in experimental studies of the flow of sand into a slot using a sand pack with a slot at the bottom, the porosity of the sand pack should be higher than the formation porosity.

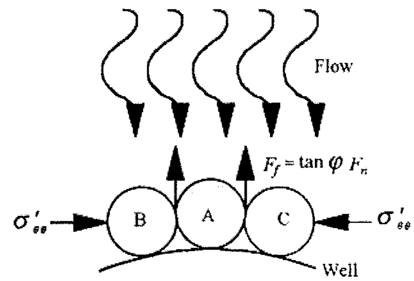

Figure 2-1: Micromechanical forces exerted on a grain lying on the borehole wall. After A. Charlez [30]

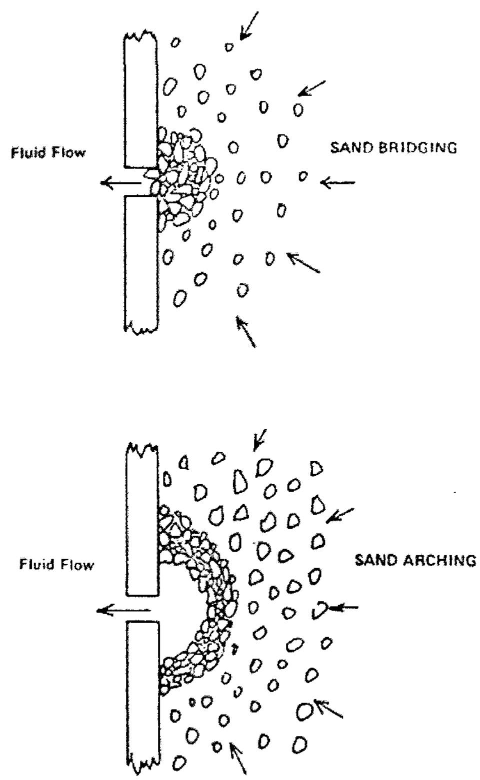

Figure 2-2: Difference between sand bridging and sand arching. After Tippie et al. [54]

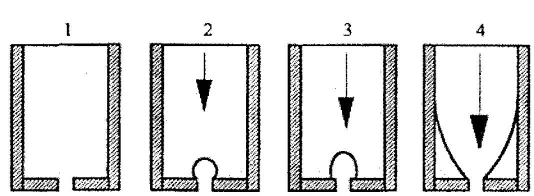

Figure 2-3: Sand arching experiment. After A. Charlez [30]

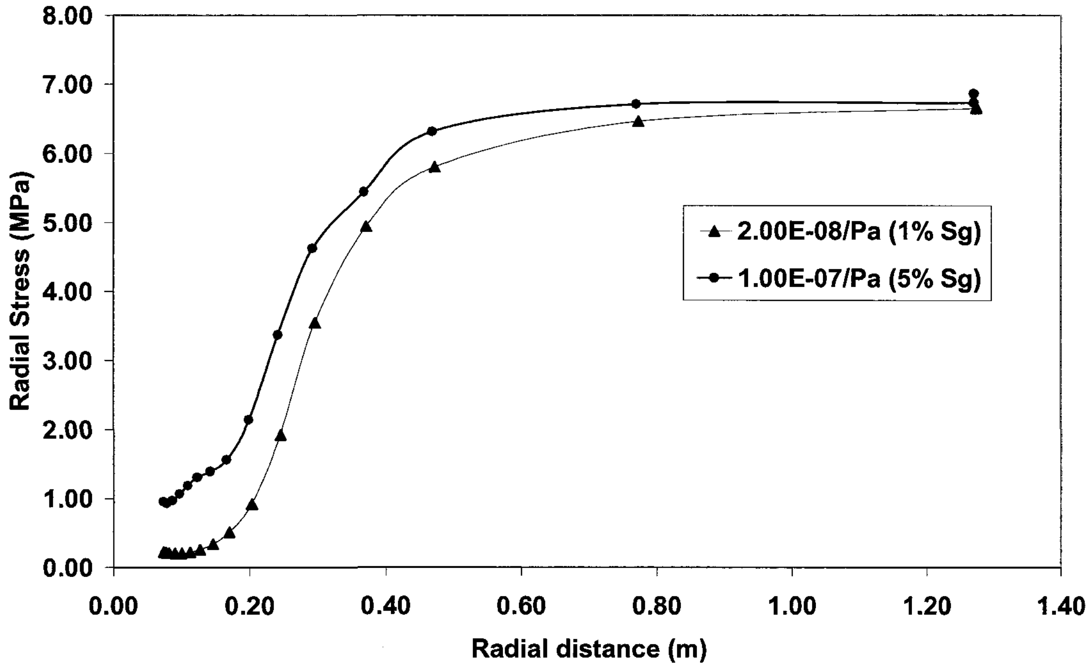

Figure 2-4: Radial stress versus distance at different compressibilities and S_g. After Yuan [70].

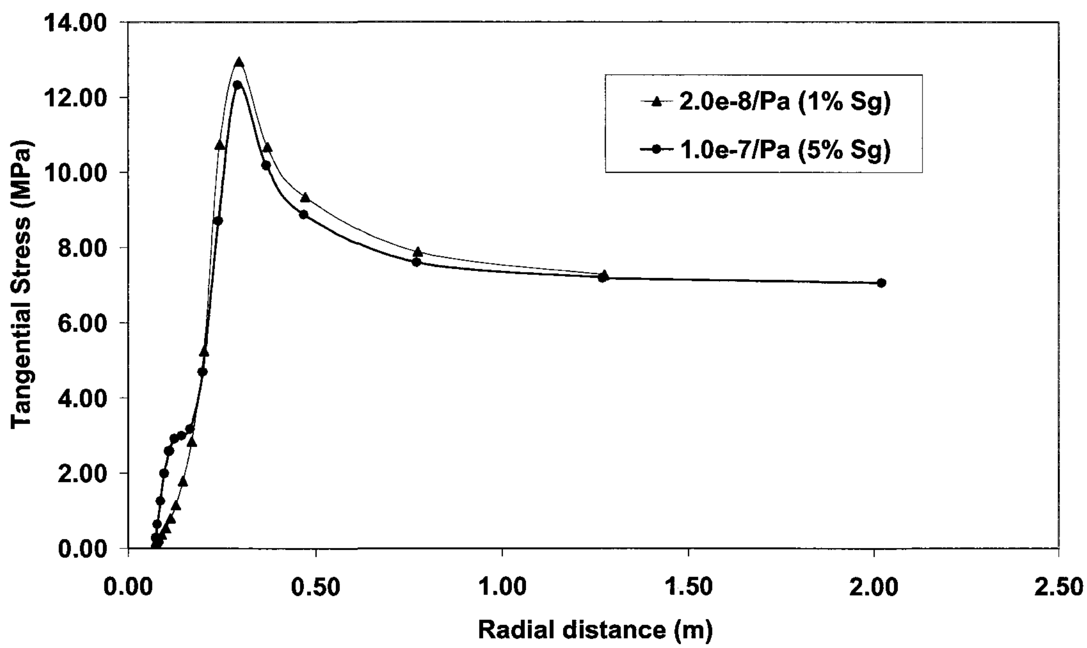

Figure 2-5: Tangential stress versus distance at different compressibilities and gas saturation. After Yuan [70].

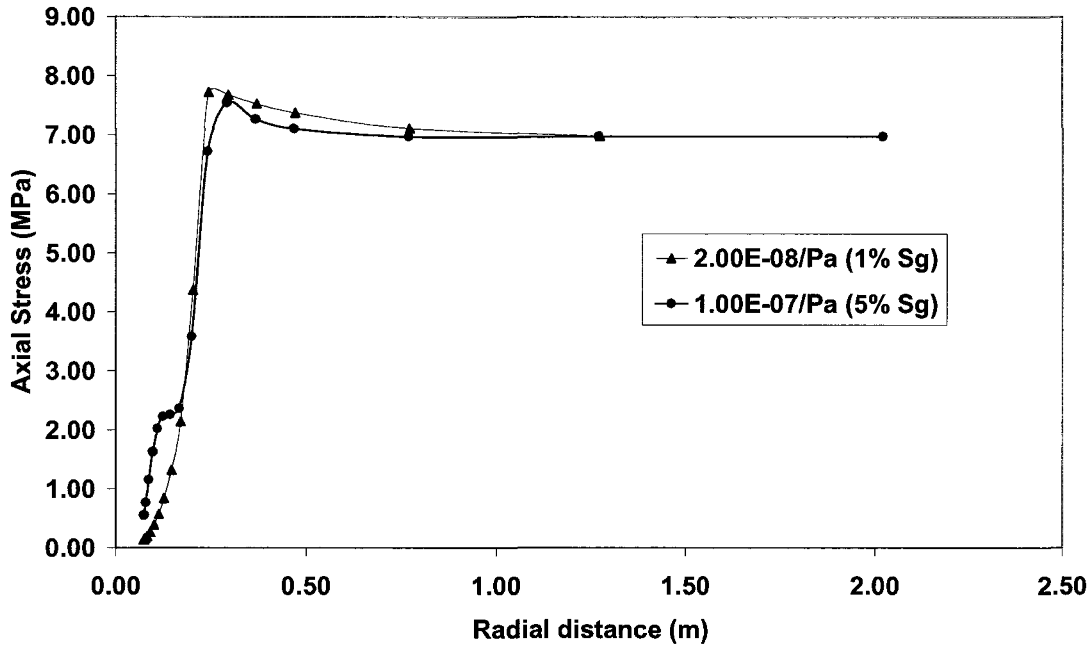

Figure 2-6: Axial stress versus distance at different compressibilities and gas saturation. After Yuan [70].

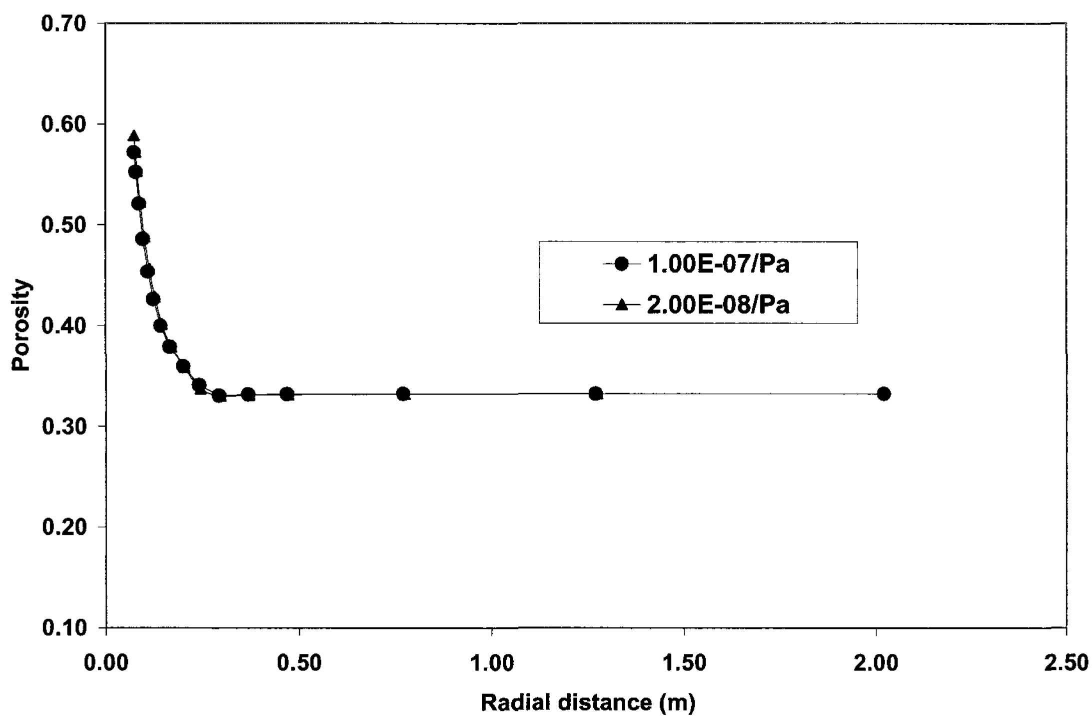

Figure 2-7: Porosity versus distance at different compressibilities. After Yuan [70]

3 Experimental Program

The flow behaviour of sand and oil in the vicinity of a slot in a horizontal well was studied under a range of experimental conditions. The physical phenomena involved in sand production are expected to occur on a relatively small scale (centimetres). These effects would occur in the vicinity of a slot during sand production, and in the vicinity of a disturbed region resulting from sand production. Consequently, mechanistic experiments exploring the behaviours involved in sand production can be performed, without a difference in scale between experimental conditions and field conditions.

The scale of the experiments needs to be large enough to capture the effects involved in sand production – so a length scale of (tens of) centimetres is clearly sufficient. The dimensions of the slot (width, length) in the experiments should be similar to the dimensions of the slot in the field. As well, the fluid flux (flow velocity) through the slot in the experiments should be matched to the fluid flux through the slot under field conditions. Since sand production behaviour is expected to be influenced by flow conditions near the slot, upstream flow conditions farther from the slot in the experiments do not have to be matched to the conditions in the field. Consequently, a linear flow regime upstream of the converging elliptical flow into the slot can be used in the experiments, even though the upstream flow regime in the field will be a combination of linear flow and converging cylindrical flow toward the horizontal well.

Field materials, or representative analogues, are required. Consequently, field produced heavy oil was selected as the principal fluid in the experiments. As a baseline for the porous medium, silica sand with a grain size distribution similar to that of unconsolidated sand formations in western Canadian heavy oil reservoirs was used; several other silica sands were also used to examine the effects of grain size distribution on sand production behaviour.

The following sections provide a description of the materials used and the experimental procedures for the various types of experiments performed in this study.

3.1 Materials Used and their Properties

3.1.1 Fluids

Four fluids were used in the laboratory experiments that were carried out for this research project: air, used in the sand production screening test; carbon dioxide (CO_2), formation water or distilled water, and produced heavy oil from a Lloydminster area reservoir (in the Dee Valley field), used to saturate the sand packs for the sand production experiments. Single-phase flow was chosen to simplify the problem. Later in the program Epoxy resin mix, EPO-THIN® resin and EPO-THIN® hardener, was used to solidify the sand packs for thin section tests.

Compressed air was supplied at 80 $\pm$ 5 psi (551.58 $\pm$ 34.47 kPa) from the ARC central plant. The Dee Valley produced oil was collected from the Husky Lashburn battery. It was dewatered and filtered. Samples collected at different times were used and are identified as Dee Valley 1 and Dee Valley 2. The viscosity and density of these heavy oils were measured over a range of temperatures (15 to 30 °C) at ARC laboratories. The accuracy of the viscosity measurements, over the range of measured viscosities, was at least 1 mPa·s. The measured oil viscosity data was fitted to the following equations:

$$\mu_1 = 25{,}680e^{-0.0945 \times T} \qquad 3\text{-}1$$

$$\mu_2 = 35{,}058e^{-0.0967 \times T} \qquad 3\text{-}2$$

where μ = viscosity (mPa·s) and T = temperature (°C).

The measured density data was fitted to the equations:

$$\rho_1 = -0.0007 \times T + 0.9819 \qquad 3\text{-}3$$

$$\rho_2 = -0.0002 \times T + 0.9848 \qquad 3\text{-}4$$

where ρ = mass density (g/cm^3). Sub indices 1 and 2 indicate Dee Valley Oil 1 and 2 respectively. The accuracy of the density measurements was 0.0001 g/cm^3.

Dead oil was used in all of the experiments. The use of dead oil has the advantage of isolating the contribution of sand production in the cold production process from the foamy oil phenomenon.

Water-wet sand packs were used in the experiments. During the first experiment, synthetic formation water with a composition typical of reservoirs under cold production (see Table 3-1) was used. In this first experiment, corrosion problems were observed in the aluminum plug that closes the slot. Consequently, it was decided to use distilled water instead of formation water in subsequent experiments.

Carbon dioxide (CO_2) was used to displace the air from the pore space within the sand pack.

3.1.2 Sands

It has been reported that the average D_{50} diameter of the sand produced by cold production in western Canada tends to be in the range of 100 to 250 μm [26]. As well, the literature on sand control identifies the uniformity of the sand as playing a key role in determining sand production behaviour [49,71]. Therefore, sands possessing a D_{50} within the range mentioned, but with different sorting, should be evaluated.

Different sands were proposed for evaluation:

1. Reservoir sand: Husky sand, obtained from cold production surface collection tanks in the Lloydminster area.

2. Synthetic sand: crystalline silica sand provided by Sil Industrial Minerals Inc.

3. Synthetic sand: Glass (soda lime) beads provided by Sil Industrial Minerals Inc.

Two sets of sands were prepared from the synthetic sands, one set with glass beads and one set with crystalline silica. The first set contained four different glass bead sands. Each of those sands possessed the same D_{50}, but their size distributions were quite different. The first sand, which will be called rounded standard, simulated the size distribution of the Husky sand. The second sand, called rounded no fine fractions, has the same particle size distribution as the Husky sand except the diameters smaller than 90 µm (170 U.S. mesh) were removed. The third sand, called rounded no large fractions, has the same particle size distribution as the Husky sand except the diameters greater than 300 µm (50 U.S. mesh) were removed. The fourth sand, called rounded well sorted, has diameters between 212 and 63 µm (70 and 230 mesh).

The second set of sands contained four different crystalline silica sands, with the same D_{50} (200 µm), but different size distributions. One of the sands is called Silica Well Sorted sand (its commercial name is Granusil 7030). It is a well-sorted sand. The other three sands were prepared using crystalline silica sand of different sizes. The second sand, identified as Silica Poorly Sorted sand, is a sand with a wide size distribution. The third sand was called Silica No Large Fractions sand. It has the same grain size distribution as the Silica Poorly Sorted sand except the diameters greater than 300 µm (50 US. mesh) were removed. The fourth sand, named Silica No Fine Fractions sand, is a sand with the same particle size distribution as the Silica Poorly Sorted sand except the diameters smaller than 90 µm (170 US mesh) were removed.

All the sands mentioned above were characterized as follows:

3.1.2.1 Grain Size Analysis

The purpose of this analysis was to determine the average grain size and particle size distribution (grain sorting) of the different sands. These two parameters have a significant influence sand production through slots, as has been pointed out in the literature [25,53,58- 61,72,].

The particle-size distribution of a sand is defined as the distribution of the percentage of the total weight of the different fractions within a given size range. Grain size is usually defined, for grains larger than 0.1 mm, as equivalent to the width of that circular or square aperture which allows the grain to just pass through [72,73].

The sands were sieved according to the ASTM Standard Test Method for Particles: ASTM # D 422-63 [74].

In this method, particles are separated into various grain-size groups or fractions. This is achieved by sieving a sample using a set of standard sieves and weighing the material retained at each sieve screen. The percentage by weight of each fraction is then calculated.

The results of this analysis can be presented either as a distribution of the weight of each fraction or as a cumulative plot of the percentage, by weight, of grains finer than the diameter denoted by the abscissa [72]. Since the grain size may vary significantly, a logarithmic scale is commonly used for the abscissa.

The slope of the sieve analysis curves indicates the sand's uniformity; the more vertical the slope; the more uniform the sand [49]. The uniformity coefficient (C_u) is representative of the uniformity of the sand [49,75]:

$$C_u = \frac{D_{60}}{D_{10}} \qquad 3\text{-}5$$

where D_{10} and D_{60}, also called effective diameters. These diameters are equal to the size of the sieve which allows a certain percentage by weight, given by the values of the subscript, to pass through.

Other percentiles that are considered important for sand production through slots are the D_{90} and D_{50} effective diameters. Also, the importance of the $D_{99.9}$ effective diameter has been discussed by Meza et al [41,42]. However, the most suitable effective diameter (or combination of diameters) to correlate with sand production is not well established for either conventional oil production or heavy oil production.

The size distribution or grain sorting is used also to classify the sands into two categories. Sand containing a wide range of grain sizes is said to be poorly sorted. A sand is well sorted when the range is narrow [76].

The uniformity coefficient (C_u) was the criteria used to define the sorting of the sands [73,75]. There is no consensus as to what the value of C_u should be to classify the sorting of the sand. Some authors reported that a sand having a uniformity coefficient smaller than 2 is considered uniform [73] while other authors [49] considered that the values of C_u for a uniform sand should be less than 3. In this project, sands with a C_u less than or equal to 2 are considered to be well sorted.

In this work, dry samples of each sand were accurately weighed and sieved through a stacked set of sieves with the sizes in US mesh indicated in Table 3-2. The equivalent metric and British unit sizes are also shown in the same table.

The particle size distribution curves of the sands used in this study are shown in Figure 3-1 and Figure 3-2 while the effective grain diameter at different percentages by weight for these sands as well as the uniformity coefficient are reported in Table 3-3.

3.1.2.2 Solids Density Measurement

The density values of the sands used (see Table 3-4) were measured based on the ASTM method designation: D1817-96 [77]. Sand densities are used in the porosity calculations as well as in the calculations of the volume of the sand produced. Details of the ASTM D1817-96 method are given in Appendix A.1.

3.1.2.3 Morphology Analysis

Since the effect of the grain shape on sand production was investigated it was necessary to determine the morphology of the sands.

The traditional morphology analysis includes the concepts of: 1) form, 2) sphericity, 3) roundness and 4) surface features [76]. Among the four factors that characterize the grain shape, the sphericity and roundness are the ones that have been cited in the literature as having an influence on sand production [53,58,61].

Sphericity is a property that states quantitatively how close the shape of an object is to that of a sphere. Wadell [76,78] introduced the following definition of sphericity:

$$\psi_w = \sqrt[3]{\frac{V_p}{V_{cs}}} \quad 3\text{-}6$$

where: V_p = volume of the particle (measured by immersion in water)

V_{cs} = volume of the circumscribed sphere (smallest sphere that will just enclose the particle).

Numerous attempts have been made to calculate sphericity based on estimating surface area. However, the most widely used method of determining sphericity is through a visual comparator. This allows a large number of grains to be classified at the same time. A comparator can be built by simply collecting a series of grains and mounting them on slides and /or photographing them. Grains to be classified are then compared with the standards. Powers [79] constructed such a comparator, shown in Figure 3-3. Powers' widely used chart presents two classes of sphericity (high sphericity and low sphericity), in combination with six classes of grain roundness.

Grain *roundness* is defined as the relative sharpness of the grain corners, or in other words, as the grain surface curvature [78]. The different roundness categories as well as the definition for each of them are presented in Table 3-5. This classification, jointly with a visual silhouette comparator, can be used for sand grain classification [78].

Scanning electron microscope (SEM) photographs of the sands used in the experiments are shown in Figure 3-4 to Figure 3-11. Figure 3-4 gives an overall picture of the Silica Well Sorted sand grains while Figure 3-5 shows two photographs of Silica Well Sorted sand single grains. The scale is given in the upper right hand corner of the photomicrograph. Comparing the photomicrograph of the sand grain with those in Powers' chart, and taking into account the sieve analysis results, the Silica Well Sorted sand was classified as well-sorted subangular sand with low sphericity.

Similarly, the Silica Poorly Sorted sand can be classified as poorly-sorted, subangular sand with low sphericity while the Husky sand was classified as a well-sorted, angular sand with low sphericity (Figures 3-6 to 3-9). An example of a well-sorted, well-rounded sand is given by the Rounded Standard Sand (Figures 3-10 and 3-11). Table 3-6 shows the classification of the other sands used in this study.

3.1.2.4 Sand Strength Experiments

Triaxial testing is the most reliable technique for obtaining the strength parameters of samples in the laboratory [80]. Knowledge of the strength parameters of the sands may help to understand the behaviour of the sands during the sand production experiments. It also allows theoretical calculations to determine critical fluid flow rates for sand production.

It is well known that the cohesive strength resulting from the interfacial tension between reservoir fluids plays an important role in the strength of unconsolidated formations [52,66,81]. Therefore, triaxial tests were performed in specimens prepared with the sands used in the sand production experiments under confining stress and saturated with produced heavy oil from the Dee Valley field and distilled de-aired water.

In a triaxial cell experiment, a cylindrical specimen of saturated sand, with cross sectional area A, is first subjected to a confining pressure σ_c, which equally stresses all surfaces of the specimen. An external axial load P is applied on the specimen cross sectional area A, and is progressively increased. The additional stress caused by P is in the axial direction only and is equal to P/A. The axial stress is increased until the specimen fails while holding the confining stress constant. Failure normally implies the condition in which the specimen can sustain no further increase in stress; i.e. the point at which it offers its maximum resistance to deformation in terms of the axial stress. Since there are no shearing stresses on the sides of the cylindrical specimen, the axial stress σ_c + P/A and the confining stress σ_c are the major and minor principal stresses, σ_1 and σ_3 respectively. Consequently, the incremental axial stress, P/A, is equal to the deviatoric stress [73,82,83]. Thus:

$$\frac{P}{A} = \sigma_1 - \sigma_3 \qquad 3\text{-}7$$

Deviatoric stress can be plotted against strain. The strength of the sand is usually determined by the stress at failure that is the peak deviatoric stress on the stress-strain plot. The major principal stress at failure is calculated from the peak deviatoric stress by using Equation 3-7, which enables the Mohr circle of stress representing failure under a particular confining pressure σ_3 to be drawn [82].

A set of Mohr circles representing failures can be constructed by measuring the peak deviatoric stress for samples of the same sand under different confining stresses. The failure envelope tangential to these circles is approximately a straight line over a range of stresses (Figure 3-13 (a)); consequently the equation of the failure envelope can be expressed in the form of Coulomb's law:

$$\tau_f = c_u + \sigma \tan \varphi \qquad 3\text{-}8$$

where τ_f = shear stress at failure
c_u = cohesion
σ = peak deviatoric stress
φ = friction angle
τ_f and σ are total stresses

Equation 3-8 represents the most widely used failure criterion for unconsolidated sands [82].

The shearing resistance is composed of two components [82]:

1. A friction force between sand grains ($\sigma \tan\varphi$), due to interlocking and friction between sand grains when sheared under a normal stress.

2. A cohesion force (denoted by c_u), which is due to the internal forces holding sand grains together in a solid mass.

When using saturated sands, pore pressure must be taken into account. Therefore effective stresses as defined by Equation 3-9 must be used instead of total stresses:

$$\sigma' = \sigma - p \qquad 3\text{-}9$$

where σ' = the effective stress
σ = the total stress
p = the pore pressure

The Coulomb equation as modified by Terzaghi is then used to represent the failure envelope [83]:

$$\tau_f' = c_u' + \sigma' \tan\varphi' \qquad 3\text{-}10$$

where σ' is the effective stress defined by Equation 3-9, τ'_f is the effective shear stress at failure, φ' is the angle of shearing resistance which measures internal friction between the sand grains, and c_u' is the corresponding cohesion (see Figure 3-13 (a)). Equation 3-10 is in accordance with the fundamental principle that changes in shearing resistance are due only to changes in the effective stress.

It is evident from equation 3-10 that the cohesion c_u' represents the shear strength of the sand in the limit as the effective normal stress becomes vanishingly small. It is obtained by extrapolating the Mohr-Coulomb failure envelope linearly to an effective normal stress of zero. An unconsolidated sand saturated with a single fluid phase normally does not possess any cohesive strength; it is referred to as cohesionless [73]. However, when the same sand is saturated by two fluid phases it acquires some cohesive strength on account of capillary forces between the two phases (see section 2.5.4). This cohesive strength is often referred to as an apparent cohesion [73,82]. Similarly, the tensile strength of an unconsolidated sand saturated with only one fluid phase will be zero, but when that sand is saturated by two fluid phases it acquires a small tensile strength.

Figure 3-13 (b) represents an alternative way to show the results of a series of triaxial tests. The plot is called a *p-q* graph and the points shown correspond to the peak points of the deviatoric stress/axial strain curves. The curve drawn through this point is also called the K_f-line. The relationship between q_f and p_f to the Mohr-Coulomb envelope is also shown [73].

Triaxial tests were performed to determine the friction angle and cohesion of the sands used in the testing program. The procedure described by Head [82,83] was followed. The DIN 18137-2 Deutsche norm was also used as a reference [84]. The applied normal stress on the prepared specimens in the triaxial tests covered the lower range of effective confining stress estimated within the sand production experiments; that is, 550 kPa, 345 kPa, and 140 kPa. A description of the apparatus and the experimental procedure used in the triaxial cell experiments is presented in the following section.

3.2 Description of the Apparatus and Experimental Procedure

All the tests carried out in this research were performed at room temperature.

3.2.1 <u>Screening Experiments With Air Without Confining Stress</u>

The air tests were performed in order to rapidly assess the influence of the particle size distribution, morphology of the sand grains and slot size on sand production through slots. Previous results reported by Meza [25] were combined with the new tests to gain a broader view of the effect of the parameters mentioned above. These measurements were helpful in selecting the slot size for the tests examining sand production under confining stress.

The tests were performed with the equipment formerly set up by Meza [25]. A schematic diagram of the apparatus is shown in Figure 3-12. The slot in the end plate is 7.57 cm in length (see Figure 3-14). Plates with five different slot widths were used: 0.018 in (0.46

mm), 0.022 in (0.56 mm), 0.028 in (0.71 mm), 0.032 in (0.81 mm) and 0.040 in (1.02 mm). These slot sizes are within the range of those machined in slotted liners for horizontal wells in western Canada.

The tests were carried out at atmospheric pressure; sand was allowed to be produced by gravity flow. Eleven sands were evaluated: Husky reservoir sand, Rounded Standard (size distribution like the Husky sand), Rounded Well Sorted, Rounded No Large Fractions, Rounded No Fine Fractions, Silica Well Sorted sand 1, Silica Well Sorted sand 2, Silica Poorly Sorted D_{50} 200 μm, Silica Poorly Sorted D_{50} 100 μm, Silica No Large Fractions, and Silica No Fine Fractions. The experimental procedure for these tests has been previously established and described in great detail by Meza [25].

3.2.2 Sand Strength Experiments

Figure 3-15 shows the essential features of a triaxial cell. The cell used in these experiments is a standard low pressure triaxial cell where a cylindrical specimen of saturated sand, with cross-sectional area A, can be tested as explained in section 3.1.2.4. The sand packs prepared for the strength tests were typically 13.8 $\pm$ 0.5 cm in length and had a radius of 3.56 + 0.06 cm (see Table 3-7). A data acquisition system was used to record the cell pressure (confining pressure), volume change, back pressures (top and bottom of the sand pack), vertical load, and piston displacement measurements.

The experimental procedure to prepare the sand packs and test their strength consisted of the following steps:

1. A PVC split mould mounted directly on the base of the triaxial cell and lined with a rubber membrane was used during the specimen preparation.

2. A sintered porous disk was placed at the bottom, on top of the cell base. The height of this hollow set up was measured for porosity calculations.

3. The set up was tamped and vibrated while pluviating the sand into the lined mould. The mass of the sand used and the final height of the core were recorded.

4. A second sintered porous disk was placed on top of the sand followed by the end cap. The rubber membrane was stretched around it and fixed with a pair of rubber O-rings. The lines for pressure drop measurements were connected at this point.

5. A vacuum was connected to the top line to evacuate the air from the sand pack. The vacuum also helped to keep the core stable while the split mould was removed.

6. The cell was put together, closed, filled with water and pressurized. A confining pressure of 20 psi was applied to the core.

7. The core was then saturated with de-aired water. The vacuum pump was kept working during this time to ensure that the pack was 100% saturated with water.

8. Transducers, thermocouples and the volume change and displacement devices were attached to the cell to monitor the test. The data acquisition system was also started.

9. The effective confining pressure was cycled up and down three times to consolidate the sand pack. To accomplish consolidation, the cell pressure was increased and decreased in steps while the pore pressure was kept constant. A minimum effective confining pressure of 20 kPa and a maximum effective confining pressure of 520 kPa were applied during each cycle.

10. The sample was flooded with dead Dee Valley heavy oil until a residual water saturation was achieved. The flow rate and pressure gradient were measured during the oil saturation. The effective permeability to oil for the pack at the residual water saturation was also calculated.

11. Confining pressure and back pressure were adjusted to obtain the desired effective confining stress for the specimen. Normally a minimum of three specimens were required to obtain the strength parameters of the sand. In this experimental project the effective confining stress ranges were between 36 and 420 kPa.

12. The compression test was started by applying a vertical load at a constant displacement rate through the piston. The test continued until the peak strength of the sand was passed and the residual strength value was reached.

3.2.3 Sand Production Experiments under Confining Stress

Experiments were conducted to study sand flow through a slot under a confining stress field and at pressure gradients comparable to those at the surface of slotted liners in a horizontal well. The influence on sand production of particle size distribution, slot width, confining pressure and pressure gradient was investigated.

A schematic diagram of the equipment used in the experiments is shown in Figure 3-16. The physical model, a triaxial cell with a slotted bottom plate, consists of a stainless steel cylindrical wall, 32.3 cm in length, 19.5 cm in diameter (ID), top and bottom flanges, and a piston and/or a diffuser. The capacity of the cell is 9.6 litres and is rated for pressures up to 1,100 psi (7,584 kPa) at temperatures between -29 and 200 °C.

A circular slotted stainless steel plate, 11.37 cm in diameter, 0.996 cm in thickness is inserted at the bottom of the cell. Figure 3-14 shows examples of the slotted plates used in the experiments. The pressure ports machined on the plate are identified in the figure with the numbers 8, 9, 10 and 11.

The apparatus has been designed so that confining (radial) and vertical (axial) stress can be applied to the sand pack. The sand pack is separated from the walls of the cell by a rubber membrane through which confining pressure is applied. A second rubber membrane separates the top flange from the sand pack and it is used to apply the vertical stress.

A displacement transducer (LVDT = Linear Variable Differential Transformer) was installed to measure the axial deformation of the pack. A positive displacement pump was attached to the cell to maintain a constant confining pressure and to record the volume changes during the consolidation and sand production tests. Both devices were connected to the cell and to the data acquisition system.

Absolute and differential pressure transmitters were used to monitor the pressure drop inside the sand pack. The locations of the pressure ports are shown in Figure 3-16 and Figure 3-17. Thermocouples are used to monitor the temperature of the triaxial cell body and the room temperature. A container placed on an electronic balance was used to collect produced sand and measure the sand production rate. A photograph of the equipment is presented in Figure 3-18.

In order to monitor the effective stress changes in the sand pack due to sand production, two total stressmeters were designed. They were stainless steel devices composed of a diaphragm disc welded to a 1/8" tubing (see Figure 3-19). The tubing was attached to an absolute pressure transmitter. The devices were evacuated and filled with de-aired water and then calibrated.

The total stressmeters were located 8.3 cm above the slots. One of the total stressmeters was designed to measure the total vertical stress while the second one was designed to measure the total radial stress. An absolute pressure transmitter located at the same height measures the pore pressure. The effective vertical and radial stress is then obtained.

The experimental procedure consisted of the following steps:

1. The slotted bottom plate was cleaned with an air jet and then closed with a plug. The plate was inserted at the bottom of the cell.

2. The walls of the cell were lined with the rubber membrane and placed on the base of the cell. A vacuum was applied to evacuate the air between the walls of the cell and the membrane. A vacuum was maintained during the packing procedure.

3. The total sand to be packed was divided into approximately 5 portions, which were poured into the vessel in turn. Manual vibration was applied between each portion to obtain the required sand density.

4. The porosity was calculated knowing the dimensions of the cell, the height of the pack and the total mass of sand used in the packing. A sample calculation is presented in Appendix A.2. The porosity values for each sand pack used are shown in Table 3-8.

5. The diffuser with the rubber membrane was placed at the top of the sand pack. The cell was covered with the upper flange.

6. The pack was isotropically consolidated. This procedure consisted of an increase in the confining pressure in steps until a maximum of 6,895 kPa (1,000 psi) is reached. Then the pressure was decreased to the working pressure. During the process the change in volume of the confining fluid was recorded. The cycle was usually repeated three times. The consolidation process was stopped when the increase in volume change between consecutives cycles became small. During the last cycle, the pressure was decreased to the working pressure. A new porosity value was obtained after the procedure is applied to the pack (see Appendix A.3). The confining pressure was kept constant at the value desired for the test.

7. The sand pack was then evacuated and flooded with carbon dioxide (CO_2) to displace the air from the pore space.

8. Subsequently the sand pack was flooded with at least two pore volumes (PV) of distilled de-aired water to wet the sand grains and to allow trapped CO_2 bubbles to dissolve into the water. The flow rate was set so that the injection pressure did not exceed the confining pressure. A positive displacement pump was used to inject the water into the pack.

9. A compressibility test was performed (see Appendix A.4) to verify that the gas saturation was as small as possible. If the gas saturation was greater than 1% water injection continued. Also, the pack was subjected to pressurization and depressurization cycles to try to promote gas dissolution and exsolution in the water, and stimulate migration of the gas out of the pack.

10. After water saturation, the pressure transducers were connected to the cell and the data acquisition system was activated. Pressure was then recorded along the cell after this time.

11. Next, the pack was flooded with oil until a residual (connate) water saturation was reached. A positive displacement pump with dual cylinders was used to displace the oil from an accumulator into the cell. Pressure was recorded along the cell during the oil flooding.

12. The effective permeability to oil for the pack at the residual water saturation was calculated (see Table 3-8).

13. The test was initiated by removing the plug from the slot(s).The pumps were run at the desired flow rate.

14. The slurry produced out of the slot(s) was collected in the containers placed on a balance. The slurry weight and pressure along the cell was recorded in real time by using the data acquisition system.

15. A video camera recorded the produced sand and oil during the experiment.

Once the test was finished the cell was opened up and the sand pack was carefully excavated to observe the physical changes undergone by the sand pack due to sand production. In all the tests performed in this research project the excavation process uncovered the formation of a channel. After this process, the channel was usually filled with epoxy resin to make a wormhole cast. Samples of the pack were taken from different sections of it, including from inside the channel. Then, Dean-Stark analysis was performed to determine the porosity and fluid saturations of the samples. The Dean-Stark analysis used is a modified soxhlet extraction method using toluene. The modified method is an in-house ARC method.

3.2.4 Visualization Experiments using CT Scanning

Computed tomography (CT) is a procedure by which a series of X-ray slices of a sample, scanned at different angles of rotation, are assembled to obtain a cross-sectional image. As an X-ray beam passes through a sample, it is attenuated proportionally to the density of the different structures found in the sample. Each cross-sectional image is subdivided into pixels. The average attenuation in each pixel can be converted to a porosity provided baseline scans of the different phases are taken before the tests.

The CT scanner used in this project is a Toshiba 64 Slice Helical Medical Scanner (see Figure 3-22). It collects 32 mm of data (0.5 mm slices) with one 0.5 second gantry revolution. The source and detector are housed within the gantry which rotates around the object/experiment as it passes through on a patient couch. X-rays are generated during the rotation creating a spiral or helical data collection. The data collected was reconstructed as axial, coronal and 3D images to study internal structure and changes within the experiment. The scans were run at 120 kV and 150 mAs with the small field of view resulting in a resolution of 0.47 mm [85].

In order to investigate the alterations in the sand matrix provoked by sand production due to changes in flow rate, two kinds of CT scanner experiments were performed. The first type of experiment was similar in design to the set of sand production experiments under confining stress described in section 3.2.3. These experiments were complementary to the sand production experiments under confining stress. The intent in the CT experiments was to scan the sand pack periodically during the course of the experiment to track changes that occurred.

These tests were conducted in a cylindrical PVC cell for which a schematic diagram is shown in Figure 3-20. This cell was designed and fabricated at the Alberta Research Council (ARC). Its maximum operating pressure is 1,930 kPa (280 psi) at 23°C. A picture of the cell components is shown in Figure 3-21.

The physical model was designed so that confining pressure could be applied. Within the limitations of the materials and fabrication procedure used, the ratio of slot length to cell diameter was kept as close as possible to the one for the cell used in the sand production experiments under confining stress. The tests were performed using water-wet sand and produced heavy oil from Dee Valley. Produced sand was monitored as in the sand production experiments under confining stress. As a result of restrictions imposed by the use of the CT scanner, pressure was monitored at just two locations, the inlet and the bottom of the cell. Only two tests were performed due to the high cost of this type of experiment.

The second type of experiment involved scanning of the epoxied sand cores obtained from the visualization experiments intended to generate thin sections (see section 3.2.5). The idea was to scan the epoxied cores before they were cut into thin sections. If the thin sections could have been obtained, the observations from the CT images could have been combined with the information from the thin sections to allow a better understanding of pore scale behaviour as sand is produced through slots.

3.2.4.1 Sand Production Under Confining Stress

The packing and saturation procedure used in the tests was similar to the one described in section 3.2.3. Two sands were evaluated: Husky and Silica No Large Fractions sand. The physical properties of the sand packs and the experimental conditions for the tests are presented in Table 3-9.

The experimental set up was modified for the second experiment after artifacts were observed during the first test. A hinge mechanism that allows the cell to be placed in a horizontal position during the scanning was added to the portable frame.

The CT scanning procedure was as follows:

1) After taking out the plug from the slot, the vessel was placed in a horizontal position for the baseline scan. Following the scanning of the sand pack, the cell was put back into the vertical position to initiate the test.

2) Oil injection began after the baseline scan was taken.

3) CT scans with the sand pack in a horizontal position were taken every 30 to 60 min depending on sand production behaviour.

4) The test was finished when the channel tip reached the top of the sand pack or when the channel had grown approximately two-thirds along the length of the pack length.

3.2.4.2 Epoxied Cores

The preparation procedure for these samples will be explained in section 3.2.5. The idea was to scan the epoxied cores before they were cut into thin sections. If the thin sections could have been obtained, the observations from the CT images could have been combined with the information from the thin sections to allow a better understanding of pore scale behaviour as sand is produced through slots.

The X-ray source was set at 120 kV, 150 mA, with a 0.9 mm $\times$ 0.8 mm focal spot size and a 240 mm field of view. The CT slices were reconstructed from scans of 0.5 mm thickness (or height) along the length of the entire epoxied core with 0.5 seconds rotation collecting 32 mm of data. Each scan was reconstructed into 20 mm thick coronal or axial views.

3.2.5 Visualization Experiments Using Thin Sections

Experiments were performed to visually investigate the structures that might form in and around a slot when sand production stops. To accomplish this, sand grains within the sand pack were immobilized after sand production. This required an experimental apparatus that is different than the one used in the previous set of experiments. It was not possible to apply a confining stress in these experiments. Otherwise the experimental conditions were similar to the previous sets of experiments.

The immobilization of the sand packs was achieved using a mixture of the EPO-THIN® resin and EPO-THIN® hardener. The tests were conducted in a split cylindrical aluminum cell 7.0 cm in diameter × 36.4 cm in length. The cell was equipped with two aluminum leads, one of which had a circular incision where a PVC slotted plate could be fixed. The slotted plates had variable width and a fixed length of 4.7 cm. The interior surface of the cell was lined with a rubber membrane to prevent the epoxy from sticking to the walls of the cell. The cell was designed and fabricated at the Alberta Research Council; with a working pressure of up to 860 kPa (125 psi) at a maximum temperature of 37.8 °C (100 °F). The cell was mounted on a portable frame, so that it could be rotated between a vertical position and a horizontal position. The experimental set up for these experiments is shown in Figure 3-23 and Figure 3-24.

Three experiments were planned using different sands: Silica Well Sorted, Silica Poorly Sorted, and Husky Sand. The slot sizes were selected after reviewing the results of the slot size and sand size distribution experiments (see Table 3-10).

The experimental procedure was as follows:

1. The split cell was put together by tightening the body bolts.
2. The rubber membrane that isolates the sand pack from the walls of the cell was placed into the cell. This includes stretching the membrane around the top and bottom of the cylinder.
3. The slotted plate was cleaned with an air jet and was inserted into the plate in the circular incision of the bottom lid. The slot was closed with the plug provided.
4. The lid was then bolted onto the bottom of the cell.
5. A vacuum was applied between the inner surface of the cell and the rubber liner to evacuate the air between the walls of the cell and the membrane. A vacuum was kept until the saturation procedure was completed.
6. The set up was tamped and vibrated while pluviating the sand into the lined mould.

7. The height and weight of the sand within the cell were recorded in order to calculate the porosity of the sand pack. Sufficient space was left at the top of the pack to pour in epoxy as described later.

8. Next, the cell was covered with the upper lid.

9. The sand pack was evacuated and then flushed with carbon dioxide (CO_2) to displace the air from the pore space. Evacuation occurred from the top of the cell. CO_2 was injected from bottom to top. The evacuation/flush procedure was repeated three times ending with the evacuation of the sand pack.

10. Subsequently, the pack was flooded with at least three pore volumes (PV) of fresh de-aired water. A vacuum was applied during the first pore volume of water saturation. After the third PV of water had been injected, the pressure transducers were connected to the cell pressure ports. Previously, the tubings that connected the transducers with the cell pressure ports were flushed and filled with fresh water.

11. Afterwards, the pack was flooded with oil until a residual (connate) water saturation was reached. A differential pressure transducer was connected to the injection port and the production end during the oil flooding.

12. To start a test, oil injection was initiated at the desired flow rate/pressure gradient.

13. The slotted plate was unplugged.

14. Produced slurry and fluids were collected and recorded. The experiments were performed at room temperature.

15. The test was finished when sand production stopped or when communication had been established between the top and the bottom of the sand pack.

16. The cell was opened at this point. The excess oil on top of the sand pack was drained. The epoxy resin was poured on top of the sand pack. Then the cell was closed by bolting the upper end cap into the cell again.

17. Air was injected to push the epoxy through the sand pack. The pressure injection was controlled so as not to exceed 414 kPa (60 psi) at room temperature since the arches

could be disturbed and the experiment might have been damaged. Air injection stopped when only sand-free epoxy resin was produced from the slot.

18. The PVC slotted plate was then plugged to prevent air from entering the slot.

19. A resin cure time of 24 h was allowed before opening the split cell and removing the epoxied core.

The idea was that the epoxied sand cores were to be sliced and thin sections were to be mounted on slides. Then it was expected to view the thin sections under a microscope to detect sand structures that might have formed in and/or around the slot. It was also planned to obtain thin sections from the central part of the core to observe if channels were formed through the core as a result of sand production. However, as will be explained in section 4.4.2, it was not possible to find a geotechnical laboratory that could properly handle this type of core.

3.3 Experimental Conditions and Parameter Selection

3.3.1 Slot Size Selection

Analysis of previous sand production data from air tests [41,42] yielded no correlation between sand production and the uniformity coefficient, the grain sand morphology and/or the sorting of the sand (Figure 3-25 and Figure 3-26). A better correlation was found between sand production and the ratio of slot width to effective diameter (SW)/$D_{99.9}$ as is shown in Figure 3-27. The results indicated that more sand can be produced as the SW/$D_{99.9}$ ratio increases.

Based on these results, the ratio SW/$D_{99.9}$ was chosen as a criterion for the selection of the slot widths to be used in this study. Table 3-11 shows the values of SW/$D_{99.9}$ for the sands indicated in column one. Sand production is also shown in the same table. The amount of sand produced in each test was used to classify the sand production into three categories as shown in the last column of Table 3-11: very limited, controlled, and massive sand production.

Taking an average of the $SW/D_{99.9}$ ratios reported in each distinct sand production classification, the following correlations were obtained:

$$SW_{min}=1.38*D_{99.9} \qquad 3\text{-}11$$

$$SW_{max}=2.24*D_{99.9} \qquad 3\text{-}12$$

$$SW_{min} \leq SW_{csp} \leq SW_{max} \qquad 3\text{-}13$$

where: SW_{min} is the probable minimum slot size to initiate sand production (below this slot size no sand production is expected to occur); SW_{max} is the probable maximum slot size for controlled sand production (at or above this size massive sand production is expected to occur); and, SW_{csp} is the slot size interval where controlled sand production might be possible. The end values of this interval are defined by SW_{min} and SW_{max} as indicated in expression 3-13.

The Silica Well Sorted sand and the Silica Poorly Sorted sand were the sands chosen to study the effect of slot size on sand production. Initially, three slot sizes were proposed for evaluation. The three slot sizes were selected based on the correlations 3-11 and 3-12. One of the slot sizes represented the probable minimum size and the other the probable maximum size for sand production. One intermediate size was selected in the middle of the other two. However, after performing and analyzing the first tests, modifications were made to the experimental matrix. Two more slot sizes were added, one for each sand (shown in bold in Table 3-12).

To study the influence of particle size distribution on the sand production behaviour a common slot size for the four sands evaluated was chosen. This slot size was 0.056 in/1.422 mm.

3.3.2 Scaling Flow Velocity at the Slot(s) to Field Conditions

The flow velocity through the slot in the experiments was matched to the flow velocity at a slot under typical field conditions. For this purpose, the following representative field conditions were used:

- Heavy oil viscosity: 2,500 mPa·s
- Oil production rate: 100 m^3/day
- Length of the horizontal section of the well (L_w): 1,000 m
- Outer Diameter of the pipe (D_w): 5.5 in. (13.97 cm)
- Open area of the slots (A_s): variable between 1.0 to 3.0% of the pipe surface
- Dimensions of the slot: variable width (W_s) and 7.62 cm length (L_s).

To estimate the flow velocity at a single slot in a horizontal well from the production rate, Equation 3-14 was used:

$$\frac{Q_{slot}}{S_s} = \frac{Q_{well}}{S_T} \qquad \text{3-14}$$

where:
Q_{slot} = the volumetric flow through a slot
Q_{well} = the volumetric flow rate into the well
S_s = the surface area of a single slot
S_T = the total surface area of the slots (open area)

The surface area of a single slot is:

$$S_s = W_s L_s \qquad \text{3-15}$$

The total surface area of all the slots is:

$$S_T = A_s \pi D_w L_w \qquad \text{3-16}$$

Applying Equations 3-14 and 3-16 with representative field values and several values for the open area A_s within the interval identified above yielded slot fluxes (Q_{slot}/S_s) of 31.65 cm/h, 47.47 cm/h and 94.94 cm/h. The flow rates for the experiments were varied depending on the slot width in order to maintain these values of the slot fluxes (see Table 3-13).

3.3.3 Analytical Methods Employed to Determine the Permeability and Porosity of the Sand Pack Before and After Sand Production

The absolute permeability to water was determined for each of the sands used in this study. A schematic diagram of the absolute permeability apparatus is presented in Figure 3-28. The absolute permeabilities were obtained by flowing distilled water at various flow rates into a sand pack prepared with the sands. The pressure drop along the sand pack was recorded for each constant flow rate and Darcy's linear flow equation was then used to calculate the absolute permeability as follows:

$$k = -\frac{Q_w \mu}{A_c dp / dL} \qquad \text{3-17}$$

where:

$Q_w =$ the volumetric flow rate of distilled water

$dL =$ length of the sand pack

$A_c =$ the cross-sectional area perpendicular to the flow, i.e. cross-sectional area of the sand pack holder

$dp =$ the pressure drop across the sand pack length dL

$\mu =$ the viscosity of the flowing fluid (in this case, distilled water)

The effective permeability to oil, k_o, at residual (connate) water saturation was calculated by flowing heavy oil at a constant flow rate into the sand pack. The pressure drop along a section of the sand pack was recorded and Darcy's linear flow equation was then used to calculate the effective permeability as follows:

$$k_o = -\frac{Q_o \mu_o}{A_c dp / dL} \qquad \text{3-18}$$

where:

$Q_o =$ the volumetric flow rate of oil

$\mu_o =$ the viscosity of the flowing fluid (in this case, Dee Valley heavy oil)

In order to determine the permeability and porosity variations due to sand production, the porosity and permeability in the sand pack after sand production takes place must be estimated and then compared with the corresponding initial values. The initial effective permeability of the pack to oil as calculated from Equation 3-18 was assumed to be constant along the pack.

The permeability around the slot can be estimated by assuming that the flow regime is elliptical in the vicinity of the slot [86]:

$$k_{os} = \frac{Q_0 \mu}{8\pi L(p_{10} - p_9)} [\ln(L_{hs} + \sqrt{L_{hs}^2 + r_{10}^2}) - \ln(-L_{hs} + \sqrt{L_{hs}^2 + r_{10}^2}) - \ln(L_{hs} + \sqrt{L_{hs}^2 + r_9^2}) + \ln(-L_{hs} + \sqrt{L_{hs}^2 + r_9^2})] \qquad 3\text{-}19$$

where L_{hs} is the half-length of the slot, r_9 is the distance from port 9 to the center of the slot, and r_{10} is the distance from port 10 to the centre of the slot (see Figure 3-14).

The applicability of the elliptical flow equation was tested in a series of sand pack flooding experiments in which a screen was welded above a single 0.711 mm (0.028 in) wide slot to prevent sand production. Three different sands were used to prepare the sand packs for these flooding experiments: a crystalline silica sand with fines (Sil-1 dry), a crystalline silica sand with fewer fines (Sil-1 wet), and a coarser glass beads sand without any fines (BT-3). The permeability in the body of the sand pack was calculated from Equation 3-18; the permeability near the slot (between the pressure ports 10 and 9) was calculated from Equation 3-19. The results are shown in Table 3-15. This table demonstrates that the permeability around the slot (k_{os}) was almost the same as the permeability within the cylindrical section of the sand pack for both the Sil-1 wet sand (2.8% difference) and the BT-3 sand (≅ 0.5% difference). Only for the Sil-1 dry sand was the permeability around the slot significantly higher than the permeability at the cylindrical section (by approximately 58%). This higher permeability may be the result of unexpected fines production out of the slot for this case. Fines production was not observed for the other two sands. These experiments provided strong evidence that the elliptical flow equation can be used to calculate the permeability around the slot.

The porosity increase in the sand pack during the sand production experiments can be estimated from the permeability increase using the Carman-Kozeny equation. For this purpose, it is convenient to express the equation in the following rearranged form (equation 3-21):

$$k = \frac{1}{c} \frac{\phi^3}{(1 - \phi)^2} \quad 3\text{-}20$$

$$\phi^3 - ck\phi^2 + 2ck\phi - ck = 0 \quad 3\text{-}21$$

where c = the "Kozeny constant", which depends on the inverse square of the average particle diameter [87], and ϕ and k are the porosity and permeability of the pack respectively. The constant c can be calculated by using the initial values of the permeability and average porosity in Equation 3-21. Once the constant c is calculated, the average porosity in the body of the cell or around the slot, between ports 10 and 9, during an experiment (after sand production has stopped) can be calculated by using Equation 3-21. Values of c for each test, shown in Table 3-16, followed the expected tendency that they would decrease when the sand particle diameter increased.

3.3.4 Measurement of the Produced Sand

Two methods were used to determine the quantity of produced sand. The first method was a direct measurement. The sand was extracted from the collected slurry and weighed. The second method was based on the material balance calculation using the slurry production rate, the injection flow rate and the densities of the sand and oil.

3.3.4.1 Extraction Process

The slurry was collected in a container. Once the slurry was collected the sand in the slurry was extracted by using solvents. The sand was then dried and weighed.

3.3.4.2 Material Balance

The incremental mass of sand produced (dm_{sp}) and the sand production rate (Q_{sp}) were also calculated by using a mass balance equation. Therefore:

$$dm_{sp} = \frac{(dm_{slurry} + Q_{oi} dt \rho_o)\rho_s}{\rho_s - \rho_o} \tag{3-22}$$

$$Q_{sp} = \frac{dm_{sp}}{dt} = \frac{(dm_{slurry} + Q_{oi} dt \rho_o)\rho_s}{(\rho_s - \rho_o)dt} \tag{3-23}$$

where:

Q_{sp} = sand production rate (g/h)

dm_{slurry}= incremental mass of slurry produced at time interval dt (g)

dm_{sp}= incremental mass of sand produced at time interval dt (g)

Q_{oi} = volumetric flow rate of oil injected (cc/h or cm^3/h)

dt = time interval (h)

ρ_o = oil mass density (g/cm^3)

ρ_s = sand mass density (g/cm^3)

The derivation of Equation 3-23 is given in Appendix A.5.

Both methods were previously used by Meza [25]. In those experiments it was found that the results generated by the two methods differed by 10%. The advantage of using Equation 3-23 is that the sand production rate can be measured very frequently and, therefore, can be related to the real-time measurements of the pressure within the cell.

3.3.5 <u>Instrumentation and Measurement Accuracy</u>

A brief description of the main instruments used in this research project, and their accuracy, is listed below:

- Absolute and differential pressure transducers: SRP PT-420 absolute pressure transducers were used to monitor confining pressures, injection pressure, pore pressure and total stress at localized points inside and outside of the sand pack. The SRP PT-420 pressure transducers have ± 0.20 % full scale (F.S) base straight line. (BSL) accuracy. Also, Rosemount differential pressure transducers were used to monitor the pressure drop inside the sand pack. The reference accuracy of these instruments is ± 0.065 % of span.

- Scale: a Mettler Toledo precision balance was used to weigh the produced fluids and slurry. The balance has a weight range of 0-6100 g, a readability of ± 0.01 g and a sensitivity accuracy of 0.025 %.

- Pumps: two Quizix QX series pumps were used in the experimental set ups, one for fluid injection into the core and the other one for the confining pressure system. They are both positive displacement, stepper motor-driven pumps with air-actuated valves. They work with the PumpWorks© software which is a program that allows complete and automated control of the pumps. The pumps offer a range of flow rates from 0.001 cc/min to 500 cc/min with an accuracy of 0.1% of the set flow rate. The manufacturer's stated resolution of the volume is in the order of 10 nanolitres.

- Thermocouples: Omega K type were used to monitor the temperature of the triaxial cell body and the room temperature. The thermocouples were calibrated to measure temperatures between 0 to 100 °C and their accuracy was 0.4% of the temperature measured (in °C).

Table 3-1: Formation water composition (Lloydminster area).

Ions	ppm (mg/l)
Sodium (Na^+)	13,300
Chloride (Cl^-)	20,828
Potassium (K^+)	208
Magnesium (Mg^{++})	806
Calcium (Ca^{++})	881

Table 3-2: Sieve opening sizes [49].

Sieve # U.S.mesh	Size (mm)	Size (in)
18	1.000	0.0394
20	0.850	0.0331
25	0.710	0.0278
35	0.500	0.0197
40	0.425	0.0165
45	0.355	0.0139
50	0.300	0.0117
60	0.250	0.0098
70	0.212	0.0083
80	0.180	0.0070
100	0.150	0.0059
120	0.125	0.0049
170	0.090	0.0035
230	0.063	0.0025
325	0.045	0.0017
400	0.038	0.0015
BP	< 0.038	<0.0015

Table 3-3: Sand grain effective diameters and uniformity coefficients.

Sands	Effective Grain Diameters (mm)						Uniformity Coefficient
	$D_{99.9}$	D_{90}	D_{60}	D_{50}	D_{40}	D_{10}	
Husky Sand	0.820	0.200	0.160	0.153	0.140	0.080	2.0
Rounded Standard	0.740	0.210	0.164	0.155	0.143	0.085	1.9
Rounded No Fine Fractions	0.690	0.208	0.161	0.152	0.134	0.099	1.6
Rounded No Large Fractions	0.295	0.183	0.158	0.149	0.128	0.073	2.2
Rounded Well Sorted	0.295	0.190	0.160	0.153	0.136	0.099	1.6
Silica Well Sorted	0.495	0.282	0.218	0.202	0.185	0.133	1.6
Silica Poorly Sorted	0.960	0.506	0.231	0.205	0.180	0.065	3.6
Silica No Large Fractions	0.465	0.325	0.230	0.203	0.180	0.065	3.5
Silica No Fine Fractions	0.940	0.487	0.220	0.207	0.185	0.112	2.0

Table 3-4: Sand densities.

Material	ρ (g/ml)
Silica Sands	2.6339 ± 0.0016
Husky Sand	2.6208 ± 0.0029
Glass Beads	2.4733 ± 0.0044

Table 3-5: Roundness classes (after Schneiderhöhn, 1954) [78].

Classes	**Definition**
Angular	Strongly developed faces with sharp corners. Sharply defined, large reentrants (indentations) with numerous small reentrants.
Subangular	Strongly developed flat faces with incipient rounding corners. Small reentrants (indentations) subdued and large reentrants preserved.
Subrounded	Poorly developed flat faces with corners well rounded. Few small and gently rounded reentrants (indentations), and large reentrants weakly.
Rounded	Flat faces nearly absent with corners all gently rounded. Small reentrants absent and large reentrants only suggested.
Well Rounded	No flat faces, corners, or reentrants discernible, and a uniform convex grain outline.

Table 3-6: Sand morphology.

Sand	Roundness Class	Sphericity	Sorting (Based on Uniformity Coefficient)
Husky Sand	Angular	Low Sphericity	Well Sorted
Rounded Standard	Well Rounded	High Sphericity	Well Sorted
Rounded No Fine Fractions	Well Rounded	High Sphericity	Well Sorted
Rounded No Large Fractions	Well Rounded	High Sphericity	Poorly Sorted
Rounded Well Sorted	Well Rounded	High Sphericity	Well Sorted
Silica Well Sorted	Sub-angular	Low Sphericity	Well Sorted
Silica Poorly Sorted	Sub-angular	Low Sphericity	Poorly Sorted
Silica No Large Fractions	Sub-angular	Low Sphericity	Poorly Sorted
Silica No Fine Fractions	Sub-angular	Low Sphericity	Well Sorted

Table 3-7: Physical properties of the sand packs used in the sand strength (triaxial cell) experiments.

Sand Type	Test #	Height (cm)	PV (cc)	ϕ	k_i (Darcies)	S_o (%)	S_w (%)
Silica Well Sorted	12	13.71	219	40.1	1.31	--	--
	13	13.57	210	40.5	2.95	92.8	7.2
	14	13.72	215	40.8	1.39	95.6	4.4
Husky Sand	16	13.75	204	37.8	1.55	89.5	10.5
	17	13.77	192	36.0	1.67	89.2	10.8
	18	13.67	207	38.7	1.33	82.0	18.0
Silica No Large Fractions	22	13.69	180	33.8	0.65	90.1	9.9
	23	13.32	178	34.2	0.45	87.4	12.7
	24	13.76	180	33.4	0.44	91.7	8.3
Silica No Fine Fractions	25	13.59	209	39.5	0.84	93.4	6.6
	26	13.64	204.	38.6	1.86	91.2	8.8
	27	13.70	210	39.4	0.52	92.5	7.5
Silica Poorly Sorted	28	13.52	175	32.6	0.19	90.1	9.9
	29	13.71	174	32.4	0.14	89.1	10.9
	30	13.67	177	33.0	0.18	89.8	10.2

Legend

PV: pore volume
ϕ: porosity
k_i: initial effective permeability to oil
S_o: oil saturation
S_w: water saturation

Table 3-8: Physical properties of the sand packs and experimental conditions used in the sand production experiments under confining stress.

Test #	Sand Type	Pore Volume (cc)	Porosity (%)	Permeability (D)	Water saturation (S_w) (%)	Oil Saturation (S_o) (%)	Slot Size (mm/in)	Confining Pressure (kPa)
1	Well Sorted	3,704	41.4	6.95	8.9	91.1	0.711/ 0.028	519
2	Well Sorted	3,651	40.6	7.51	5.9	94.1	0.864/ 0.034	531
3	Well Sorted	3,667	41.0	6.25	7.2	92.8	1.016/ 0.040	982
4	Well Sorted	3,691	41.5	5.62	7.4	92.6	0.102/ 0.040	513
5	Well Sorted	3,690	41..0	5.92	8.1	91.9	0.142/ 0.056	506
6	Poorly Sorted	2,742	31.6	0.37	7.8	92.2	0.142/ 0.056	2,472
7	Poorly Sorted	2,918	32.8	0.60	9.5	90.5	0.198/ 0.078	2,471
8	Well Sorted	3,561	40.4	5.71	9.2	90.8	0.142/ 0.056	2,469
9	Well Sorted	3,706	41.0	5.63	5.9	94.1	1.016/ 0.040	2,472
10	Well Sorted	3,648	41.1	4.10	4.7	95.3	1.016/ 0.040	733
11	Well Sorted	3,676	41.1	4.12	2.5	97.5	1.016/ 0.040	157
12	Well Sorted	3,631	40.8	3.34	7.7	92.3	1.016/ 0.040	150
13	Well Sorted	3,572	40.5	3.64	6.2	93.8	1.016/ 0.040	1,002

Continuation of Table 3-8.....

Test #	Sand Type	Pore Volume (cc)	Porosity (%)	Permeability (D)	Water saturation (S_w)	Oil Saturation (S_o)	Slot Size (in/mm)	Confining Pressure (kPa)
14	Poorly Sorted	2,723	30.2	0.67	6.0	94.0	0.234/ 5.94	2,499
15	Silica No Large Fractions	2,953	33.2	0.51	5.6	94.4	0.142/ 0.056	2,497
16	Silica No Fine Fractions	3,460	38.4	2.04	6.1	93.9	0.142/ 0.056	2,494
17	Husky Sand	3,460	38.2	0.73	4.1	95.9	0.142/ 0.056	508

Table 3-9: Physical properties of the sand packs and experimental conditions used in the sand production visualization experiments using CT scanning.

	Test 19: Husky sand	Test 20: Silica No Large Fractions sand
Porosity (%)	37.8	33.1
Permeability (D)	0.54	0.79
Water Saturation (S_W)	6.9	13.4
Oil Saturation (S_O)	93.1	86.6
Pore Volume (cm^3)	1092	961
Slot Size (in/mm)	0.056/1.422	0.056/1.422
Initial Flow Rate (cm^3/h)	10	17
Confining pressure (kPa)	1,700	1,700

Table 3-10: Physical properties of the sand packs and experimental conditions used in the sand production visualization experiments using thin sections.

Sand Type	ϕ (%)	PV (cc)	Slot Size mm(in)
Silica Well Sorted pack 1	42.7	394	0.965 (0.038)
Husky Sand pack 1	38.6	352	1.016 (0.040)
Husky Sand pack 2	38.7	375	1.016 (0.040)
Husky Sand pack 3	39.4	358	0.813 (0.032)
Silica Well Sorted pack 2	43.0	348	0.711 (0.028)
Silica Poorly Sorted pack 1	34.7	316	4.293 (0.169)

Table 3-11: Slot width/$D_{99.9}$ ratio and sand production for different sands.

Sands	$SW/D_{99.9}$		Sand Production	
	0.028 in (0.711 mm)	0.041 in (1.016 mm)	Amount (g)	Classification
Poorly Sorted sand 1	0.74		0	Very Limited Sand Production
Poorly Sorted sand 2	0.99		0	
Husky Sand	0.87		117	
Rounded Standard	0.96		55	
Rounded No Fine Fractions	1.03		69	
Well Sorted Sand 1	1.44		684	Controlled Sand Production
Well Sorted Sand 2	1.45		625	
Husky Sand		1.24	3,850	
Rounded No Large Fractions	2.41		13,800	Massive Sand Production
Rounded Well Sorted	2.41		10,300	
Well Sorted Sand 1		2.05	6,000	
Well Sorted Sand 2		2.07	12,610	

Table 3-12: Proposed experimental matrix to study the effect of grain size distribution and slot size on sand production.

Sands	Theoretical Sizes mm (in)		Proposed sizes mm (in)			
	SW_{min}	SW_{max}	SW_{min}	Intermediate Size	SW_{max}	Additional Size
Well Sorted Sand	0.660 (0.026)	1.016 (0.040)	0.711 (0.028)	0.813 (0.032)	1.016 (0.040)	1.422 (0.056)
Poorly Sorted Sand	1.295 (0.051)	2.184 (0.086)	1.422 (0.056)	1.702 (0.067)	1.981 (0.078)	5.944 (0.234)

Table 3-13: Proposed flow rates for a given slot size at a constant fluid velocity.

Slot ID	Slot Size mm (in)	Q_{Slot} (cm^3/h)		
		@ 94.94 cm/h slot flux and 1 % A_S	@ 47.47 cm/h slot flux and 2 % A_S	@ 31.65 cm/h slot flux and 3 % A_S
Slot1	0.711 (0.028)	51	26	17
Slot2	0.813 (0.032)	59	29	20
Slot3	1.016 (0.040)	74	37	25
Slot4	1.422 (0.056)	103	51	34
Slot5	1.702 (0.067)	123	61	41
Slot6	1.981 (0.078)	143	72	48
Slot7	5.944 (0.234)	430	215	143

Table 3-14: Absolute permeability of the sands used.

Sand	Porosity (%)	Permeability (D)			Average Permeability (D)
		Q_1 (cc/h)	Q_2 (cc/h)	Q_3 (cc/h)	
Silica Well Sorted	41.8	19.9	19.9	19.5	19.8
Husky Sand	37.4	3.9	3.9	3.9	3.9
Silica No Large Fractions	32.5	1.0	1.0	1.0	1.0
Silica No Fine Fractions	40.2	18.5	18.5	18.5	18.5
Silica Poorly Sorted	32.0	1.4	1.5	1.5	1.4

Table 3-15: Permeability tests without sand production. Slot size: 0.028 in (0.711 mm).

Sand	Flow rate (cm3/h)	k_p (D)	k_s(D)	Difference (%)
Sil-1 dry	120	21.2	33.5	57.9
Sil-1 wet	120	23.4	22.7	2.8
Glass Beads (BT-3)	300	243.5	244.1	0.2
	400	242.5	241.9	0.3
	500	243.6	245.6	0.8

k_p = permeability in the pack, k_s = permeability in the vicinity of the slot

Table 3-16: Calculated values for the Kozeny constant *c*.

Sand	Test #	$c_{average}$ (m^{-2})
Silica Well Sorted	Test 1	3.00E+10
	Test 2	2.66E+10
	Test 3	3.19E+10
	Test 4	3.76E+10
	Test 5	3.34E+10
Silica Poorly Sorted	Test 6	1.84E+11
	Test 7	1.32E+11
Silica Well Sorted	Test 8	3.27E+10
	Test 9	3.52E+10
	Test 10	4.92E+10
	Test 11	4.93E+10
	Test 12	5.86E+10
	Test 13	5.24E+10
Silica Poorly Sorted	Test 14	8.02E+10
Silica No Large Fractions	Test 15	1.61E+11
Silica No Fine Fractions	Test 16	7.41E+10
Husky Sand	Test 17	2.14E+11

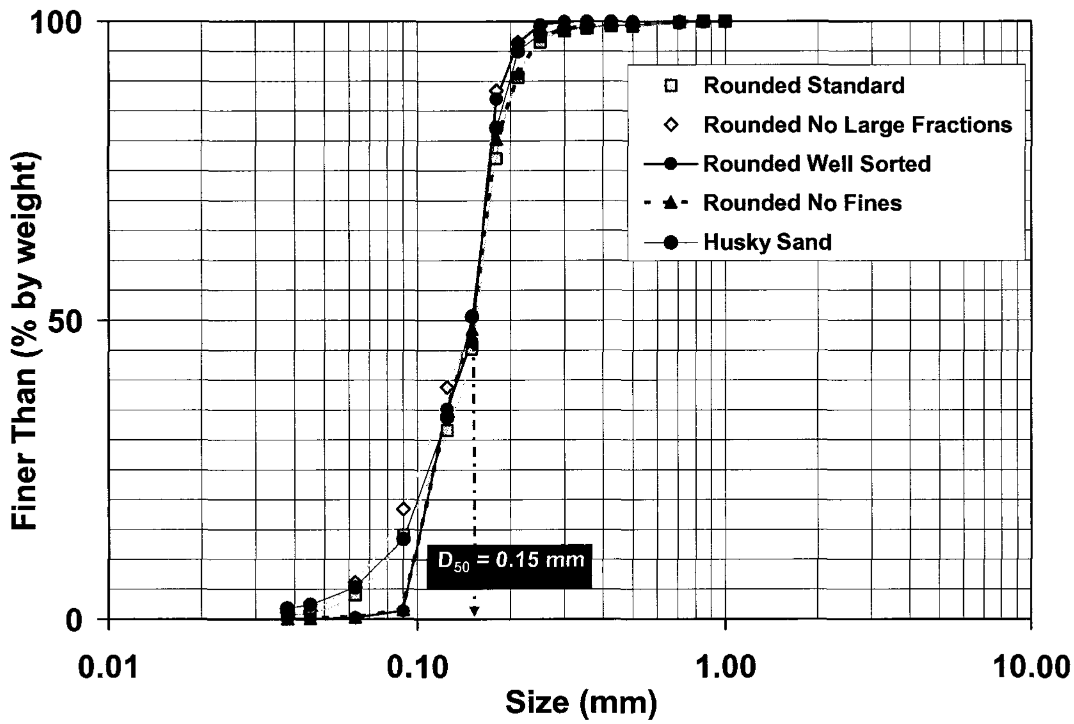

Figure 3-1: Particle size distribution curves for the rounded and Husky sands.

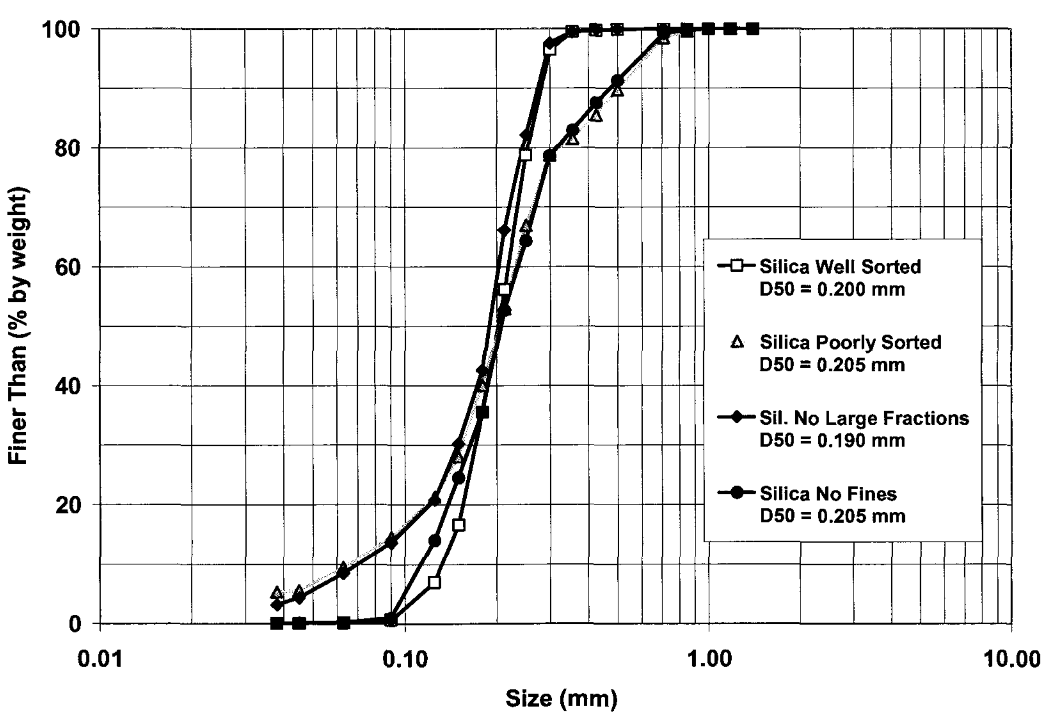

Figure 3-2: Particle size distribution curves for the silica sands

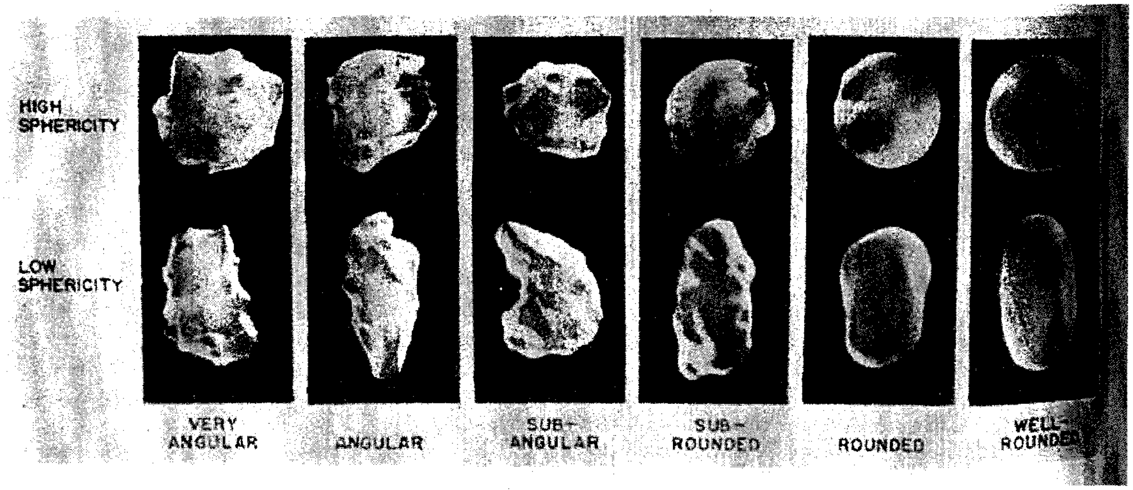

Figure 3-3: Roundness scale of Maurice Powers [52]

Figure 3-4: SEM photomicrograph of the Silica Well Sorted sand. MAG: X20.

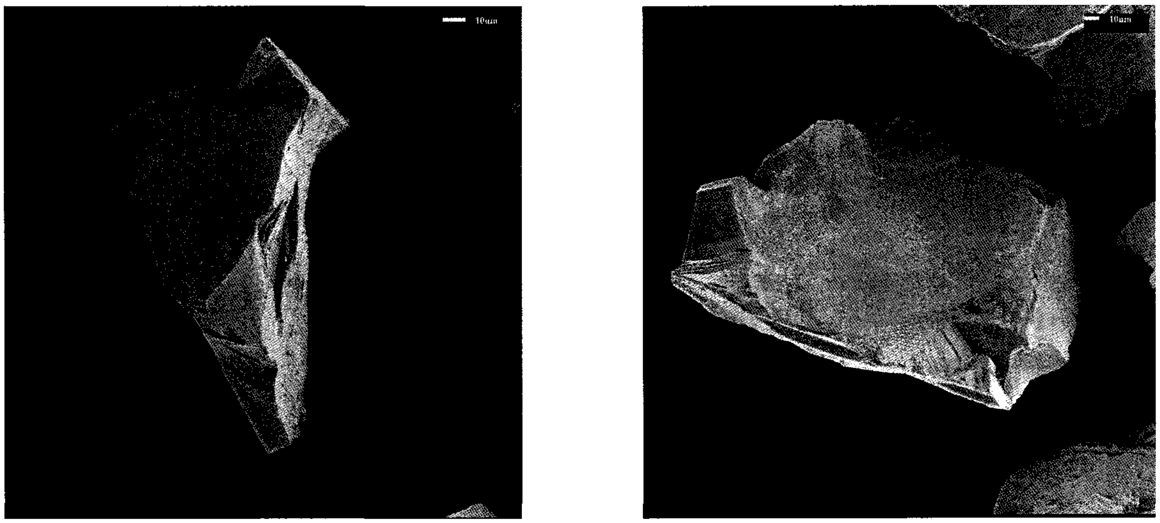

(a) MAG X300 (b) MAG 200

Figure 3-5: SEM photomicrograph of Silica Well Sorted sand grains.

Figure 3-6: SEM photomicrograph of the Husky sand. MAG: X60.

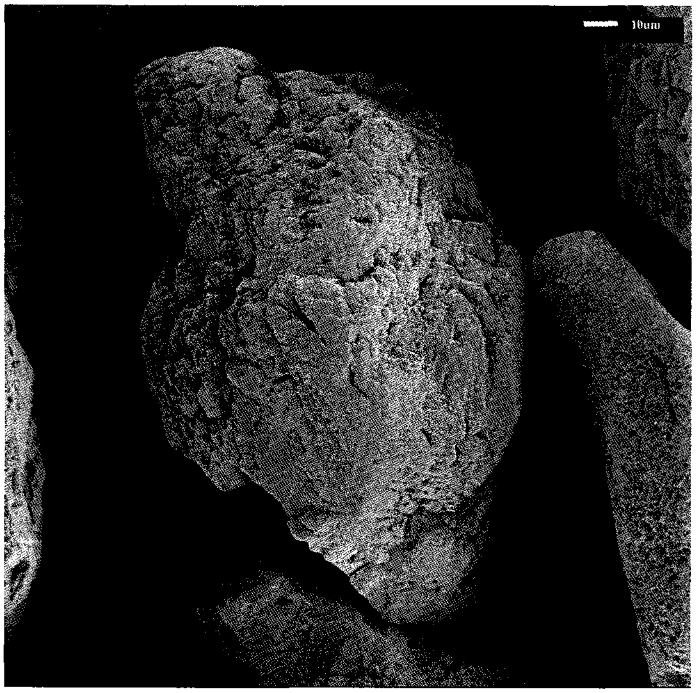

Figure 3-7: SEM photomicrograph of a Husky sand grain. MAG X400

Figure 3-8: SEM photomicrograph of the Silica Poorly Sorted sand. MAG: X60.

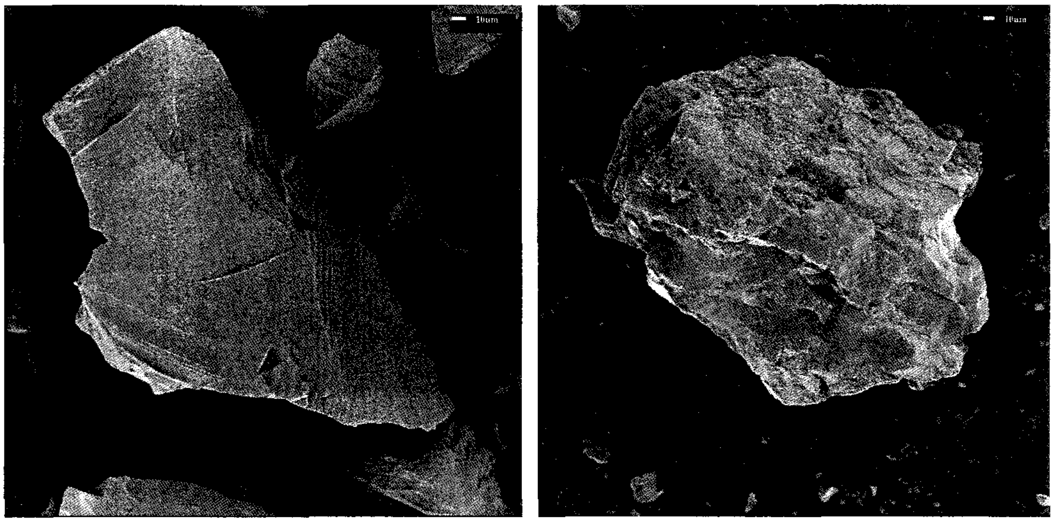

(a) MAG X200

(b) MAG 100

Figure 3-9: SEM photomicrograph of Silica Poorly Sorted sand grains.

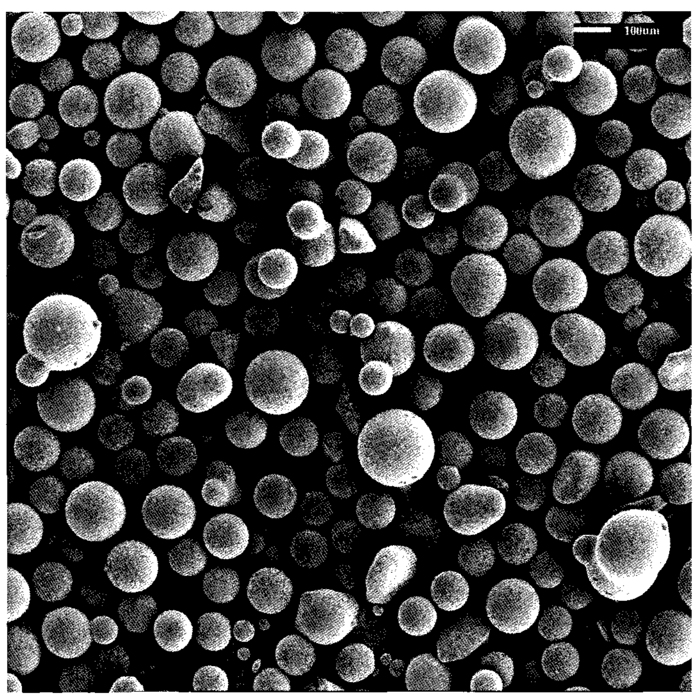

Figure 3-10: SEM photomicrograph of the Rounded Standard sand. MAG: X70.

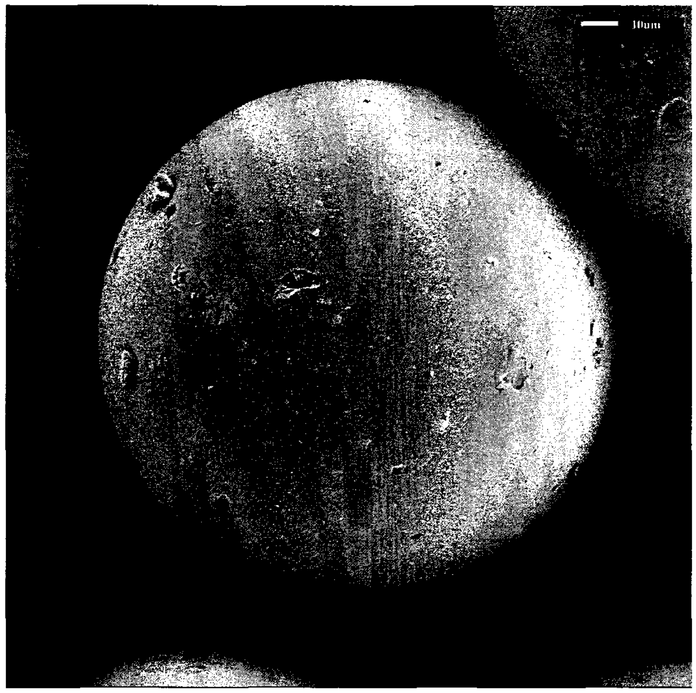

Figure 3-11: SEM photomicrograph of a Glass Bead. MAG X500.

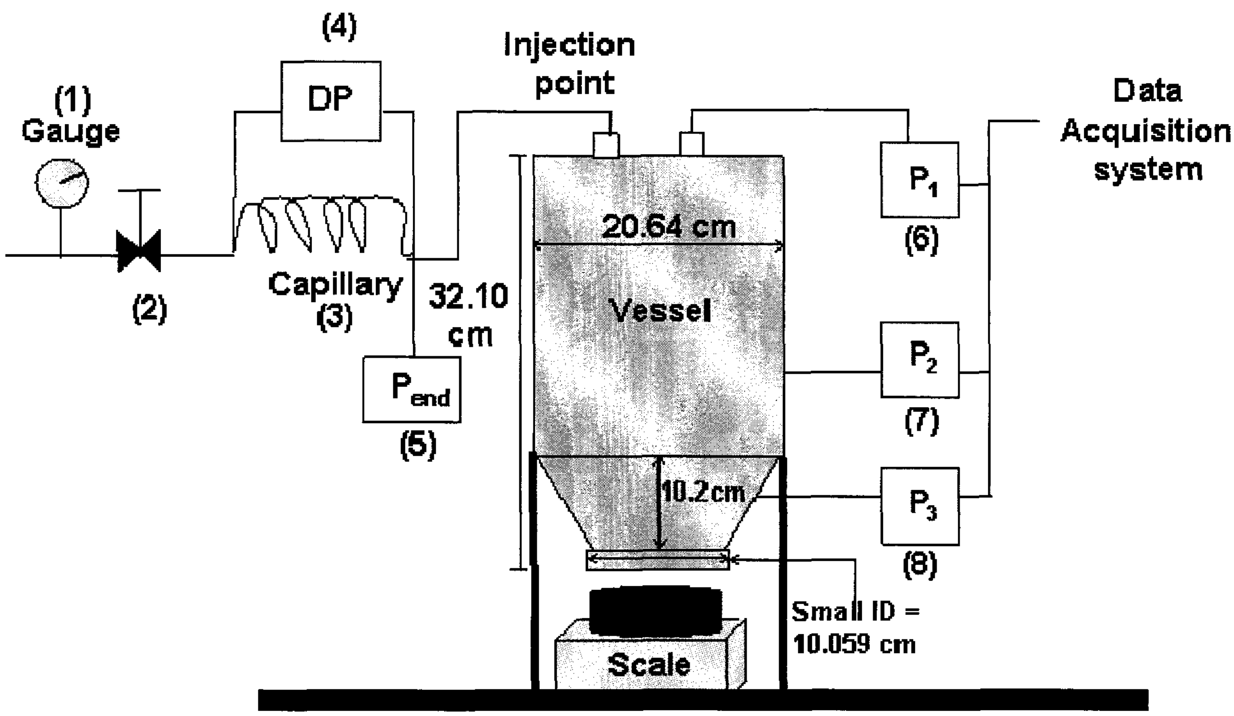

Figure 3-12: Schematic of sand production apparatus for the air tests (not to scale).

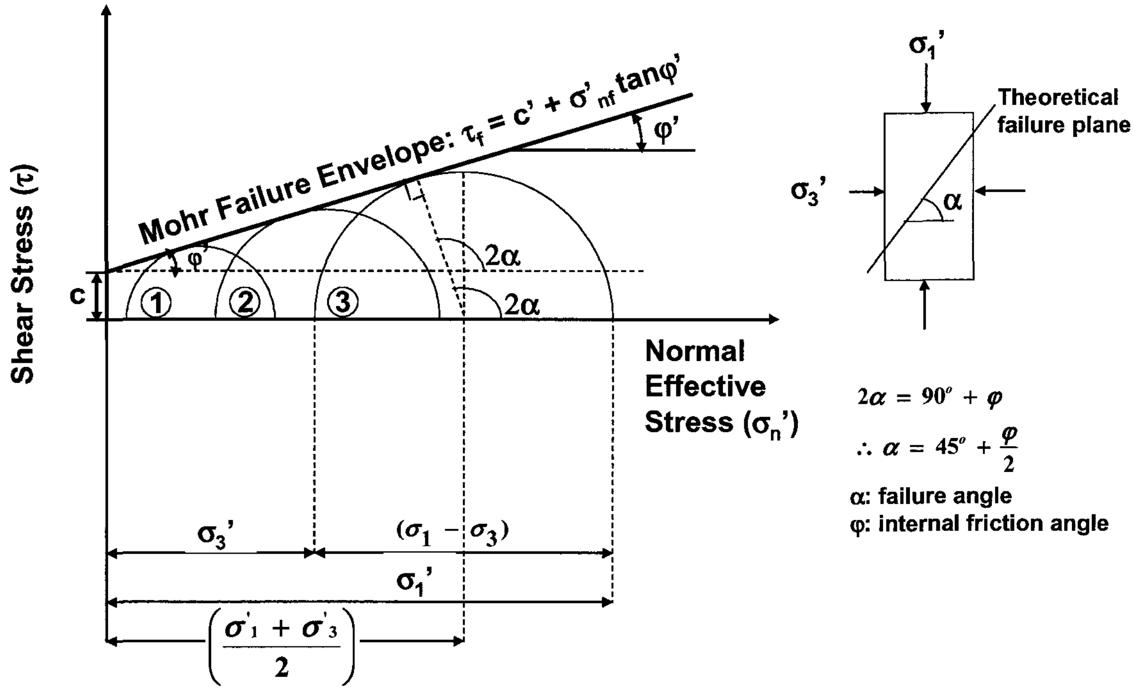

(a) Use of Mohr circles to determine strength parameters

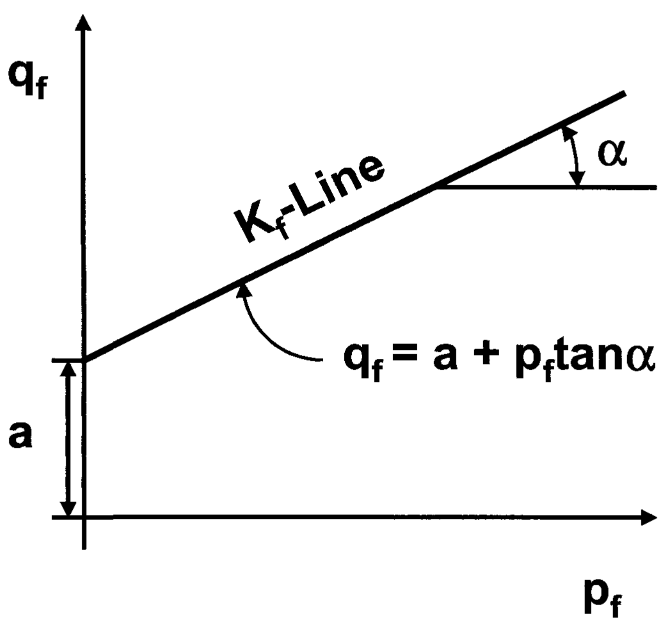

$$q_f = \left(\frac{\sigma_1 - \sigma_3}{2}\right)_f$$

$$p_f = \left(\frac{\sigma_1^{'} + \sigma_3^{'}}{2}\right)_f$$

$$\sin\varphi = \tan\alpha$$

$$c = \frac{a}{\cos\varphi}$$

(b) p-q diagram showing the relation of q_f and p_f to Mohr – Coulomb envelope.

Figure 3-13: Strength parameters calculation. After Lambe [72] and Head [81]

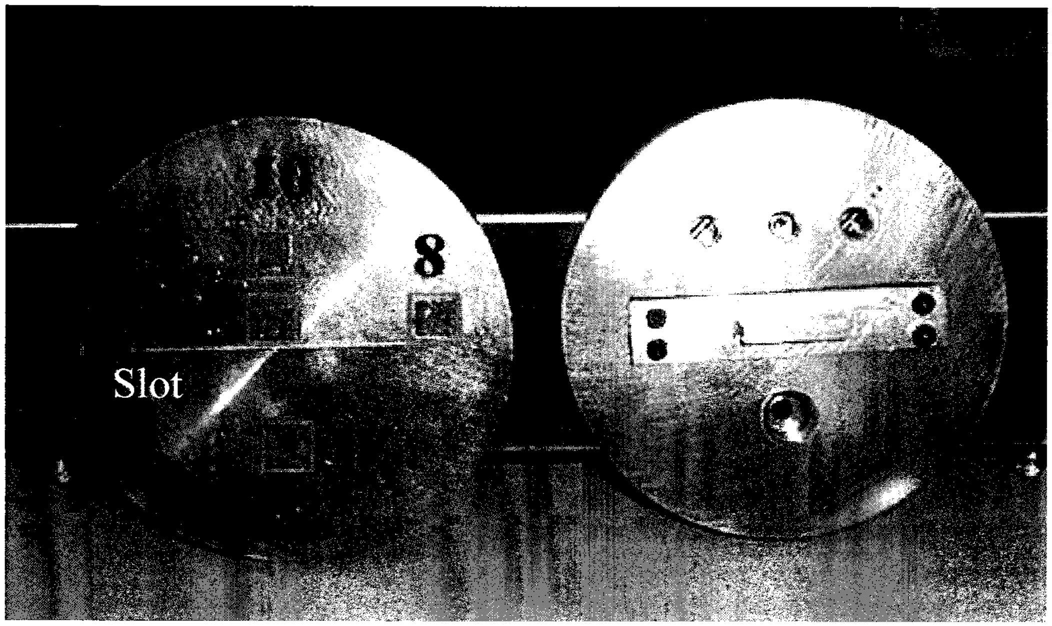

Figure 3-14: Slot plates used in the sand production experiments

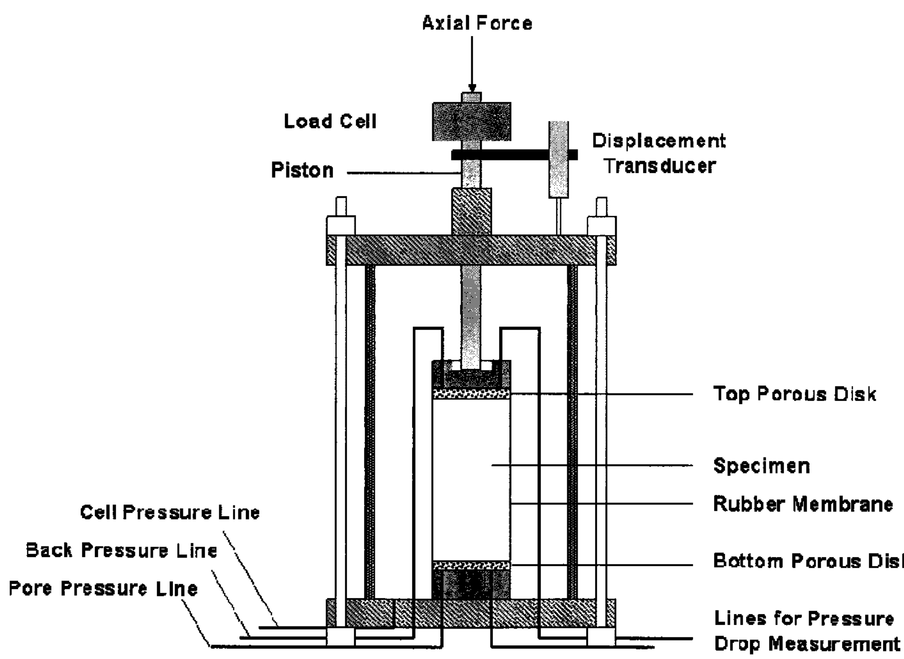

Figure 3-15: Schematic of low pressure triaxial cell.

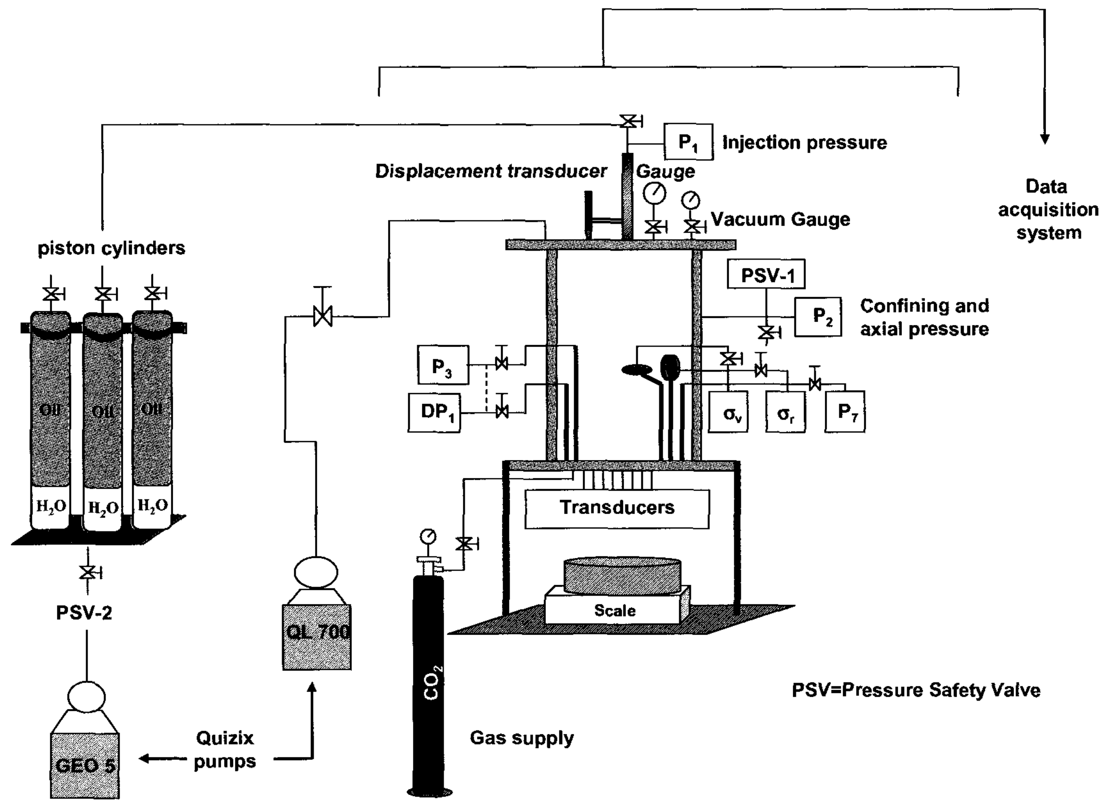

Figure 3-16: Schematic of the sand production under stress apparatus (not to scale). Cell ID: 19.5 cm. Cell Length: 32.3cm

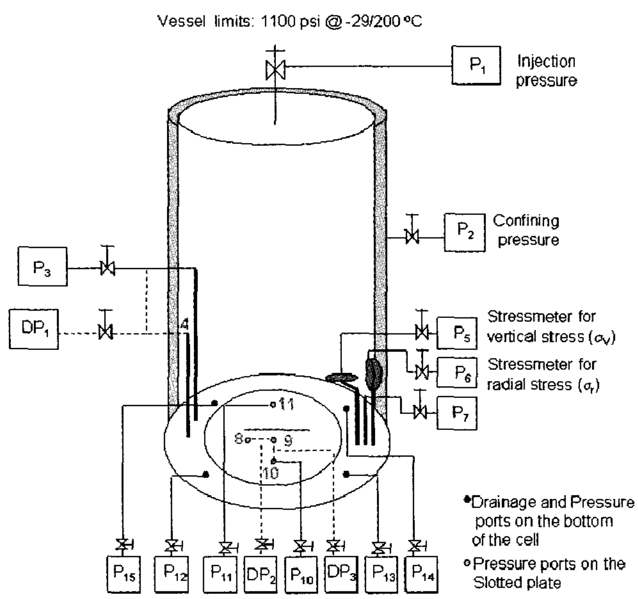

Figure 3-17: Schematic of the sand production apparatus under confining stress showing the pressure ports (not to scale). DP1, DP2 and DP3 measure the differential pressure between ports 3 and 4, 8 and 9, and 10 and 11 respectively.

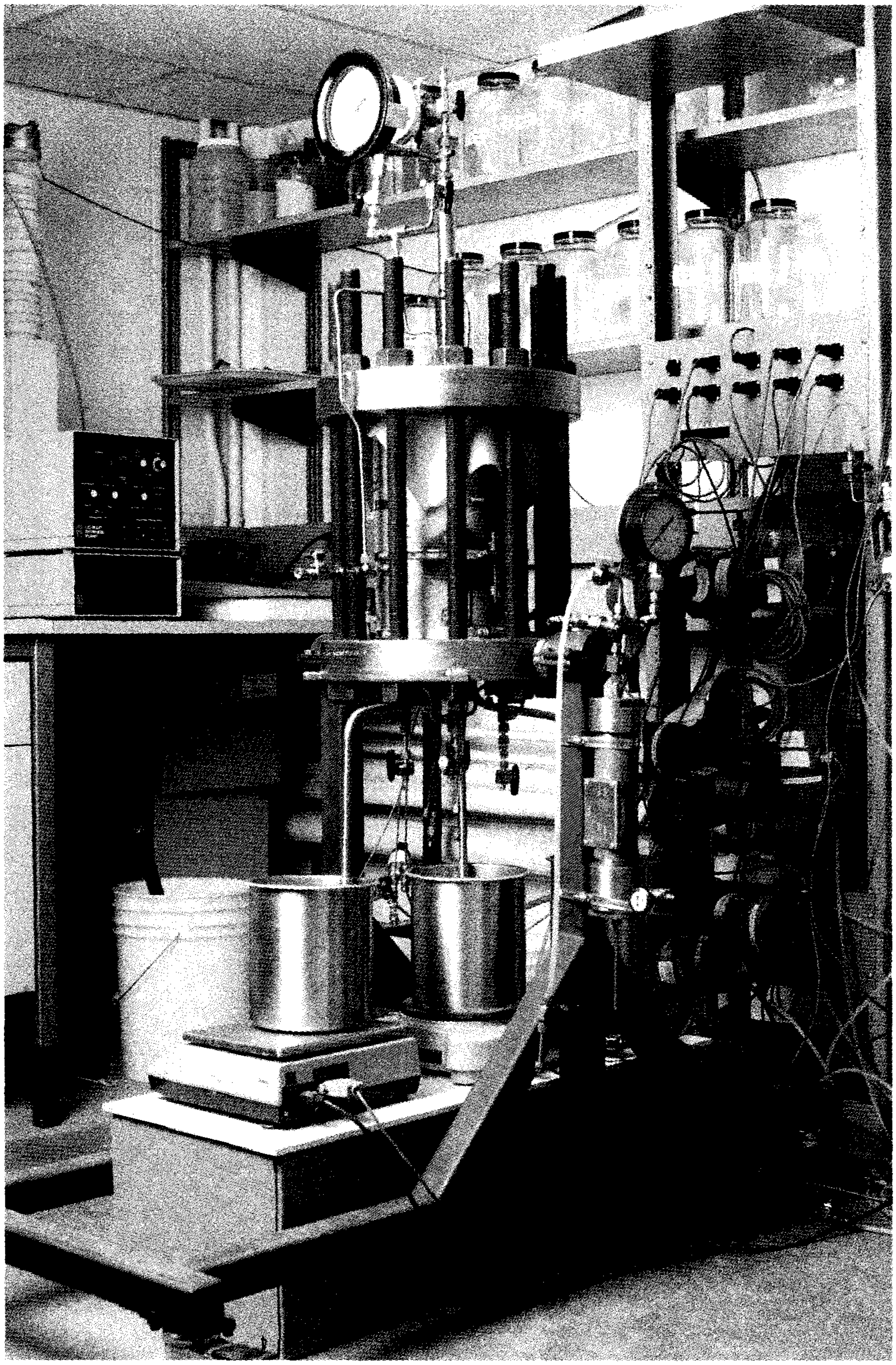

Figure 3-18: Picture of the equipment for the sand production experiments under confining stress.

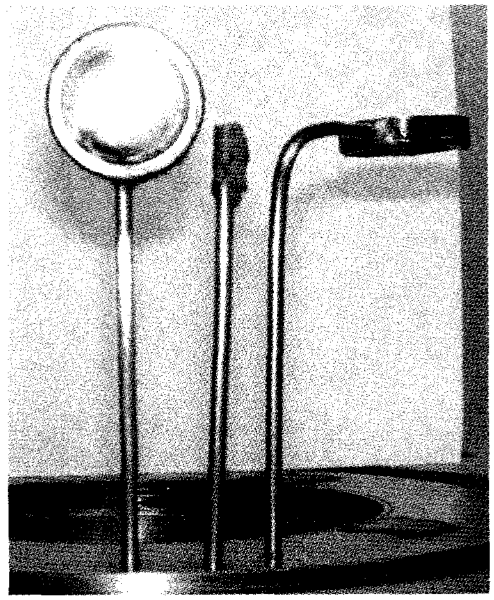

Figure 3-19: Total stressmeter for vertical and radial stress.

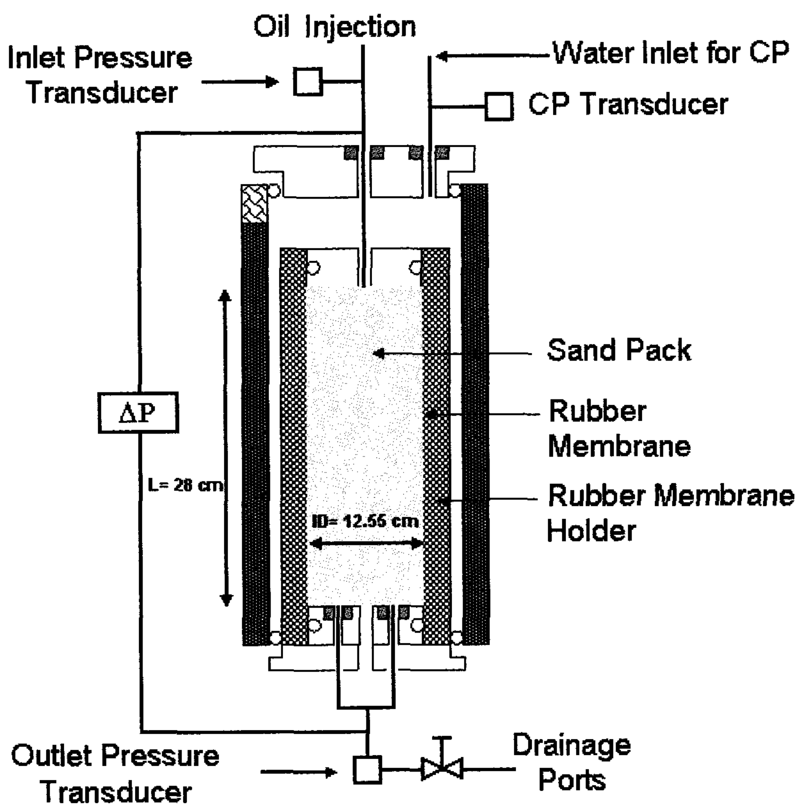

Figure 3-20: Schematic of the sand production under stress apparatus used in the CT scanner test (not to scale).

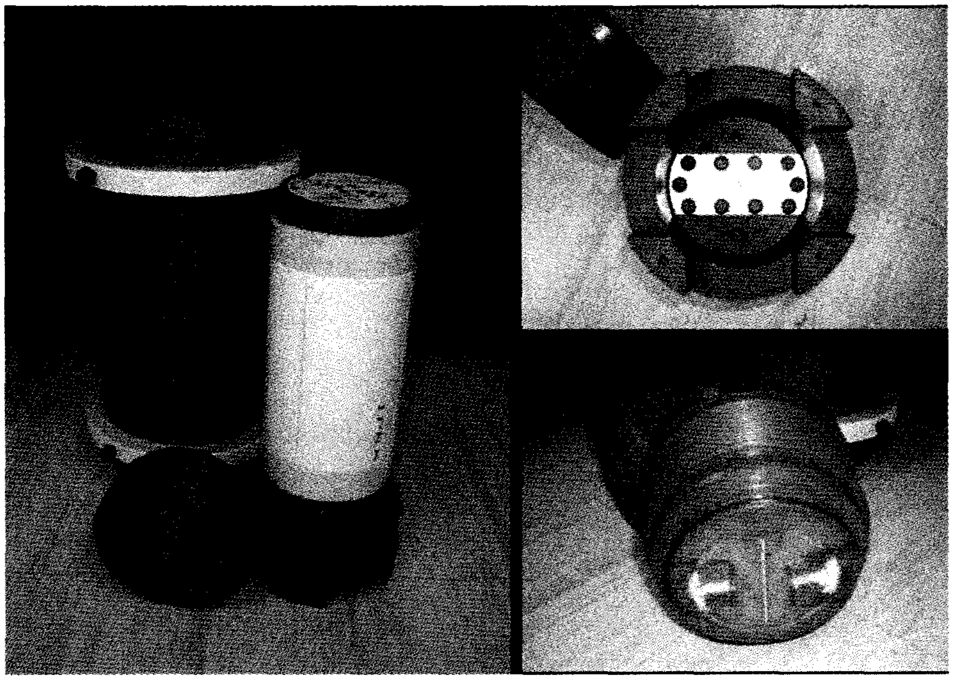

(a) the core holder and sand pack (b) end cap with slot and plug

Figure 3-21: Pictures of the sand production under stress apparatus used in the CT scanner test.

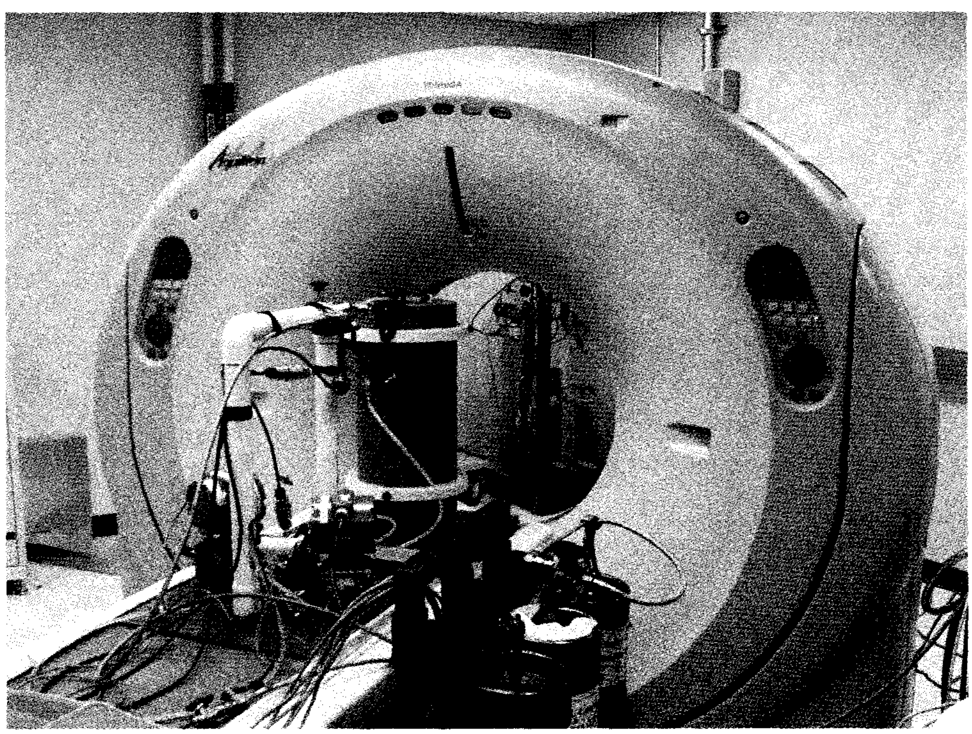

Figure 3-22: Pictures of the CT Scanner experimental set up for the sand production experiments under confining stress.

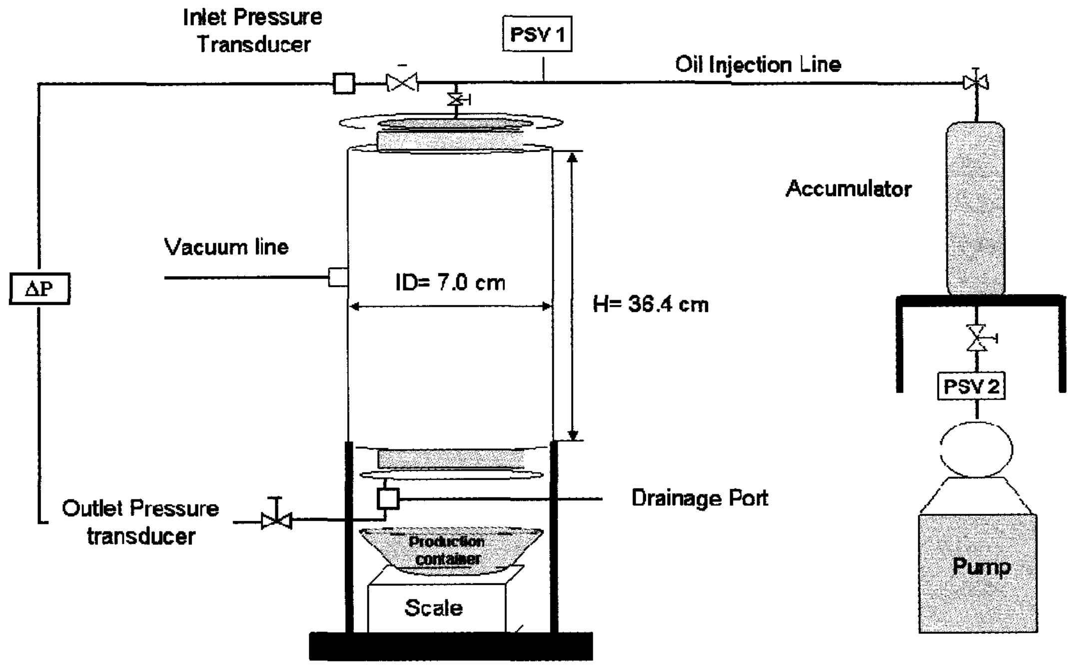

Figure 3-23: Schematic of the experimental apparatus to prepare the epoxied cores for the thin sections.

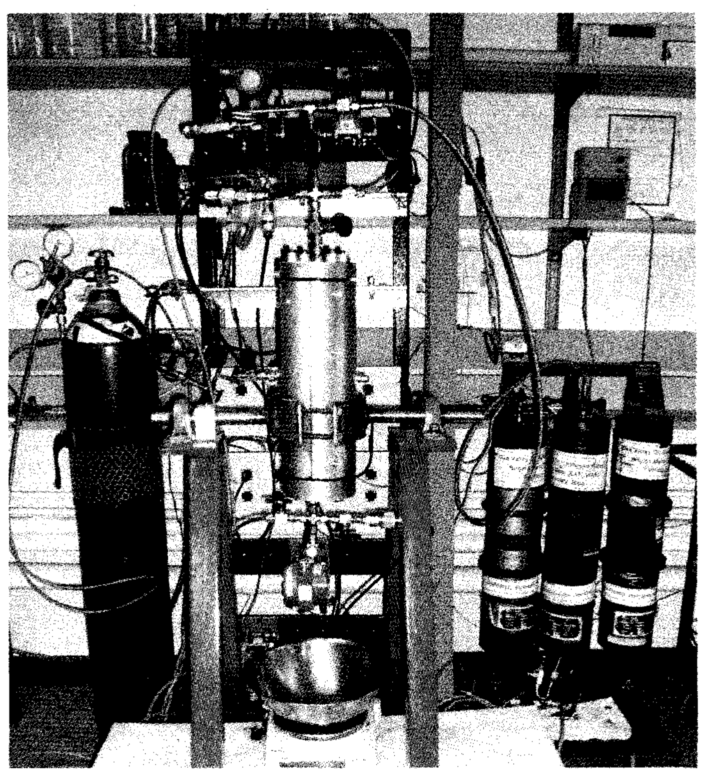

Figure 3-24: Picture of the experimental set up for the sand production epoxied cores.

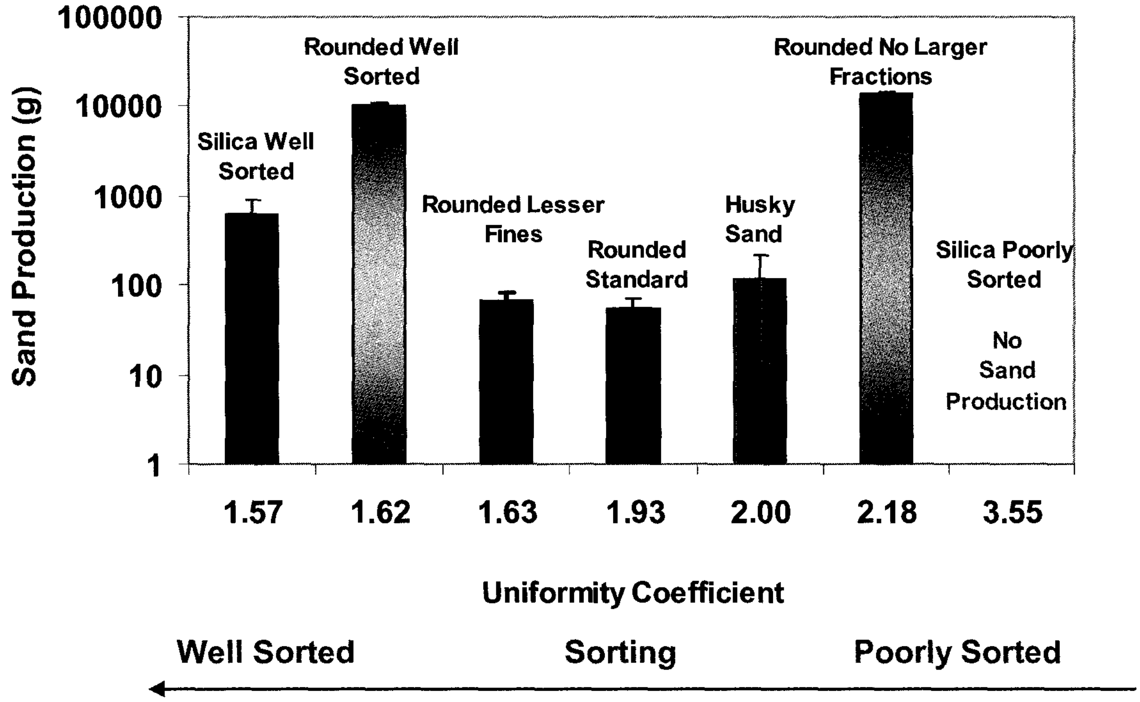

Figure 3-25: Effect of sorting-uniformity coefficient on sand production.

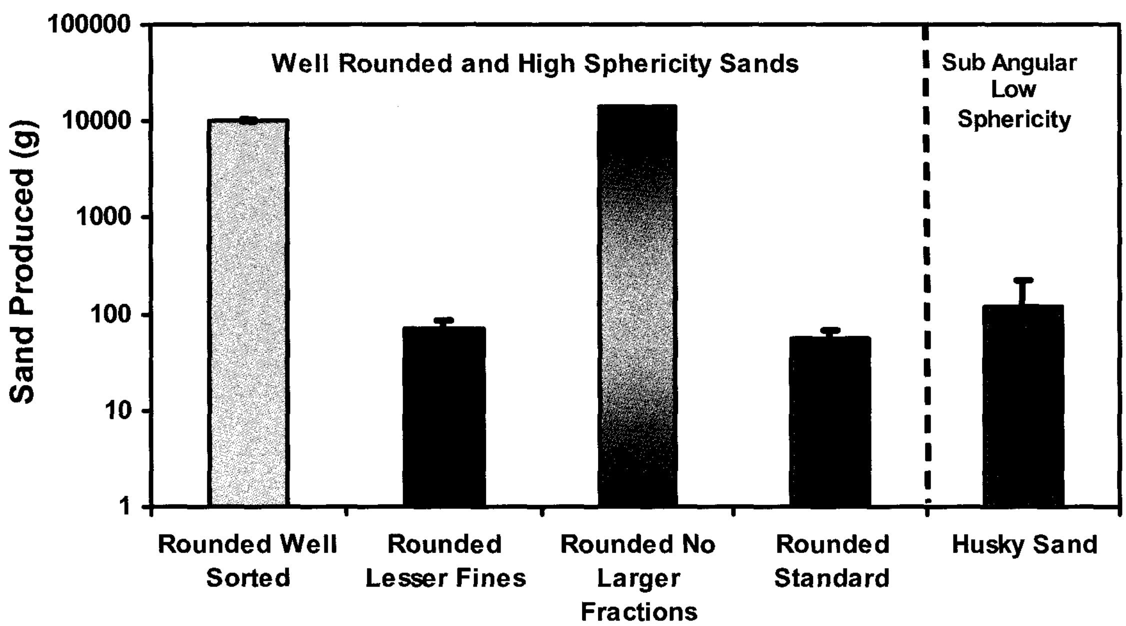

Figure 3-26: Effect of grain morphology on sand production.

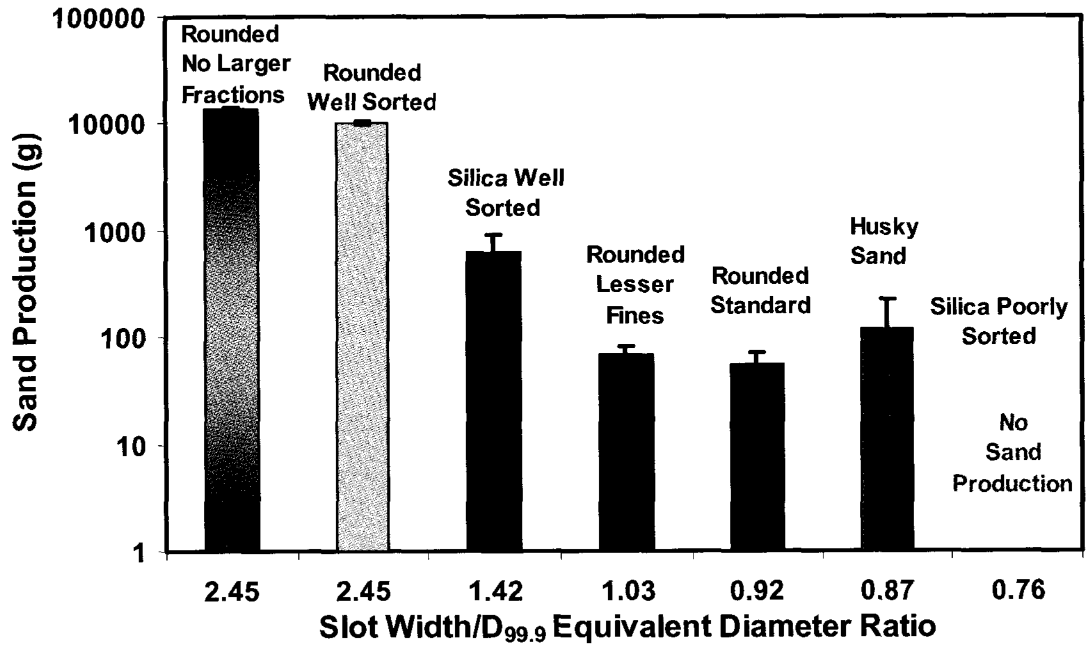

Figure 3-27: Sand production against Slot Width/D99.9 Equivalent Diameter ratio.

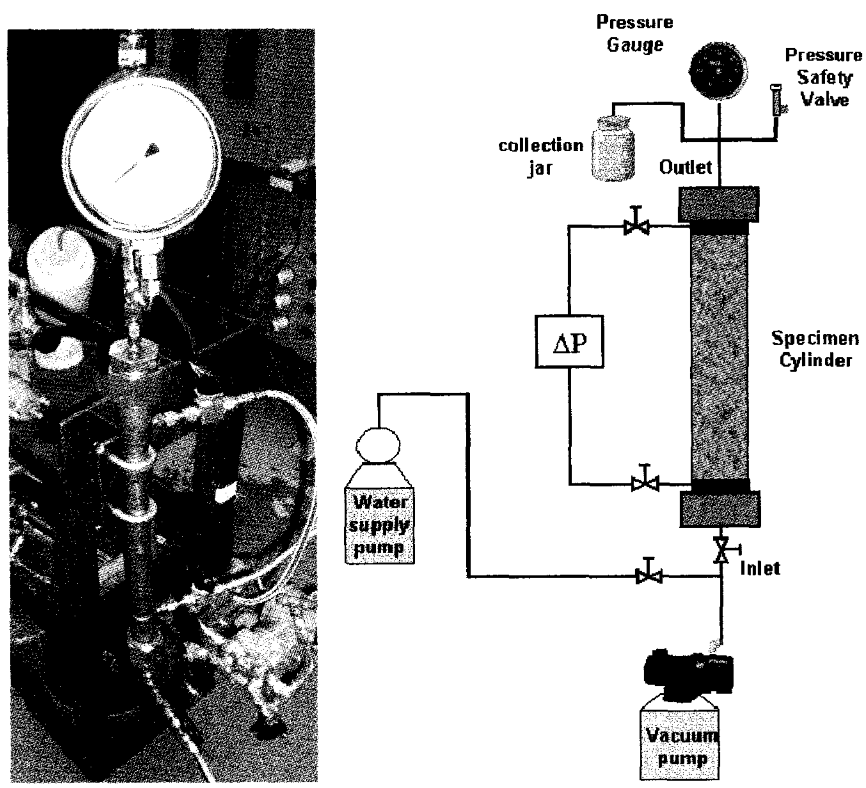

Figure 3-28: Absolute permeability apparatus.

4 Experimental Results and Discussion

The presentation of the results is divided into four main sections: screening experiments with air, sand production experiments under confining stress, sand strength experiments, and visualization experiments using a CT scanner. The experimental results are discussed in the following sections.

4.1 Screening Experiments with Air without Confining Stress

The sand production experiments using air as the flowing fluid allowed a rapid scoping of the factors affecting sand production. A continuation of the work initiated by Meza during her M.Sc. thesis is presented in this section. Additional air tests were performed and a more complete analysis was carried out. The results of this analysis yielded a correlation between slot size and grain size distribution regarding sand production behaviour (see section 3.3.1 and equations 3-11 to 3-13). The correlation was used to choose the slot sizes for the confining experiments with water wet sand packs saturated with dead heavy oil. Details of this analysis were given in section 3.3.1 and will not be repeated here. However, a summary of the findings and the basic reasons for choosing the sands evaluated in this study are given below.

4.1.1 Reproducibility of the Tests

It is very important to emphasize that sand production through narrow openings is a highly variable process in terms of the quantity of sand produced. For example, the production of sand through a slot is very sensitive to the ratio of the slot width to the diameter of the sand grains. The randomness of this process has been mentioned in the literature previously [55,86].

Several tests were repeated to evaluate the reproducibility of the air flow experiments. In spite of the large scatter in the data, a trend in the sand production behaviour can be observed. Examples of this trend are evident in Figure 4-1 and Figure 4-2. In analyzing and interpreting the results of the sand production experiments, this randomness needs to be taken into consideration.

4.1.2 <u>Summary of Findings from Screening Experiments with Air</u>

The sands used during the air screening experiments are shown in Table 4-1. The average sand production from the air experiments, as well as the range of sand production observed, is also reported in this table for each sand at different slot sizes.

The first sands previously evaluated by Meza [25] were the Silica Well Sorted 1 sand and the Husky sand. In spite of the randomness of the tests, a definite difference was observed between the average production of Silica Well Sorted 1 sand and Husky sand as shown in Table 4-1 for a 0.711 mm (0.028 in) slot. It appears that Husky sand could arch/bridge more easily than Silica Well Sorted 1 sand although the average diameter (D_{50}) of the Husky sand is smaller than the average diameter of the Silica Well Sorted 1 sand (see Table 4-1). Significantly more Silica Well Sorted 1 sand than Husky sand was also produced from the 0.040 in (1.02 mm) slot (see Table 4-1).

At first the large amount of Silica Well Sorted 1 sand produced compared to Husky sand, for a given slot size, was thought to be due to the greater angularity of the Husky sand. Another explanation given was that the larger sand grains of the Husky sand within the highest sand fraction could make the sand arch more easily. More air experiments were planned to try to distinguish between the two explanations of the observed behaviour.

A test with a glass bead sand, identified as Rounded Standard, having the same size distribution as the Husky sand, was prepared to investigate the effect of roundness and angularity on sand production. The tests were performed using the 0.711mm (0.028 in) slot under gravity flow. Table 4-1 shows the results obtained with the Rounded Standard sand in comparison to those obtained with the Husky sand. The results show that the roundness of the grains, given the inherent randomness of the process, did not seem to play as critical a role in the sand production behaviour observed as the sand particle size distribution. The difference in sand production between the two sands is within the standard deviation observed in this type of experiment.

From this result, there was left the explanation that the lower production of the Husky sand compared to the Silica Well Sorted 1 sand was a consequence of the broader size distribution for the Husky sand, particularly in the largest fractions. This could increase the probability of forming sand arches/bridges due to an increase in the frictional force between the grains. The stress in the arch/bridge is better transmitted for larger sand grains. It has been reported previously that arch stability is strongly dependent on, in addition to the flow rate, the characteristics of the sand grains that form the porous material and the size of the perforation [58,59,64]. Larger perforations required larger grains to form stable arches.

Therefore, three more sands were prepared and tested to evaluate the influence of the different sand fractions on sand production: Rounded No Fine Fractions, Rounded No Large Fractions and Rounded Well Sorted (see section 3.1.2). A greater production of Rounded No Fine Fractions sand compared with Rounded Standard sand would be expected if the fines were the key to explaining arching/bridging behaviour. However, approximately the same quantity of sand was produced with the Rounded No Fine Fractions sand as with the Rounded Standard sand. Also, the sand pack made with Rounded No Large Fractions sand was completely produced through the 0.711mm (0.028 in) slot (Table 4-1). This result indicated that the bigger fractions, i.e. grains bigger than 0.25 mm (60 mesh), played an important role in stopping sand production, although these fractions represented a relatively small percentage of the size distribution (approximately 3 wt.% in this case). The results found with the Rounded Well Sorted sand (no fines, no fractions bigger than 212 μm) supported the previous results with the other glass bead sands. In the test with this sand, the entire sand contained in the pack was produced (Table 4-1).

To evaluate the effect of the grain sorting on sand production, four Silica sands were tested. Two of the sands were well sorted sands with a relatively narrow size distribution (see Figure 4-3). They were identified as Silica Well Sorted 1 and Silica Well Sorted 2.

The other two sands were sands with a much broader size distribution. They were named Silica Poorly Sorted 1 and Silica Poorly Sorted 2. The uniformity coefficients (C_u) of the four sands are shown in Table 4-1. It is important to notice that the C_u of the poorly sorted sands is more than twice the C_u of the well sorted sands. Furthermore, the average grain size diameter (D_{50}) of the two Well Sorted sands and the Poorly Sorted 2 sand is approximately the same (0.200 mm) while the Poorly Sorted 1 has a D_{50} of 0.100 mm.

The results showed that under the experimental conditions applied in these tests the size distribution has a remarkable influence on sand production. The well sorted sands were produced initially and then able to arch/bridge with the 0.711 mm (0.028 in) slot size but were produced profusely with the 1.016 mm (0.040 in) slot size. The poorly sorted sands were not produced at any of the slot sizes tested (see Table 4-1). Also, the average grain size diameter might be important in the selection of slot size for uniform sands but does not represent a reliable criterion for non-uniform sands. The D_{50} of the Poorly Sorted 2 is twice the D_{50} of the Poorly Sorted 1, but neither sand could be produced.

Although the air experiments represent a very simplified system (i.e. cohesionless sand, no stress field, single fluid system), they provided the foundation for choosing the parameters and type of sands to be evaluated. Based on the results of the air tests and taking into consideration that the average diameter (D_{50}) of the sand produced by cold production in western Canada tends to be in the range of 100 to 250 μm [26], the Silica Poorly Sorted 2 (D_{50} = 0.205 mm) and the Silica Well Sorted 2 sands (D_{50} = 0.203 mm) (shown in bold in Table 4-1) were chosen for subsequent testing. Two more sands were also prepared, the Silica No Large Fractions and Silica No Fine Fractions (see section 3.1.2) to evaluate the influence of grain size distribution on sand production under conditions closer to field conditions. Finally, a reservoir sand (Husky sand) was selected for evaluation. To simplify the nomenclature, from this point on the Silica Poorly Sorted 2 and the Silica Well Sorted 2 sands will be referred to simply as Silica Poorly Sorted and Silica Well Sorted sands.

Table 4-1: Summary of screening experiments with air.

Sands	D_{50} (mm)	Slot Size in (mm)	Sand Production g (wt%)	C_u
Silica Poorly Sorted 2 sand	0.205	0.032 (0.813)	0	3.6
		0.040 (1.016)	0	
Silica Poorly Sorted 1 sand	0.100	0.028 (0.711)	0	3.4
		0.040 (1.016)	0	
HUSKY Sand	0.153	0.018 (0.457)	0	2.0
		0.022 (0.559)	N/A	
		0.028 (0.711)	203 ± 148 (2.1-2.9)	
		0.040 (1.016)	3,820 ± 1065 (35-52)	
Rounded Standard	0.155	0.028 (0.711)	55 ±12 (0.1- 0.5)	1.9
Rounded No Fine Fractions	0.152	0.028 (0.711)	69 ±17 (0.1-0.6)	1.6
Silica Well Sorted 1 sand	0.280	0.018 (0.457)	0	1.6
		0.022 (0.559)	N/A	
		0.028 (0.711)	626 ± 319 (2.9-6.0)	
		0.040 (1.016)	10,800 (100)	
Silica Well Sorted 2 sand	0.202	0.022 (0.559)	0	1.6
		0.028 (0.711)	684 ± 81 (0.74-6.2)	
		0.032 (0.813)	1,808 ± 569 (7-25)	
		0.040 (1.016)	5,495 ± 2,219 (18-46)	
Rounded No Large Fractions	0.149	0.028 (0.711)	13,800 (100)	2.2
Rounded Well Sorted	0.153	0.028 (0.711)	10,300 (100)	1.6

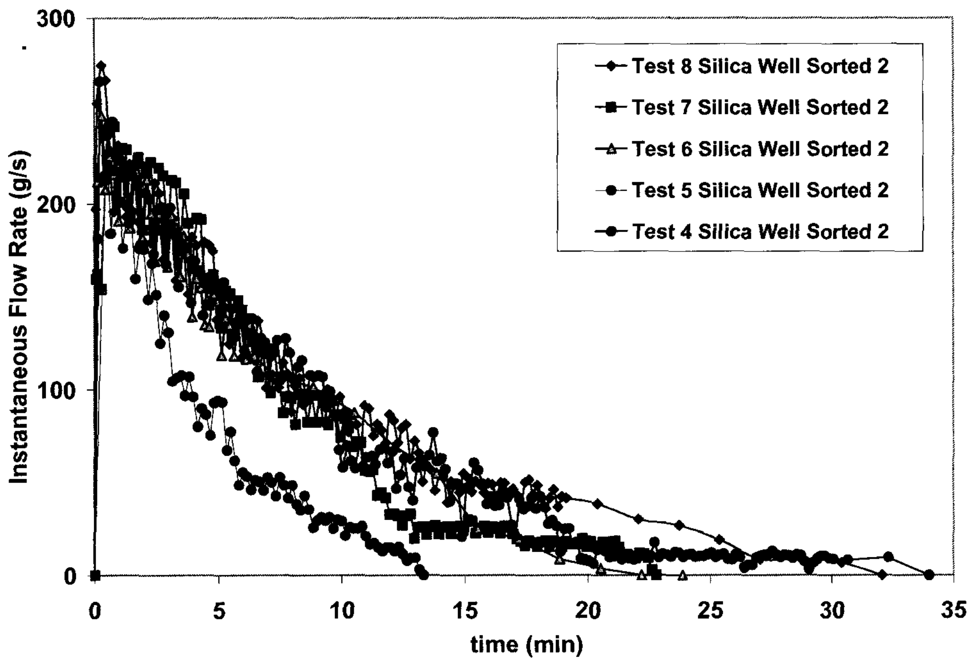

Figure 4-1: Sand flow rate versus time. Gravity Flow. Silica Well Sorted 2 sand. Slot Size: 0.032 in (0.864 mm). Reproducibility tests.

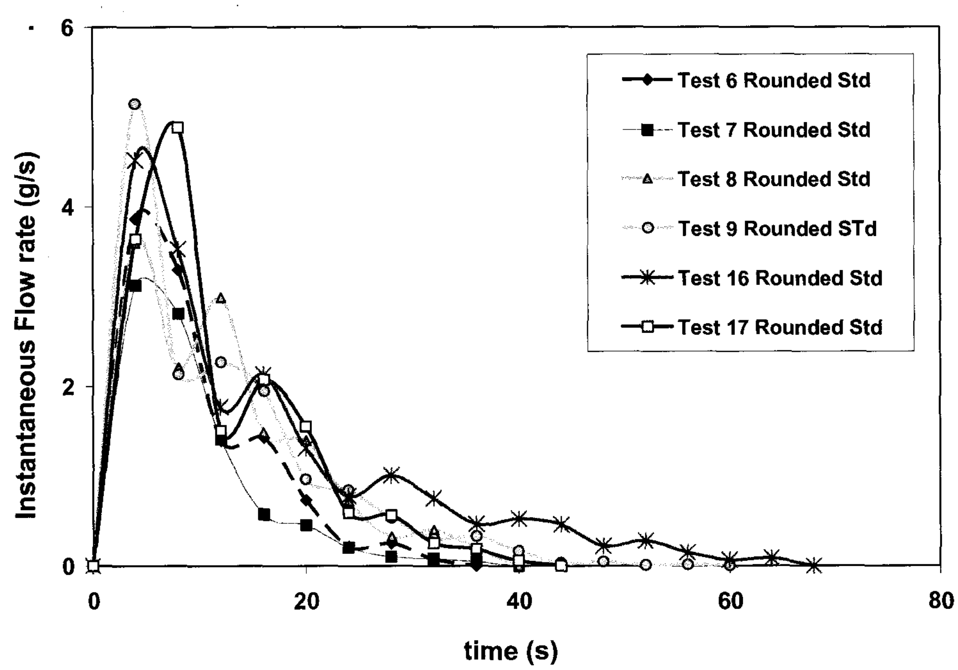

Figure 4-2: Sand flow rate versus time. Gravity Flow. Rounded Standard sand. Slot Size: 0.711 mm (0.028 in). Reproducibility tests.

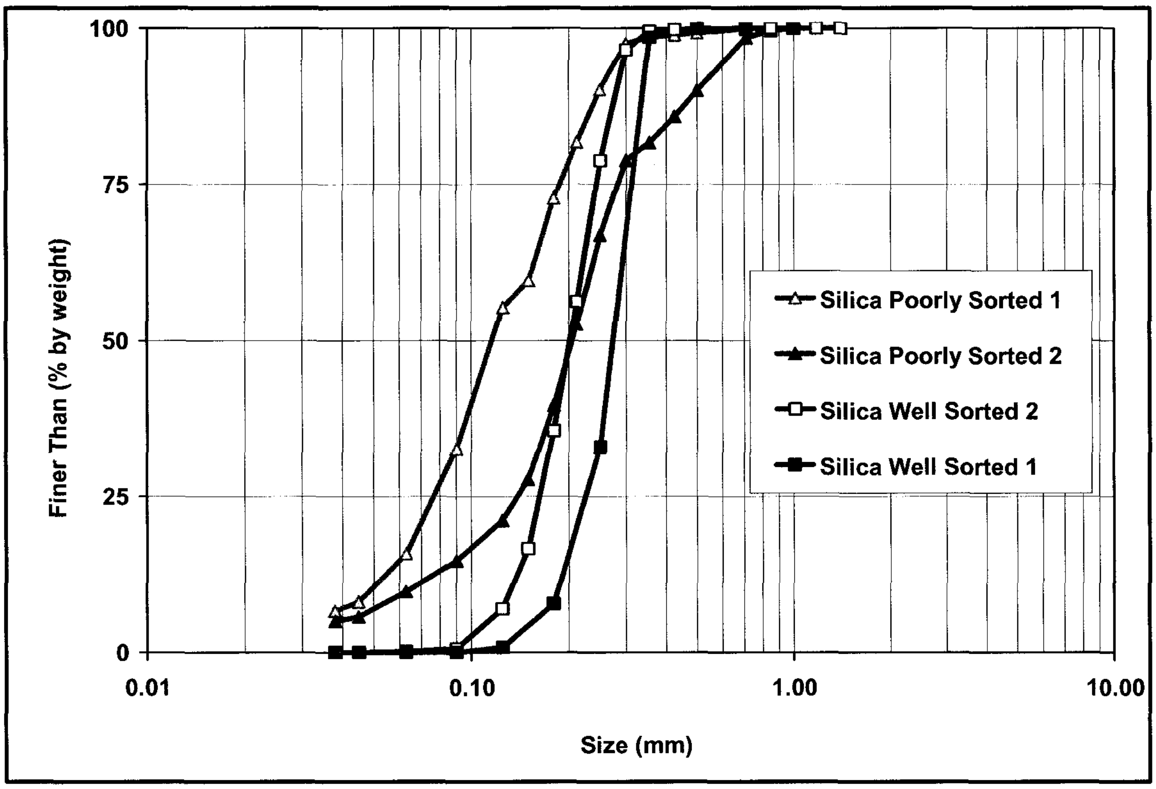

Figure 4-3: Particle size distribution curves for the silica sands used in the screening experiments with air.

4.2 Sand Production Experiments Under Confining Stress

Seventeen sand production experiments were performed using water-wet sand packs saturated with dead Dee Valley heavy oil to analyze the effect of slot size, fluid flow rate, grain size distribution, and confining stress on sand production behaviour.

In order to evaluate the influence of slot size on sand production, seven experiments were performed. Two sands were evaluated, the Silica Well Sorted sand and the Silica Poorly Sorted sand. Four slot sizes were chosen (see section 3.3.1 and Table 3-12) for the evaluation of the Silica Well Sorted sand: 0.711 mm (0.028 in), 0.812 mm (0.032 in), 1.016 mm (0.040) and, 1.422 mm (0.056 in). Three slot sizes were used in the evaluation of the Poorly Sorted sand: 1.422 mm (0.056 in), 1.981 mm (0.078 in) and 5.944 mm (0.234 in). The effect of the grain size distribution was investigated by comparing the sand production behaviour of four Silica sands. The sands had the same average particle size diameter but differed significantly in their size distribution (see section 3.1.2).

The effect of the stress field on sand production behaviour was assessed by applying different confining stresses (ranging from 150 kPa to 2,500 kPa) to Silica Well Sorted sand packs. Two slot sizes were used: 1.016 mm (0.040 in) and, 1.422 mm (0.056 in).

In each experiment, the flow rate was varied in steps according to a specified program (see Table 3-13). These steps were varied depending on the slot width in order to maintain the slot fluxes proposed in this table. Depending on the behaviour of a particular experiment, departures from the specified program were carried out sometimes by increasing or decreasing the steps in the flow rates by arbitrary amounts.

The procedure employed in these experiments was described in detail in Section 3.2.3. Production of sand and oil out of the slot was filmed on video. An analysis of the results obtained from the experiments is presented in the following sections.

Two different runs (3 and 6) with two different sands will be described in detail in order to present typical behaviours observed in the experiments. The results from the other tests are summarized in tabular form (see Table 4-4, Table 4-5, and Table 4-6). Selected results are illustrated graphically in the body of this chapter, in support of comments in the text. Further, a summary of the results for each experiment is presented in graphical form in Appendix B-1.

4.2.1 Data Analysis Procedure

4.2.1.1 Slot width to effective grain diameter ratio

The ratio of the slot width to sand grain diameter is an important parameter in controlling sand production through a slot. Since the sands used are not uniform in size, different effective diameters of the sand grains will be used (see section 3.1.2.1). The ratio of the slot width to effective grain diameter at different percentages by weight for these sands (i.e. D_i) was calculated and tabulated in Table 4-2. The values of the effective grain diameters listed in the first column on the left in Table 4-2 are calculated and tabulated in Table 3-3.

4.2.1.2 Determination of the variations in the properties of the sand pack

Sand production is usually associated with improvement in primary recovery in Alberta and Saskatchewan heavy oil reservoirs. One postulated mechanism for this field-based observation is the creation of a zone of enhanced permeability and high porosity around the wellbore, which allows the viscous oil to flow more easily to the perforations. Another mechanism which has been put forward to explain the higher oil recoveries during cold production is the formation of high permeability channels (wormholes). For the CHOPS process, with massive sand production from vertical (or slant or deviated) wells, the latter mechanism has been largely accepted as the predominant one. For sand production from horizontal wells, it is not yet clear which phenomenon is more likely to occur. In either case, the overall effect of sand production is to increase the permeability of the formation. It is therefore important to determine the permeability enhancement within the pack caused by sand production.

The calculated porosity and permeability of the sand pack were compared with the corresponding initial values. These two parameters were calculated by using the pressure drop measurements within the body of the sand pack (Ports 3 and 4) and around the slot (Ports 10 and 9). A detailed description of the analytical methods employed in these calculations was provided in section 3.3.3.

4.2.1.3 Pressure Gradient Calculations

Calculation of Pressure Gradients From Pressure Drop Measurements

The pressure data obtained in each test was used to calculate pressure gradients (dp/dL) in the cell and in the vicinity of the slot. The distances between the pressure ports are shown in Table 4-3, along with the designation of the pressure gradients. The pressure gradient $(dp/dL)_{11,slot}$ between port 11 and the entrance of the slot was also calculated. The location of port 11 with respect to the slot can be seen in Figure 3-14.

The pressure at the entrance of the slot (p_{slot}) must be calculated in order to calculate $(dp/dL)_{11,slot}$. If the flow through the slot is assumed to be the same as the flow between two infinite parallel planes a distance 2W apart, then the Hagen-Poiseuille equation for the slot can be used to estimate p_{slot} as follows [88]:

$$Q = \frac{2}{3}\frac{(p_{slot} - p_B)W^3 L_s}{\mu b} \qquad \text{4-1}$$

where: p_B = pressure at the end of the slot, atmospheric pressure
W = width of the slot divided by 2
L_s = length of the slot
b = depth of the slot = thickness of the plate
μ=viscosity of the slurry or oil flowing out of the slot
Q = the slurry or oil flow rate

All pressure measurements in this thesis are given in terms of the gauge pressure, so p_B=0; therefore p_{slot} can be obtained by rearranging Equation 4-1:

$$p_{slot} = \frac{3}{2}\frac{bQ\mu}{W^3 L_s} \qquad \text{4-2}$$

The pressure gradient $(dp/dL)_{11,slot}$ is calculated simply as the ratio of the pressure drop $(p_{11}-p_{slot})$ to the distance, $\Delta L_{11,slot}$, between pressure port 11 and the entrance to the slot. The viscosity of the produced slurry varied since the sand cut also varied. Therefore the viscosity of the slurry should be calculated and used in Equation 4-2 when sand was produced. This approach is approximate since the sand and oil do not exactly flow as a continuum through the slot.

The viscosity of the sand-oil slurry can be calculated as follows:

$$\mu_{Slurry} = \mu_r \mu_o \qquad 4\text{-}3$$

where μ_r is the relative viscosity of the slurry and μ_o is the oil viscosity.

The relative viscosity of Husky sand slurries was measured previously [89] at ARC and was fitted to the following equation:

$$\mu_r = e^{\frac{5c_s}{2(1-1.48c_s)}} \qquad 4\text{-}4$$

where c_s is the sand concentration.

The relative viscosity of a Unimin (Ottawa) sand slurry was measured at the Saskatchewan Research Council (SRC). The measurements were fitted with the following equation [89]:

$$\mu_r = 1 + 2.5c_s + 10c_s^2 + 0.0019e^{20c_s} \qquad 4\text{-}5$$

This equation was used to calculate the relative viscosity of the sand-oil slurries comprised of Silica sands which are also synthetic sands with similar characteristics.

Estimate of Critical Pressure Gradients During Sand Production

Two approaches were taken to estimate critical pressure gradients during sand production. In the first approach, Darcy's linear flow equation (see equation 3-18) was used to approximate the pressure gradient into the slot:

$$\frac{dp}{dL} = \frac{Q_o \mu_o}{S_s k_o} \quad \text{4-6}$$

where S_s is the slot surface area defined in equation 3-15.

This approach is based on the assumption that the flow into the slot is predominantly vertical (i.e. perpendicular to the plane of the slot). Thus the area perpendicular to the flow is simply S_s, the area of the slot. Flow in the horizontal plane of the slot is taken to be sufficiently small to be neglected. This is supported by the pressure drop measurements obtained from ports near the slot in these sand production experiments; the maximum pressure gradients reported in the horizontal plane of the slot (see, for example, the curve labelled $(dp/dL)_{11,slot}$ in Figure 4-6) were at least two orders of magnitude lower than the estimated vertical pressure gradient into the slot (see the column labelled $(dp/dL)_{isp}$ in Table 4-6). In the analysis of the sand production experiments, the estimated pressure gradient obtained from equation 4-6 will be applied to evaluate sand failure within the sand pack; it will be used to evaluate the critical pressure gradient required for the initiation of sand production and the critical pressure gradient required for the onset of continuous sand production.

The second approach is similar to the one taken by Bratli and Risnes [55] (see Fjær et al. [47]) in establishing a criterion for stability/failure of sand arches. In this approach, a spherical cavity around the production opening is assumed to be created by a small amount of initial sand production. The radius of this cavity can be estimated from the volume of initial sand production (see expression 2-11). The fluid pressure gradient into this cavity can be calculated using Darcy's law, assuming that inflow occurs through the outward facing hemisphere of the cavity [47]:

$$\frac{dp}{dr} = \frac{\mu_o Q}{2\pi k_o r^2} \qquad 4\text{-}7$$

In addition, the predicted critical pressure gradient at which the arch surrounding a cavity will fail can be estimated using the results of Bratli and Risnes [55] (see Fjær et al. [47]). Their results are based on the observation that an arch will not remain stable if the pressure gradient at the surface of the arch exceeds the gradient of the radial stress there. In their analysis of arch failure, Bratli and Risnes [55] obtained the following representation for the radial stress profile near the surface of the arch under the assumption that the sand matrix adjacent to the arch was in a plastic state that could be described by the Mohr-Coulomb failure envelope:

$$\frac{d\sigma}{dr} = 2\frac{C_o}{r} \qquad 4\text{-}8$$

where C_o is the uniaxial compressive strength and r is the cavity radius. Consequently, the critical pressure gradient for arch failure becomes

$$\left(\frac{dp}{dr}\right)_{Cr} = 2\frac{C_o}{r} \qquad 4\text{-}9$$

Alternatively, arch failure can be expressed in terms of a predicted critical flow rate. This is obtained by substituting equation 4-7 into equation 4-9:

$$\frac{\mu_o Q_{cr}}{2\pi k_o r} = 2C_o \qquad 4\text{-}10$$

In the analysis of the sand production experiments, the estimated pressure gradient obtained from equation 4-7 and the predicted critical pressure gradient and flow rate obtained from equations 4-9 and 4-10 offer a different perspective on sand failure behaviour in the experiments. They are applied to sand failure occurring within the sand pack following the first episode of (small) sand production. That is, these quantities will be calculated for the first flow rate during which sand production was observed. The arch radius will be estimated from the volume of sand produced before a channel started to grow (assuming a spherical cavity) using expression 2-11. Typically, the arch radius calculated in this manner will be an upper bound on the radius of the arch around the cavity formed by sand production. For example, in section 4.4 on the visualization experiments using CT scanning, the production of small amounts of sand created a cylindrical cavity with a hemispherical tip (see Figure 4-48). The radius of the hemispherical tip is equal to the radius of the cylinder (see Table 4-12), and somewhat less than the radius of a sphere of equal volume. Consequently, the estimated pressure gradient for flow into the cavity and the critical pressure gradient for arch failure around the cavity obtained by using the radius for a spherical cavity will provide lower bounds on the actual values of these parameters.

Effective Stress Calculations

Isotropic confining stress was applied to the sand pack in these sand production experiments. Also, two total stressmeters were located inside the pack (see section 3.2.3) to measure the total vertical and radial stress. However, the total radial stressmeter did not work properly due to an unresolved leak. Therefore, only the values of the total vertical stress are reported. The effective radial stress was calculated using the confining pressure and the pore pressure provided by the pressure transducer located at port 7 (see Figure 3-17), close to the walls of the cell. The same port pressure value was used to calculate the effective vertical stress. Both the total vertical stressmeter and port 7 were at the same height (see Figure 3-17). The effective vertical stress at the top of the pack (hereafter referred as the effective axial stress) was also computed. The confining stress and the injection pressure were used in the calculations. Therefore:

$$\text{Effective Vertical Stress} = \sigma'_V = \sigma_c - p_7 \qquad 4\text{-}11$$

$$\text{Effective Axial Stress} = \sigma'_A = \sigma_c - p_1 \qquad 4\text{-}12$$

$$\text{Effective Radial Stress} = \sigma'_R = \sigma_c - p_7 \qquad 4\text{-}13$$

where: σ_c is the confining stress, p_1 is the pressure at the injection point and p_7 is the pressure at port 7.

The objective was to follow up the changes of the state of stresses inside the pack during sand production.

4.2.1.4 Sand Concentration or Sand Cut

The sand cut is the incremental volume of sand produced (see equation 3-22 in section 3.3.4.2) with respect to the volume of slurry produced and was calculated using the following expression:

$$C_s = \frac{\left(\frac{dm_{sp}}{\rho_s}\right)}{\left(\frac{dm_{sp}}{\rho_s}\right)+\left(\frac{dm_o}{\rho_o}\right)}*100 \qquad \text{4-14}$$

4.2.2 <u>History of a Typical Sand Production Experiment Under Confining Stress</u>

4.2.2.1 Silica Well Sorted Sand: Test 3

Test 3 was carried out with the Silica Well Sorted sand using a 1.016 mm (0.040 in) slot size. The confining stress in this experiment was 1,000 kPa. Figure 4-4 to Figure 4-7 show cumulative sand production and sand cut versus time, permeability versus time, pressure gradient versus time, and stress versus time for each flow rate evaluated, respectively. Table 4-4 and Table 4-5 show the properties of the sand pack before and after the experiment and the sand produced during the experiment. The results for the other tests are also shown.

The run was started with the pack close to atmospheric pressure. The plug was removed from the slot and almost simultaneously the flow rate was increased to the initial flow rate corresponding to this slot size; i.e. 25 cc/h (Table 3-13). According to the material balance a small amount of sand was produced during the period of injection at this flow rate (14 g). This was confirmed from the produced sample, which contained a small amount of sand at the bottom of the container. However, during this injection period, the sand contained in the produced slurry could not be detected. A visual examination of the slurry did not identify the presence of any sand. Moreover, when a sample of the slurry was spread on a glass plate with a spatula, no sand was detected. These observations indicated the difficulty in detecting the presence of sand at small sand cuts (~ 0.6 % average and peak sand cuts between 1-3% as shown in Figure 4-4) when heavy oil is used.

Since only a small amount of sand was produced at the initial flow rate, the flow rate was increased to the next selected level (37 cc/h, see Table 3-13). At this new flow rate a similar behaviour was found; a relatively small amount of sand produced (10 g in 23 h, see Table 4-5) with low sand cuts (~ 0.5.% average and peak sand cuts between 1-3% as shown in Figure 4-4). Moreover, no significant changes were observed in the permeability of the pack as shown by the flat straight line from the initial value in the permeability vs. time graph (Figure 4-5). This is true for both the permeability of the pack and the permeability around the slot.

The flow rate was then increased further to the last selected flow rate (Table 3-13). The new flow rate was 74 cc/h. Under this condition no significant change in sand production and in the sand cut behaviour was observed (see Table 4-5 and Figure 4-4). The permeability remained constant.

It can be suggested that the variations observed in the sand cut profile correspond to the dynamic sequence of formation and destruction of sand arches in the vicinity of the slot, assuming that sand arching is the main mechanism that stops sand production. The fact that relatively small amounts of sand were produced during these three flow rates indicates that the sand arches were broken but able to rebuild and remain stable during the process.

Given that no enhancement in the properties of the sand pack were found until this point, it was decided to increase the flow rate until enough sand was produced to cause changes in the permeability of the sand pack. Thus, the flow rate was arbitrarily raised, first to 100 cc/h where no significant changes were registered and later to 148 cc/h. At this last flow rate, and after 6 h, the first significant sand production episode occurred (see Figure 4-4). Sand started to be produced and did not stop until the end of the test. The permeability also peaked right after sand production started (Figure 4-5). The calculated permeability values after this point were more than three orders of magnitude higher than the original permeability.

The pressure gradient data is presented in Figure 4-6. The ports at which the pressure gradients were measured are shown in Figure 3-17. The pressure gradient profiles shown tracked one another closely at each flow rate. Moreover, the magnitude of the pressure gradients becomes higher as the slot was approached except for the pressure gradient $(dp/dL)_{8,9}$ which is measured along the length of the slot. As the slot is further approached the flux of oil increases which explains the higher pressure gradients $(dp/dL)_{10,9}$ and $(dp/dL)_{11,slot}$. The magnitude of the pressure gradient $(dp/dL)_{8,9}$ was much smaller than at other locations within the sand pack. This result is evidence of little or no fluid flow along the horizontal plane next to and parallel to the slot. The lower pressure gradients (i.e. lower driving force) along that direction meant that little flow was occurring in the transverse direction, even in the region near the slot. There could be cases in the field where horizontal permeability could be much larger than the vertical permeability. As such, flow in the horizontal plane parallel to the slot could be significant. In such a case, the pressure gradient in the transverse direction might behave slightly differently from what was observed in the experiments.

The pressure gradient follows a staircase type of behaviour. It increased right after the flow rate is raised and then stabilized and remained practically constant during the duration of the step. The small amount of sand produced seems to have little impact on the measured pressure gradients. The pressure gradients suddenly decreased to values close to zero after massive sand production occurred in the last flow rate. The low pressure and pressure gradient readings along the cell are indicative of a high permeability zone or channel.

The drop in pressure gradient with time can be explained by referring to the analytical model of Geilikman et al.[90] or the flow of oil and sand into a vertical well as described in the book by Charlez [30]. In this model, as sand is produced massively with the oil a remolded zone of higher porosity, ϕ_y, is created. The difference between the oil velocity, v_o, and the sand velocity, v_s, is given from Darcy's law by:

$$v_o - v_s = -\frac{k_y}{\mu_o}\frac{\partial p}{\partial r} \qquad 4\text{-}15$$

Therefore the pressure gradient in the yielded zone will be given by:

$$\frac{\partial p}{\partial r} = -\mu_o \frac{(v_o - v_s)}{k_y} \qquad 4\text{-}16$$

where k_y is the permeability of the yielded region. Equation 4-16 indicates that as the sand is mobilized, and the difference between the oil velocity and the sand velocity is reduced, the pressure gradient will decrease.

The velocities v_o and v_s are related to the oil and sand flow rates Q_o and Q_s respectively by [90]:

$$Q_o = S_s \phi_y v_o \qquad 4\text{-}17$$

$$Q_s = S_s(1 - \phi_y)v_s \qquad 4\text{-}18$$

where ϕ_y is the porosity of the yielded region and S_s is the surface area of the slot. At the very start of massive sand production, considerable changes in the porosity can occur. If the porosity within the sand pack stabilizes then the sand flow rate in the yielded region will be the same as the sand flow rate produced out of the slot. Therefore:

$$Q_o = \phi_{slurry} Q_i \qquad 4\text{-}19$$

$$Q_s = (1 - \phi_{slurry})Q_i \qquad 4\text{-}20$$

where ϕ_{slurry} is the porosity of the produced slurry and Q_i = injection flow rate. The pressure gradient can then be written as:

$$\frac{\partial p}{\partial r} = \frac{\mu_o}{k_y}\left[\frac{\phi_{Slurry}Q_i}{S_s\phi_y} - \frac{(1-\phi_{Slurry})Q_i}{S_s(1-\phi_y)}\right] \qquad 4\text{-}21$$

Rearranging equation 4-21 leads to:

$$\frac{\partial p}{\partial r} = -\frac{\mu_o}{k_y}\frac{Q_i}{S_s}\left[\frac{\phi_{slurry} - \phi_y}{\phi_y(1-\phi_y)}\right] \qquad 4\text{-}22$$

This equation shows that the pressure gradient decreases when the difference ϕ_{slurry}-ϕ_y decreases and/or when the permeability k_y increases. Alternatively, for a given pressure gradient, the permeability k_y increases as the difference ϕ_{slurry}-ϕ_y decreases [13,91].

Figure 4-7 shows the stress distribution in the sand pack as calculated using equations 4-11 to 4-13. The confining stress and the total stress are also included in the graph. The effective stress profiles reflect the change in pore pressure that occurred after each flow rate change. They decrease as the flow rate increases. Also the axial stress is the smallest effect stress shown in Figure 4-7 since the pore pressure is greatest at the top of the pack. The sudden peak observed on both the total and effective vertical stress is due to a decrease in the cross-sectional area of the pack due to the massive sand production observed and the growth of a high-permeability channel above the level of the total stressmeter. The confining stress remained constant during the test until the massive sand production made the rubber membrane collapse. Shortly after this event, the test was stopped.

After the test was stopped, the sand pack was excavated. The top of a channel was found 6 cm below the top of the cell. The channel was not centered along the axis of the pack but a bit lateral to it. The porosity around the channel was determined from samples taken at different locations in the sand pack. The Dean-Stark technique was used in the analysis. The results are shown in Table 4-4. The porosity obtained from the samples taken at the top and the middle of the pack was close to the original porosity. However, the samples taken at the bottom of the sand pack yielded a higher porosity. It is believed that the samples taken at the bottom of the pack contain part of the slurry still present in the high permeability channel. Results from the other sand production tests and the CT scanner visualization tests confirmed that outside the channel the porosity of the pack remained largely unchanged.

4.2.2.2 Silica Poorly Sorted Sand: Test 6

Test 6 was carried out with the Silica Poorly Sorted sand using a 1.42 mm (0.056 in) slot size. The confining stress in this experiment was 2,500 kPa. Figure 4-8 to Figure 4-11 show cumulative sand production and sand cut versus time, permeability vs. time, pressure gradient versus time, and stress versus time for each flow rate evaluated, respectively. Table 4-4 and Table 4-5 show the properties of the sand pack before and after the experiment and the sand produced during the experiment.

The wide grain size distribution and the presence of more than 5% by weight of fines in this sand made the handling of the experiments somewhat more challenging than for the Silica Well Sorted sand. The first characteristic observed with this sand was the low permeability of its sand pack (see Table 3-8). The low permeability of the sand pack for the Silica Poorly Sorted sand is most likely due to the wide grain size distribution and the presence of fines in the sand. Consequently, the sand packs made with this sand have a lower injectivity than the other sands in the study. As a result, they require a higher injection pressure (and therefore a higher pore pressure inside the pack) to achieve the same fluid injection rate. To preserve the integrity of the sand pack, to avoid fracturing for example, the confining pressure must always be set above the maximum pore pressure in the pack. Therefore, it was necessary to raise the confining pressure in the experiment with the Silica Poorly Sorted sand as the fluid injection rate was increased. For example, the confining stress for the second flow rate evaluated in this experiment had to be increased from 1,000 to 2,500 kPa to keep the confining stress sufficiently above the pore pressure. For the last three flow rates evaluated in this experiment, the confining pressure continued to be raised as the injection pressure was increased to increase the fluid injection rate (see Table 4-7).

Figure 4-8 shows the cumulative sand production and sand cut as a function of time. Once again, it was not easy to detect the presence of sand in the production stream. The first impression from the experiment was that just trace amounts of sand were produced. The pressure and pressure drop behaviour of the pack during the experiment did not show significant changes. Therefore, to promote the sand production, the fluid injection rate was increased until the pressure limit of the physical model was approached. The fluid injection rates were increased from 17 cc/h to 150 cc/h (refer to Table 4-7), equivalent to a range of fluid velocities between 16 cm/h and 138.40 cm/h.

After analyzing the data from the experiment, it was found that some sand had been produced during the initial two flow rates. For example, 21 g of sand were produced during the first flow rate period (~ 22 h). The average sand cut was about 2%. The sand cuts at the end of this period peaked and varied from 3 to 12.5%. For the second flow rate, the amount of sand produced was higher, approximately 55 g. However, this amount of sand was produced over a longer period of time, 65 h. The average sand cut was 0.85% with sand cut peaks between 4 to 6%. Sand production hardly occurred after these two flow rates (see Table 4-5 and Figure 4-8) although the flow rate was increased four more times, to a maximum of about 4.5 times the second flow rate. Therefore, it can be assumed that the arches/bridges formed were quite stable.

Figure 4-9 shows the permeability behaviour as a function of time for experiment 6. During the first flow rate period the permeability profiles track one another. The permeability around the slot was higher than the permeability in the pack. A drop in the permeabilities can be observed at the end of the first flow rate period although some sand was produced. During the period of the second flow rate (34 cc/h), the permeabilities leveled off to a value close to the original permeability of the pack (~ 0.4 Darcies). Then, both permeabilities increased at a time that coincides with the sand production reported during this period.

For the next flow rate, i.e.51 cc/h, the permeabilities slightly increased although only a tiny amount of sand was produced (2 g). A surge in the permeability around the slot was observed for the subsequent flow rate of 76 cc/h (see Figure 4-9). However, this permeability variation does not seem to be permanent: when the flow rate was increased again to 101 cc/h, the permeability around the slot dropped, although not to the previous level. The peak in the permeability around the slot and the variability observed in the permeability of the pack during the period of the 76 cc/h flow rate is possibly due to the migration and production of fines near the slot since no sand production occurred at this flow rate.

In general, it can be hypothesized that the movement and production of fines jointly with the small amount of sand produced in the experiment are responsible for the permeability increases observed during the experiment. However, the observed improvement in the permeability (from 0.4 to 0.8 Darcies, refer to Table 4-5) is not likely to be sufficient to enhance oil production rates.

Figure 4-10 shows the behaviour of the pressure gradients as a function of time. The pressure gradients within the sand pack began to increase when oil injection began. The pressure gradients continued to build up even during the period of sand production, probably due to the limited flow of sand through the slot. The pressure gradients levelled off after some time and remained constant for the duration of the first flow rate (17 cc/h). The pressure gradients then increased due to the increase in flow rate (34 cc/h). However, after reaching a maximum, the pressure gradients close to the slot declined. The decline in the pressure gradients coincided with the period of sand production.

When the flow rate was increased again, to 51 cc/h, the pressure gradients near the slot increased initially and then dropped slightly while the pressure gradient in the middle of the sand pack increased initially and then remained constant. During this flow rate just 2 g of sand were produced. This sand was produced at the same time as the drop in pressure gradient near the slot occurred. It is possible that this small amount of sand production (perhaps including the production of fines) may have reduced the pressure drop around the slot. Since the amount of sand produced was small, the pressure drop in the middle of the pack was not affected. As discussed above, the drop in the pressure gradients around the slot during the 76 cc/h flow rate could be attributed to the production of fines since sand production was not observed during this period. The fact that the pressure gradient inside the pack followed the usual behaviour of increasing in magnitude when the flow rate was raised supports this hypothesis. The flow rate was increased twice more to 101 and 150 cc/h in an attempt to find out if sand could be produced continuously from this pack; it could not. The pressure transducers and pressure drop transducers were out of range under these conditions.

Figure 4-11 shows the effective stress distribution in the sand pack for experiment 6. The confining stress and the total stress are also included in the graph. The first thing to notice is the increase in confining stress from the first flow rate (17 cc/h) to the second flow rate (34 cc/h). As noted above, the confining stress had to be increased to preserve the integrity of the sand pack when the fluid injection rate was increased. For the subsequent flow rates of 34 cc/h and 51 cc/h, the effective stress profiles reflect the changes in pore pressure that occurred after each flow rate change (similar to experiment 3 with the Silica Well Sorted sand). The effective stress profiles decreased as the flow rate increased. In the next stage of the test (76 cc/h), both the pore pressure and the confining pressure were increased. The net effect was an increase in effective stress. For the remaining two flow rates, it was not possible to record much information. Many of the absolute pressure transducers were out of range under these conditions.

An inspection of the pack after the experiment did not indicate the presence of either a dilated zone or a high permeability channel. This observation is supported by the analysis of samples taken from the pack following the experiments. There was no evidence of significant porosity changes in these samples (see Table 4-4). However, a higher porosity was estimated using the Carman-Kozeny correlation. These porosity values were computed from the permeabilities obtained at the end of the tests. The results obtained from the Carman-Kozeny correlation in this case may not be very accurate. It is possible that the permeability improvement is due mainly to the production of the finer sand fractions; the Carman-Kozeny correlation does not take this into account.

4.2.3 Critical Pressure Gradient Analysis for Sand Production

In addition to the formation strength and in situ stresses, a successful sand production strategy must take into consideration the drag forces that may develop in the reservoir during the oil production process. The literature contains a significant body of work on the formulation and assessment of different models for sand failure and production that take into account drag forces [55,56,47].

In the analysis of the results of this experimental study on sand production through slots, the estimated pressure gradient at the slot as calculated from equation 4-6 will be used to determine the critical pressure gradient required for the initiation of sand production and the critical pressure gradient required for the onset of continuous sand production. The pressure gradient at the slot is used to select these critical pressure gradients associated with sand production since it is the largest pressure gradient involved in the process (see the discussion below) so it should present the greatest hurdle to sand production.

Table 4-6 shows that the critical pressure gradient at the slot for the initiation of sand production $(dp/dL)_{isp}$ varied between 0.27 and 1.79 MPa/cm for the Silica Well Sorted sands. For continuous sand production, the critical pressure gradient $(dp/dL)_{csp}$ spanned a range from 0.22 to 2.58 MPa/cm.

The critical pressure gradient for initiation of sand production for the Silica Poorly Sorted sand was much higher (by one order of magnitude) than for the Silica Well Sorted sand. For this sand continuous sand production was not achieved.

There are two other pressure gradients involved in the process of sand production that should be considered. One is the pressure gradient at the edge of the cavity/tip of the channel $(dp/dr)_{AH}$; the second one is the pressure gradient needed to transport the failed sand alone the cavity /channel to the slot.

The pressure gradient to transport the sand is the smallest of the three pressure gradients that have been identified. It has been estimated to be on the order of 2-10 kPa/m [91].

This is at least four orders of magnitude smaller than the least of the critical pressure gradients through the slot.

The third pressure gradient is the one calculated at the edge of the cavity $(dp/dr)_{AH}$. Such a cavity is assumed to be created by a small amount of initial sand production. This last pressure gradient has been estimated for all of the sand production experiments (under confining stress) discussed in this section using the procedure described in section 4.2.1.3 (see equation 4-7). The results are presented in Table 4-6. For both sands, $(dp/dr)_{AH}$ is about two orders of magnitude smaller than the critical pressure gradient through the slot for the initiation of sand production $(dp/dL)_{isp}$.

Another way of evaluating the pressure gradient at the edge of the cavity is to compare it with the critical pressure gradient estimated from the Bratli and Risnes criterion (see equation 4-9). To calculate the critical pressure gradient estimated from the Bratli and Risnes criterion, the unconfined compressive strength of the sands measured from the sand strength experiments was used (see Table 4-9). Further, the radius of the arch was estimated from the volume of initial sand production using expression 2-11 as outlined in section 4.2.1.3. The estimated arch radii are shown in Table 4-6. Interestingly, the critical pressure gradient from the Bratli and Risnes criterion is very close to the estimated pressure gradient at the edge of the cavity (see Table 4-6). On the whole, the differences between the estimated pressure gradients at the edge of a cavity for these sand production experiments with the critical pressure gradients predicted by the Bratli and Risnes criterion are much smaller than the differences that have been reported in the literature for sand production experiments with perforations [13,56,81].

In most of the experiments discussed here, the critical pressure gradient calculated using the Bratli and Risnes criterion was a bit larger than the estimated pressure gradient at the cavity when sand production had not yet been initiated, and a bit smaller than the estimated pressure gradient at the cavity when sand production was being initiated. There was one exception to this trend for the Silica Well Sorted sand that is within the margin of uncertainty for both the estimation of the pressure gradient at the cavity and the predicted critical pressure gradient from the Bratli and Risnes criterion. In this case, the critical pressure gradient obtained from the Bratli and Risnes criterion was a bit larger than the estimated pressure gradient at the cavity even though sand production was being initiated.

There were also two other cases, for sands that were not well sorted, in which the relationship between the estimated pressure gradient at the edge of a cavity and the critical pressure gradient calculated using the Bratli and Risnes criterion did not match the observed sand production behaviour. For the experiment with the Silica No Large Fractions sand the estimated pressure gradient at the edge of the cavity was about 25% larger than the critical pressure gradient from the Bratli and Risnes criterion prior to the initiation of sand production. On the other hand, for the Silica Poorly Sorted sand in which sand production was initiated the critical pressure gradient from the Bratli and Risnes criterion was much larger than the estimated pressure gradient at the edge of the cavity.

As a final point of interest, in three of the experiments with well sorted sands the critical flow rate obtained from the Bratli and Risnes criterion (see equation 4-10) is very close to the experimental flow rate at which sand production was initiated. In two other experiments with well sorted sands, the critical flow rate from the Bratli and Risnes criterion was reasonably close to the experimental flow rate at which sand production was initiated, given the discrete steps at which the flow rate was increased in the experiments and the uncertainties in estimating the parameters (particularly the radius of the arch) in the Bratli and Risnes criterion. In the remaining two experiments with well sorted sands, the critical flow rate from the Bratli and Risnes criterion is significantly greater than the experimental flow rate at which sand production was initiated; this implies that the Bratli and Risnes criterion may have overpredicted the critical pressure gradient for sand failure at the edge of a cavity in these experiments. Overall, the results of the experiments with well sorted sands indicate that the critical pressure gradient for sand failure at the edge of the cavity may have required a fluid injection rate that is fairly similar to the fluid injection rate required to achieve a critical pressure gradient at the slot. Consequently, in the experiments with well sorted sands, the critical pressure gradient for sand failure at the edge of the cavity may play a role that is at an equal level of importance with that of the critical pressure gradient at the slot as a limiting factor for sand production

For two of the experiments with the Silica Poorly Sorted sand, the critical flow rate given by the Bratli and Risnes criterion is one order of magnitude smaller than the largest experimental flow rate tested in the experiments, for which no sand production occurred. This suggests that in these experiments the critical pressure gradient at the slot is the limiting factor for sand production, rather than the critical pressure gradient for sand failure at the edge of a cavity within the sand pack.

From this analysis, it appears reasonable to have selected the estimated pressure gradient at the slot as the basis for determining the critical pressure gradient required for the initiation of sand production and the critical pressure gradient required for the onset of continuous sand production. Furthermore, it appears that the Bratli and Risnes criterion for predicting sand failure at the edge of a cavity is consistent with the pressure gradients at the edge of the cavity estimated from the experiments.

4.2.4 Effect of Velocity and Slot Size

The effect of fluid velocity on sand production through perforations has been studied extensively. The results presented in the literature show that the fluid flow rate is a factor in determining arch size and stability. Furthermore, the transport of failed sand is sensitive to the flow rate. Flow rate variations can have significant effects on the producing characteristics of unconsolidated sand reservoirs [54,61,63,67].

Arch stability is also strongly dependent on the size of the openings (perforations/slots). Larger openings require larger grains to form stable arches. The selection of opening diameters is used as a sand production control design strategy [49,58].

The results of the experiments investigating the effects of slot size and fluid velocity (Table 3-12 and Table 3-13) on sand production during heavy oil production will be described in this section. The experiments were conducted using the Silica Well Sorted sand and the Silica Poorly Sorted sand, single slotted plates with different slot sizes (see Table 3-12), and dead heavy crude oil. The sand packs were water wet and subject to constant confining pressure. For each of the two sands used in the study, a water-saturated sand pack was generated to measure the absolute permeability to water (k) for each sand. The results of the absolute permeability measurements are reported in Table 3-14.

4.2.4.1 Silica Well Sorted Sand

A total of four experiments with the well sorted sand were performed investigating the effect of slot size on sand production, using slot sizes of 0.711, 0.813, 1.016 and 1.422 mm (0.028, 0.032, 0.040 and 0.056 in). In these experiments, fluid velocities ranged from 16 cm/h to 376 cm/h. The confining stress was kept constant at 500 kPa. Sand production was recorded as a function of time.

The physical properties of each sand pack before the sand production experiments started are presented in Table 3-8. The porosity and the pore volume varied within relatively narrow intervals, 39.5 to 41.3% and 3,600 to 3,700 cc respectively. However, the effective permeability to oil had a wider variation, ranging from 3.5 to 7.5 darcies. The average oil saturation was 93.1% while the average water saturation was 6.9% (see Table 3-8).

Slurry samples were collected and cleaned, as were samples taken from the area around the slot for each sand pack following the completion of the experiment. The mass of produced sand in the slurry samples and the porosity of the sand pack samples were determined using the Dean-Stark method. The presence of a high permeability channel was usually observed when sand production occurred. A summary of the results are presented in Table 4-5. Usually a test was stopped when the rubber membrane collapsed due to sand production or when the channel reached the top of the pack as indicated by an abrupt decrease (essentially to zero) in the pressure drop between the injection and production ends of the sand pack (caused by pressure communication between the injection and production ends).

The effect of the slot size and pressure gradient (fluid velocity) on sand production behaviour for the well sorted sand is presented as an operation-completion graph in Figure 4-12. There are two trend lines in the pressure gradient vs. slot size graph. The lower trend line represents the pressure gradients at which sand production was initiated in each test while the upper line represents the pressure gradients at which continuous sand production was maintained. These two lines divide the graph into three zones. The first zone can be identified as the sand production free zone. The second zone is the sand production initiation zone. Within this zone, a delicate equilibrium between "sand production on demand" and massive sand production would occur. The third zone is the massive sand production zone. In this area, once sand production started, it could not be stopped.

In the sand production experiment with the smallest slot size (0.711 mm/0.028 in), sand production was mechanically induced but then it stopped. During this first experiment synthetic reservoir water was used. The slot plug was oxidized by the salty water. Consequently, the plug got stuck inside the slot. After the slot was opened no sand production was observed for the first 3 h. The injection pressure was higher than expected. Hence, it was thought that small pieces of the plug were still inside the slot. To verify that the slot was clean, a knife was used to gently sweep any external particles that could be obstructing the slot. The process was repeated more than once. Sand started to be produced after repeating this procedure for the third time. Apparently, nothing was blocking the slot. It seemed that the sand was able to bridge or arch. These arch/bridges must have been quite stable since the mechanical disturbance had to be applied more than once before sand production started. Following the initial limited sand production at a flow rate of 51 cc/h, the flow rate was dropped to 26 cc/h. The sand was able to arch at this flow rate. The arches remained stable for the rest of the experiment. A much higher flow rate (204 cc/h)/pressure gradient was required to re-start sand production; at this pressure gradient continuous sand production was maintained (see Figure 4-12 and Figure B-17 in Appendix B-1).

When sand production occurred, a channel and/or a dilated zone formed (see Figure 4-13). The dilated zone usually had an elliptical shape, possibly due to the flow regime induced by the presence of the slot (Figure 4-13c). The porosity of this dilated zone was higher than the original porosity (see Table 4-4).

Different actions were taken to try to stop sand production. In one approach, the flow rate was decreased. This did not cause sand production to be reduced. In the second approach, oil injection was stopped and re-started again at a lower flow rate. However, the results were the same; the pack continued to produce sand. These observations suggest that in order to control and manage sand production in well sorted sands, the focus should be on slot sizes that are at the lower end of the interval identified in equation 3-11.

4.2.4.2 Silica Poorly Sorted Sand

To investigate the effect of the slot width on the production of the Silica Poorly Sorted sand, three slot sizes were proposed (see Table 3-12): 1.422, 1.702, and 1.981 mm (0.056, 0.067, and 0.078 in respectively). The experiments with the 1.422 and 1.981 mm slot sizes were performed first. It was observed that bigger slot sizes need to be employed to have continuous sand production using this poorly sorted sand under the experimental conditions that were selected for this study. Therefore, the intermediate size (0.702 mm) was not evaluated; instead a 5.944 mm (0.234 in) slot was used (see Table 3-12).

The physical properties of the sand packs before the sand production experiments started are presented in Table 3-8. The pore volume and porosity of the packs were quite similar in these three experiments, as in the case of the experiments with the well sorted sand. Note that the effective permeability to oil was relatively low for these sands (between 0.4 and 0.7 Darcies). This is lower than typical permeabilities of unconsolidated heavy oil reservoirs in western Canada (usually 2-5 Darcies). This was probably due to the wide grain size distribution of the sand and/or the relatively high content of the finer fractions (less than 90 μm) in the sand.

The initial confining pressure for the experiments was set at a relatively high level (2,500 kPa), as a consequence of the relatively low permeability of the sand packs. A confining pressure at this level was required in order to exceed the injection pressure needed for the flow rates that were selected initially in the first two tests. The fluid velocities in the tests ranged from about 3 cm/h initially to as high as 138 cm/h ultimately, depending on the slot size (see Table 4-7). To preserve the integrity of the pack, the confining pressure was increased once the pore pressure started to approach the 2,500 kPa initial confining pressure as shown in Table 4-7. To promote continuous sand production, fluid velocities were increased until the pressure limit of the physical model was approached in the case of experiments 6 and 7 (see Table 4-7). Sand production was not significant in either experiment. Therefore, a bigger slot size was evaluated. The new slot size was three times larger than the last size evaluated; i.e. 5.94 mm (0.234 in). Continuous sand production was observed from the beginning of the test at a relatively low pressure gradient, 0.381 MPa/cm (see Table 4-6). During the first flow rate, the arches broke and reformed several times as indicated by the periods of zero sand production and continuing sand production. This behaviour was observed throughout the whole test.

The experiment was carried out for 14 days. Since the perception was that just small amount of sand were being produced, the flow rate was increased nine times during the duration of the experiment. The average sand cut was 1.4 % with rare episodes of sand cut peaks of 10% (see Figure 4-14). At the end of the experiment, it was discovered that a narrow high permeability channel had been created in the sand pack during the experiment. A cast of the channel is shown in Figure 4-15. An important inference can be made from this test. The production of sand at relatively low and steady sand cuts for a long period of time might bring two benefits; a way to transport the sand out of the well and the creation of high permeability channels that can improve the production of the reservoir. Although the Silica Poorly Sorted sand does not represent a typical heavy oil sand due to its rather wide grain size distribution, it might be possible to find similar behaviour for other sands that are more well sorted if the correct slot size is chosen. In the case of the Silica Well Sorted sand this behaviour might have been induced for the first two slot sizes tested (0.711 mm/0.028 in and 0.813 mm/0.032 in) had the flow rate changes been made in smaller intervals as they were in experiment 14 for the Silica Poorly Sorted sand.

Figure 4-16 shows the operation-completion design map for controlled sand production in horizontal wells for the Silica Poorly Sorted sand under the conditions studied. As in the case of the Silica Well Sorted sand different zones can be identified. The first zone is at the far left of the graph and is the sand production free zone. It corresponds to slot sizes less than 1.981 mm (0.078 in) and pressure gradients less than 16 MPa/cm. Opposite to this zone, on the far right of the graph, the massive sand production zone is located. It corresponds to slot sizes bigger than 5.944 mm (0.234 in) at any pressure gradient. The area in between the two zones is less well defined. It was sub-divided into two regions: in the upper zone there is a possibility that sand production could be continuous and massive, while in the lower zone it was unlikely that sand production could be initiated. These regions were identified as a “Probable Massive Sand Production Area” and a “Probable Sand Production Free Area” on the operation-completion design map, since they were not explored in these experiments.

These observations suggest that in order to control and manage sand production in poorly sorted sands, the focus should be on slot sizes that are at upper end of the interval identified in equation 3-11. Also, continuous sand production at low sand cuts (less than 1.5 %) can be achieved if the initial flow rates are low (corresponding to a fluid velocity of 2.70 cm/h) and are later increased in small increments. In this manner there is an opportunity to transport the sand produced by the heavy oil and at the same time generate zones (channels) with high permeability.

No porosity changes were observed in the sand pack with the Silica Poorly Sorted sand from experiment 14 outside the channel using the Dean-Stark method (see Table 4-4). Due to the very limited sand production, the sand packs from experiments 6 and 7 did not show significant porosity changes either (see Table 4-4).

4.2.5 Effect of Grain Size Distribution

Meza et al. [41] reported a previous experimental investigation of the flow of oil and sand into a horizontal well slot. Among other parameters they studied the influence of the grain size distribution on sand production. They used three types of sands in their study: a Silica Well Sorted sand named Sil-1, a reservoir sand (Husky Sand) and two sands made of glass beads.

The difference in sand production behaviour between the Sil-1 sand and Husky sand was thought to be mainly due to differences in grain size distribution. The hypothesis was that either the finer particles or the largest particles were responsible for the difference in sand production between the Husky and Sil-1 sands. After performing experiments with the glass bead sands, one of which contained a fraction finer sizes, they concluded that particles with greater average diameter have a more significant influence on the formation of arches/bridges.

In their study Meza et al. [41] emphasized the importance of the slot width to effective sand grain diameter ratio (SW/D_i) as an important parameter in the investigation of sand production through the slots. They calculated the effective diameter D_i for various percentiles (by weight) of these sands and determined this ratio (SW/D_i) for each sand. They observed, in comparing the Sil-1 and Husky sands, that the slot width to grain diameter ratio was smaller for the Sil-1 sand for all effective diameters except the $D_{99.9}$ diameter.

One of the goals of this research is to investigate further the role of the grain size distribution on sand production with a more realistic fluid system; i.e. heavy crude oil and irreducible water saturation and with synthetic sands having the same D_{50} (200 μm) but different size distributions (see section 3.1.2 and Figure 3-2). Thus the Silica Well Sorted sand, the Silica No Large Fractions sand, the Silica No Fine Fractions sand and the Silica Poorly Sorted sand were evaluated.

Although the Silica Poorly Sorted sand had a lower permeability than is typical of unconsolidated heavy oil reservoirs in western Canada, it represents the other side of the spectrum in grain sorting. This sand was selected to investigate the effect of a wide grain size distribution on sand production.

The results of the experiments investigating the effect of slot size on sand production indicated that the well sorted sands and the poorly sorted sands behaved quite differently. In these experiments, the experimental conditions were not identical. The wide grain size distribution and the presence of more than 5% by weight of fines in the Silica Poorly Sorted sand made the conditions of the experiments somewhat different than the experiments with the Silica Well Sorted sand. The first difference observed was the permeability of the sands. The absolute permeability of the Silica Well Sorted sand was about 20 Darcies while for the Silica Poorly Sorted sand the absolute permeability was about 1.4 Darcies (See Table 3-14). The second difference was the injectivity of the pack and the effective permeability to oil. The effective permeability of the sand packs prepared with the Silica Poorly Sorted sand ranged from 0.4 to 0.7 Darcies while the effective permeabilities of the sand packs with the Silica Well Sorted sand were between 4 to 7 Darcies. The low injectivity of the Silica Poorly Sorted sand packs meant that the tests could not be performed at the same confining pressure selected for the standard tests of the Silica Well Sorted sand. The actual confining stress selected to perform the Silica Poorly Sorted sand experiments was five times higher, at 2,500 kPa.

Consequently, it was decided to perform an experiment with the Silica Well Sorted sand under the same experimental conditions as one of the experiments with the Silica Poorly Sorted sand. A slot size of 1.422 mm and a confining pressure of 2,500 kPa were chosen for this experiment. The initial flow velocity was 15.68 cm/h, as in the test with the Silica Poorly Sorted sand. Figure 4-17 presents the results obtained from the comparative tests. In the case of the well sorted sand, sand was produced from the beginning. The test was stopped 19 hours after being initiated due to the collapse of the rubber membrane. In the case of the poorly sorted sand, just a few grams of sand were produced, although the flow velocity was increased to more than eight times its original value (see Table 4-5 and

Table 4-7). A detailed description of this experiment was given in section 4.2.2.2. Figure 4-8 and Figure 4-18 show the cumulative sand produced and the sand cuts for each sand.

Figure 4-19 and Figure 4-20 show the cumulative sand production and the sand cut for the other two sands evaluated. The experiments were performed under the same conditions; i.e. at a confining stress of 2,500 kPa confining stress, a slot size of 1.422 mm (0.056 in) and an initial fluid velocity of 15.68 cm/h.

The Silica No Fine Fractions sand was produced from the beginning, as in the case of the Silica Well Sorted sand. The sand cut and the sand production behaviour were quite similar (see Figure 4-18 and Figure 4-19). The original porosity of each sand pack was also similar (see Table 4-4). However, the permeabilities were different. The permeability of the Silica Well Sorted sand was more than twice the permeability of the Silica No Fine Fractions sand (i.e. 5.75 vs 2.04 Darcies, see Table 4-4). The difference in permeability between the two sands yields a different critical pressure gradient for continuing sand production. Consequently, the calculated critical pressure gradient for continuing sand production for the Silica No Fine Fractions sand (0.64 MPa/cm) was almost three times bigger than the one for the Silica Well Sorted sand (0.22 MPa/cm) as shown in Table 4-6.

On the other hand, the Silica No Large Fractions sand behaved similarly to the Silica Poorly Sorted sand. The characteristics of the pack (porosity and permeability) were also similar as shown in Table 4-4 (experiments 6 and 15). As in the case of the Silica Poorly Sorted sand, small amounts of sand were produced during the first two flow rates in the test (see Table 4-5 and Figure 4-20). The sand cuts were also relatively low, ~0.85 and 1% for each flow rate respectively. However, there was an important difference. Continuing sand production was achieved with the Silica No Large Fractions sand after a threshold fluid velocity of 93.18 cm/h was reached. Different actions were taken to try to stop the sand production, such as sudden decreases and increases in flow rate. However, none of these actions caused the sand production to stop.

After the experiment with the Silica No Large Fractions sand had been completed, a high permeability channel was discovered in the pack. It extended from the slot all the way to the top of the pack. It is reasonable to assume that if a more gradual increase in flow rate had been applied it would have been possible to produce sand in a more controlled manner.

Table 4-2 shows the slot width to effective grain diameter ratio (SWEGD) for various percentiles (by weight) of the sands used. The values reported in this table were calculated using the effective diameters presented in Table 3-3. From previous work [25], it was thought that the larger fractions of the sand had a decisive influence in the arching of the sand and consequently in stopping sand production. Although the large fractions may indeed be important, the results of this experimental work indicate that this fraction of the sand is not likely to be the only factor to be taken into consideration.

If we take as a criterion that the SWEGD must be less than 1.5 for the $D_{99.9}$ percentile in order not to produce sand, then this criterion works for the Silica Well Sorted sand. The ratio for this sand is 1.44 when a slot size of 0.711 mm (0.028 in) was used in the sand production experiment and 2.88 when a 1.422 mm (0.056 in) slot size was in place (see Table 4-2). Therefore, it will be hard to produce this sand with the 0.711 mm (0.028) slotted plate while it will be easier to produce with the 1.422 mm one. This was certainly observed.

The criterion also works with the Silica Poorly Sorted sand. A ratio of 1.48 with the 1.422 mm slotted plate indicates that the sand will be difficult to produce. This was observed. However, the criterion does not work in the case of the Silica No Large Fractions sand and the Silica No Fine Fractions sand. The Silica No Large Fractions sand has a SWEGD for the $D_{99.9}$ percentile of 3.058 with the 1.422 mm (0.056 in) slot size. This means that massive sand production should occur when the 1.422 mm (0.056 in) slot size is used. This was not the case. Extremely high fluid velocities had to be applied to achieve continuing sand production (see Table 4-5 and Table 4-7).

Quite the opposite was found with the Silica No Fine Fractions sand. This sand was massively produced from the beginning of the experiment at a fluid velocity of 15.68 cm/h with the 1.422 mm (0.056 in) slot size. This sand had a SWEGD for the $D_{99.9}$

percentile of 1.51 (Table 4-2). No meaningful correlation could be found between sand production behaviour and the SWEGD ratio at any of the effective diameters D_i presented in Table 4-2.

It seems that a wider grain size distribution has an important role in the formation of stable arches/bridges. To quantify the uniformity of the grain size distribution of a sand, the uniformity coefficient is used typically (see equation 3-5). The uniformity coefficients (C_u) of the sands used in this study are shown in Table 3-3. It seems that sands with a C_u bigger than 3 (the poorly sorted sands) are more difficult to produce.

In section 3.3.1 it was noted that no direct correlation could be found between sand production and the uniformity coefficient based on the air experiment results (see Figure 3-25). A sand like the Rounded No Larger Fractions sand with a C_u of 2.18 was entirely produced by gravity in the air experiment. According to the initial convention adopted in this dissertation, the Rounded No Larger Fractions is a poorly sorted sand ($C_u > 2$). No sand was produced in later air experiments performed with two other Silica Poorly Sorted Sands (see Table 4-1). These latter sands had uniformity coefficients of 3.41 and 3.55 (refer to Table 4-1); i.e. much broader grain size distribution. These results may indicate that it is more appropriate to take a limit of 3 for C_u for the category of well sorted sands instead of 2. Also, in the case of the results found in the air experiments, it might be possible that a C_u of 2.00 and a C_u of 2.18 are actually no different, and that there is indeed a correlation between sand production and the sorting of the sands. This discussion helps to highlight why there is not consensus in the literature as to what the value of C_u should be to classify the sorting of the sand.

In the case of this study, we basically have two types of sands. The poorly sorted sands are represented by the Silica No Large Fractions sand and the Silica Poorly Sorted sand with a C_u of 3.54 and 3.55 respectively. The well sorted sands are represented by the Silica Well Sorted sand and the Silica No Fine Fractions sand with a C_u 1.64 and 2.00 respectively. It is recommended to conduct a more detailed study with sands that present intermediate values of C_u, i.e. between 2 and 3, to have a more complete picture of the effect of C_u on sand production.

It is quite clear from the results found that the poorly sorted sands are much harder to produce than the well sorted ones. It is possible that the wide sand grain size distribution not only makes the sand arch more easily but it may also promote sand bridging. The slot may act like a filter whose porous material is the sand particles bridging inside.

Later in this thesis, in section 4.3, further discussions about the influence of grain sorting on sand production will be addressed. Those discussions will be focused on the link to the sand strength.

For all four sands, the Dean-Stark analysis of the sand packs after the experiment finished yielded the same result. No change in porosity outside the high permeability channel or affected zone (refer to Table 4-4) was detected.

4.2.6 Effect of Confining Stress

A series of experiments was conducted to study the influence of the effective stress of the formation on sand production behaviour through slots. A range of confining stresses was chosen; the following considerations guided the selection of the range of confining stresses in the experiments. Under field conditions, the effective radial stress increases monotonically from a value of zero at the slot entrance (sand face) to a far-field effective stress. For western Canadian heavy oil reservoirs, the far-field effective stress is likely to be in the range of 4 – 7 MPa. As sand is produced from a slot in the field, the sand matrix in the vicinity of the slot will undergo a deformation in response. Correspondingly, the effective radial stress in the vicinity of the slot will relax. The length scale over which these effects occur is likely to be on the order of centimetres (perhaps up to 50 cm) [70].

Since there is no difference in scale between the conditions in the sand production experiments and field conditions, the confining stress applied in the experiments should be representative of the effective stress in the field at a similar distance from the slot. From the discussion above, an appropriate boundary stress condition for the sand production experiments would be to apply a confining stress that relaxes from its initial value during the course of the experiment (as sand is produced through the slot).

Unfortunately, it is difficult to calculate this relaxation *a priori* (in general, it will be time-dependent). A simpler approach, and a suitable one, is to apply a fixed confining stress during a given sand production experiment. Several experiments were performed, with different fixed confining stresses over a selected range, to assess the influence of confining stress on the results of the sand production experiments.

The focus was on confining stresses below 1,000 kPa. This focus was based on the results of previous studies in which the stress distribution around a slotted liner under representative field conditions was estimated to be below 1,000 kPa. Initial analyses of the stress distribution and matrix deformation around a slotted liner were performed by Boone et al. [69], who examined the collapse of a heavy oil formation around a slotted liner as the result of a rapid depressurization of a horizontal well; however, these authors did not report the range of effective stresses around the horizontal well that they obtained from their calculations. Subsequently, their results were extended in a simulation study by Yuan [70]. In the latter study, the calculated effective radial stress in the vicinity of the well bore was below 1,000 kPa.

The selected values of confining stress for the current experimental study were 150, 500, 750, and 1,000 kPa. Another test using a confining pressure of 2,500 kPa was later added to the experimental matrix to cover a wider range of confining pressure values. Two slot sizes were used in the experiments: 1.016 mm (0.040 in) and 1.422 mm (0.056 in). In general, for a given slot size, the threshold fluid velocity (or equivalently, pressure gradient) required to produce sand decreased as the confining stress increased (see Figure 4-21). Also shown in Figure 4-21 are the results of two experiments that are out of the trend line (red points in Figure 4-21 (a)). This kind of behaviour is not unusual in sand production experiments, as has been reported by several authors [55,64]. As explained in section 4.1.1, trends instead of individual experiments must be analyzed to obtain conclusions from sand production experiments.

In the experimental literature on sand production through openings, mixed results on the influence of confining stress have been obtained. For example, Selby and Farouq Ali [61] found in their experiments that sand production increased when the overburden pressure was increased. They also found that it was easier for the sand to arch at low overburden loads. However, other authors [63,64] found that arch stability increased with increasing stress. There is a possibility that the apparent differences among these experimental results are caused by the choice of fluids, confining stresses, and experimental systems. For example, Cleary et al. [63] observed that the influence of confining stress in a kerosene/water system was not the same as in a mineral spirit/ water system. They believed that differences in capillary cohesion between the two fluid systems were responsible. Moreover, at lower confining stresses (within the range considered in the current study), the experimental results presented in Cleary et al. [63] appear to indicate that a reduction in the threshold velocity at which sand arches became unstable occurred. It was only at higher confining stresses that the opposite trend was observed.

A qualitative explanation of the influence of confining stress on sand production behaviour that was observed in the current study is presented below. The appearance of a small cavity in a sand pack, such as the one occurred after the removal of the plug from the slotted plate in the experiments (or after a well was completed in the field) causes a redistribution of stresses around it. The stresses in front of the cavity would tend to decrease since the sand can deform there more easily. Consequently, to balance the external stresses applied to the system, the stresses lateral to the cavity contour must increase. Eventually, the hoop stresses around the cavity would increase and the radial stresses decrease. The ratio of these effective stresses would be largest at the edge of the cavity in the direction of the smallest effective stress, so this is where shear failure of the sand matrix would occur first. The direction of the smallest effective stress is along the axis of the sand pack, on account of the pore pressure gradient generated by the injected oil. Consequently, growth of the cavity would tend to occur in this direction. Further, at higher confining stress the ratio of effective stresses would be higher at the edge of the cavity, leading more readily to failure of the sand arches there (i.e. under lower loading from fluid drag). This argument has some similarity to the arguments used to explain the phenomenon of borehole breakout.

4.2.7 Reservoir Sand Behaviour

The Husky sand was included in this study as an example of field sand. The slot selected for the experiment was 1.422 mm (0.056 in). This slot size is in the middle of the range provided by equation 3-13.

Figure 4-22 to Figure 4-25 show cumulative sand production and sand cut versus time, permeability versus time, pressure gradient versus time, and stress versus time respectively for each flow rate evaluated in the experiment performed with the Husky sand. Table 4-4 and Table 4-6 show the properties of the sand pack before and after the experiment and the sand produced during the experiment.

The initial flow rate was 17 cc/h, equivalent to a fluid velocity of 15.68 cm/h. The flow rate was decreased to 10 cc/h two hours later to preserve the integrity of the pack since the pore pressure was close to the confining pressure. Sand production started 10 h after the flow rate was changed. High sand cuts were observed from the beginning of the sand production period (see Figure 4-22). Sand did not stop for the duration of the experiment. The rubber membrane failed 90 h after the experiment started. The total amount of sand produced was 900 g (see Table 4-5).

Figure 4-23 shows the permeability of the pack as a function of time along the pack and around the slot. The permeability remains constant close to its initial value before sand production. The permeability starts to increase as soon as sand production begins. It continues increasing steadily as sand is produced during the first 10 h after sand production started. After this period it continues increasing but at a lower pace. The sudden drop and increase in the permeability occurred when the membrane first started to leak and ultimately failed. A high permeability channel was observed in the pack after the experiment was completed.

The behaviour of the pressure gradients as a function of time is shown in Figure 4-24. The behaviour observed is similar to what was observed in the other experiments with the Silica sands, i.e. the pressure gradients close to the slot are higher in magnitude than the pressure gradient inside the pack. The pressure gradients decreased dramatically when sand production started.

Figure 4-25 shows the effective stress distribution in the Husky sand pack. The behaviour follows the trend observed with the other tests. First the magnitude of the effective stress profiles drops due to the increase in the pore pressure. The effective stress profiles stay relatively constant until sand production starts. The peak in the total and effective vertical stress profiles coincide with the maximum peak in the sand cut (~ 80%, see Figure 4-22 and Figure 4-25). The stress profiles then increased as a consequence of the decrease in the pore pressure due to sand production. The total vertical and effective vertical stress profiles are the lowest among the four stresses profiles. It is clear that they were the most affected by the sand production, most probably because they are the ones that measure the stresses inside the pack rather than at the border of the pack like the axial and radial stresses.

An inspection of the sand pack after the experiment revealed the presence of a high permeability channel. According to the Dean-Stark analysis the porosity outside the channel did not experience any significant change as in the other experiments reported in this dissertation (see Table 4-4).

As in the case of the Silica Well Sorted sand, it might be necessary, in order to control and manage sand production with the Husky sand, to focus on slot sizes that are at the lower end of the interval identified in equation 3-13.

4.2.8 Size Distribution of the Produced Sand

Figure 4-26 to Figure 4-29 show the particle size distribution of selected sand production samples from different experiments. The analysis of the produced sand was performed to investigate if certain fractions of the sand might be preferentially produced through a slot. That could have had implications on the sand production behaviour observed. Random samples of each of the Silica sands were taken for the analysis. The samples evaluated were from experiment 8 (Silica Well Sorted sand), experiment 14 (Silica Poorly Sorted sand), experiment 15 (Silica No Large Fractions sand) and experiment 16 (Silica No Fine Fractions sand).

Similar results were obtained in all the cases analyzed. The sieve analysis yielded particle size distribution curves very similar to that of the original sand. The results imply that the bulk of the sands were produced through the slot. Similar results have been reported in the literature previously [11,25].

4.2.9 Section Summary

- From the preliminary experiments on sand production with air-saturated packs, the coarsest fraction of the sand had the largest impact on sand production. Based on the observations from these experiments, two correlations were obtained between the parameter $SW/D_{99.9}$ and the sand production behaviour that allowed minimum and maximum slot width sizes to be estimated for controlled sand production.

- For the sand production experiments that form the core of the thesis, experiments using water wet sand packs under confining stress saturated with heavy oil, the performance of the correlations was mixed. For a well sorted sand, the results of the experiments with heavy oil were consistent with the correlation. However, with sands that were not as well sorted, the results of the sand production experiments were not consistent with the predictions of the correlation. This suggests that the effect of the relationship between the slot width and grain size distribution on sand production is more complex than that indicated by a correlation simply between the very largest sand grains and the slot width. Evidently, the shape of the grain size distribution also has an important effect on sand production.

- From the results of the sand production experiments with heavy oil, operation-completion graphs were generated for two of the sands used in the study: a well sorted sand, and a poorly sorted sand. The operation-completion graphs show the influence of velocity and slot size on sand production. For the well sorted sand, three well defined zones were identified:

- ❖ Zone where sand production did not occur;
- ❖ Zone where sand production was continuous and massive;
- ❖ Zone where sand production could be initiated, but was intermittent – within this zone, a delicate equilibrium existed between intermittent sand production, i.e. "sand production on demand", and continuing (and massive) sand production;

- The operation-completion graph generated for the well sorted sand indicates that, for the control and management of sand production in these sands, the focus should be on slot sizes that are at the lower end of the interval defined by the correlation obtained from the preliminary air experiments.

- Flow rates are clearly a key factor in managing sand production through slots. As the slot width is increased, the critical pressure gradient (flow rate) required to initiate sand production decreases.

- The operation-completion graph for the poorly sorted sand did not yield characteristic sand production zones that were as well defined as in the case of the well sorted sand. Nevertheless, four zones indicative of different sand production behaviours could be identified. The transition between these zones were not nearly as sharp as in the case of the well sorted sand:

- ❖ Zone where sand production did not occur;
- ❖ Zone where continuous and massive sand production was likely to occur;
- ❖ Transition zone between the two zones described above where sand production behaviour is less certain. This transition zone could be sub-divided in two regions: in a lower zone (smaller pressure gradient or flow rate), it was unlikely that sand production could be initiated; in an upper zone (larger pressure gradient or flow rate), there is a possibility that sand production could be continuous and massive, although this region was not explored in the sand production experiments with heavy oil. In the transition between these regions, sand production behaviour was

uncertain, as it too could not be explored in the sand production experiments with heavy oil. There is a possibility that the sand production behaviour in this region would be similar to that in the experiments with well sorted sands; i.e. sand production might be initiated but would be intermittent.

- From the operation-completion graphs, it is evident that sand production behaviour is influenced strongly by a critical pressure gradient:

  - ❖ The critical pressure gradient for initiation of sand production is much lower for a well sorted sand than for a poorly sorted sand;

  - ❖ The critical pressure gradient decreases as confining stress increases;

  - ❖ A sufficiently large pressure gradient leads to persistent sand production and growth of channels.

- The effect of sand production on the sand packs used in the experiments were confined to localized regions (channels) where there was a large permeability and porosity increase. Outside these regions no changes in permeability and or porosity were observed. This suggests that the localized regions affected by sand production need to continue to grow into the reservoir to maintain oil production rates.

- Continuing sand production at low sand cuts (less than 1.5%) could be achieved if the initial flow rates were low and later increased in small increments. With this operating strategy, there is an opportunity to transport the sand produced by heavy oil along a horizontal well while simultaneously generating regions (channels) with high permeability.

- The grain size distribution of the sand plays an important role in the formation of stable arches/bridges. A wide grain size distribution appears to be conducive to the formation of arches; it likely also promotes sand bridging.

- Sand production did not select for certain fractions of the sand; the grain size distribution of the produced sand in the experiments matched the grain size distribution of the sand packs.

- The results of the sand production experiments as expressed in the operation-completion graphs could be considered in the design of slotted liners for managing sand production in horizontal wells; as an example, since the critical pressure for the initiation of sand production decreases as the slot size increases, a distribution of slot sizes could be envisaged along the length of the horizontal well with a higher proportion of narrow slot sizes at the heel of the well (where the pressure gradient into the well would be highest) and a higher proportion of wider slot size at the toe (where the pressure gradient into the well would be lowest). This would allow a better opportunity for intermittent sand production to occur along the entire length of the well, rather than preferentially near the heel.

Table 4-2: Ratio of slot width to effective grain diameter for different percentiles of the sands used.

Percentile Less than	SWEGD Ratio										
	Silica Well Sorted				Silica Poorly Sorted				Silica No Large Fractions	Silica No Fine Fractions	Husky Sand
	0.711 mm (0.028 in)	0.813 mm (0.032 in)	1.016 mm (0.040 in)	1.422 mm (0.056 in)	1.422 mm (0.056 in)	1.702 mm (0.067 in)	2.007 mm (0.078 in)	5.944 mm (0.234 in)	1.422 mm (0.056 in)	1.422 mm (0.056 in)	1.422 mm (0.056 in)
$D_{99.9}$	1.436	1.642	2.053	2.873	1.481	1.773	2.091	6.192	3.058	1.513	1.734
D_{90}	2.521	2.883	3.603	5.043	2.810	3.364	3.966	11.747	4.375	2.920	7.110
D_{60}	3.261	3.729	4.661	6.523	6.156	7.368	8.688	25.732	6.183	6.464	8.888
D_{50}	3.520	4.025	5.030	7.040	6.937	8.302	9.790	28.995	7.005	6.870	9.294
D_{40}	3.843	4.395	5.492	7.686	7.900	9.456	11.150	33.022	7.900	7.686	10.157
D_{10}	5.346	6.113	7.639	10.692	21.877	26.185	30.877	91.446	21.877	12.696	17.775

Table 4-3: Distance between pressure ports and identification of the estimated pressure gradients.

Distance Location	Distance (cm)	Pressure Gradient Identification
Port 3 and 4 ($D_{3,4}$)	11.90	$(dp/dL)_{3,4}$
Port 10 and 9 ($D_{10,9}$)	1.91	$(dp/dL)_{10,9}$
Port 9 and 8 ($D_{9,8}$)	4.01	$(dp/dL)_{9,8}$
Port 11 to edge of the slot ($D_{11,slot}$)	2.44	$(dp/dL)_{11,slot}$

Table 4-4: Properties of the sand pack before and after sand production

Test #	Sand	Slot size (mm/(in))	Confining Stress, σ_c (kPa)	Initial k_o @ σ_c (D)	k_o at the end of the test (D)		Initial ϕ (%)	ϕ (%)at the end of the test Carman-Kozeny		ϕ (%) at the end of the test from Dean-Stark analysis		
					k_{op}	k_{os}		ϕ_p	ϕ_s	ϕ_T	ϕ_M	ϕ_B
1	Silica Well Sorted	0.711 (0.028)	519	6.95	16.6	34.7	41.4	49.8	57.3	---	---	---
2		0.813 (0.032)	531	7.51	> 500	> 500	40.6	N/A	N/A	---	---	---
3		1.016 (0.040)	982	6.25	> 500	> 500	41.0	N/A	N/A	43.3	41.3	48.7
4		1.016 (0.040)	513	5.62	> 500	> 200	41.5	N/A	N/A	39.1	40.6	44.6
5		1.422 (0.056)	506	5.92	> 42.9	> 35.4	40.9	N/A	N/A	42.1	39.5	49.1
6	Silica Poorly Sorted	1.422 (0.056)	2,472	0.37	0.77	0.84	31.6	37.8	38.7	34.0	29.8	28.7
7		1.981 (0.078)	2,471	0.60	0.59	2.22	32.8	32.570	44.6	33.1	32.1	30.4
8	Silica Well Sorted	1.422 (0.056)	2,469	5.75	6.78*	131.20*	40.4	41.9	68.9	41.3	39.6	45.2
9		1.016 (0.040)	2,472	5.63	7.80*	27.52*	41.0	43.8	55.9	41.2	40.0	44.4
10		1.016 (0.040)	733	4.10	> 500	17.06	41.1	N/A	55.2	40.3	42.3	44.9

k_{op}= oil effective permeability in the pack
k_{os} = oil effective permeability @ the slot
ϕ_p= porosity in the pack, ϕ_s = porosity @ the slot
ϕ_T = Porosity at the top of the pack
ϕ_M= Porosity in the middle of the pack
ϕ_B= Porosity at the bottom of the pack
* Before membrane collapsed
**Test was stopped prematurely

Continuation....

Test #	Sand	Slot size (mm/(in))	Confining Stress, σ_c (kPa)	Initial k_o @ σ_c (D)	k_o at the end of the test (D)		Initial ϕ (%)	ϕ (%)at the end of the test Carman-Kozeny		ϕ (%) at the end of the test from Dean-Stark analysis		
					k_{op}	k_{os}		ϕ_p	ϕ_s	ϕ_T	ϕ_M	ϕ_B
11	Silica Well Sorted	1.016 (0.040)	157	4.12	4.35**	3.26**	41.1	41.6	37.8	39.8	38.9	39.8
12		1.016 (0.040)	150	3.34	4.82*	6.24*	40.8	44.5	47.1	40.9	38.4	39.2
13		1.016 (0.040)	1,000	3.64	4.55	12.4	40.5	42.8	52.3	41.4	39.8	43.2
14	Silica Poorly Sorted	5.944 (0.234)	2,495	0.67	> 530	> 93	30.2	N/A	N/A	32.3	30.9	27.8
15	Silica No Large Fractions	1.422 (0.056)	2,495	0.51	> 200	> 9.79	33.2	N/A	N/A	35.1	33.7	32.1
16	Silica No Fine Fractions	1.422 (0.056))	2,493	2.04	2.27	6.17	38.4	39.3	48.6	40.1	36.1	39.6
17	Husky Sand	1.422 (0.056)	507	0.73	14.9	7.82	38.2	68.2	62.0	39.7	37.6	36.0

k_{op}= oil effective permeability in the pack k_{os} = oil effective permeability @ the slot ϕ_p= porosity in the pack, ϕ_s = porosity @ the slot

ϕ_T = Porosity at the top of the pack ϕ_M= Porosity in the middle of the pack ϕ_B= Porosity at the bottom of the pack

* Test was stopped to avoid membrane collapse

Table 4-5: Sand produced in the heavy oil experiments under confining stress.

Test #	Sand	Slot Size (mm/(in))	Confining Stress (kPa)	Mass of Sand in the pack (g)	Flow Rate (cc/h)	Estimated M.B. (g)	Actual (g)	Total		High k channel
								M.B. (g)	Actual (g)	
1	Silica Well Sorted	0.711 (0.028)	519	13,813	51	73.46	31.51	179.9	142.6	Yes
					26	23.27	17.75			
					102	4.22	Traces			
					204	78.90	93.35			
2		0.813 (0.032)	531	14,038	21	8.97	*	1,148	1,074	Yes
					31	2.40	Traces			
					61	0.00	0.00			
					122	1,136	1,074			
3		1.016 (0.040)	982	13,950	25	14.40	*	677.4	544.7	Yes
					37	10.60	Traces			
					74	21.25	*			
					100	3.72	Traces			
					148	627.3	544.58			
4		1.016 (0.040)	513	13,695	25	0.00	0.00	974.1	942.8	Yes
					37	12.86	traces			
					74	961.3	942.77			
					After **	---	129.17		129.2	
5		1.422 (0.056)	506	14,046	17	10.66	Traces	536.5	499.4	Yes
					34	60.42	55.30			
					17 (II)	465.43	444.11			

* The amount was considered too small to be cleaned **After the pumps were stopped. Slurry was being produced by gravity

Continuation…

Test #	Sand	Slot Size (mm/(in))	Confining Stress (kPa)	Mass of Sand in the pack (g)	Flow Rate (cc/h)	Estimated M.B. (g)	Actual (g)	Total		High k channel
								M.B.(g)	Actual (g)	
6	Silica Poorly Sorted	1.422 (0.056)	2,472	15,650	17	21.26	†	78.96	N/A	No
					34	55.26	†			
					51	2.44	Traces			
					76	0.00	0.00			
					101	0.00	0.00			
					150	0.00	0.00			
7	Silica Poorly Sorted	1.981 (0.078)	2,471	15,722	25	27.73	†	97.20	N/A	No
					49	0.00	0.00			
					68	20.07	†			
					75	47.55	†			
					110	0.00	0.00			
					147	1.85	Traces			
8	Silica Well Sorted	1.422 (0.056)	2,469	13,805.76	17	390.7	400.64	390.67	400.64	Membrane collapsed
9		1.016 (0.040)	2,472	14,020.41	25	430.4	304.13	164.36‡	304.13	
10			733	13,776	25.00	75.02	83.67	1,005‡	1,438	Yes. Also membrane collapsed
					13	930.1	1354.14			
11			157	13,846	25	4.43	Traces	117.09	N/A	N/A
					37	84.25	†			
					74	28.41	†			
					100	Test was stopped by mistake when apparently massive sand production would have started				

† It was not cleaned. The perception from a visual examination of the produced samples was that the amount of sand produced was too small to be cleaned. ‡ M.B. was performed until the membrane collapsed. The collapse of the membrane caused water from the confining system to come into the pack. This is the reason for the difference between M.B. and actual.

Continuation…

Test #	Sand	Slot Size (mm/(in))	Confining Stress (kPa)	Mass of Sand in the pack (g)	Flow Rate (cc/h)	Estimated M.B. (g)	Actual (g)	Total M.B. (g)	Total Actual (g)	High k channel
12	Silica Well Sorted	1.016 (0.040)	150	13,884	25	3.78	Traces	98.0	73.3	Yes
					37	60.73	73.32☼			
					13	33.46				
13			1,000	13,800	25	467.9	466.61	467.9	466.6	Membrane collapsed
14	Silica Poorly Sorted	5.944 (0.234)	2,500	16,627	123	65.87	27.4	275.7	148.7	Yes
					17	38.02	4.08			
					25	14.19	10.72			
					34	24.00	17.52			
					40	16.02	8.65			
					49	22	9.41			
					62	0.36	1.05			
					74	40.63	31.03			
					110	54.64	38.82			
15	Silica No Large Fractions	1.422 (0.056)	2,500	15,706	17	8.917	†	995.9	913.1	Yes
					34	22.39	16.12			
					51	0.00	0.00			
					76	20.30	15.50			
					101	471.0	461.73			
					17	291.5	243.66			
					51	202.10	176.12			

☼ Included both flow rates † It was not cleaned. The perception from a visual examination of the produced samples was that the amount of sand produced was too small to be cleaned.

Continuation …

Test #	Sand	Slot Size (mm/(in))	Confining Stress (kPa)	Mass of Sand in the pack (g)	Flow Rate (cc/h)	Estimated M.B. (g)	Actual (g)	Total		High k channel
								M.B. (g)	Actual. (g)	
16	Silica No Fine Fractions	1.422 (0.056)	2,500	14,614	17	291.7	327.37	291.7	327.4	Yes. Membrane broke
17	Husky Sand	1.422 (0.056)	500	14,676	17	0.00	0.00	852.4	900.4	Yes. Membrane broke
					10	852.4	900.35			

Table 4-6: Pressure gradient and critical flow rate calculations for each test.

Test #	Sand	Slot Size (mm (in))	Q_{isp} (cc/h)	$(dp/dL)_{isp}$ (MPa/cm)	Q_{csp} (cc/h)	$(dp/dL)_{csp}$ (MPa/cm)	Q_{cavity} (cc/h)	r_{sc} (cm)	$(dp/dr)_{AH}$ (MPa/cm)	$(dp/dr)_{cr}$ (MPa/cm)	Q_{cr} (cc/h)
1	Silica Well Sorted	0.711 (0.028)	102	1.34	204	2.54	51	2.25	0.022	0.0420	97.6
2	Silica Well Sorted	0.813 (0.032)	61	1.12	122	2.45	21	1.11	0.0409	0.0849	68.7
3	Silica Well Sorted	1.016 (0.040)	100	1.79	148	2.58	25	1.12	0.0592	0.0843	56.3
4	Silica Well Sorted	1.016 (0.040)	25	0.69	37	1.35	37	1.26	0.0867	0.0750	46.7
5	Silica Well Sorted	1.422 (0.056)	17	0.27	34	0.546	17	1.18	0.0508	0.0801	36.8
6	Silica Poorly Sorted	1.422 (0.056)	150*	17.1	--	--	17	1.42	0.136	0.262	15.3
7	Silica Poorly Sorted	1.981 (0.078)	147*	13.7	--	--	25	1.56	0.122	0.238	26.1
8	Silica Well Sorted	1.422 (0.056)	--	--	17	0.22	--	--	--	--	--
9	Silica Well Sorted	1.016 (0.040)	--	--	25	0.49	--	--	--	--	--
10	Silica Well Sorted	1.016 (0.040)	--	--	25	0.74	--	--	--	--	--
11	Silica Well Sorted	1.016 (0.040)	37	1.06	100	2.11	25	0.88	0.0997	0.107	26.8

Q_{isp} = Critical flow rate for initiation of sand production

Q_{csp} = Critical flow rate for continuing sand production

Q_{cavity} = Flow rate at which small amount of sand is produced initially forming small cavity

$(dp/dr)_{AH}$ = Pressure gradient into a hemisphere

$(dp/dL)_{isp}$ = Critical pressure gradient (calculated through the slot) for initiation of sand production

$(dp/dL)_{csp}$ = Critical pressure gradient (calculated through the slot) for continuing sand production

r_{sc} = Radius of spherical cavity form after small amount of sand production

$(dp/dr)_{Cr}$ = Critical pressure gradient for sand failure from Bratli and Risnes criterion

Q_{cr} = Critical flow rate for sand failure from Bratli and Risnes criterion

* Last flow rates that could be applied without observing continuing sand production

Continuation …

Test #	Sand	Slot Size (mm (in))	Q_{isp} (cc/h)	$(dp/dL)_{isp}$ (MPa/cm)	Q_{csp} (cc/h)	$(dp/dL)_{csp}$ (MPa/cm)	Q_{cavity} (cc/h)	r_{sc} (cm)	$(dp/dr)_{AH}$ (MPa/cm)	$(dp/dr)_{cr}$ (MPa/cm)	Q_{cr} (cc/h)
12	Silica Well Sorted	1.016 (0.040)	25	0.718	37	1.30	25	0.83	0.173	0.113	25.5
13	Silica Well Sorted	1.016 (0.040)	--	--	25	0.754	--	--	--	--	--
14	Silica Poorly Sorted	5.944 (0.234)	12.3	0.381	--	--	12.3	2.04	0.0328	0.182	39.6
15	Silica No Large Fractions	1.422 (0.056)	76	9.38	101	3.98	17	1.06	0.504	0.407	18.1
16	Silica No Fine Fractions	1.422 (0.056)	--	--	17	0.637	--	--	--	--	--
17	Husky sand	1.422 (0.056)	--	--	17	2.07	--	--	--	--	--

Q_{isp} = Critical flow rate for initiation of sand production

Q_{csp} = Critical flow rate for continuing sand production

Q_{cavity} = Flow rate at which small amount of sand is produced initially forming small cavity

$(dp/dr)_{AH}$ = Pressure gradient into a hemisphere

$(dp/dL)_{isp}$ = Critical pressure gradient (calculated through the slot) for initiation of sand production

$(dp/dL)_{csp}$ = Critical pressure gradient (calculated through the slot) for continuing sand production

r_{sc} = Radius of spherical cavity form after small amount of sand production

$(dp/dr)_{Cr}$ = Critical pressure gradient for sand failure from Bratli and Risnes criterion

Qcr = Critical flow rate for sand failure from Bratli and Risnes criterion

Table 4-7: Fluid flow rates and fluid velocities for each test.

Test #	Sand	Slot Sizes	Confining Stress (kPa)	Fluid Flow Rates (cc/h)	Fluid Velocities (cm/h)
1	Silica Well Sorted	0.711 (0.028)	519	51.0	94.1
				26.0	48.0
				102.0	31.4
				204.0	188.2
2	Silica Well Sorted	0.813 (0.032)	531	21.0	31.9
				31.0	47.1
				61.0	92.7
				122.0	185.4
3	Silica Well Sorted	1.016 (0.040)	982	25.0	32.3
				37.0	47.8
				74.0	95.6
				100.0	129.2
				148.0	191.2
4	Silica Well Sorted	1.016 (0.040)	513	25.0	32.3
				37.0	47.8
				74.0	95.6
5	Silica Well Sorted	1.422 (0.056)	506	17.0	15.7
				34.0	31.4
				17 (II)	15.7
6	Silica Poorly Sorted	1.422 (0.056)	979	17.0	15.7
			2,473	34.0	31.4
			2,475	51.0	47.1
			3,138	76.0	70.1
			3,885	101.0	93.2
			4,904	150.0	138.4
7	Silica Poorly Sorted	1.981 (0.078)	2,471	24.5	16.2
			2,472	49.0	32.5
			3,472 to 3,613	67.5	44.7
			3,821	74.5	49.0
			2,800 to 4,461	110.0	72.9
			2,800 to 5,200	147.0	97.4
8	Silica Well Sorted	0.813 (0.032)	2,469	17.0	15.7
9	Silica Well Sorted	1.016 (0.040)	2,472	25.0	32.3
10	Silica Well Sorted	1.016 (0.040)	733	25.0	32.3
				12.5	16.2
11	Silica Well Sorted	1.016 (0.040)	157	25.0	32.3
				37.0	47.8
				74.0	95.6
				100.0	129.2
12	Silica Well Sorted	1.016 (0.040)	150	25.0	32.3
				37.0	47.8
				12.5	16.2
13	Silica Well Sorted	1.016 (0.040)	1,000	25.0	32.3

Continuation ...

Test #	Sand	Slot Sizes	Confining Stress (kPa)	Fluid Flow Rates (cc/h)	Fluid Velocities (cm/h)
14	Silica Poorly Sorted	5.944 (0.234)	2,498	12.3	2.7
				17.3	3.8
				25.0	5.5
				34.0	7.5
				40.0	8.8
				49.0	10.8
				61.5	13.6
				74.0	16.3
				110.0	24.3
15	Silica No Large Fractions	1.422 (0.056)	2,497	17.0	15.7
				34.0	31.4
				51.0	47.1
			2,833	76.0	70.1
			4,991 to 2,491	101.0	93.2
			2,498	17.0	15.7
			2,498	51.0	47.1
16	Silica No Fine Fractions	1.422 (0.056)	2,493	17.0	15.7
17	:Husky Sand	1.422 (0.056)	508	17.0	15.7
				10.0	

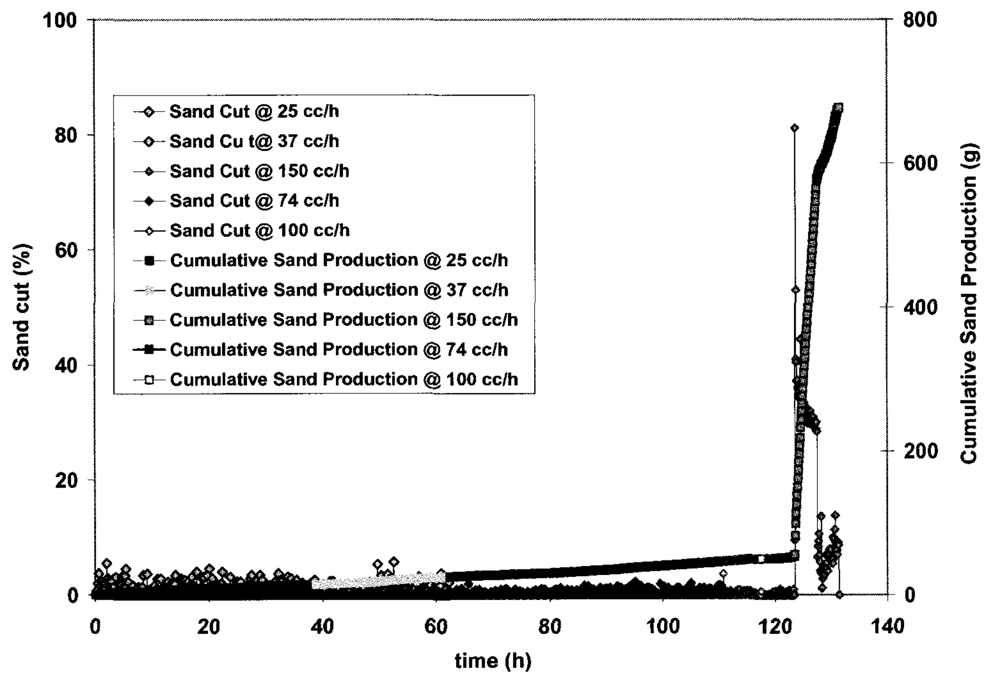

Figure 4-4: Sand cut and cumulative sand production as a function of time for experiment #3. Sand: Silica Well Sorted. Slot size: 1.016 mm (0.040 in).

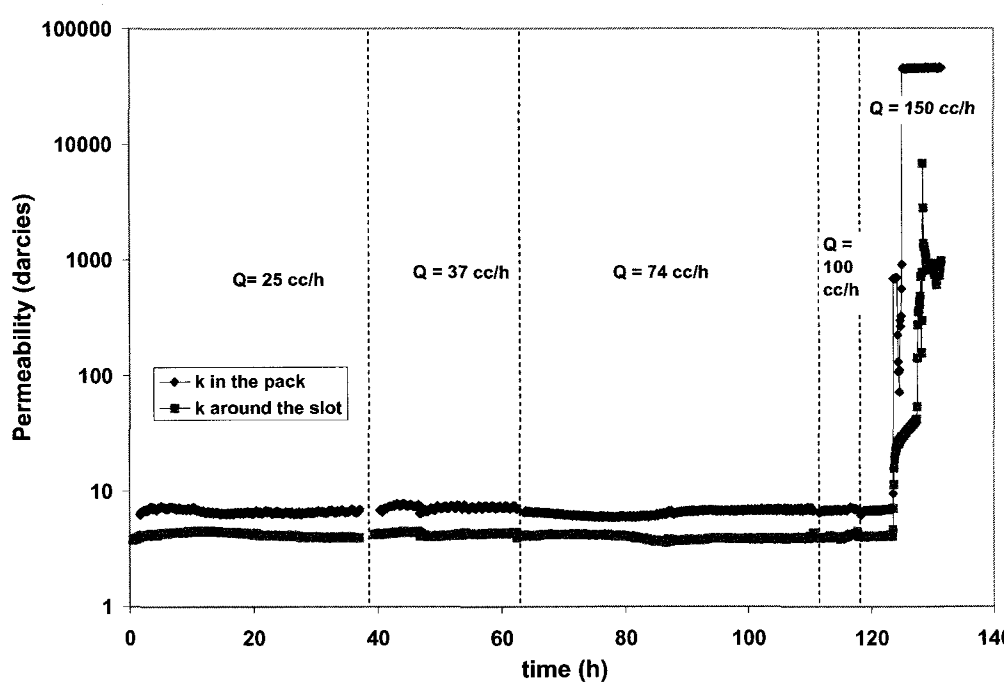

Figure 4-5: Permeability inside pack and around the slot as a function of time for experiment #3. Sand: Silica Well Sorted. Slot size: 1.016 mm (0.040 in).

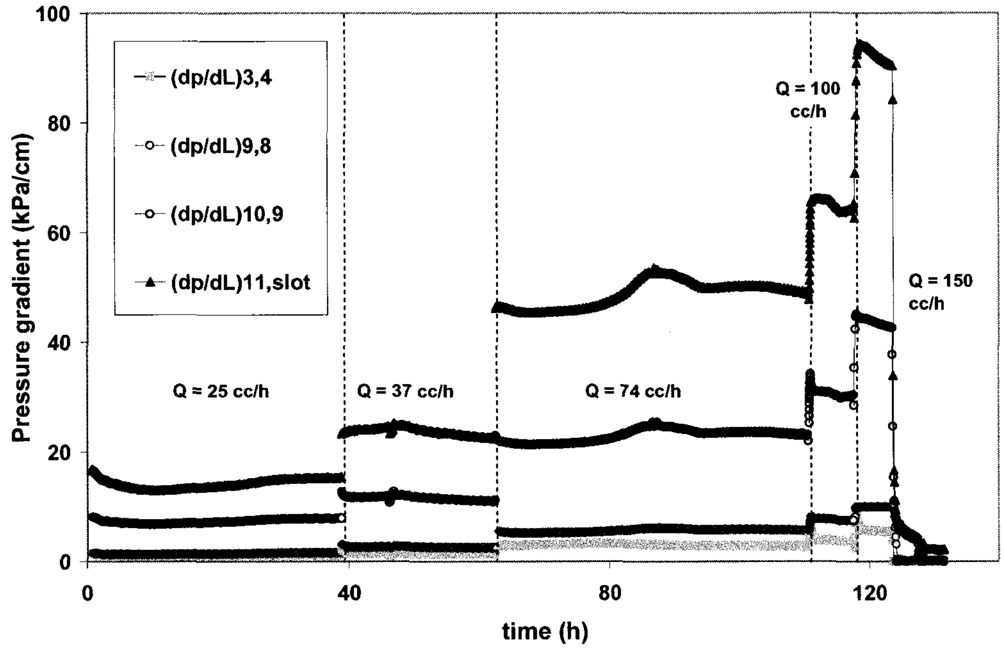

Figure 4-6: Pressure Gradient as a function of time for experiment #3. Sand: Silica Well Sorted. Slot size: 1.016 mm (0.040 in).

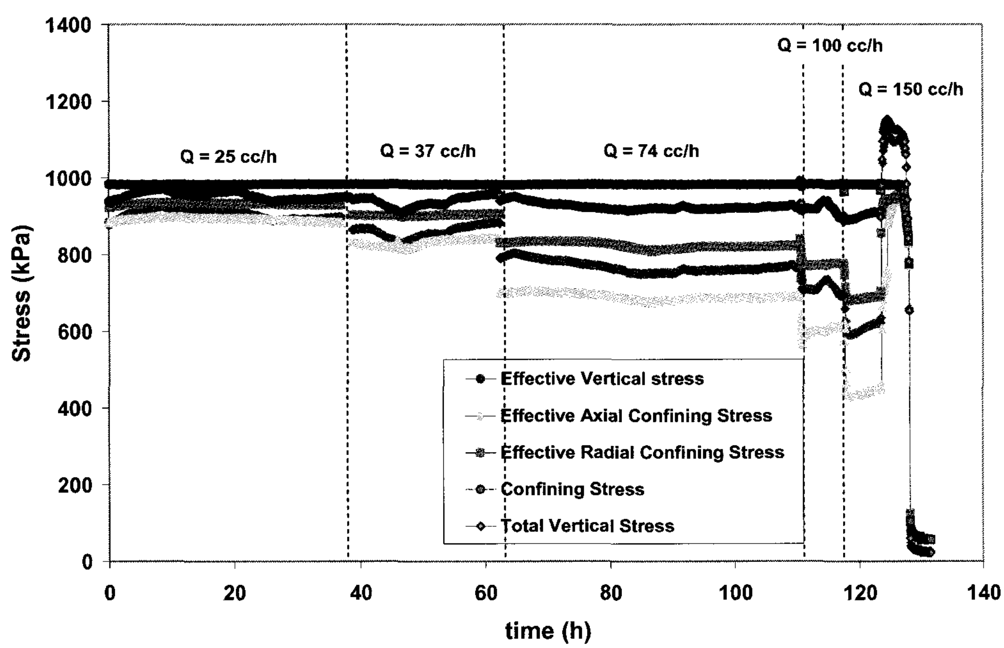

Figure 4-7: Stress distribution in the sand pack as a function of time for experiment #3. Sand: Silica Well Sorted. Slot Size: 1.016 mm (0.040 in).

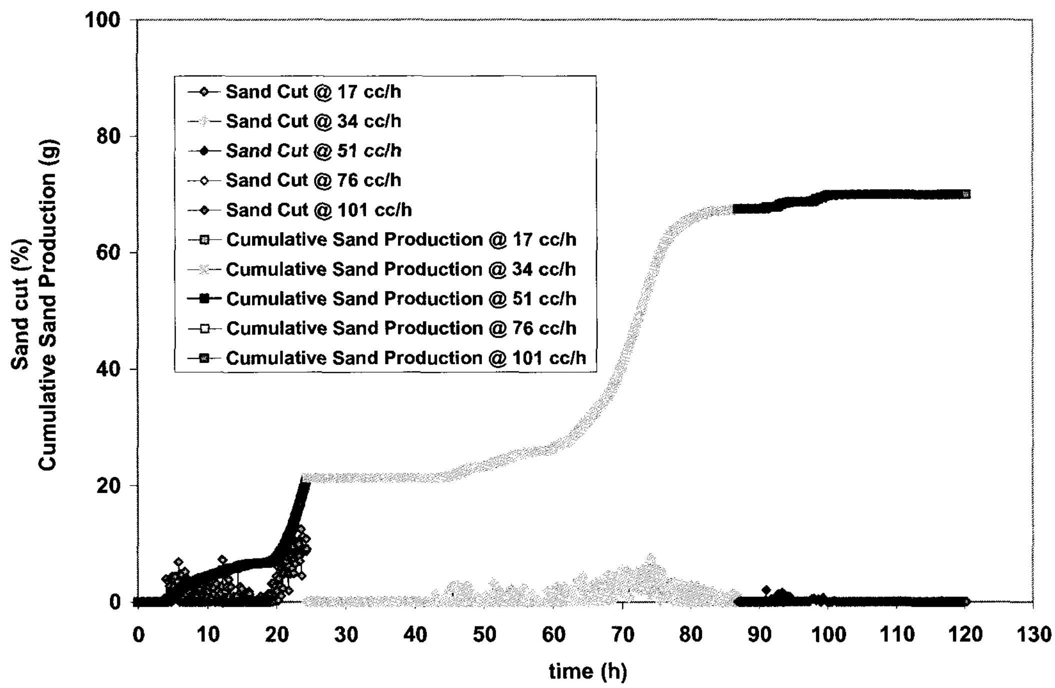

Figure 4-8: Sand cut and cumulative sand production as a function of time for experiment #6. Sand: Silica Poorly Sorted. Slot size: 1.422 mm (0.056 in).

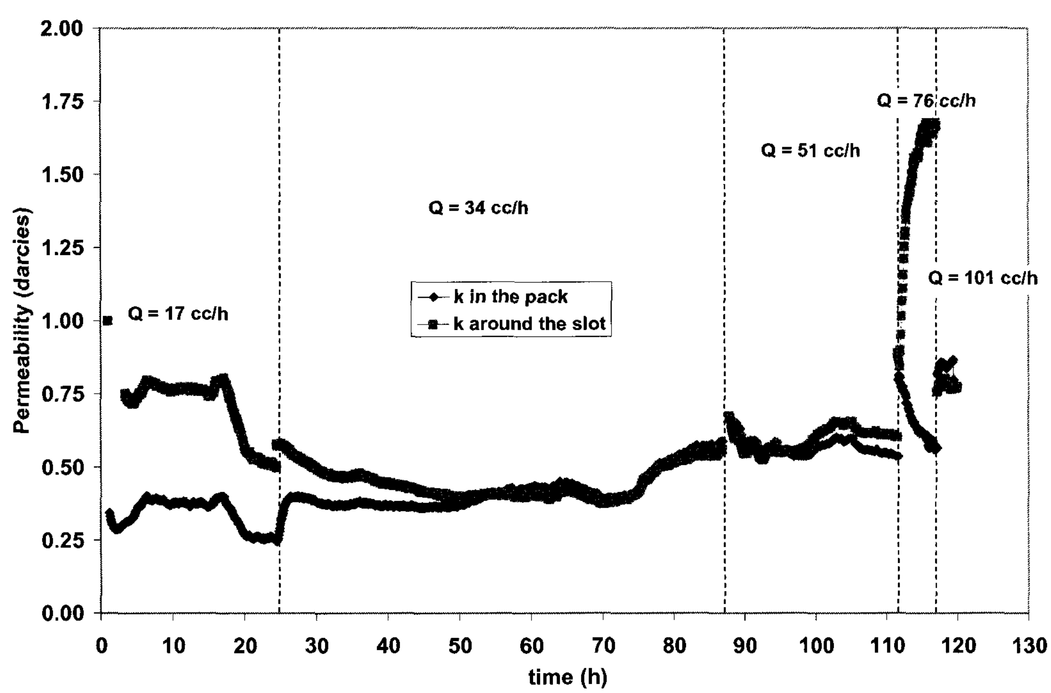

Figure 4-9: Permeability inside pack and around the slot as a function of time for experiment #6. Sand: Silica Poorly Sorted. Slot size: 1.422 mm (0.056 in).

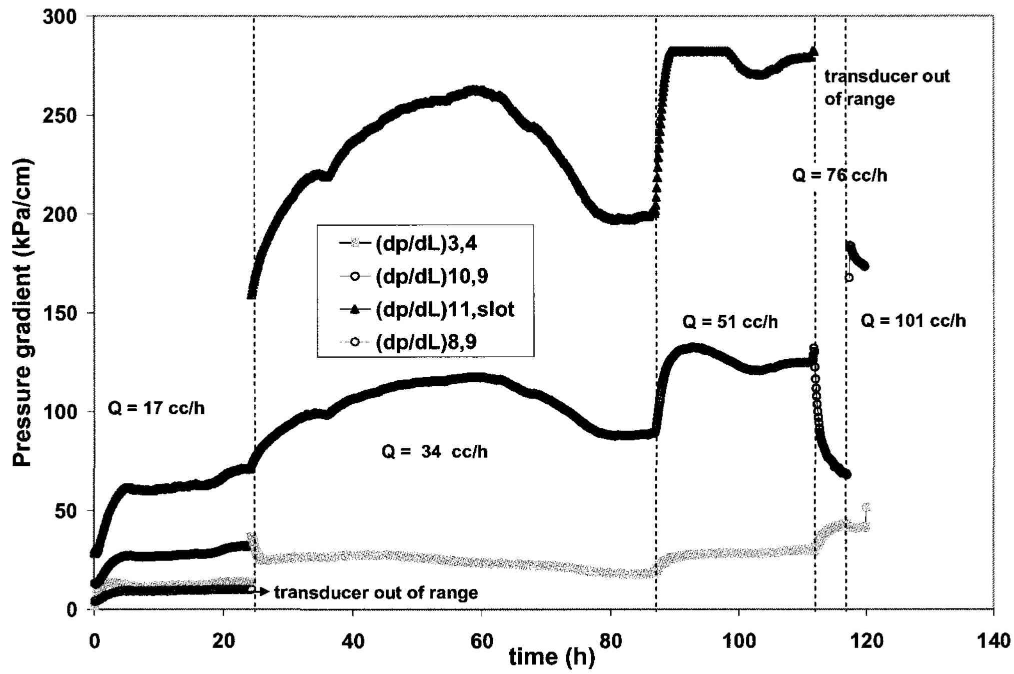

Figure 4-10: Pressure Gradient as a function of time for experiment #6. Sand: Silica Poorly Sorted. Slot size: 1.422 mm (0.056 in).

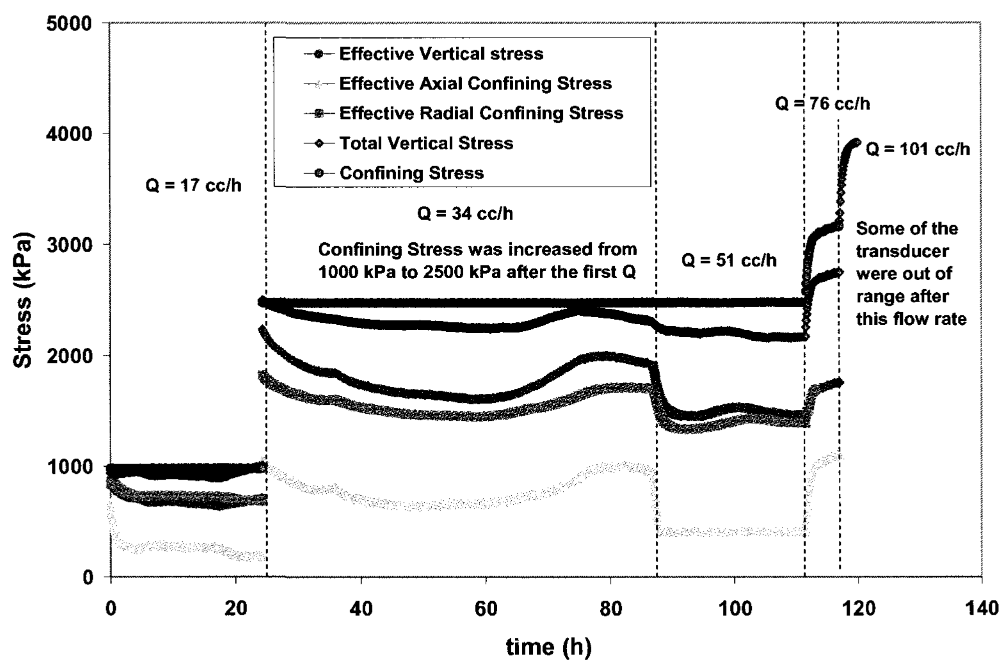

Figure 4-11: Stress distribution in the sand pack as a function of time for experiment #6. Sand: Silica Poorly Sorted. Slot Size: 1.422 mm (0.056 in).

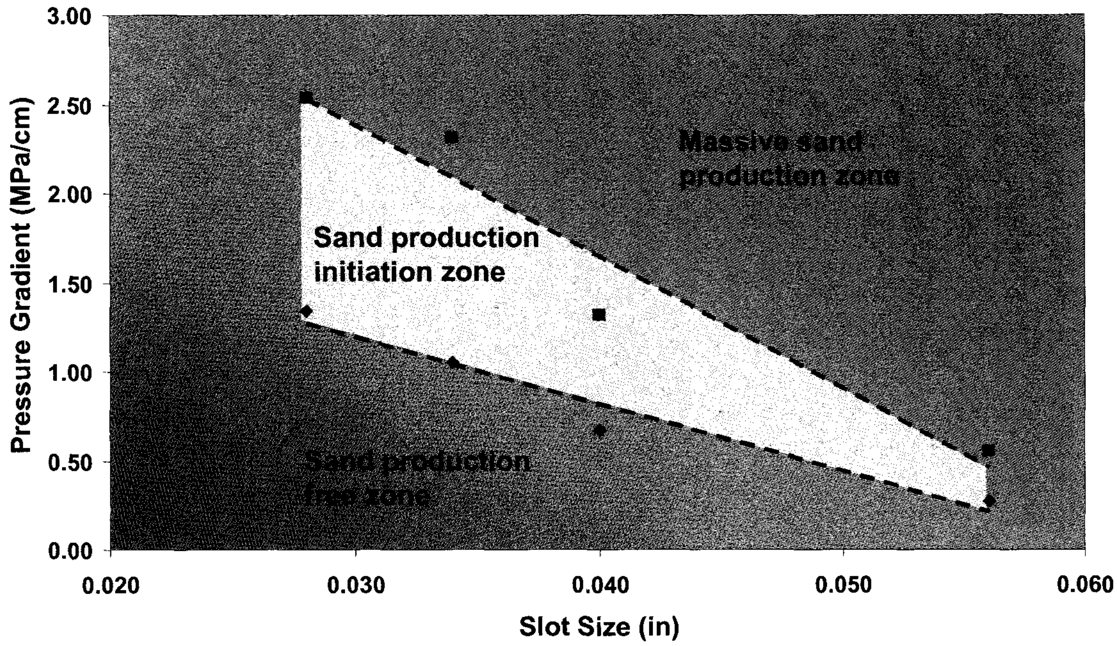

Figure 4-12: Operation-completion design map for controlled sand production in horizontal wells; well sorted sand, confining stress 500 kPa

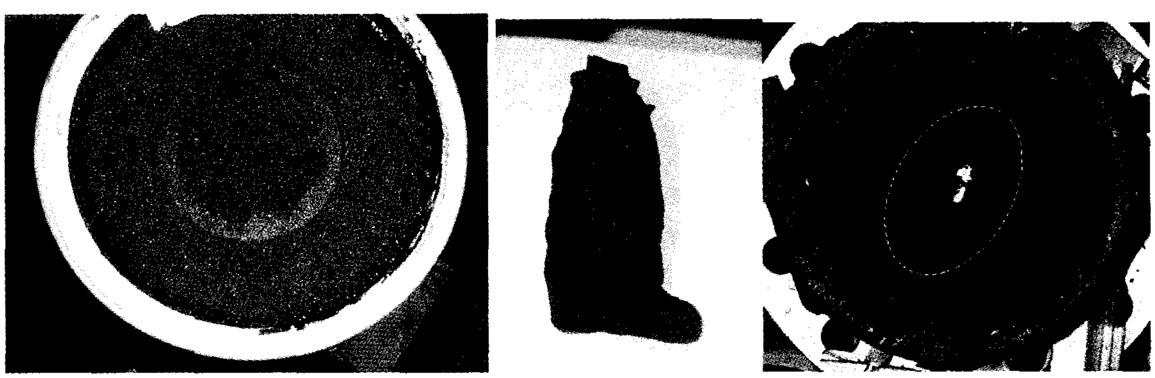

(a) (b) (c)

Figure 4-13: View of different sand packs composed of a well sorted sand after sand production; (a) view of the tip of the high permeability channel at the top of the sand pack in test 2, (b) high permeability channel cast from test 1, (c) dilated zone shape from test 4

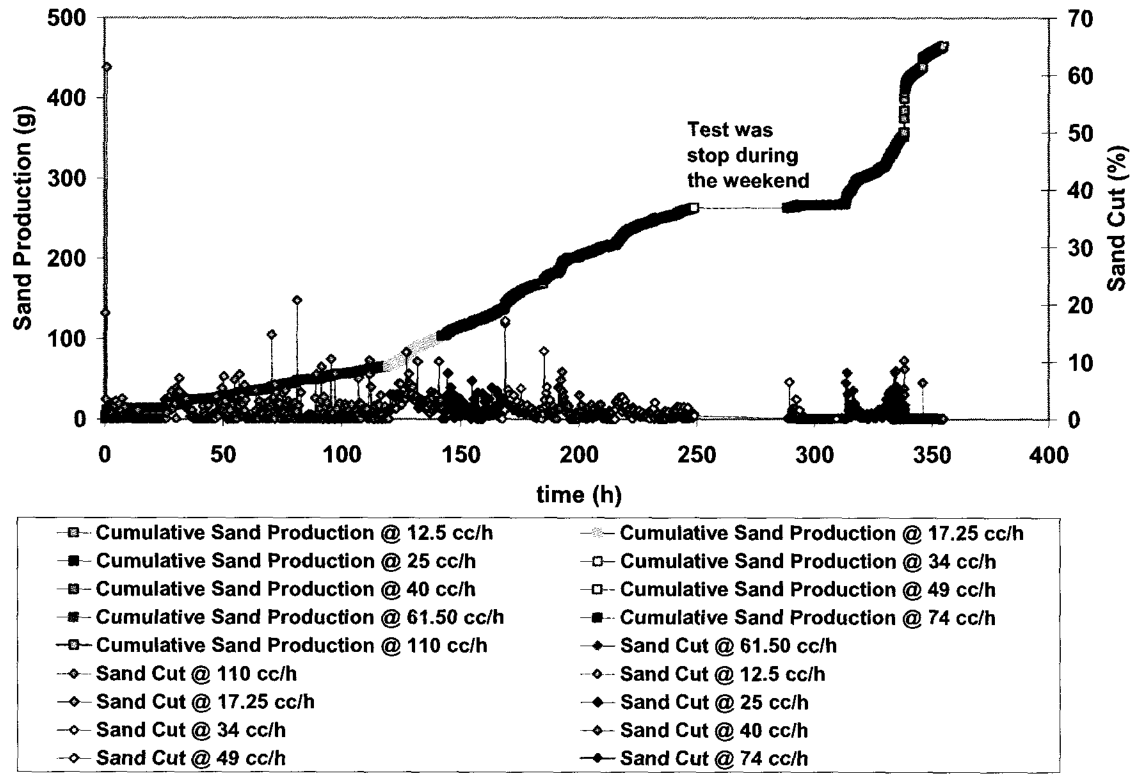

Figure 4-14: Sand cut and cumulative sand production as a function of time for experiment # 14. Sand: Silica Poorly Sorted. Slot size: 5.944 mm (0.234 in).

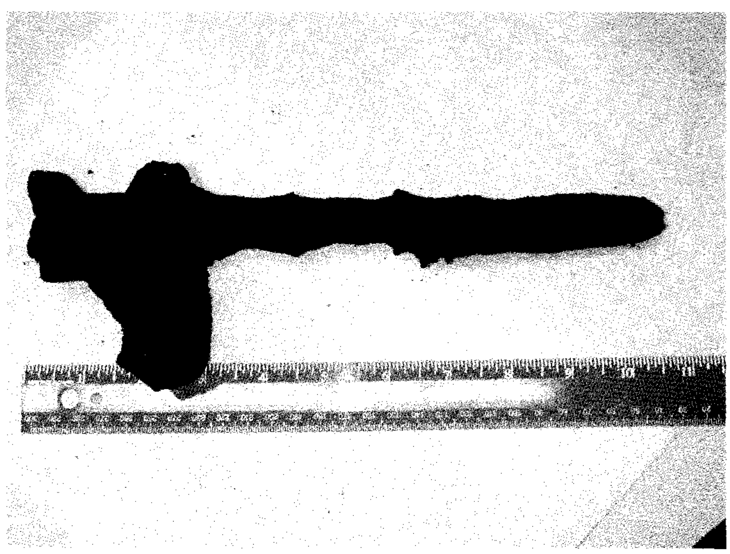

Figure 4-15: View of a high permeability channel cast from experiment 14. Sand: Silica Poorly Sorted sand. Slot size: 5.944 mm (0.234 in).

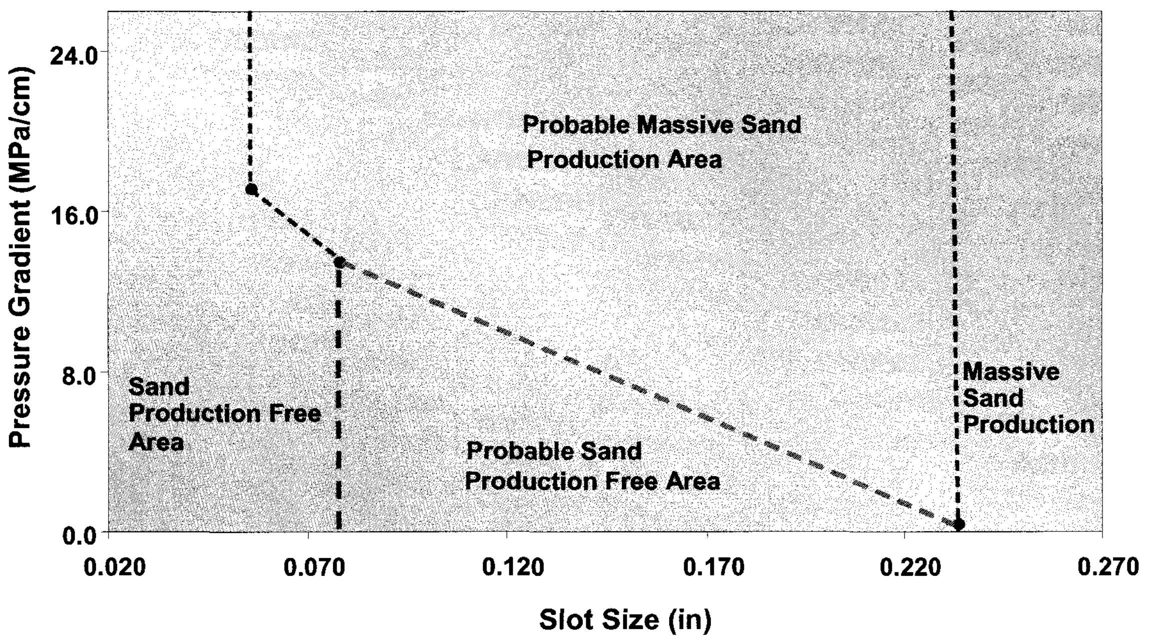

Figure 4-16: Operation-completion design map for controlled sand production in horizontal wells; poorly sorted sand, confining stress 2500 kPa

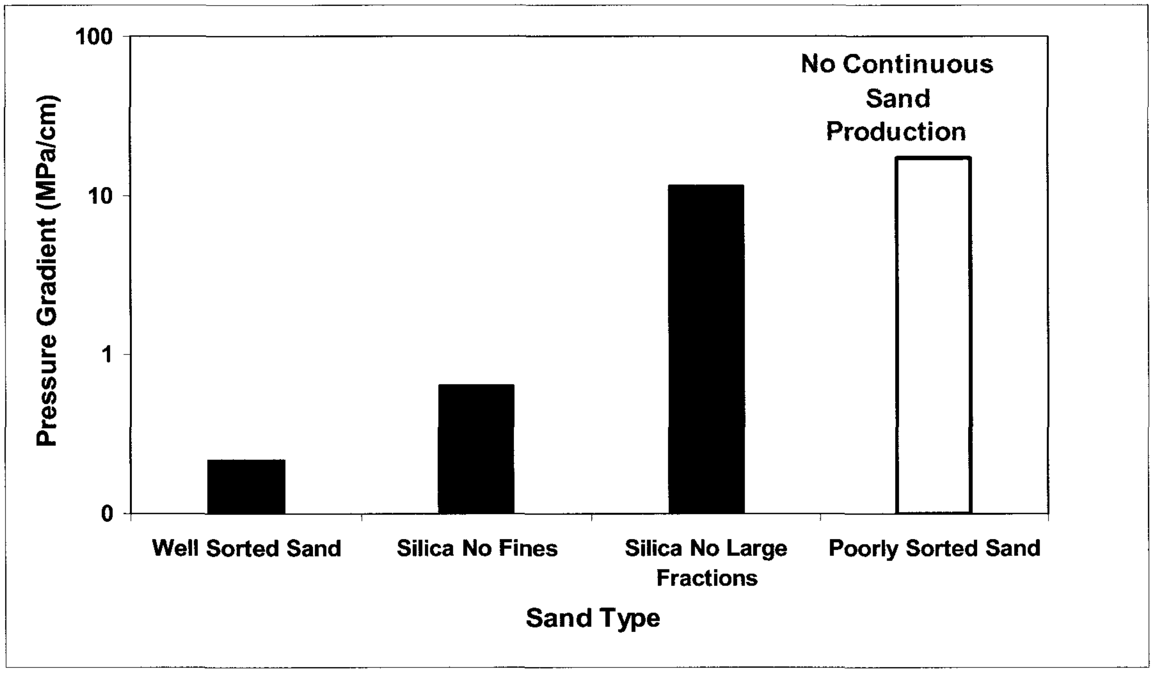

Figure 4-17: Effect of particle size distribution on sand production; slot size 1.422 mm (0.056 in), confining stress 2,500 kPa

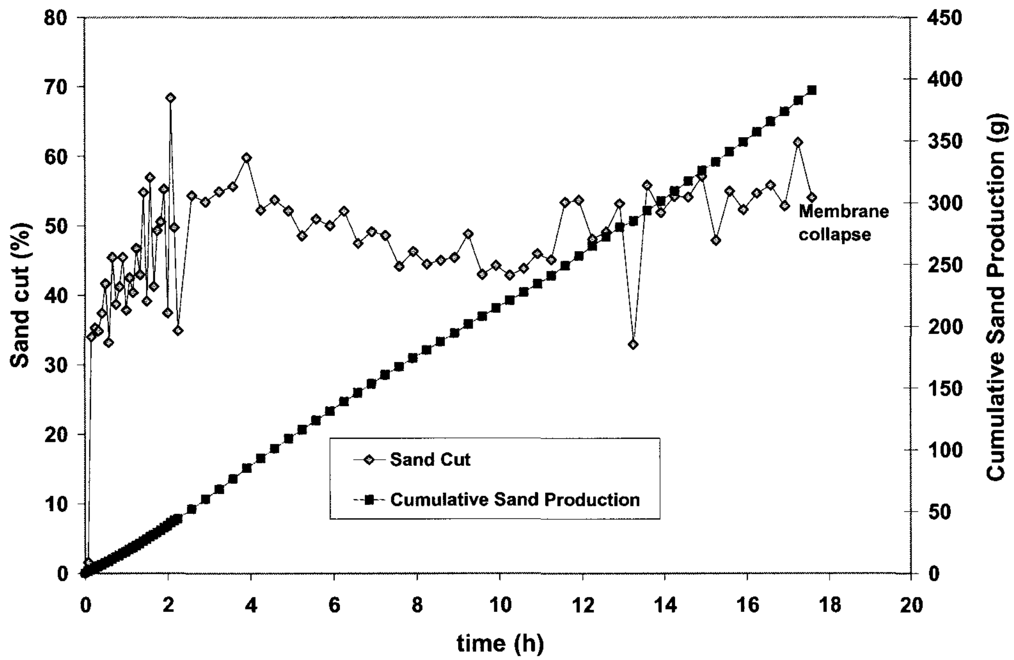

Figure 4-18: Sand cut and cumulative sand production as a function of time for experiment # 8. Sand: Silica Well Sorted. Slot size: 1.422 mm (0.056 in). $\sigma_c = 2469$ kPa

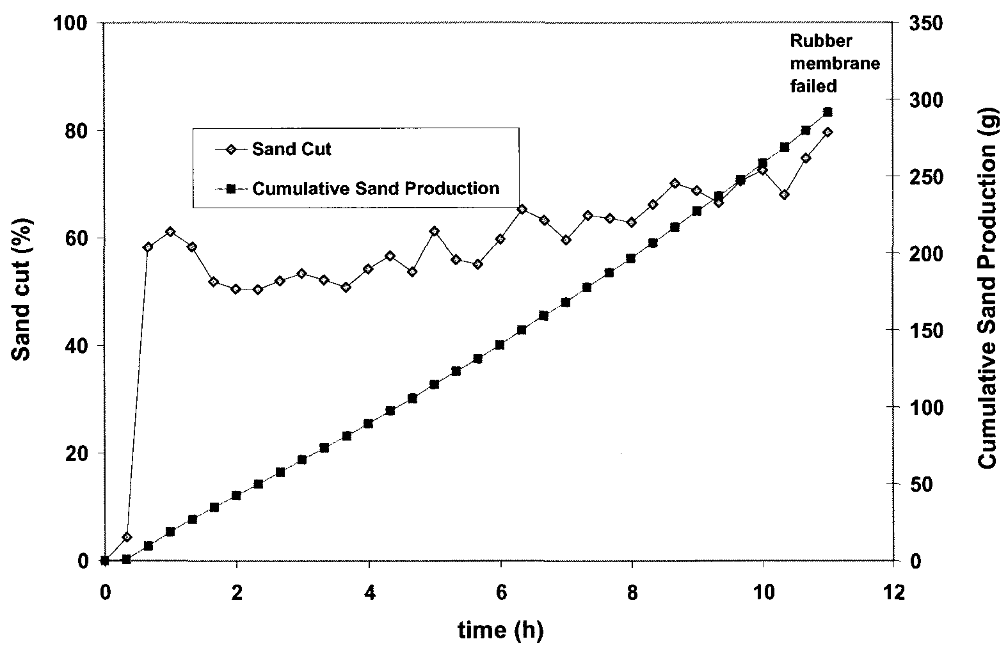

Figure 4-19: Sand cut and cumulative sand production as a function of time for experiment # 16. Sand: Silica No Fines. Slot size: 1.422 mm (0.056 in). $\sigma_c = 2469$ kPa

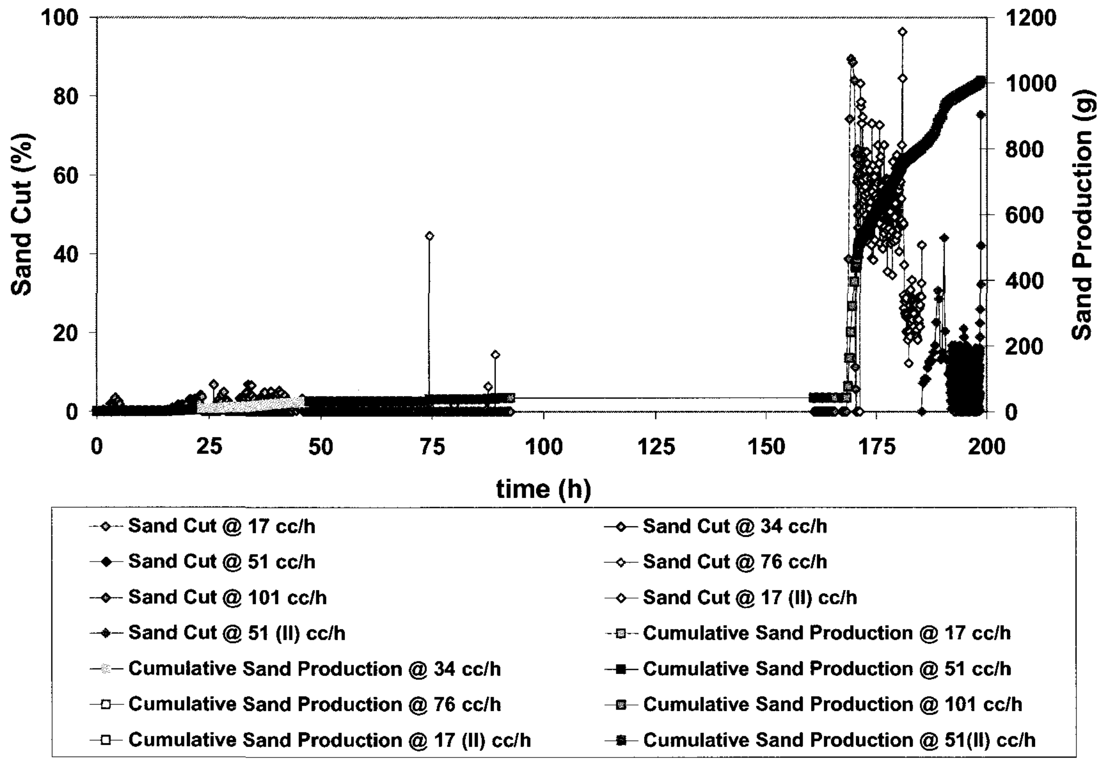

Figure 4-20: Sand cut and cumulative sand production as a function of time for experiment #15. Sand: Silica No Large Fractions. Slot size: 1.422 mm (0.056 in). σ_c = 2469 kPa

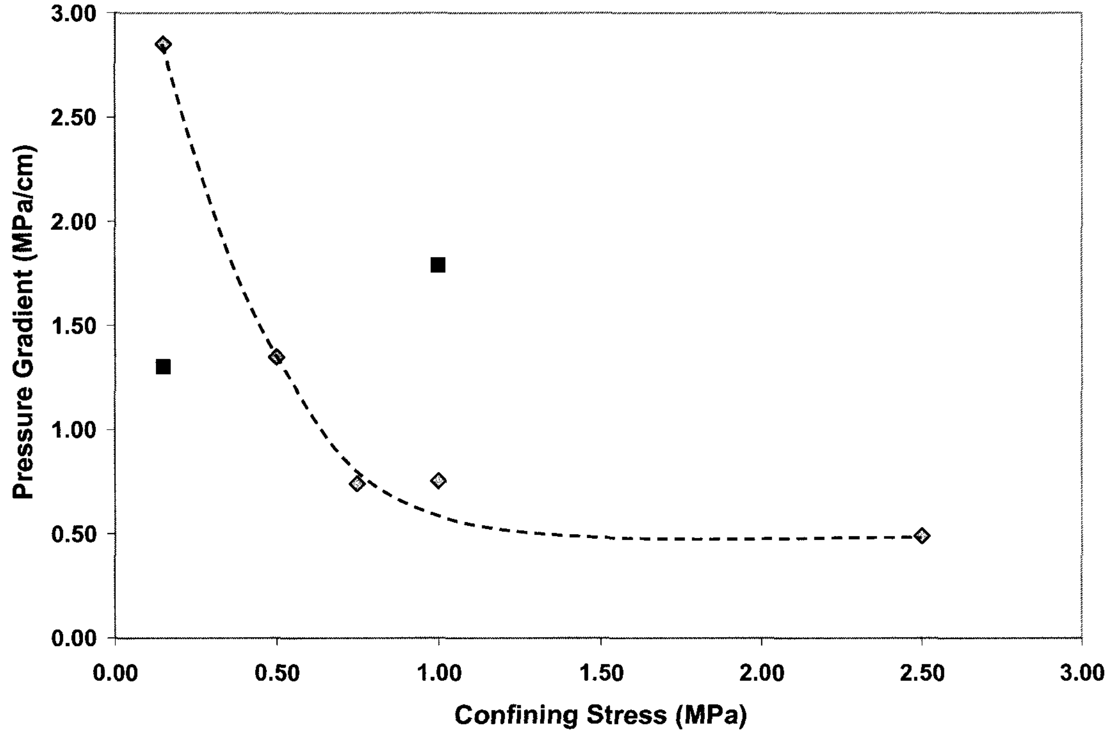

(a) slot size 1.016 mm (0.040 in)

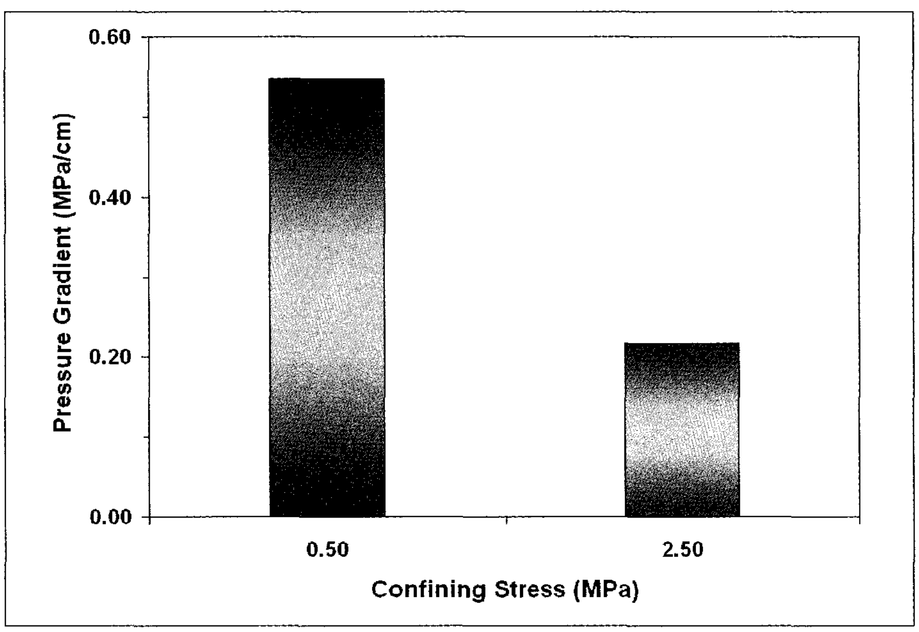

(b) slot size 1.422 mm (0.056 in)

Figure 4-21: Effect of confining stress on sand production initiation. Silica Well Sorted sand

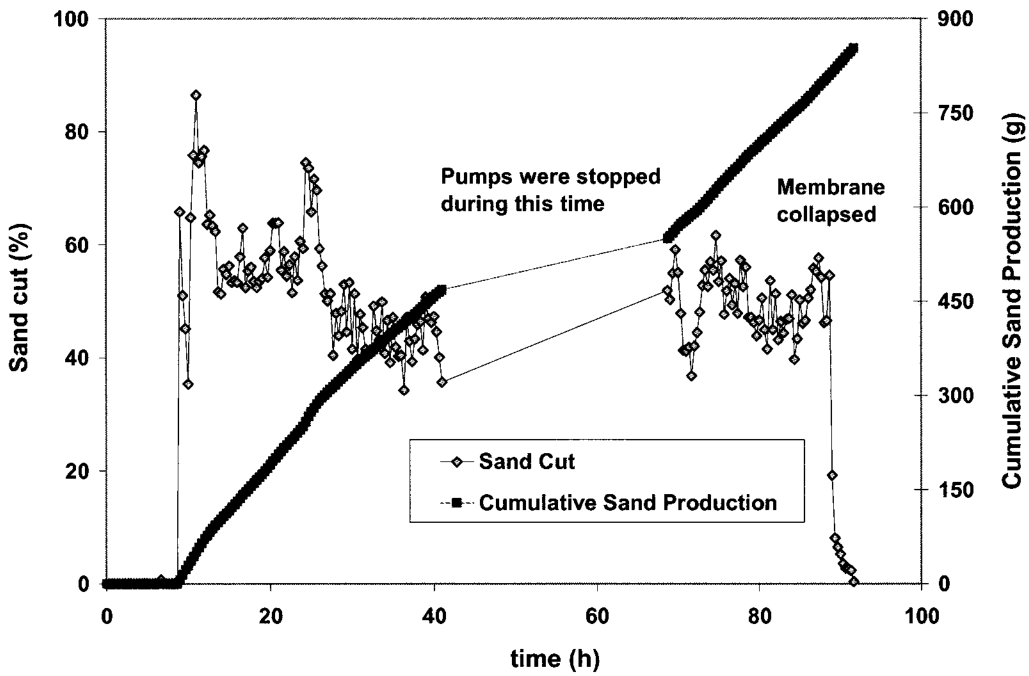

Figure 4-22: Sand cut and cumulative sand production vs. time for experiment # 17. Husky sand. Slot size: 1.422 mm (0.056 in). σ_c = 507 kPa

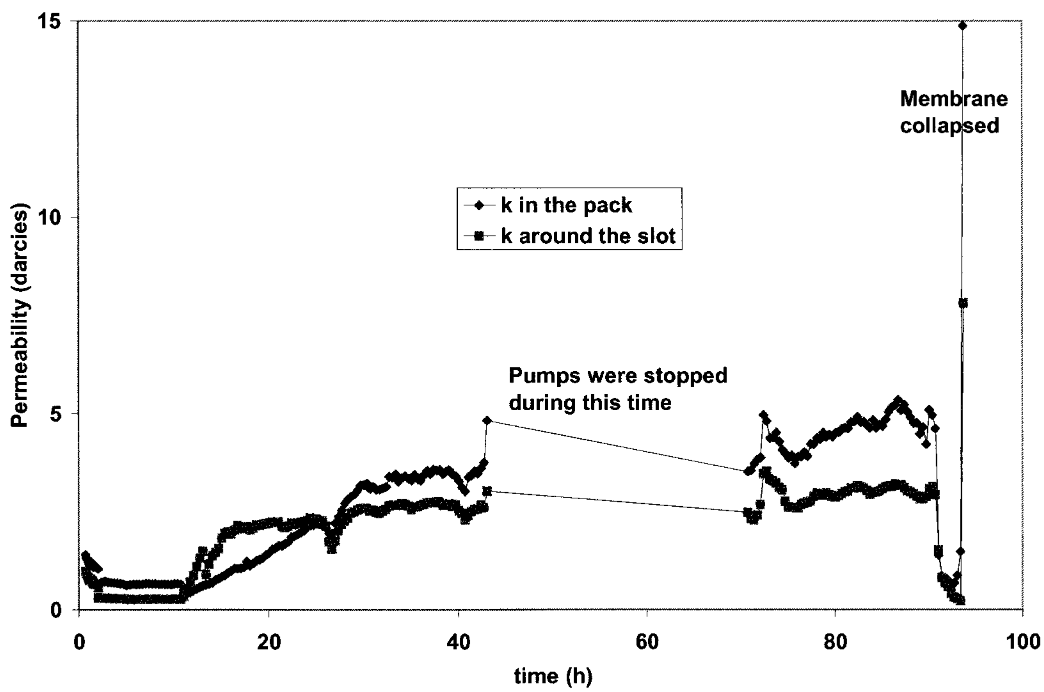

Figure 4-23: Permeability inside pack and around the slot vs. time for experiment # 17. Husky sand. Slot size: 1.422 mm (0.056 in). σ_c = 507 kPa

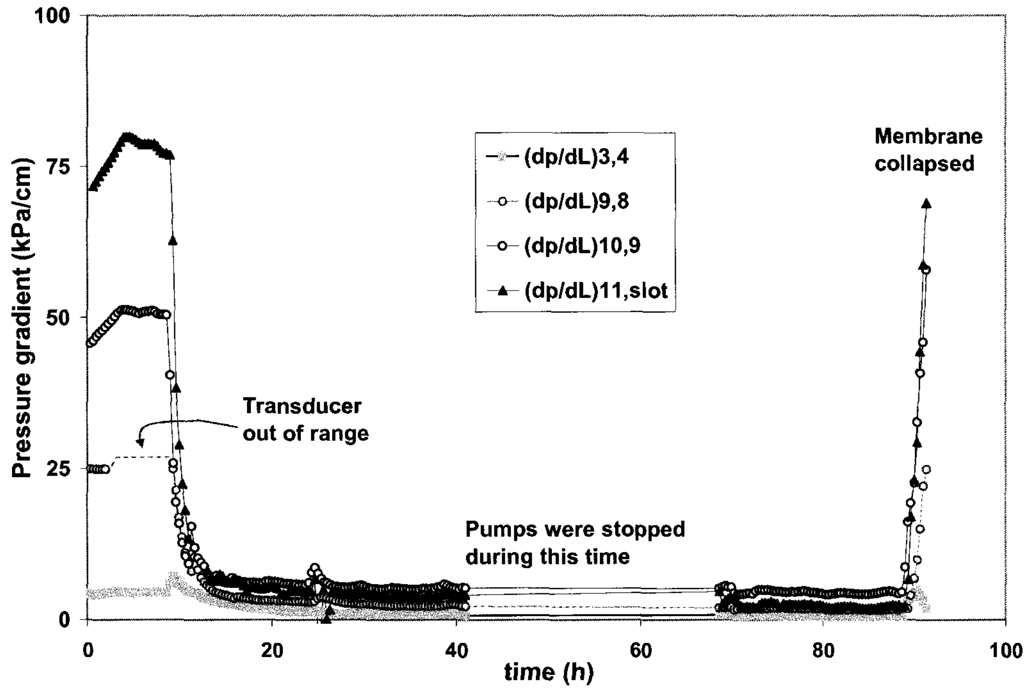

Figure 4-24: Pressure Gradient vs. time for experiment # 17. Husky sand. Slot size: 1.422 mm (0.056 in). σ_c = 507 kPa

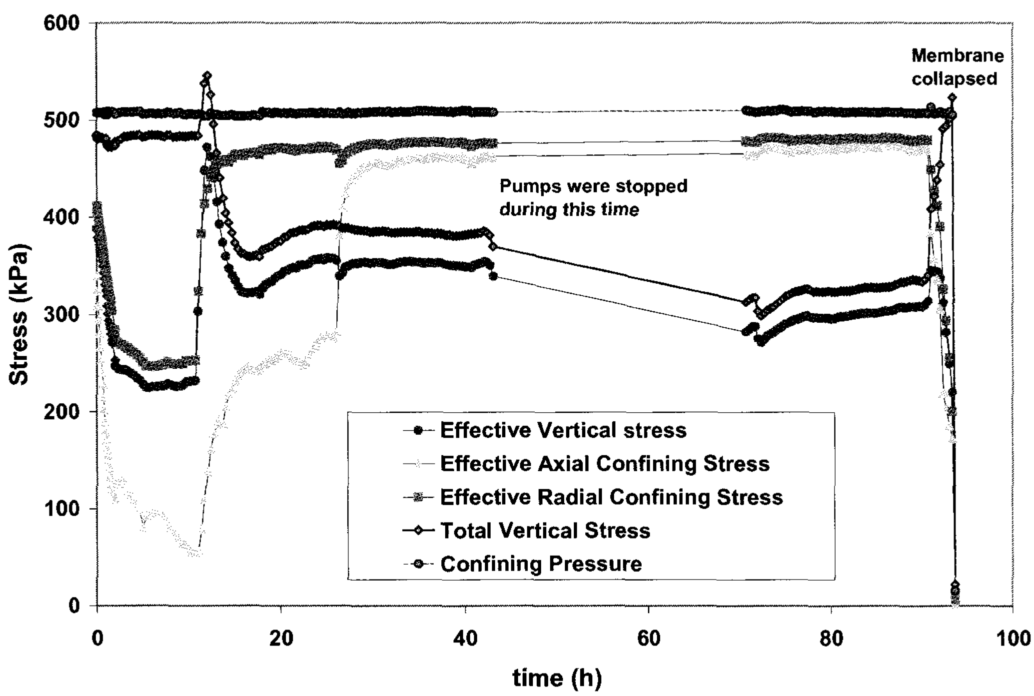

Figure 4-25: Stress distribution in the sand pack as a function of time for experiment # 17. Husky sand. Slot size: 1.422 mm (0.056 in). σ_c = 507 kPa

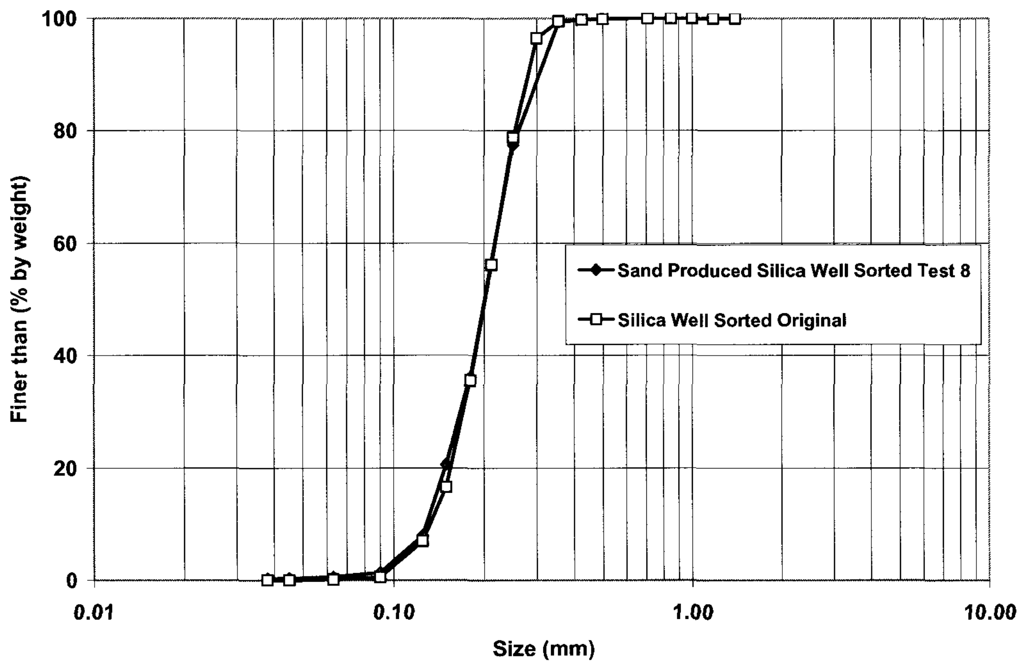

Figure 4-26: Particle size distribution curves for the sand produced in experiment 8. Sand: Silica Well Sorted. Slot Size: 1.422 mm (0.056 in). σ_c: 2469 kPa

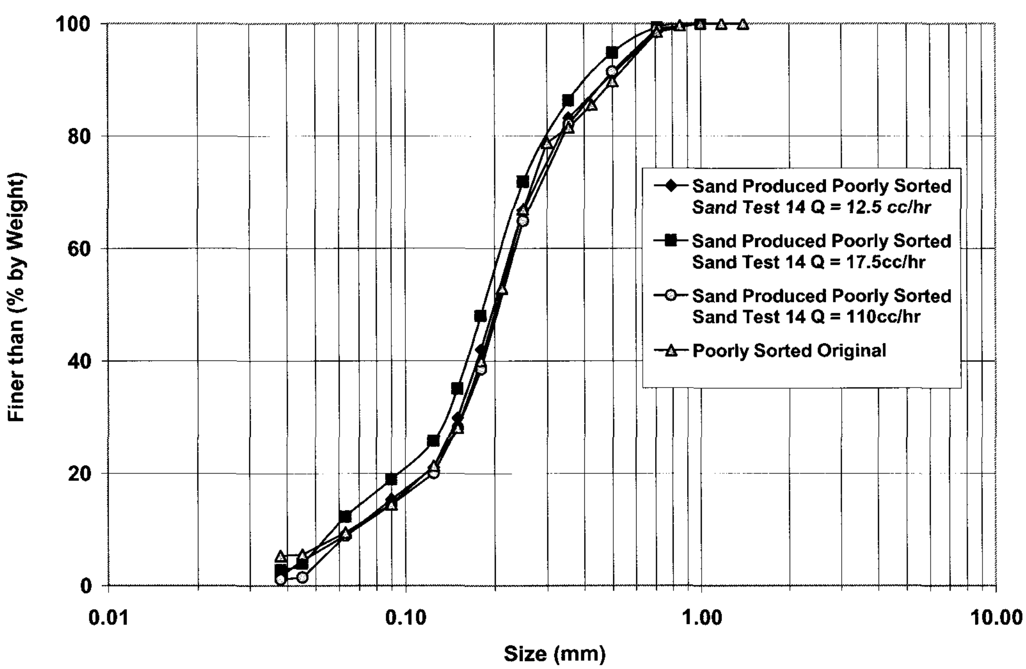

Figure 4-27: Particle size distribution curves for the sand produced in experiment 14. Sand: Silica Poorly Sorted. Slot Size: 5.944 mm (0.234 in). σ_c: 2495 kPa

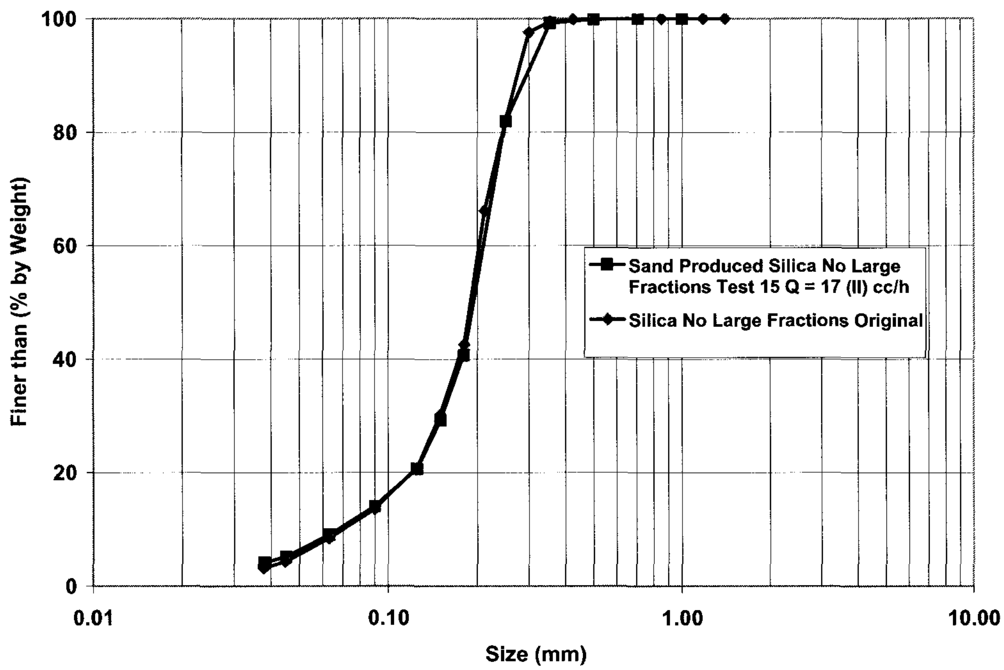

Figure 4-28: Particle size distribution curves for the sand produced in experiment 15. Sand: Silica No Large Fractions. Slot Size: 1.422 mm (0.056 in). σ_c: 2495 kPa

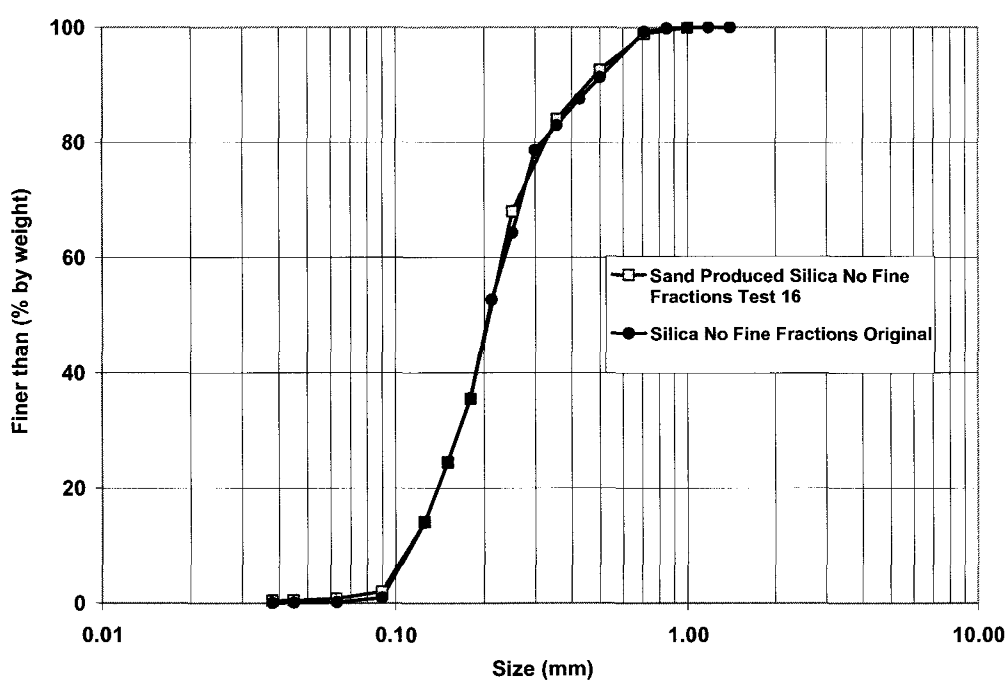

Figure 4-29: Particle size distribution curves for the sand produced in experiment 16. Sand: Silica No Fines. Slot Size: 1.422 mm (0.056 in). σ_c: 2493 kPa

4.3 Sand Strength Experiments

A successful sand production strategy involves knowledge of the different factors that provoke sand influx into the wells. Among the most critical ones are [80]:

- formation strength
- in situ stress; and
- production rate.

According to Zhang et al. [80] the key factor for predicting sand production and recommending sand control completions is the mechanical strength of a reservoir formation. However, the interconnection between the aforesaid parameters is critical in controlling the sand production process.

Knowledge of the strength parameters of the sands may help to understand the behaviour of the sands during the sand production experiments. It will also allow theoretical calculations to be performed to determine critical fluid flow rates and pressure gradients for sand production.

This section presents the results of triaxial cell experiments performed on sand packs prepared with the different sands used in this experimental program. The sand packs were saturated with residual water and dead Dee Valley heavy oil. The experiments were conducted following the method described in section 3.2.2. For each sand, a set of three tests was carried out to determine the failure envelope. The effective confining pressures chosen for each set of measurements were based on the effective confining pressure values used in the sand production tests (under confining stress); that is, 550 kPa, 345 kPa, and 140 kPa. Table 3-7 shows the initial physical properties of each sand pack used in the sand strength experiments.

An example of the deviatoric stress/axial strain graph and volumetric strain/axial strain graph obtained from the sand strength experiments is shown in Figure 4-30 for the Husky sand. The corresponding graphs for the other sands used in this experimental study are shown in Appendix B.2, Figures B-69 to B-72. As mentioned in section 3.1.2.4 on the experimental program, the strength of the sand is usually determined by the stress at failure; that is, by the peak deviatoric stress on the stress-strain plot. The corresponding stress path and the K_f-line for the Husky sand from which the cohesion and friction angle were calculated are shown in Figure 4-31. Figures B-73 to B-76 in Appendix B.2 present the corresponding graphs for the other sands evaluated.

Figure 4-32 shows the failure envelope constructed for the Husky sand using Mohr circles. The corresponding graphs for the rest on the sands are presented in Appendix B.2, Figures B-77 to B-80.

A summary of the results of the triaxial compression strength experiments (peak stress and strain conditions at failure) is displayed in Table 4-8 while the calculated cohesion and friction angles determined graphically using the Mohr circles and analytically using the p-q graphs for the sands evaluated are presented in Table 4-9. The slight differences observed between the two types of analysis can be attributed to the lack of precision inherent in the drawing of the Mohr failure envelope by a graphical method.

In previous sand production studies by Meza and colleagues [41], it was found that the grain size and/or the grain size distribution of a sand had an important influence on the sand production from sand packs saturated with a single fluid (air or silicone oil).

Those findings agreed with Lambe and Whitman [73]. They stated that the average particle size, the sorting, and the angularity affects the friction angle of a sand in two ways. First it affects the porosity that can be obtained under the same packing conditions; second, it affects the friction angle that is achieved at that porosity. Since the sands used in this experimental project have approximately the same angularity and average particle size (D_{50}), the grain size distribution will likely be the characteristic having the greatest impact on the differences in the strength of the sands.

Figure 4-33 shows a comparison of the K_f-lines of the five sands tested. The chart indicates that the sands can be divided into two main groups. The first group consists of the two stronger sands. These sands are the ones with the highest uniformity coefficient;

i.e. the poorly sorted sands (see Table 3-3 and Table 3-6) named Silica Poorly Sorted sand and Silica No Large Fractions sand. The second group consists of the three weaker sands whose uniformity coefficients allow us to classify them as well sorted sands. They are the Silica Well Sorted sand, Husky sand and Silica No Fine Fractions sand (see Table 3-3 and Table 3-6).

It has been reported [73] that poorly sorted sands have both smaller initial porosities and larger friction angles. It is certain that the poorly sorted sands in this study have smaller porosities (see Table 3-7). They also present the highest friction angle among the group (see Table 4-9). However, it can be argued that the differences in the friction angle between the Silica No Large Fractions sand and the other three weaker sands is quite small and can be considered within experimental error. Nevertheless, the Silica No Large Fractions sand has the highest cohesion among all the sands. In the subsequent discussion, it will become evident that this parameter has to be taken into consideration too in exploring the relationship between sand strength and sand production in unconsolidated sands.

Figure 4-34 presents the pressure gradient needed for continuous sand production as a function of cohesive strength for two synthetic sands (Silica Well Sorted, Silica Poorly Sorted) and a reservoir sand (Husky sand). The sand production experiments were performed using a slot size of 0.056 in and confining stresses of 500 kPa for the Silica Well Sorted and Husky sands and 970 kPa for the Poorly Sorted sand. The reason for the difference in the confining stress between the experiments performed with the Silica Well Sorted sand and the Silica Poorly Sorted sand was mentioned in section 4.2.2.2. The Silica Poorly Sorted sand has a lower permeability than the other two sands (see Table 3-8). Consequently, the sand packs made with this sand have a lower injectivity than the other sands in the study. This requires a higher injection pressure (and therefore a higher pore pressure inside the pack) to achieve the same fluid injection rate. To preserve the integrity of the sand pack, to avoid fracturing for example, the confining pressure must always be set above the maximum pore pressure in the pack. Therefore, it was necessary to set the confining pressure in the experiment with the Silica Poorly Sorted sand at a higher value than the confining pressure for the two other sands. The difference in confining pressure in this case is not expected to affect the trends in behaviour that were observed.

There appears to be a clear trend between cohesion and the pressure gradient needed for continuous sand production. The calculated friction angles were the same for the Silica Well Sorted sand and the Husky sand but the cohesive strength was much greater for the Husky sand than for the Silica Well Sorted sand. The pressure gradient required for continuous sand production with the Husky sand was more than three times higher than the pressure gradient required for continuous sand production with the Silica Well Sorted sand. The Silica Poorly Sorted sand had both a higher friction angle and a higher cohesion. This sand could not be produced continuously even at pressure gradients as high as 17 MPa/cm.

The literature on sand control identifies the uniformity of the sand as playing a key role in determining sand production behaviour [49,71]. This lead to the decision to include sands with the same D_{50} but with different sorting (see Figure 3-2) in this study. Figure 4-35 presents the pressure gradient needed for continuous sand production as a function of cohesive strength for these four sands. At first glance, there does not seem to be any clear tendency between sand production behaviour and either cohesion or friction angle. However, when the data is organized differently, taking into consideration both strength parameters, a more coherent picture emerges (see Figure 4-36). The conclusion drawn from the latter figure is that both parameters appear to be important.

A strength parameter that depends on both the friction angle and the cohesion is the unconfined compressive strength (C_o). Tremblay et al. [81] stated that since the friction angle (φ) is constant within the range of normal stress under which the sands are usually tested, the unconfined compressive strength could be calculated from [81]:

$$C_o = \frac{2c_u \cos\varphi}{1-\sin\varphi} = 2c_u \tan\left(\frac{\pi}{4}+\frac{\varphi}{2}\right) \qquad \text{4-23}$$

where c_u is the cohesion and φ is the friction angle.

The unconfined compressive strength for the five sands tested in this study is reported in Table 4-9. On the basis of the unconfined compressive strength, the Silica Well Sorted sand is the weakest sand of the five sands. This was indeed observed in the sand production experiments under confining stress. On the other hand, the sand with the highest unconfined compressive strength is the Silica No Large Fractions sand. However, in the sand production experiments, it was the Silica Poorly Sorted sand and not the Silica No Large Fractions sand that required the highest pressure gradient for continuous sand production. Although the unconfined compressive strength provides a relationship between friction angle and cohesion, it does not offer a good correlation to the behaviour observed in the sand production experiments.

An alternative approach for comparing the results of the sand strength measurements with the sand production behaviour for these sands is to consider a definition of sand strength based on the shear stress at which the sands failed in the strength tests. Table 4-10 and Figure 4-37 show the shear stress at failure for the five sands over a range of normal stress. Three main zones were identified in the graph/data. The border of each zone has been marked with a dashed line in Figure 4-37 and bold characters in Table 4-10. The first zone is at low normal stress; i.e. less than 80 kPa. Over this range of normal stress, particularly at the lower end of the range, three of the sands present very similar shear stress at failure; i.e. Silica No Large Fractions sand, Silica Poorly Sorted sand, and Silica No Fine Fractions sand. In the next zone, between a normal stress of 80 kPa and 200 kPa, the Silica Poorly Sorted sand became the strongest sand, followed in turn by the Silica No Large Fractions sand, the Silica No Fine Fractions sand, and finally the Husky sand and the Silica Well Sorted sand. This order in the strength of the sands is consistent with the results found in the sand production experiments (Figure 4-34 and Figure 4-36). The third zone occurs at a normal stress greater than 200 kPa. This is the point where the failure envelopes of the Silica Well Sorted sand and the Silica No Fine Fractions sand cross. For values of the normal stress greater than this stress, the Silica Well Sorted sand shows greater strength than the Silica No Fine Fractions sand. The strength of the Silica Poorly Sorted sand and the Silica No Large Fractions sand is emphasized in this zone. The

Husky sand is slightly stronger than the Silica Well Sorted sand throughout the range of normal stress evaluated.

As mentioned in section 3.1.2.4 on the experimental program, shearing resistance has two components [82]: a friction force between sand grains ($\sigma \tan \varphi$) due to interlocking and friction between sand grains when sheared under a normal stress, and a cohesion force (c_u) which is due to the internal forces holding sand grains together in a solid mass. At lower normal stresses, the shear stress along the failure envelope is affected most by the cohesion term. Therefore, the sands with higher cohesion will be the ones with highest strength under conditions of lower normal stress (zone 1). However, when the normal stress increases, friction begins to play more of an equal role with cohesion in establishing sand strength at failure.

A calculation of the stress distribution within the sand packs during the sand production experiments is beyond the scope of this experimental program. However, the effective normal and shear stresses in the region of the pack that subsequently failed during sand production would reasonably be expected to lie between 0 (where the sand face had experienced tensile failure) and the value of the confining stress applied to the sand pack during the experiment. Typically, the confining stress lay within zone 2 or zone 3 as defined above. The consistency of the trend between the sand production behaviour and the order of the strength of the sands for zone 2, combined with the inconsistencies in the trend between the sand production behaviour and the order of the strength of the sands for zones 1 and 3 suggests that the effective normal and shear stresses in the region of the sand pack that failed during the experiments initially lay in zone 2.

The data was also plotted against the uniformity coefficient. The results are shown in Figure 4-38. Evidently, there is a strong correlation between the uniformity coefficient of the sands and the pressure gradient required for continuous sand production obtained from the sand production experiments. The results of the triaxial experiments indicate that sands with a higher uniformity coefficient (i.e. less well sorted) were stronger. This behaviour has been attributed to better interlocking of the sand grains [73] which increases the frictional forces.

4.3.1 Section Summary

The strength parameters (internal friction angle and apparent cohesion) of sand packs prepared with the different sands used in this experimental program were determined from triaxial cell experiments. The sand packs were saturated with residual water and dead heavy oil.

The measured cohesion and friction angles allowed the set of sands studied to be divided into two main groups. The first group were the stronger sands: the Silica Poorly Sorted sand and the Silica No Large Fractions sand. The second group were the weaker sands: the Silica Well Sorted sand and the Husky sand. The Silica No Fine Fractions sand did not fit in a single category. At low normal stresses it belonged to the group of stronger sands, while at higher normal stresses, it belonged to the group of weaker sands.

Both friction angle and cohesive strength play an important role in the relationship between sand production behaviour and sand strength; it appeared that the strength of the sand as defined by the shear stress at failure provided the most consistent correlation with sand production behaviour.

From the measurements of sand strength, sands with a higher uniformity coefficient (i.e. not as well sorted) were stronger. This result is consistent with reports in the literature which state that a wider sand grain size distribution is associated with better grain interlocking within the sand which increases the frictional forces. It also reinforces the observation from the sand production experiments that a sand with a wider grain size distribution is more difficult to produce.

Table 4-8: Summary of the results of the triaxial compression strength experiments (peak stress and strain conditions at failure).

Sand	Test #	$q_f = \left(\frac{\sigma_1 - \sigma_3}{2}\right)_f$ (kPa)	$p_f = \left(\frac{\sigma_1' + \sigma_3'}{2}\right)_f$ (kPa)	σ'₃ (kPa)	σ'₁ (kPa)	ε_l (%)	ε_v (%)
Silica Well Sorted	12	965.2	1383	417.2	2348	6.4	2.0
	13	350.0	490.1	138.6	840.2	4.7	2.7
	14	88.69	125.2	36.37	213.9	4.5	4.4
Husky Sand	16	662.7	945.5	282.8	1608	4.4	2.5
	17	366.6	509.5	142.9	876.0	3.7	3.0
	18	199.4	273.2	73.83	472.6	2.3	2.1
Silica No Large Fractions	22	300.7	383.5	82.86	684.2	2.2	2.2
	23	496.2	646.9	150.8	1143	2.7	2.3
	24	806.0	1,096	290.2	1902	3.5	2.3
Silica No Fine Fractions	25	214.3	294.1	79.78	508.3	3.0	2.2
	26	315.4	451.8	136.5	767.2	3.0	1.5
	27	559.6	839.6	280.0	1399	5.9	1.7
Silica Poorly Sorted	28	524.6	669.4	144.8	1194	3.1	2.3
	29	972.8	1,269	296.2	2242	3.53	1.87
	30	286.8	354.3	67.53	641.1	2.7	2.7
	19	230.4	277.4	46.94	507.9	2.2	2.6

<u>Legend</u>

p_f and q_f: peak points of stress-strain curves

σ'_3 : effective confining (radial) stress: $\sigma'_3 = \sigma_3$-u

σ'_1 : effective principal (axial) stress: $\sigma'_1 = \sigma_1$-u

u: pore pressure

ε_l: axial strain

ε_v: volumetric strain

Table 4-9: Friction angle, cohesion and unconfined compressive strength for the different sands used in the experiments

Sands	Strength Parameters from Mohr Circles			Strength Parameters from p-q Graphs		
	Friction Angle	Cohesion	Unconfined compressive strength	Friction Angle	Cohesion	Unconfined compressive strength
	φ' (°)	c_u (kPa)	C_o (kPa)	φ' (°)	c_u (kPa)	C_o (kPa)
Husky Sand	44	20	95	44	18	93
Well Sorted Sand	44	10	48	44	7	47
No Large Fractions	45	45	217	45	47	217
No Fine Fractions	39	40	168	39	36	169
Poorly Sorted Sand	49	35	188	49	34	186

Table 4-10: Shear stress* on the failure plane in function of normal stresses for the sands evaluated in the experiments

σ_{nf} (kPa)	τ_f (kPa)				
	Poorly Sorted Sand	No Large Fractions Sand	No Fine Fractions Sand	Husky Sand	Well Sorted Sand
5	41	50	44	25	15
10	47	55	48	30	20
20	58	65	56	40	30
40	81	85	73	59	49
60	104	105	89	79	69
80	**127**	**125**	**105**	**98**	**88**
100	150	145	121	118	108
200	**266**	**245**	**203**	**215**	**205**
400	497	445	365	410	400
600	727	645	528	606	596

* The Mohr Coulomb envelopes obtained from the Mohr circles were used in the calculations

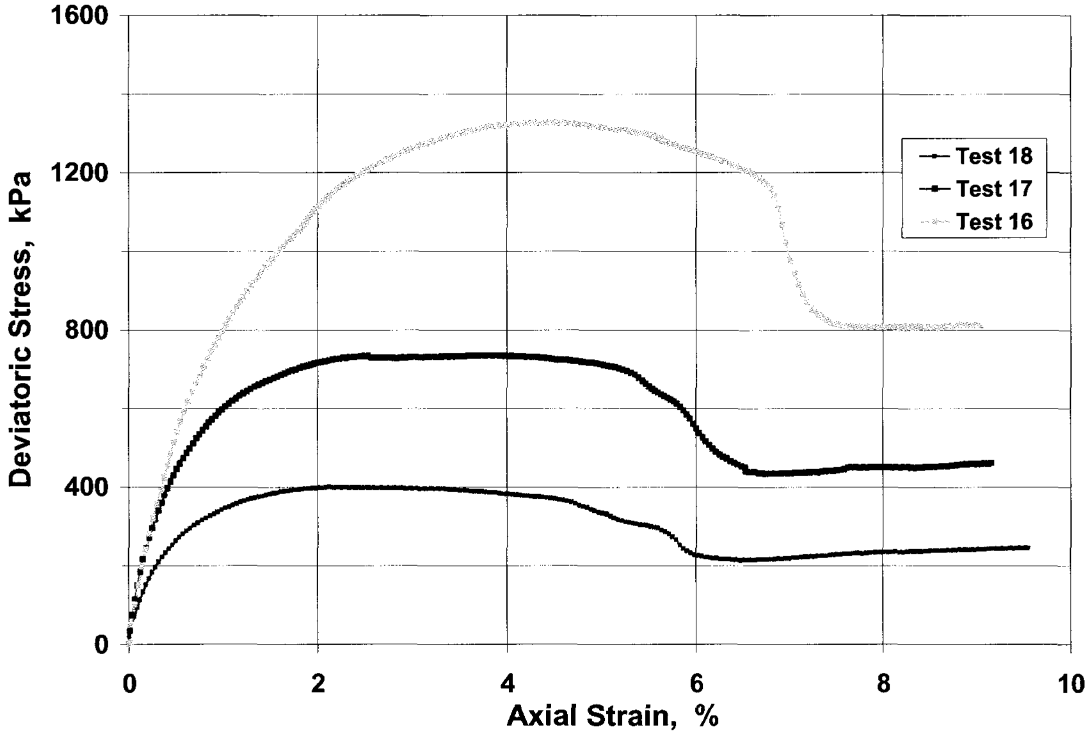

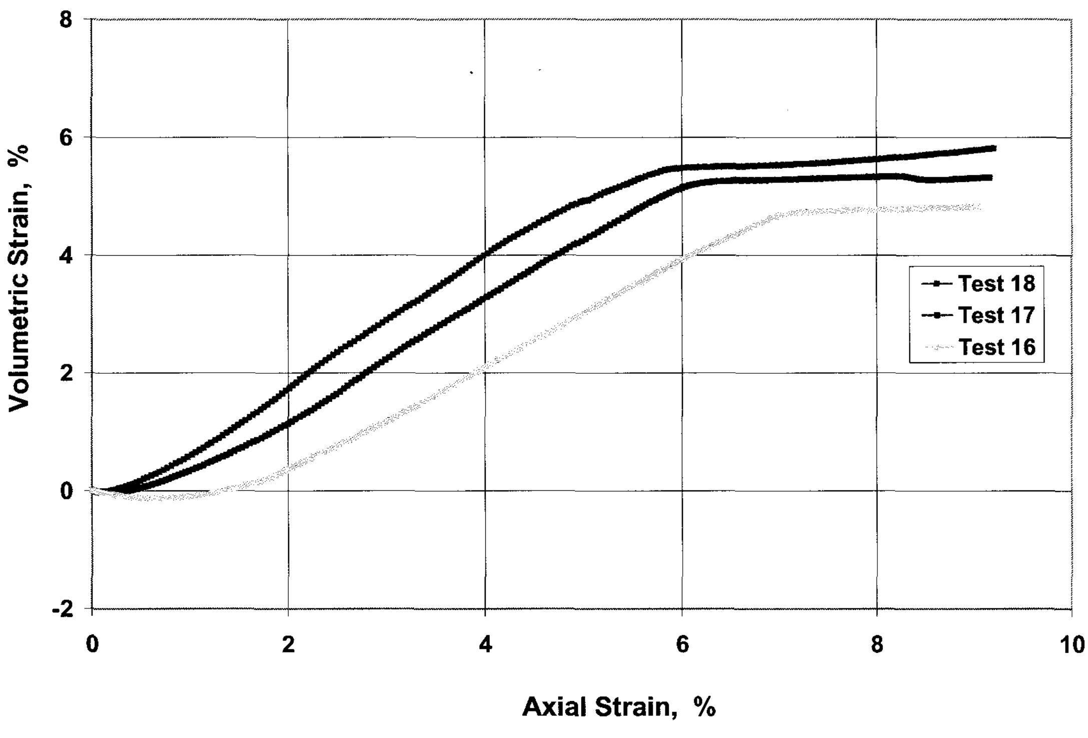

Figure 4-30: Deviatoric stress and volumetric strain vs. axial strain for the Husky sand.

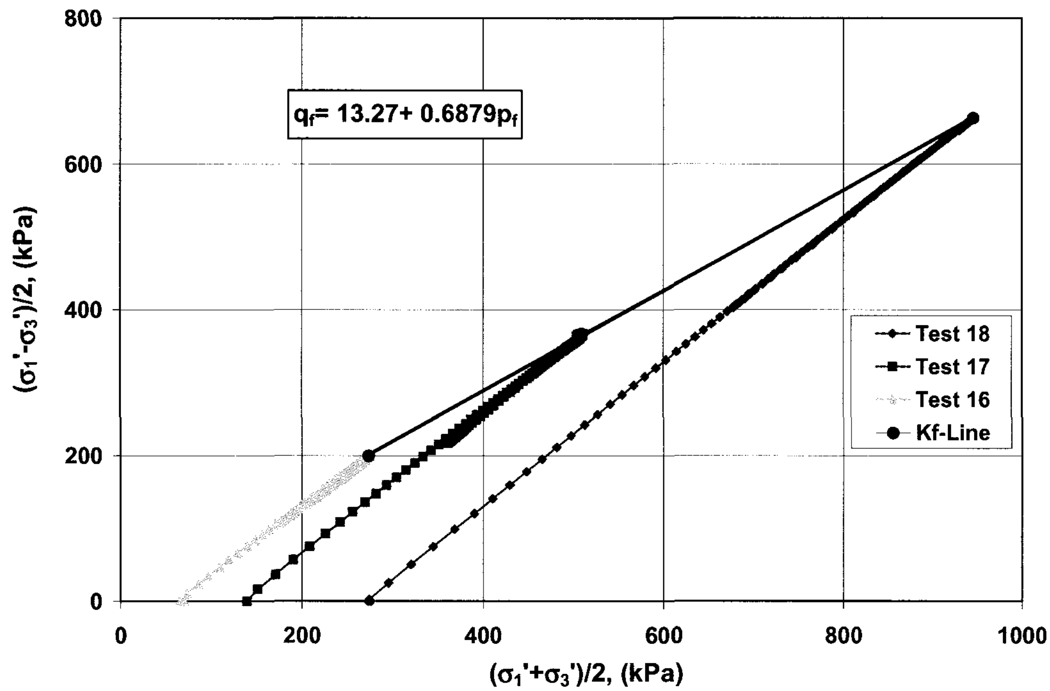

Figure 4-31: Stress path and K_f-line for the Husky sand

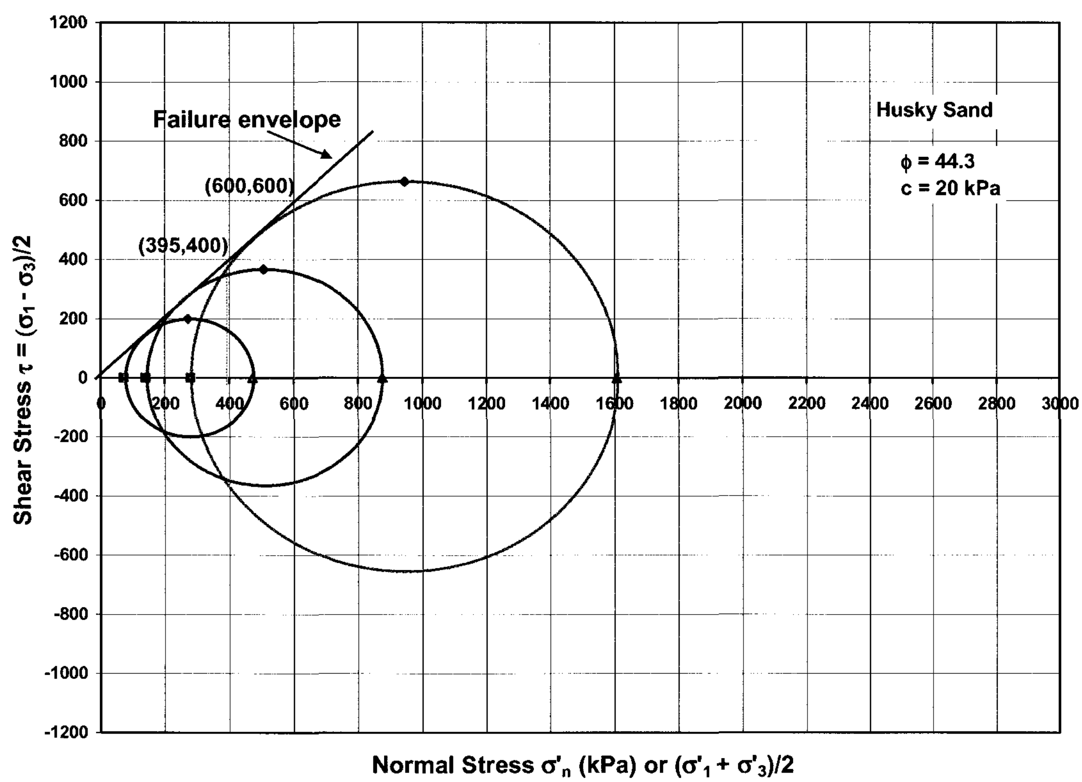

Figure 4-32: Mohr circles, failure envelope and strength parameters for the Husky sand

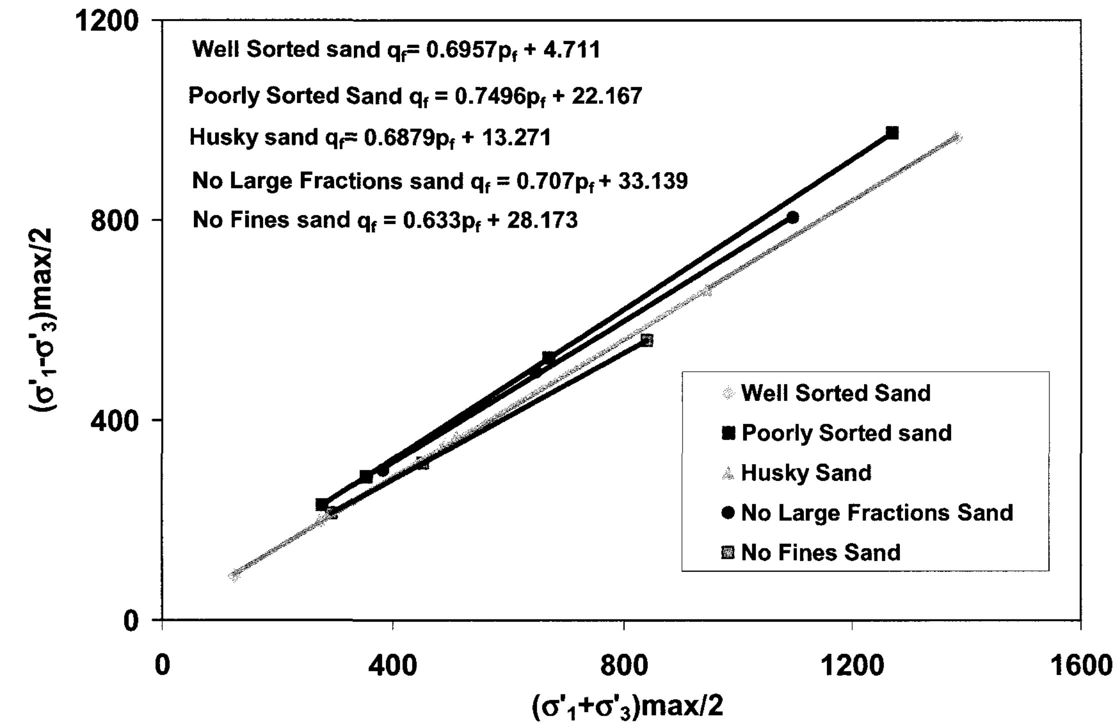

Figure 4-33: Comparative chart of the K_f-lines for the sands tested.

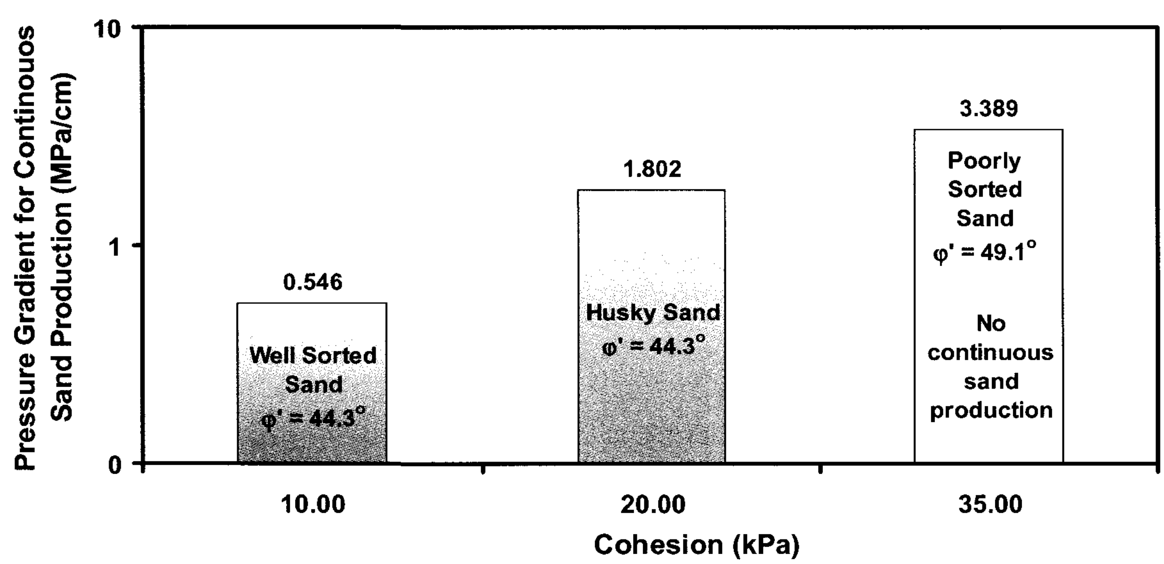

Figure 4-34: Effect of sand strength on continuous sand production; slot size: 0.056 in., confining pressure: 500 kPa.

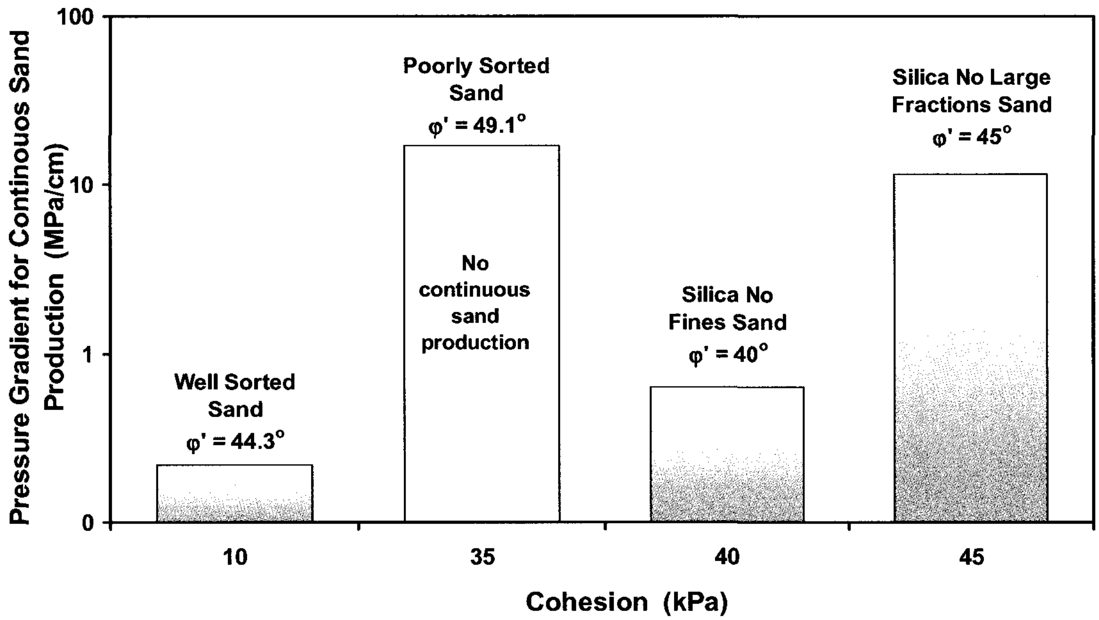

Figure 4-35: Pressure gradient for continuous sand production as a function of cohesive strength

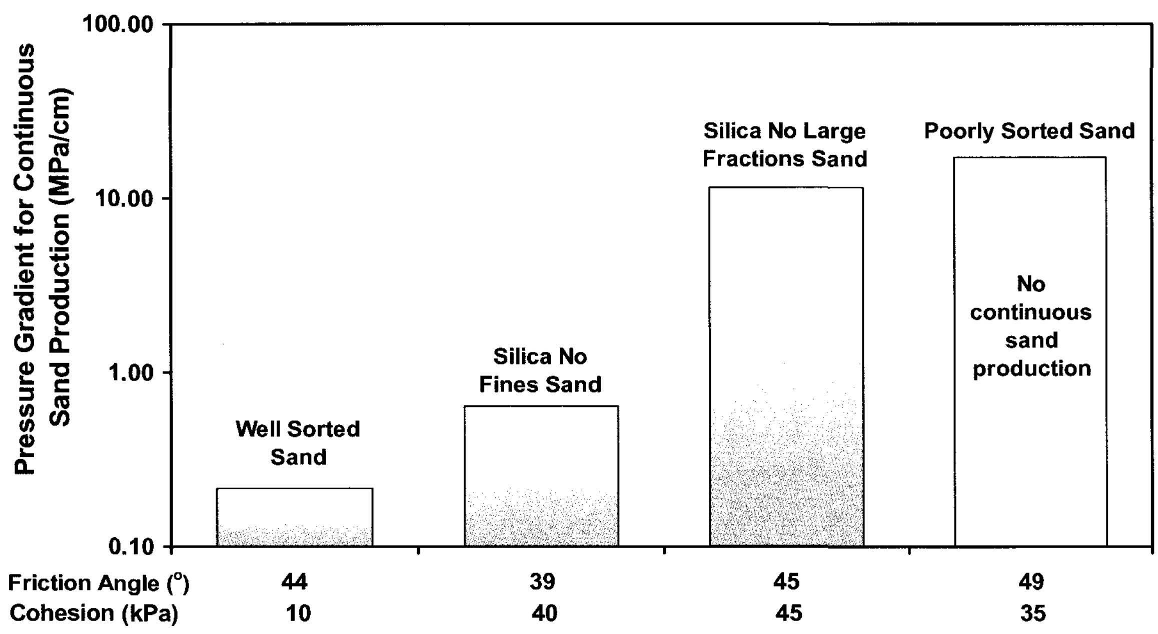

Figure 4-36: Pressure gradient for continuous sand production as a function of both friction angle and cohesive strength

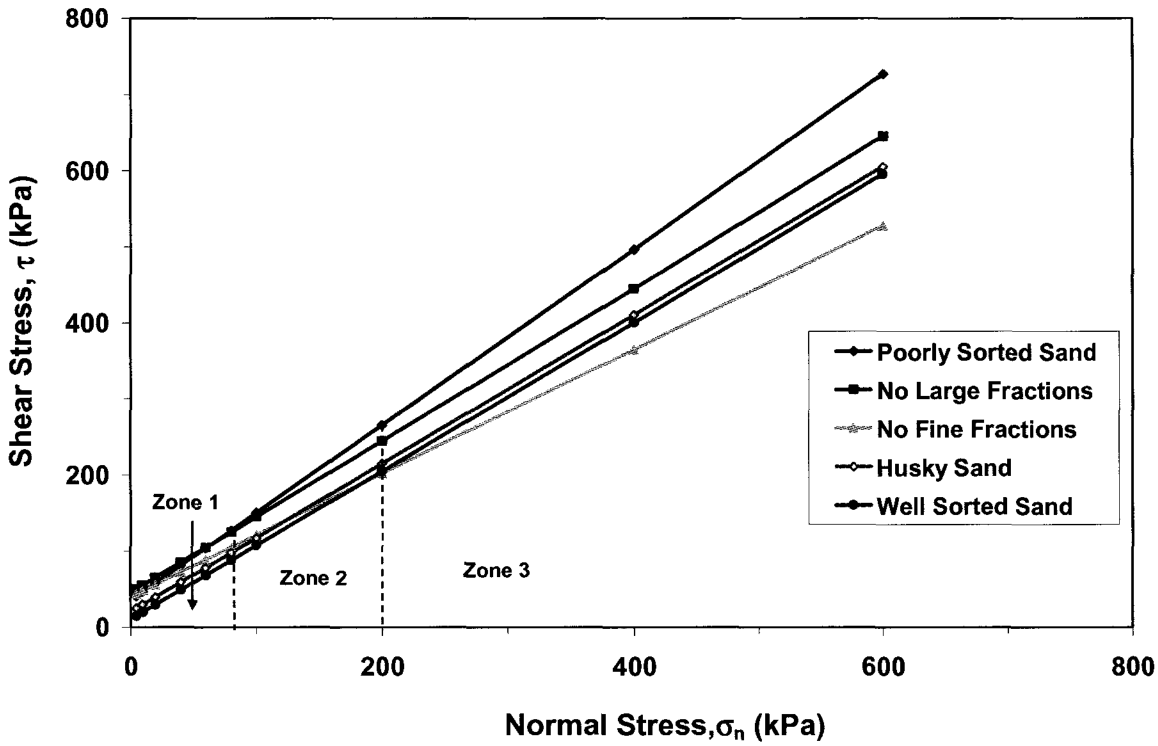

Figure 4-37: Shear stress on the failure plane as a function of normal stress

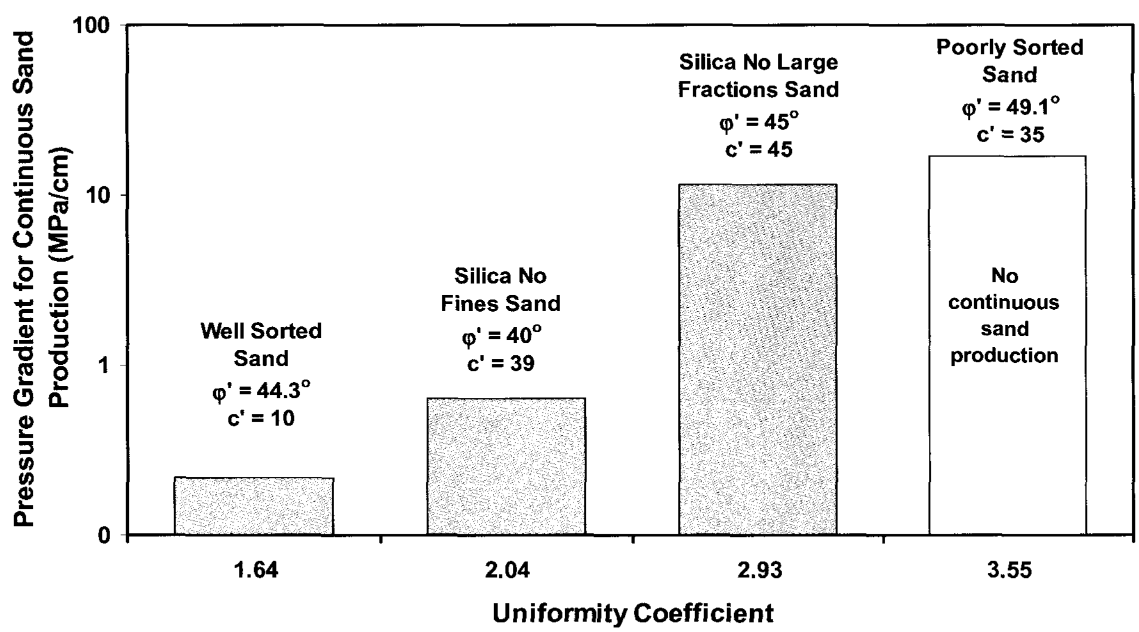

Figure 4-38: Pressure gradient for continuous sand production as a function of the uniformity coefficient of the sand.

4.4 Visualization Experiments Using CT Scanning

In order to investigate the effect of sand production on the porosity distribution within the sand packs, two kinds of CT scanning experiments were performed. The first type of experiment, called dynamic experiments, was similar in design to the set of sand production experiments under confining stress described in section 3.2.3. The dynamic experiments with CT scanning are complementary to the sand production experiments under confining stress. The intent in the CT experiments was to scan the sand pack periodically during the course of the experiment to track changes that occurred.

The second type of experiment involved scanning of the epoxied sand cores obtained from the visualization experiments intended to generate thin sections (see section 3.2.5). The idea was to scan the epoxied cores before they were cut into thin sections. If the thin sections could have been obtained, the observations from the CT images could have been combined with the information from the thin sections to allow a better understanding of pore scale behaviour as sand is produced through slots.

A detailed description of the procedure used to perform the tests was given in section 3.2.4.

4.4.1 Dynamic Experiments

Two sands were evaluated, the Husky sand and the Silica No Large Fractions sand. In this type of test, the objective was to image through CT scanning the alterations in the sand matrix provoked by sand production due to changes in flow rate. The scanner proved to be invaluable in these dynamic experiments. Real time images could be displayed with a delay of only 0.33 seconds after X-ray exposure began and continued at 12 frames/second while scanning was performed. This provided important data for guiding decisions on changes in fluid injection rate during the course of the experiment. Consequently, better control of the sand production process in the experiment was achieved.

The data collected was reconstructed as axial, coronal, and 3D images to study internal structure and changes within the experiment. The scans were run at 120 kV and 150 mAs with a small field of view resulting in a resolution of 0.47 mm. The slot size used in the experiments was 1.422 mm (0.056 in). Table 4-11 summarizes the changes in the properties of the sand packs and the total quantity of sand produced during the experiments.

The CT scanner test performed with the Husky sand presented many challenges. It involved a new experimental design with newly purchased CT equipment. The first challenge was the design of the vessel. The vessel had to be re-designed three times for different reasons including functionality and CT scanner restrictions. The final design had the slot cut directly into the bottom end cap (see section 3.2.4.1 and Figure 3-21). This design helped avoid leaks through the slot but had the drawback that the slot size could not be changed as desired as in the case of the sand production experiments under confining stress. Consequently, one intermediate slot size was chosen to evaluate the sands selected (Husky sand and Silica No Large Fractions sand). It turned out that this was not the best size for the Husky sand (see section 4.4.1.1).

It should be noted that the experiments with sand production through the slot were performed with the model in a vertical position. Scanning of the vessel in this vertical position introduced X-shaped artefacts [92]. Furthermore, the external support rings, used as a precautionary measurement in the second design to avoid the expansion of the PVC vessel under pressure, also contributed artefacts. The external support rings were later eliminated during the experiment with the Silica No Large Fractions sand after it was confirmed that it was safe to operate the vessel without them. Moreover, a hinge mechanism that allowed the cell to be placed in a horizontal position during scanning was added to the portable frame so that the X-shaped artefacts could be minimized in later experiments.

Therefore, the real time images obtained from the Husky sand experiment could not be processed since the artefacts completely distorted the images (see Figure 4-39). CT images taken of the core itself (without the vessel) after the experiment finished yielded valuable information about the experiment. However, some X-shaped artefacts were still present in the images since the sample was scanned in a vertical position due to the presence of free heavy oil at the top of the high permeability channel that had formed in the pack during the experiment. It was also determined through the course of the experiment that a higher kV setting would have allowed better penetration of X-rays through the sand pack and resulted in less noisy images.

4.4.1.1 Husky Sand

Figure 4-40 and Figure 4-41 show the cumulative sand produced, the sand cut, and the permeability behaviour as a function of time during experiment 19. Sand was produced from the beginning and did not stop for the duration of the test. The average sand cut was 40%. The cumulative sand production shown in Figure 4-40 is practically a straight line from the origin. Approximately 275 g, representing 5.85% of the total mass of sand in the sand pack, was produced (see Table 4-11). This large production of sand provoked the formation of a high permeability channel (see Figure 4-42). The initiation of the channel was observed as early as two hours after the experiment started. Initially, a cavity formed with a shape similar to what Bratli and Risnes [55] report in their experiments. The shape of the cavity has been highlighted in Figure 4-42 by black rectangles. The cavity was not at the center of the pack indicating that sand was preferentially produced from one side of the slot.

The continued sand production, indicative of continued sand failure and transport, ultimately allowed the formation of a channel (scans 4 and 9 in Figure 4-42). Two well defined zones were identified in the permeability vs. time graph (Figure 4-41). The first zone spanned approximately the first nine hours of the test and is characterized by a slight increase in the permeability. It is believed that during this time both processes occurred, channel development and scouring [13]. The permeability measurements were not initially affected by the formation of the channel. The reason for this is that, as a result of restrictions imposed by use of the CT scanner, pressure was monitored at just two locations, at the inlet and at the bottom of the cell. Therefore, the permeability reported here is the average permeability along the length of the pack. The sudden increase in permeability nine hours after the test began indicates that the channel tip had reached the inlet of the pack. At this point the channel was full of failed sand with a high porosity, 46.55% from Dean-Stark analysis (Table 4-11). After this point, sand transport of the failed sand out of the slot by the flowing heavy oil would be the predominant process during the remainder of the experiment. It is very noticeable in Figure 4-42, scan 4, that the upper part of the channel was already empty 18 hours after the initiation of the experiment. A sharper increase in the permeability measurement was observed after 25 h (see Figure 4-41). At this point 36% of the channel was empty or filled mainly with oil (Figure 4-42, scan 9). This observation was confirmed by direct inspection of the pack at the end of the test.

Figure 4-43 shows CT images of the sand pack taken without the vessel after the experiment was finished. The Hounsfield units or CT numbers scale and the equivalent porosity scale are also shown. Furthermore, CT number profiles along selected lines are represented in the graphs shown to the right of the scans. Also, square boxes were drawn in different parts of the pack. For two of these boxes, histograms of the mean CT numbers for the area circumscribed by the boxes are shown in Figure 4-43. The profile line identified as 1 in the upper scan and B-1 in the profile graph shows two shoulders and a deep valley. The Hounsfield unit values at the shoulder are close to 1200. The Hounsfield unit values decrease to -800 in the valley. Akin and Kovscek [92] reported that the CT number for air is -1000. Therefore, the valley observed indicates that the channel was empty at the top. Direct observation of the pack confirmed this inference.

The Hounsfield units value of 1200 is believed to represent the original porosity of the sand pack. Figure 4-44 presents CT images of a water-wet Husky sand pack saturated with Dee Valley oil. This sand pack did not undergo sand production. Its porosity was similar to the sand pack in experiment 19 (see Table 3-9 and Table 3-10). The row profiles in Figure 4-44 indicate that the CT numbers for the pack are quite close to 1200. The CT numbers along the sand pack are fairly uniform indicative of a relatively homogenous packing. This evidence supports the assumption that the Hounsfield units value of 1200 is equivalent to the original porosity.

The second profile line graph A-2 in Figure 4-43 corresponds to line 2 in the lower CT scan image. The shape of the graph is similar to the one described before but in this case the valley CT numbers are close to 200, or more precisely 146, from box 4. The CT number for water is 0. The density of water is close to that of heavy oil [93]. Therefore, it is reasonable to assume that the Hounsfield units value of 146 corresponds to a material that is mostly oil.

Box 5 is located inside the channel filled with failed sand. The mean CT number in this area is 895.8. This number was associated with a porosity of 46.55%. This value was obtained from Dean-Stark analysis. The last value, considered jointly with the CT number associated with the original porosity, allowed the construction of the porosity scale shown in Figure 4-43.

An important observation from the test is that the properties of the sand pack outside the high permeability channel did not change. This has been demonstrated throughout the experimental study. The experiments under confining stress also support this finding as well as the CT images obtained from the epoxied sand packs for the thin sections (see section 4.4.2). Tremblay et al. [11] have reported similar behaviour in their sand production studies. A more detailed discussion of the field implications of this result will be given in the section 4.4.2.

A pressure gradient of 2.39 MPa/cm at the slot (as calculated from equation 4-6) provided by the initial flow rate of the experiment (10 cc/h) was sufficient for the formation of a high permeability channel. This pressure gradient is quite close to the critical pressure gradient at the slot (2.07 MPa/cm as shown in Table 4-6) obtained for continuing production of the Husky sand in the sand production experiments under confining stress discussed in section 4.2.3.

Figure 4-45 represents a comparison between the scan of the sand pack taken without the vessel and an actual picture of the sand pack after it was cut longitudinally. It is evident that the CT images closely represent the actual sand pack.

Figure 4-46 shows the particle size distribution of the produced sand. The curves almost superimpose on each other. Therefore, there is no evidence that any of the fractions of the sand were preferentially produced. This result agrees with previous results from the experiments under confining stress (see section 4.2) and with reports found in the literature [11,25].

4.4.1.2 Silica No Large Fractions Sand

The sand production experiment performed with the water wet Silica No Large Fractions sand pack and saturated with dead Dee Valley heavy oil represents the most successful experiment from point of view of controlling sand production behaviour. The success of this test is greatly due to the use of the X-ray computed tomography technique.

Figure 4-47 shows how the growth of the high permeability channel could be controlled by varying the flow rate. To some extent, it also shows how sand production could be controlled. The growth of the channel was measured by measuring the length of the channel evident in the CT scanner images (Figure 4-48).

The initial flow rate for the experiment was 17 cc/h (yellow pattern in the graph). This represents a fluid velocity of 25.43 cm/h at the slot. Sand production started 30 minutes after the experiment began. The critical pressure gradient calculated at the slot for this initial flow rate (using equation 4-6) was 3.39 MPa/cm.

The flow rate was kept constant for two hours to investigate if the sand was able to arch under this condition. However, sand production did not stop during this period of time. Therefore, it was decided to decrease the flow rate by 25%. The new flow rate was 12.75 cc/h (light blue pattern in Figure 4-47). This flow rate was kept constant for approximately 18 hours. During this time, the size of the channel was stable (see Figure

4-47 and Figure 4-48). Subsequently, the flow rate was increased in steps in order to identify the new threshold flow rate for channel growth. More importantly, it was crucial to find out once the channel started to grow again, if it would be possible to stabilize/stop the sand through manipulation of the flow rate. The flow rate was successively increased to 14.88, 15.94, 17, and finally up to 21.25 cc/h. At this last flow rate, the channel started to grow again (see Figure 4-47). Consequently, the flow rate was successively reduced to 17 and 15.94 cc/h. This strategy was successful since the length of the channel stabilized again. Subsequently, a third cycle of flow rate increase was initiated. First the flow rate was raised to 17 cc/h and then to 19 cc/h; at this point the channel grew more sharply. It was possible to stabilize the channel growth again as shown in cycle three of Figure 4-47. At this point, the experiment was concluded.

A summary of the strategy adopted to decide the changes in flow rate follows. Figure 4-48 shows the coronal images of the sand pack. They are images reconstructed perpendicular to the slot. The first image shows the first scan at initial conditions. The initiation of the channel was observed 30 minutes after the test began (scan 1). At this point it was also evident that sand production had started by physical observation of the slurry produced. To track the channel growth, its length was measured by using a vertical line similar to the one shown in Figure 4-48. After the flow rate was dropped from 17 to 12.75 cc/h, the channel did not show variations in its length as seen in Figure 4-48 scans 4 and 14 and Table 4-13. Scans 15 to 22 (Figure 4-48) are examples of the images taken at the different flow rate increases applied during cycle one (Figure 4-47). The length of the channel remains constant in all of them. Scan 25 shows the increase in length of the channel at 21.25 cc/h while scans 28 to 34 show the stabilization of the channel during the subsequent decreases in flow rate during cycle two. The further development of the channel with an increase in flow rate in cycle three can be observed in Scans 36 to 38 while the re-stabilization of the channel is again reached at 15.94 cc/h. Scan 40 is an example of the last two scans taken from the pack. The shape and length of the pack remained constant in scans 39 and 40. The total channel length was approximately 75% (17.1 cm) of the length of the sand pack (23.25 cm).

An analysis of the pressure gradients involved in this sand production experiment can be performed, similar to the analysis of the sand production experiments under confining stress that was described in section 4.2.3. As noted above, the pressure gradient at the slot for the initial flow rate in the experiment was 3.39 MPa/cm. Unlike the situation with the sand production experiments under confining stress, it is difficult to estimate changes in the pressure gradient at the slot during the course of this sand production experiment. The main difficulty is that, in this case, it is not possible to track changes in the permeability near the slot caused by sand production, since the pressure could only be monitored at the inlet and at the bottom of the cell. However, it is possible in these experiments to estimate changes to the pressure gradient at the tip of the channel generated in the sand pack. The CT images obtained during the experiment allow an ideal opportunity to track changes to the shape (with a focus on the diameter) of the channel during the experiment. From this information, the pressure gradient at the tip of the channel can be estimated in a straightforward manner. For this reason, the remainder of the pressure gradient analysis in this section is focused on the pressure gradient at the tip of the channel.

For the purpose of this analysis, it is assumed that the flow into the tip of the channel was spherically symmetric. Therefore the surface area for the flow at this location was assumed to be a hemisphere with the same diameter as the channel [14]. Consequently, equation 4-7 could be used to estimate the pressure gradient at the tip of the channel. The results are shown in Table 4-12. The radius of the channel was calculated using the CT images; it is also reported in Table 4-12. The second pressure gradient shown in Table 4-12 is the critical pressure gradient for sand failure obtained from the Bratli and Risnes criterion (equation 4-9). The unconfined compressive strength of the Silica No Large Fractions sand obtained from the sand strength experiments was used in the computations (see Table 4-9). The initial permeability of the sand pack as calculated using equation 3-18 (for linear Darcy flow) and shown in Table 4-11 this should provide a suitable estimate of the permeability of the undisturbed sand pack upstream of the tip of the channel. Finally, the corresponding critical flow rate from the Bratli and Risnes criterion (calculated using equation 4-10) is shown in Table 4-12. The rows containing the flow rates at which channel growth was observed have been highlighted in turquoise in this table.

A comparison between the two pressure gradient columns indicates that channel growth was observed each time the pressure gradient into the channel exceeded the critical pressure gradient. The first calculated critical flow rate was smaller (~ 12 cc/h) than the initial flow rate in the test (17 cc/h). Therefore, the Bratli and Risnes criterion predicted that sand production would occur, as it certainly did. Following the initial flow rate, the calculated critical flow rate increased to the interval 15-17 cc/h, mainly due to an increase in the channel diameter following its initial formation. Subsequently, the channel diameter remained fairly constant. Channel growth was observed consistently in the experiments when the flow rate was greater than 17 cc/h. This agrees closely with the critical flow rate determined from the Bratli and Risnes criterion. Notwithstanding any restrictions on sand production imposed by the slot, it is evident from this analysis that the critical pressure gradient at the tip of the channel was a key factor in determining whether channel growth and subsequent sand production would occur.

Figure 4-49 shows the sand cut as a function of time. The flow rates used are represented in different colours. It might have been expected to have zero sand cuts during the periods where the channel was stable. However, in the sand production process there are two stages: 1) sand failure, and 2) sand transport [12,13]. The two stages are identified in Figure 4-49. The first stage was identified as the active growth stage. This means that during this period, sand failure occurred and, as a consequence, channel growth. These are the periods where a surge in sand production was observed (Figure 4-49). The second stage is identified in Figure 4-49 as the clean up period. In this period, although the channel does not grow the failed sand is transported to the slot by the drag force exerted by the heavy oil.

Graphs of sand cut vs. time are part of the typical information that can be obtained from the sand production experiments under confining stress. However, in a regular sand production experiment, it is not possible to identify the two stages described. It could be observed from production samples whether sand was being produced or not, but it is a more difficult task to identify if the sand produced is a consequence of channel growth or if the channel is being emptied out by scouring. This meant that any decisions to change the flow rate in the sand production experiments under confining stress were much more poorly informed. Consequently, it was more difficult to control the channel growth in these experiments.

Figure 4-50 presents the permeability of the pack in test 20 as a function of time. The cumulative sand production obtained during experiment 20 is also plotted. The original permeability of the pack was 0.79 Darcy (see Table 4-11). Slight changes in permeability were calculated during the first 40 hours of the test. As explained in experiment 19 with the Husky sand, the permeability values reported in the experiment are the average values for the pack. It is important to remember that as a result of restrictions imposed by the use of the CT scanner, pressure was monitored at just two locations, the inlet and the bottom of the cell. Also, as is discussed in the next paragraphs, the properties of the pack did not seem to change outside the channel, so a big percentage of the pack was practically unchanged during this part of the experiment. A rapid increase of the permeability was observed when the channel had grown to around 50% of the pack length. From this point on, the pressure drop began to decrease significantly. The inlet transducer was clearly registering the changes in the pack. A continuation of the test at this point could have yielded a completed clean up of the channel and consequently a major increase in permeability could have been registered.

Figure 4-51 shows the sand pack at initial conditions (t = 0). The CT numbers along the pack are quite consistent and are shown above the rectangles in the figure. Taking an average of the numbers provided, it was ascertained that the initial porosity of 33% is equivalent to 1183 Hounsfield units. The number was close to the value of 1200 Hounsfield units in the porosity scale shown in Figure 4-51. There are also four lines drawn across the pack. Each line has a corresponding graph identified as A-1, 2, 3, and 4 in the black rectangle next to the CT image. These graphs give the CT number profiles along those lines. The red lines were drawn just to isolate the information in the pack. As in the case of the CT numbers along the length of the pack, consistent CT numbers were obtained across the width of the pack at these locations.

Figure 4-51 also shows the last scan taken of the pack. Four lines were drawn across the pack. Three of them intercept the channel while the fourth one is in the upper, apparently undisturbed, part of the pack. Next to the scan are the corresponding graphs that illustrate CT number profiles along these lines.

There are two important observations that must be highlighted. First, the porosity of the pack outside the channel seems to be undisturbed as per the results observed in the upper line (A-1), above the channel, and via the values given by the other graphs outside the channel. The second observation is that the CT numbers registered inside the channel are lower than those outside the channel as shown by the valleys in the graphs A-2, A-3, and A-4. However, the porosity inside the channel is not constant. Lines A-2 and A-3 show Hounsfield units close to 500 which is approximately equivalent to 50% porosity from the scale presented in Figure 4-51. The A-4 line at the bottom of the channel represents higher porosity which is consistent with the results obtained with the Dean-Stark analysis. The Dean-Stark analysis of a sample taken at the end of the channel yields a value of 40% porosity. This is the second porosity value shown on the scale at the bottom of the figure. The variability inside the channel is captured by the high standard deviation (σ_s) of 473.7 Hounsfield units compared with the average value of 622.8 units found for the channel (see Figure 4-43).

Figure 4-52 presents the last image taken from the pack as well as a photograph of the pack. The white rectangle in the photograph isolates the channel from the rest of the pack. The CT image also shows, in this case with great precision, what happened in the pack. It can be observed that the channel is full of sand, so not enough time had elapsed for the channel to be scoured. The CT image perfectly captures the size and shape of the channel. The 3D representation of the channel in Figure 4-52 indicates that the entire area around the slot is affected. Furthermore, the channel does not seem to be in the center of the pack.

4.4.2 Epoxied Sand Packs

Experiments were performed to try to investigate visually the structures that might form in and around a slot when sand production stops. To accomplish this, sand grains within the sand pack were immobilized after sand production. The immobilization of the sand packs was achieved using a mixture of the EPO-THIN® resin and EPO-THIN® hardener. Details of the test are given in section 3.2.5. Coronal and axial CT images were taken of the epoxied sand packs prepared for the thin section tests. It was thought that the combination of both results (CT images and thin sections) could help to explain the mechanisms involved in the sand production process. However, problems during the preparation of the sand packs for the thin sections and with the preparation of the thin sections later did not allow the original objective to be accomplished. A brief description of the challenges found during the preparation of the epoxy cores will be given and the CT images of the epoxied sand packs presented.

The first challenge was to inject the epoxy resin in the core. The idea was to partially displace the oil from the pore space to cement the sand pack after sand production took place. This would have facilitated the preparation of the thin sections.

Although the initial viscosity of the resin is less than 10 mPa·s, which implies that the fluid mobility ratio was unfavourable for displacement, it increases with time as the curing process starts. As a consequence, the pressure that had to be applied during the displacement process was high (up to 500 kPa). Therefore, it is likely that the sand packs were disturbed; in particular, any arch that may have formed in them could have been disrupted. This assumption would have been resolved by observing the thin sections.

The second challenge was the preparation of the thin sections. Due to the nature of the sand packs (unconsolidated sands) and the limited success with the cementation process (epoxy injection) the sand packs were not hard enough for the standards of the companies that performed the thin section services (Vancouver Geothec-Lab and AGAT

Laboratories). A last attempt was made at the University of Alberta by the Earth Sciences Department (geological laboratory) without success.

4.4.2.1 Silica Well Sorted Sand

Two sand packs were prepared with the Silica Well Sorted sand. The slot sizes used were 0.965 mm (0.038 in) and 0.711 mm (0.028 in). The initial flow rate was 25 cc/h. Massive sand production was observed with the first slot size. A high permeability channel was formed as observed in Figure 4-54. The sand pack was partially emptied out by the epoxy resin. High porosity failed sand still remained at the end of the channel close to the slot. The row profile presented to the right of the CT image, corresponding to the line drawn in the lower part of the pack, indicates that outside the channel the porosity remained unchanged (at ~ 43%). The slurry produced during the epoxy resin injection was analyzed by Dean-Stark and a porosity of 65% was determined. The total amount of sand produced during the experiment is reported in Table 4-14.

No sand production was observed initially when the second slot size was used (0.711 mm/0.028 in) at a flow rate of 17 cc/h. To assure arch formation, sand production was stimulated by disturbing the sand around the slot with a sharp knife. Sand was produced (see Table 4-14) but eventually production stopped. The CT image of the sand pack is presented on the right hand side of Figure 4-54. There is a high permeability channel full of failed sand in the center of the pack. Once again, outside the channel the Hounsfield units are high (~ 1300), indicative of the original porosity of the pack. The bright blue color at the top of the images and inside the high permeability channel corresponds to the epoxy resin. Its Hounsfield units are ~ 150. A void is also observed at the bottom of the pack.

The packs were preserved in a freezer before they were taken to the thin section lab.

4.4.2.2 Silica Poorly Sorted Sand

One sand pack was prepared with the Silica Poorly Sorted sand. The slot size used was 0.711 mm (0.169 in). Sand was produced at the beginning of the test at the initial flow rate of 12.5 cc/h but stopped shortly thereafter. A relatively small amount of sand (26.53 g) was produced (see Table 4-14).

Figure 4-55 shows the CT image of the pack. As in the case of the sand production experiments under confining stress (see, for example, the channel cast from experiment 14 as shown in Figure 4-15), a narrow channel was observed. It seems that stronger sands have the tendency to produce narrower channels than weaker sands. The channel is observed closer to the right edge of the pack in the CT image. The channel is not emptied; it is rather filled with sand at a higher porosity than the original sand pack (see the left hand side scale and raw profile graph in Figure 4-55).Outside the channel the porosity remains unchanged.

4.4.2.3 Husky Sand

Two sand packs were prepared with the Husky sand. The first slot size used was 0.965 mm (0.038 in). The initial flow rate was 25 cc/h. Massive sand production occurred. A big empty void was observed in the CT image (see Figure 4-56). The void is not filled with the epoxy resin but rather with air as indicated by the row profile graph to the right of the CT image in the upper part of Figure 4-56. The Hounsfield unit for air is -1000 [92]. However, the fact that the sand pack was in one piece indicates that some epoxy resin must have penetrated the pack.

A second experiment was performed with a smaller slot size. The second slot size selected was 0.813 mm (0.032 in). The initial flow rate this time was 10.5 cc/h. Sand was produced at the beginning and stopped 4 hours later. The arches were stable since an increase in flow rate to 15 cc/h did not yield sand production. However, the pressure inside the cell with the new flow rate was close to the working limit for the cell. Therefore the flow rate was decreased to12 cc/h. No sand was spontaneously produced during this flow rate. To investigate if the sand could arch if sand production would have occurred naturally; sand production was induced by introducing the tip of a knife into the slot. A small amount of sand was produced (11 g). Sand production stopped two hours after the knife disturbed the arches.

The CT image of this sand pack is presented in the lower part of Figure 4-56. There was no channel formation. The Hounsfield units for the sand pack are relatively high, close to 1200. This value may represent the original porosity according to a CT image of a Husky sand pack that did not undergo sand production (Figure 4-44). The latter sand pack showed average Hounsfield units of 1300. This difference in the CT numbers between the two sand packs could be considered within experimental error. The sharp drop in the row profile graph corresponds to the presence of air. The pack had a fracture that was created when the sand pack was taken out of the split cell.

4.4.3 Section Summary

The computed tomography (CT) technique allowed changes in the sand pack, due to changes in the oil flow rate, to be tracked in real time. CT observations provided critical input to decisions on flow rate alterations during the test. It was found that channel growth could be controlled successfully (i.e. stopped/started) through flow rate changes. It was also found that the estimated pressure gradient at which sand failure occurred at the channel tip, provoking channel growth, agreed remarkably well with the predicted critical pressure gradient for sand failure at the tip of a channel provided by the Bratli and Risnes [55] stability criterion. Furthermore, as in previous experimental results, it was found that outside of the channel, porosity (and permeability) did not change.

Sand packs were prepared to make thin sections from the pack following sand production. Unfortunately, challenges in preparing the packs for creating thin sections and in preparing the thin sections later could not be overcome, so no thin sections were generated. However, the sand packs prepared to make the thin sections were generated, and these packs were scanned. The results of the scanning supported previous findings from the visualization experiments using CT scanning and from the sand production experiments under confining stress.

Table 4-11: Dynamic CT scanner tests. Characteristics of the sand packs after sand production and amount of sand produced.

Test #	Sand	k_{oi} (D)	k_{of} (D)	ϕ_i (%)	ϕ_f (%) Carman-Kozeny	Amount of Sand Produced (g)		ϕ_f (%) from Dean-Stark analysis						
						M.B.	Actual	ϕ_T		ϕ_M		ϕ_B		Channel
								Left	Right	Left	Right	Left	Right	
19	Husky Sand	0.54	10.11	37.8	66.4	274.9	274.61	38.2	37.8	38.5	39.0	37.2	37.4	46.6
20	Silica No Large Fractions	0.79	1.63	33.1	40.1	98.9	81.77	31.1	30.7	30.6	31.2	31.4	30.7	39.1

k_{oi} = Initial oil effective permeability
k_{of} = Final oil effective permeability
ϕ_i = Initial Porosity
ϕ_f = Final porosity
ϕ_T = Porosity at the top of the pack
ϕ_M = Porosity in the middle of the pack
ϕ_B = Porosity at the bottom of the pack
Left = left side of the pack
Right = right side of the pack

Table 4-12: Computed pressure gradients and sand produced for each flow rate in experiment 20.

μ_o* (mPa·s)	Q (cc/h)	Average r_{Ch} (cm)	$(dp/dr)_{Ch}$ (MPa/cm)	$(dp/dr)_{Cr}$ (MPa/cm)	Q_{cr} (cc/h)	Sand Produced (g)
3,615.45	17.00	0.5	1.2	0.80	11.2	5.85
3,424.23	12.75	0.8	0.44	0.58	11.6	21.24
3,831.79	14.88	0.8	0.58	0.58	16.8	6.77
3,309.08	15.94	0.8	0.53	0.58	15.0	2.70
3,755.79	17.00	0.8	0.65	0.58	17.4	4.41
3,537.71	21.25	0.7	0.84	0.61	15.3	17.82
3,740.56	17.00	0.8	0.54	0.53	15.5	8.39
3,537.71	15.94	0.8	0.48	0.53	16.8	10.32
3,781.79	17.00	0.8	0.55	0.53	17.7	2.86
3,815.17	19.13	0.8	0.62	0.53	16.6	0.91
3,675.39	17.00	0.6	0.95	0.71	16.4	0.03
3,777.50	15.94	0.8	0.51	0.53	12.8	17.64

*Viscosity variations are due to small changes in the cell temperature from 20 °C
r_{Ch} = average radius of the channel

$(dp/dr)_{Ch}$ = pressure gradient at the tip of the channel

$(dp/dr)_{Cr}$ = critical pressure gradient for sand failure

Table 4-13: Tracking the high permeability channel growth from the CT images.

CT Scan Number	Time (h)	Flow Rate (cc/h)	Length of the Channel (cm)
0	0.00	17.00	0.00
1	0.33	17.00	1.1
2	0.83	17.00	3.2
3	1.33	17.00	4.5
4	1.83	12.75	5.1
5	2.17	12.75	5.1
6	2.83	12.75	5.1
7	3.17	12.75	5.1
8	3.83	12.75	5.1
9	4.33	12.75	5.1
10	4.83	12.75	5.1
11	5.83	12.75	5.1
12	8.67	12.75	5.1
13	19.00	12.75	5.1
14	20.67	12.75	5.1
15	21.83	14.88	5.1
16	23.00	14.88	5.1
17	25.83	14.88	5.1
18	26.33	15.94	5.1
19	28.33	15.94	5.1
20	29.33	17.00	5.1
21	30.00	17.00	5.1
22	32.00	17.00	5.1
23	33.17	21.25	5.8
24	33.83	21.25	6.7
25	34.33	21.25	7.0
26	34.83	21.25	7.7
27	35.33	17.00	8.3
28	35.67	17.00	8.6
29	35.83	17.00	8.6
30	36.17	17.00	8.6
31	44.67	15.94	8.6
32	45.00	15.94	8.6
33	47.33	17.00	8.6
34	49.00	17.00	8.9
35	49.83	19.13	9.3
36	50.83	19.13	10.9
37	51.33	17.00	11.8
38	51.83	15.94	12.5
39	52.33	15.94	17.1
40	55.83	15.94	17.1

Table 4-14: Amount of sand produced during the sand production experiments with the sand packs prepared for the thin sections.

Sand	Slot Size (mm (in))	Sand produced (g)	ϕ_i (%)	ϕ_{Ch} (%)
Silica Well Sorted	0.711 (0.028)	155.67	42.7	--
	0.965 (0.038)	309.74	42.9	65.7
Husky Sand	0.813 (0.032)	45.75	39.4	--
	0.965 (0.038)	171.93	38.7	59.9
Silica Poorly Sorted	4.293 (0.169)	26.53	34.7	--

ϕ_i = initial porosity

ϕ_{Ch} = porosity inside the channel

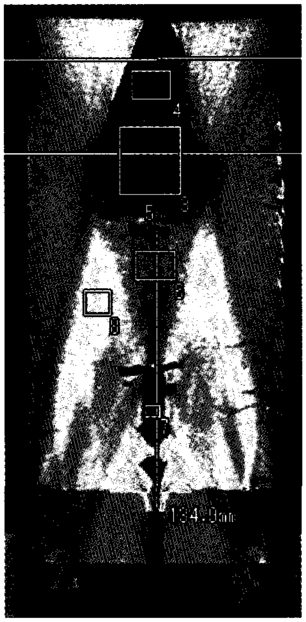

Figure 4-39: CT image from experiment 19 showing the X-shaped artefacts. Husky sand. Slot size 1.422 mm (0.056in)

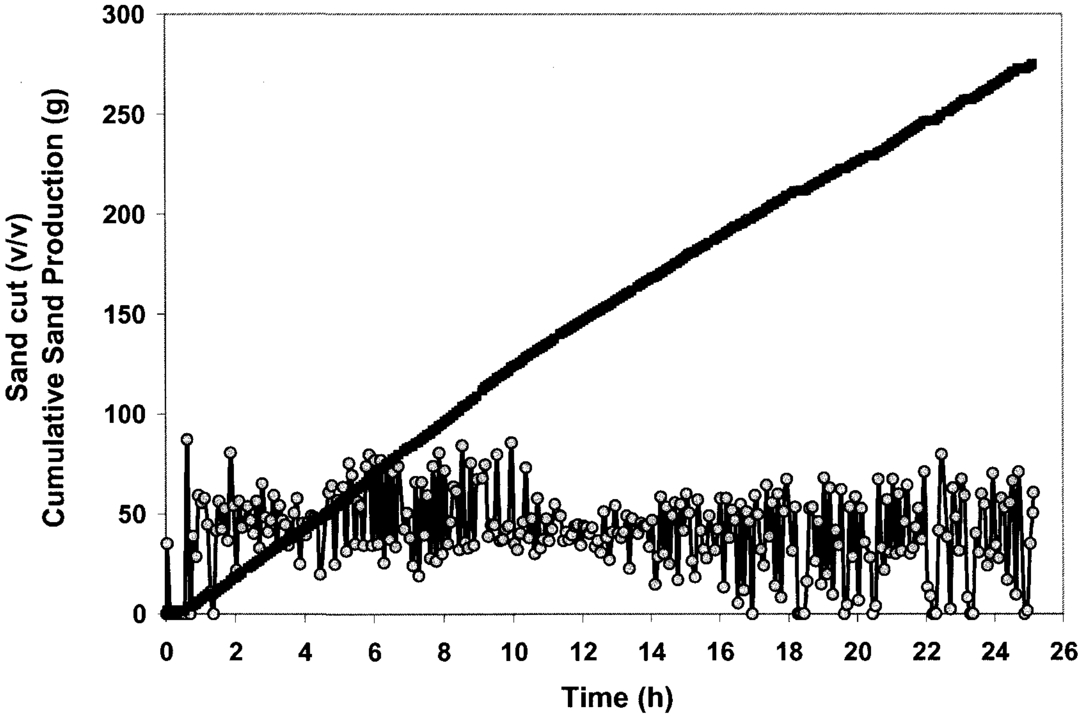

Figure 4-40: Sand cut and cumulative sand production as a function of time. CT scanner experiment 19. Husky sand. Slot size: 1.422 (0.056 in)

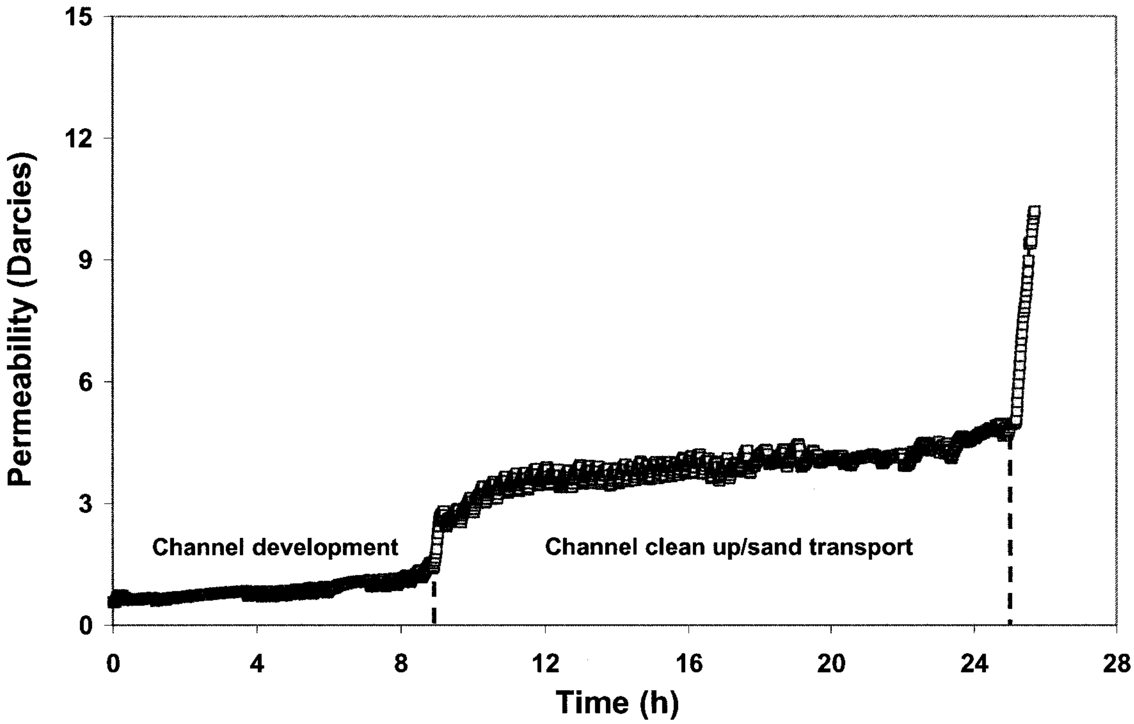

Figure 4-41: Permeability as a function of time. CT scanner experiment 19. Husky sand. Slot size: 1.422 (0.056 in)

Scan 1	Scan 2	Scan 3	Scan 4	Scan 9
t = 0	t = 2h	t = 3h	t = 18.5h	t = 25h

Figure 4-42: Sagittal images of the sand pack during experiment 19. Husky sand. Slot size: 1.422 (0.056 in)

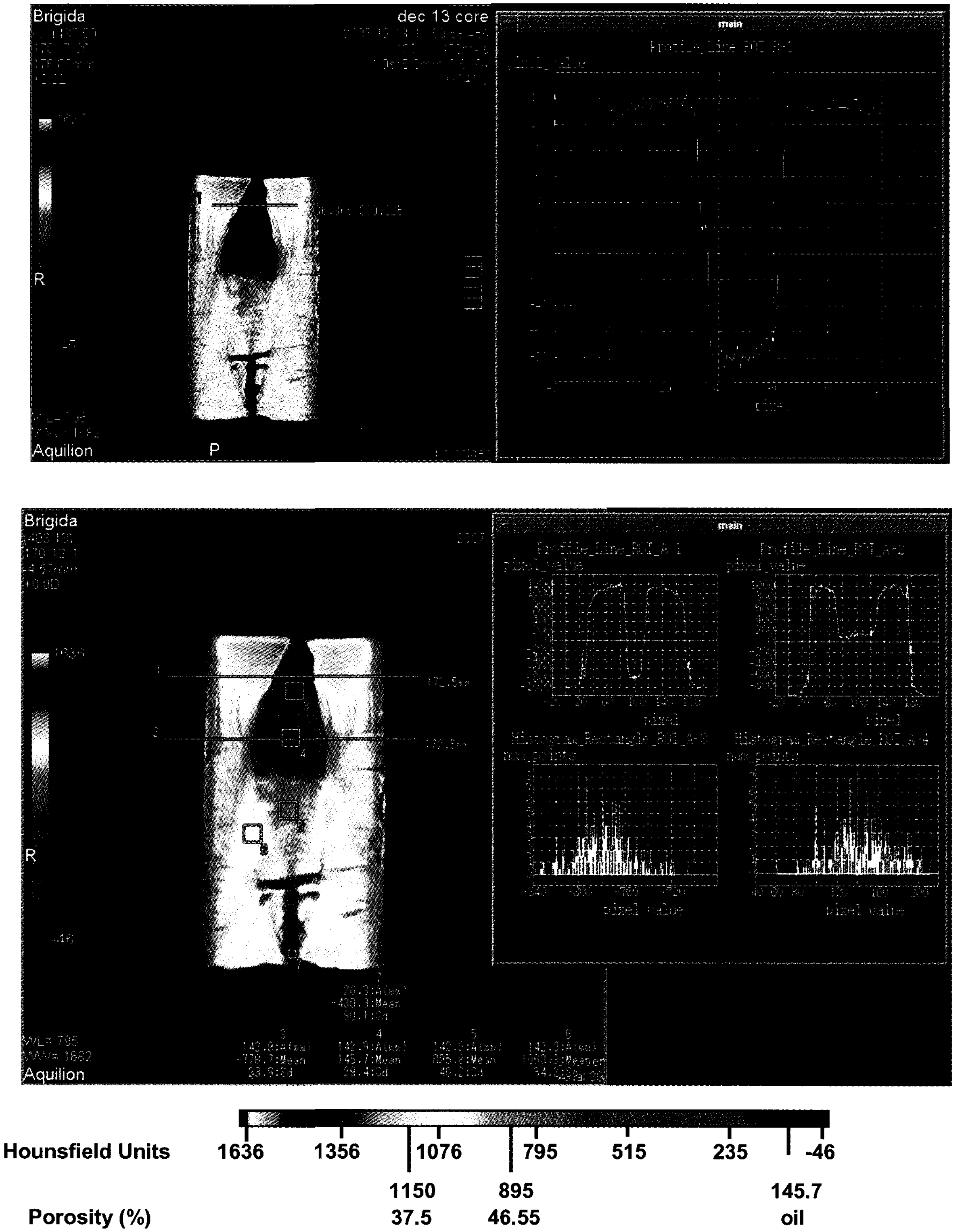

Figure 4-43 : CT scanner images and sand pack statistics at the end of experiment 19.

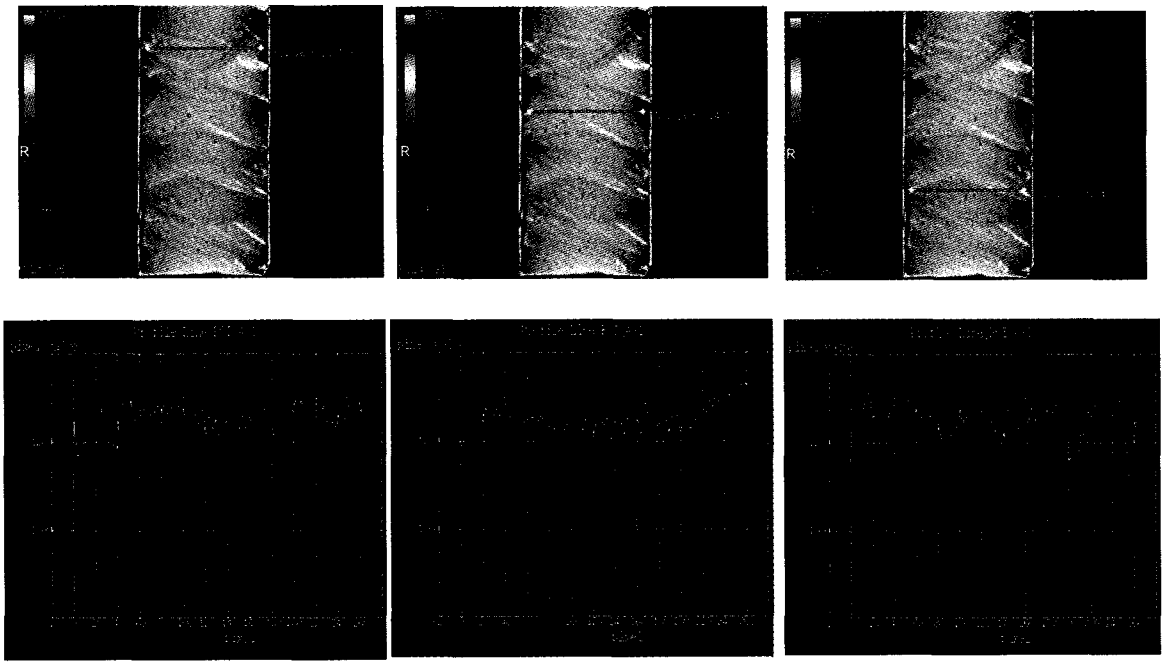

Figure 4-44: Water wet Husky sand pack saturated with Dee Valley Oil.

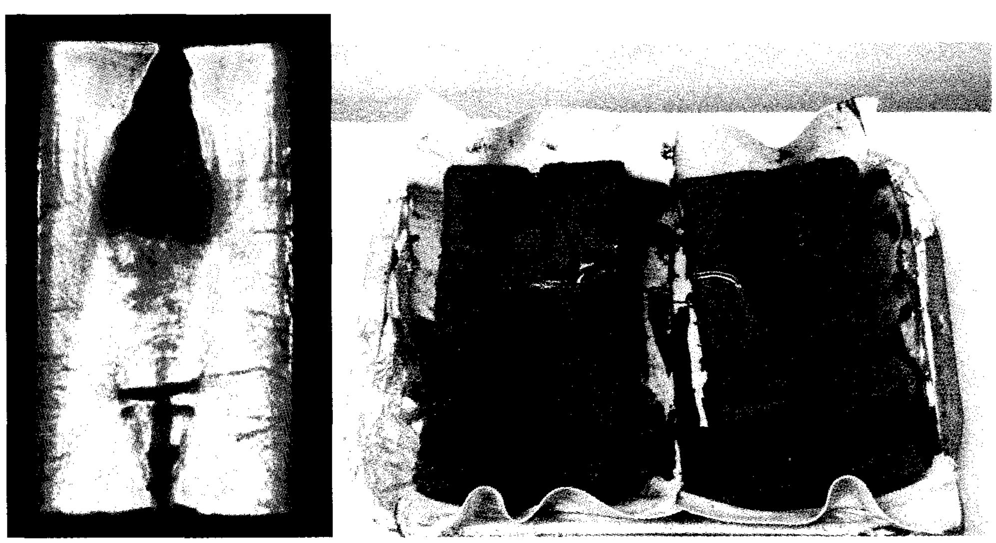

Figure 4-45: Experiment 19 Sand Pack. Husky sand. Slot size: 1.422 (0.056 in). CT Scanner image at the end of the experiment vs actual sand pack.

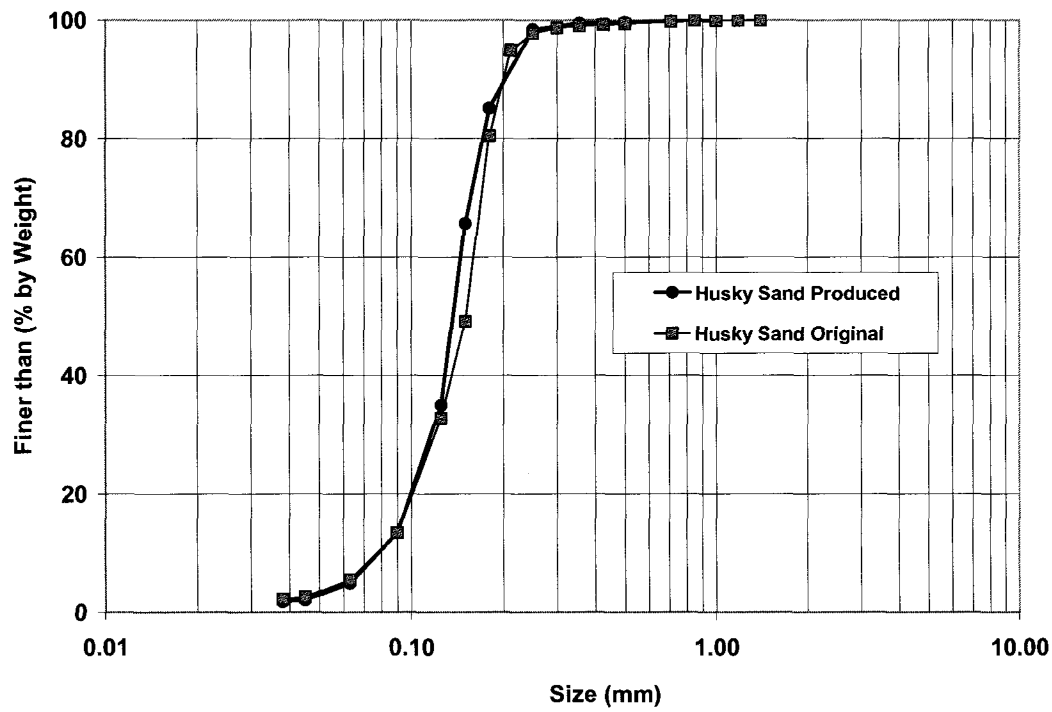

Figure 4-46: Grain size analysis of the sand produced during experiment 19.

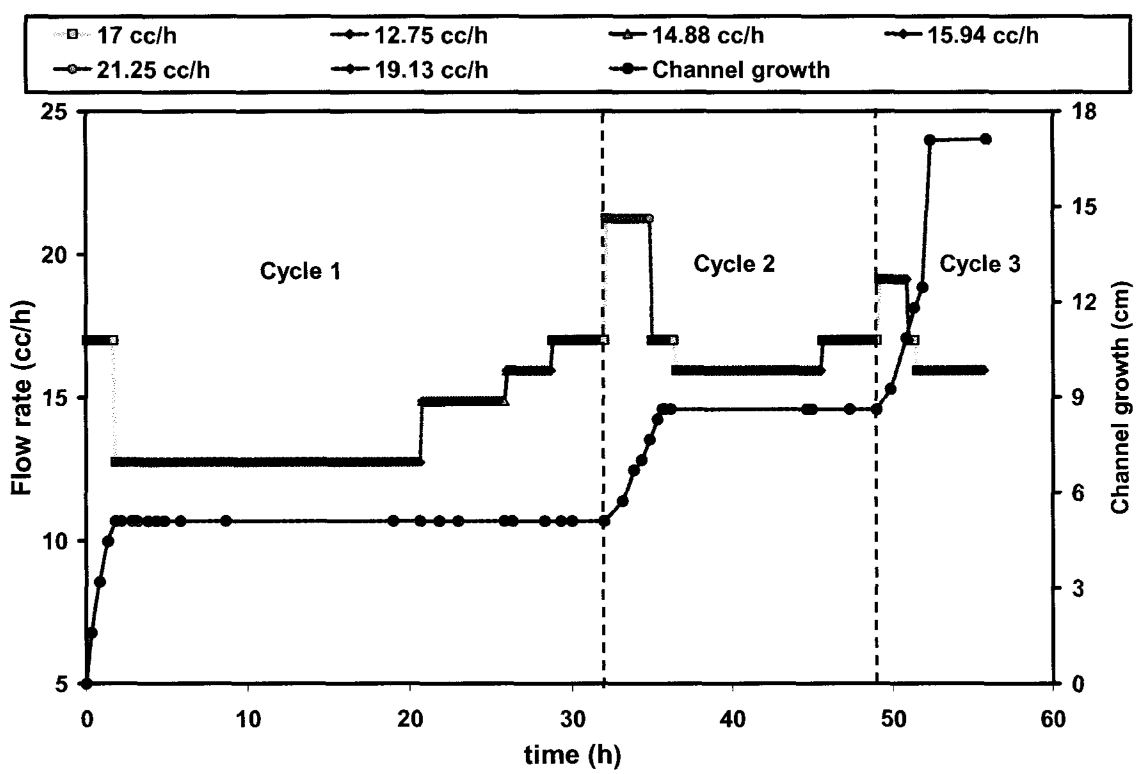

Figure 4-47: Controlled channel growth through flow rate changes.

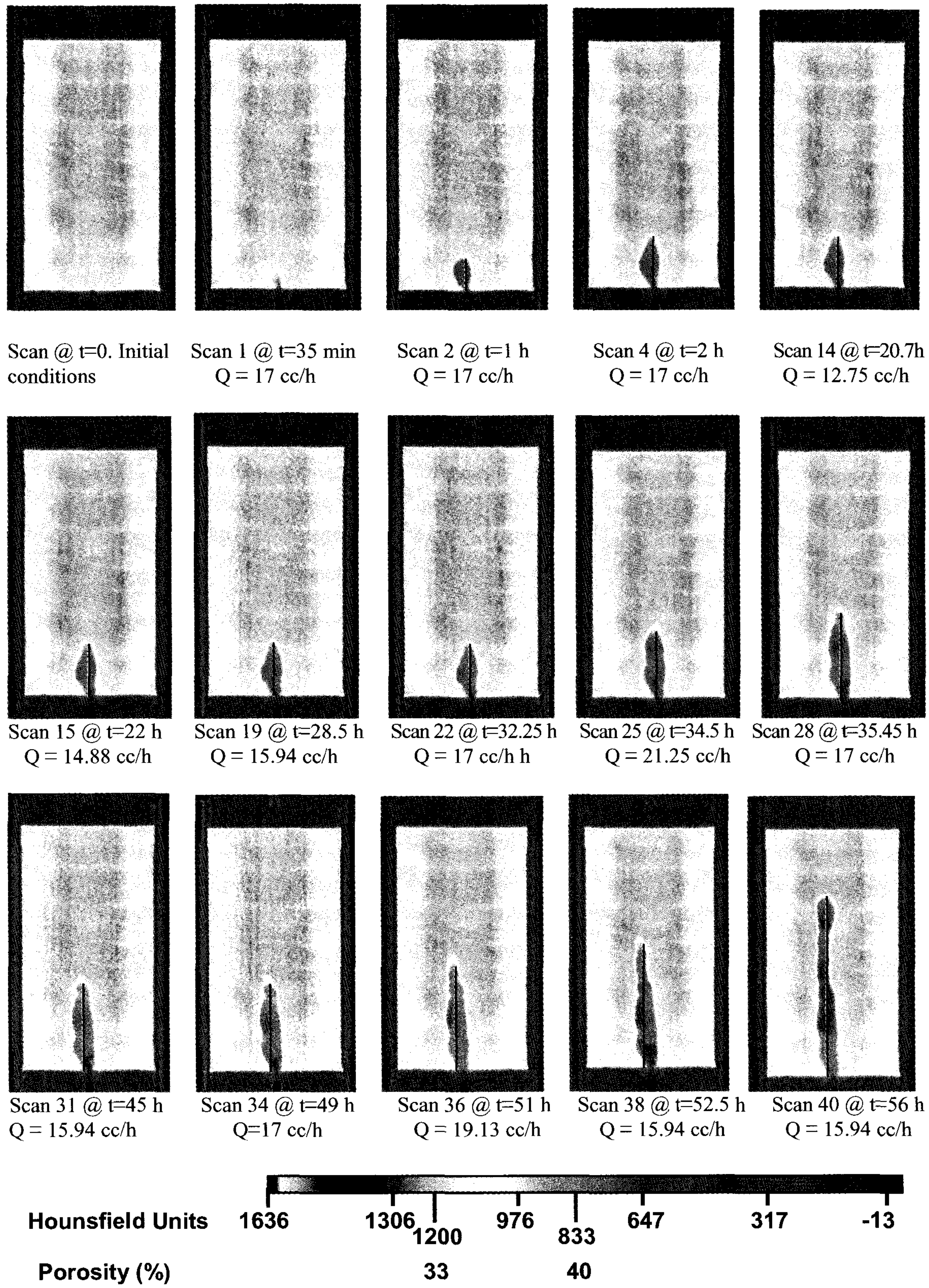

Figure 4-48: Channel growth follow up with the CT scanner

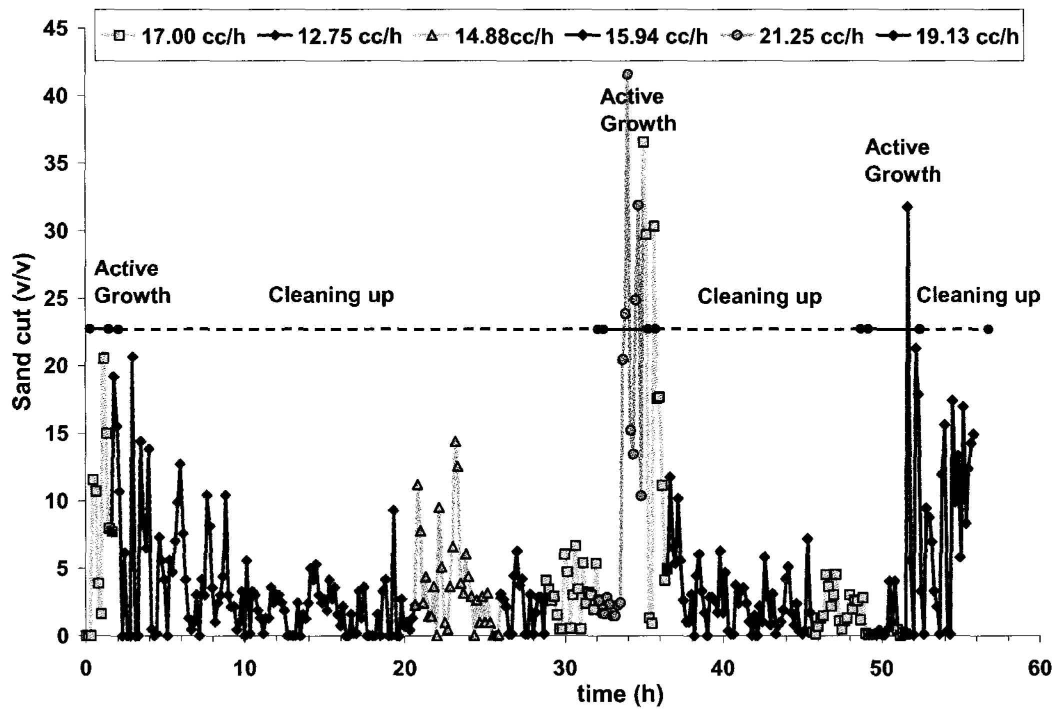

Figure 4-49: Sand cut as a function of time. CT scanner experiment 20. Silica No Large Fractions sand. Slot size: 1.422 (0.056 in)

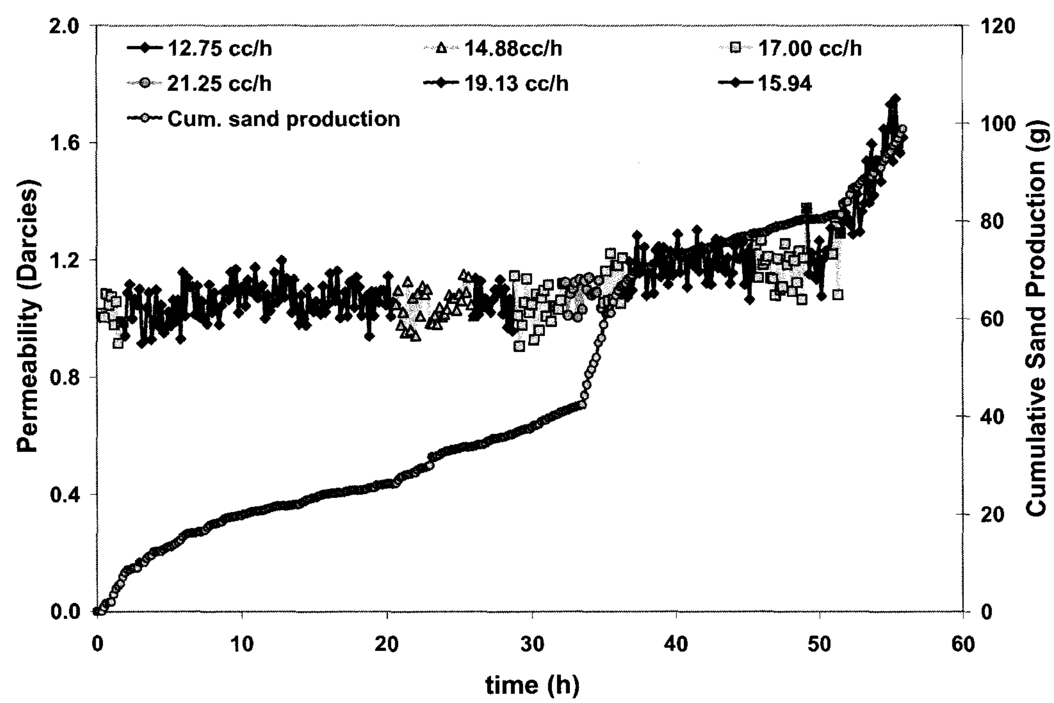

Figure 4-50: Permeability and cumulative sand production as a function of time. CT scanner experiment 20. Silica No Large Fractions. Slot size: 1.422 (0.056 in)

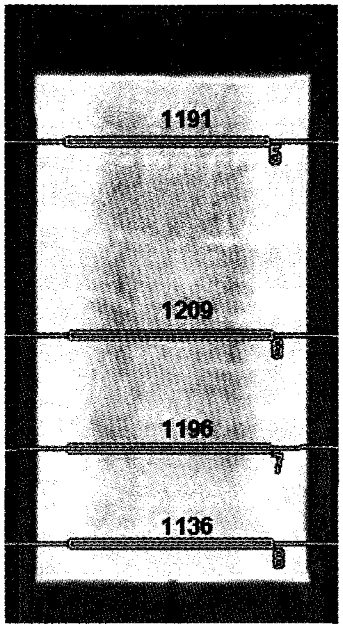

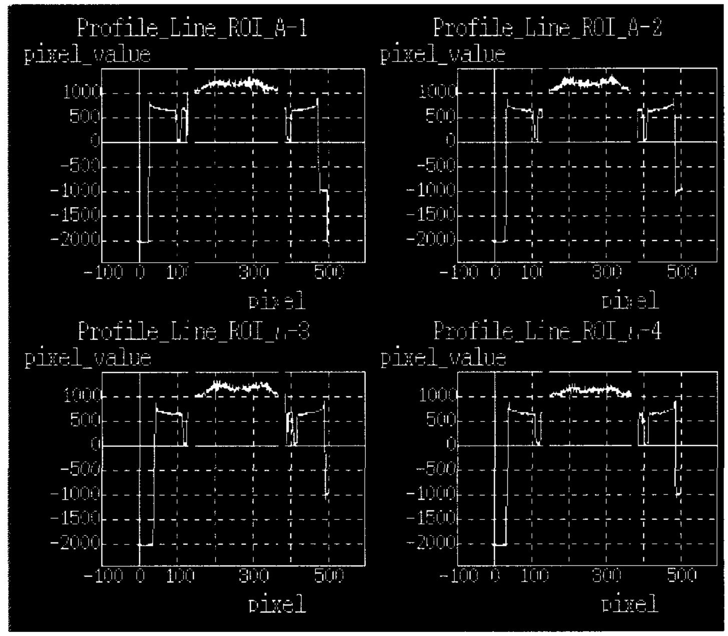

Initial Conditions @ t=0

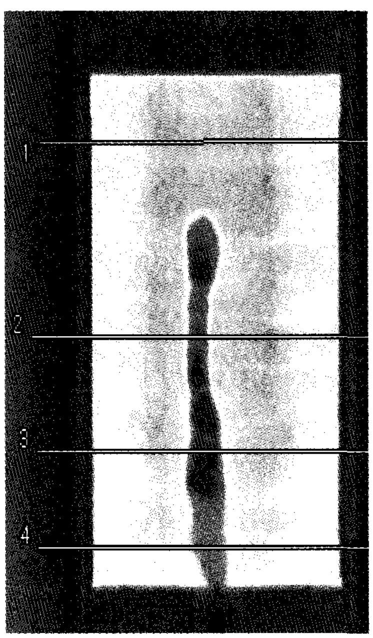

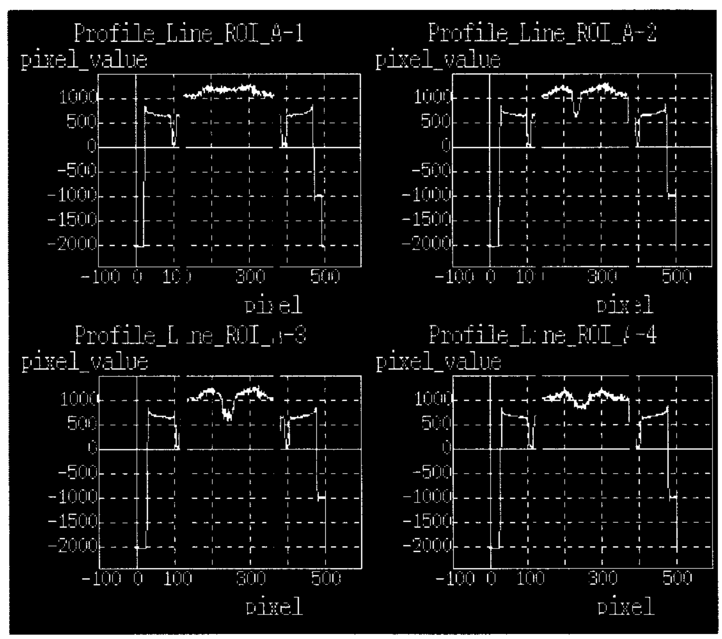

Final conditions @ t=56h

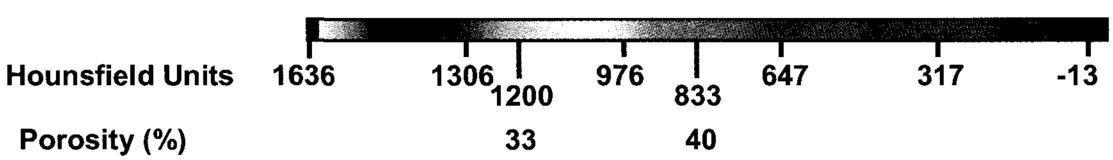

Figure 4-51: CT number profiles along selected lines

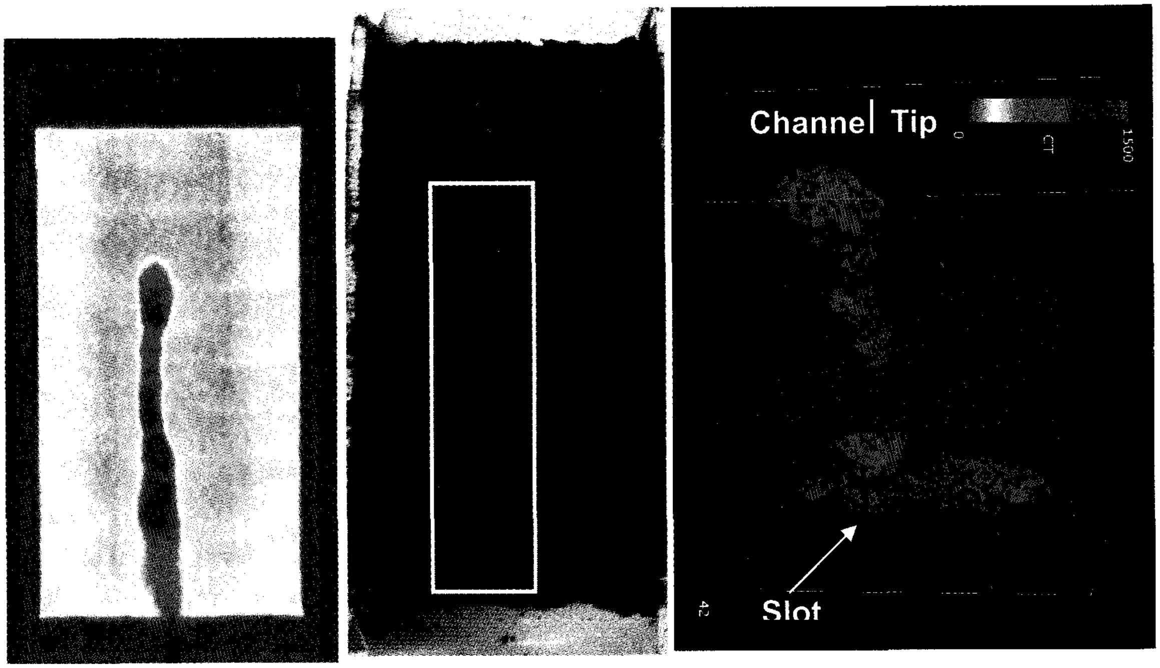

Figure 4-52: Silica No Large Fractions sand. Slot size: 1.422 (0.056 in). CT Scanner image at the end of the experiment vs actual sand pack. 3D representation of the high permeability channel.

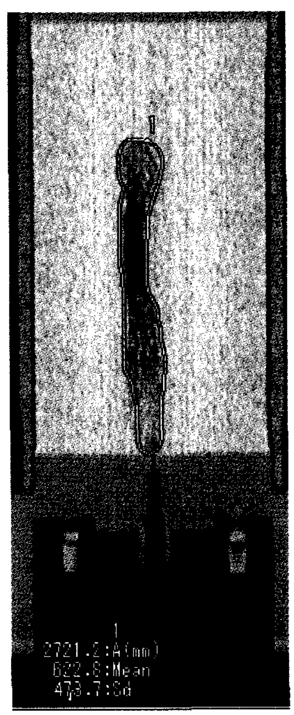

Figure 4-53: Average CT numbers inside the channel

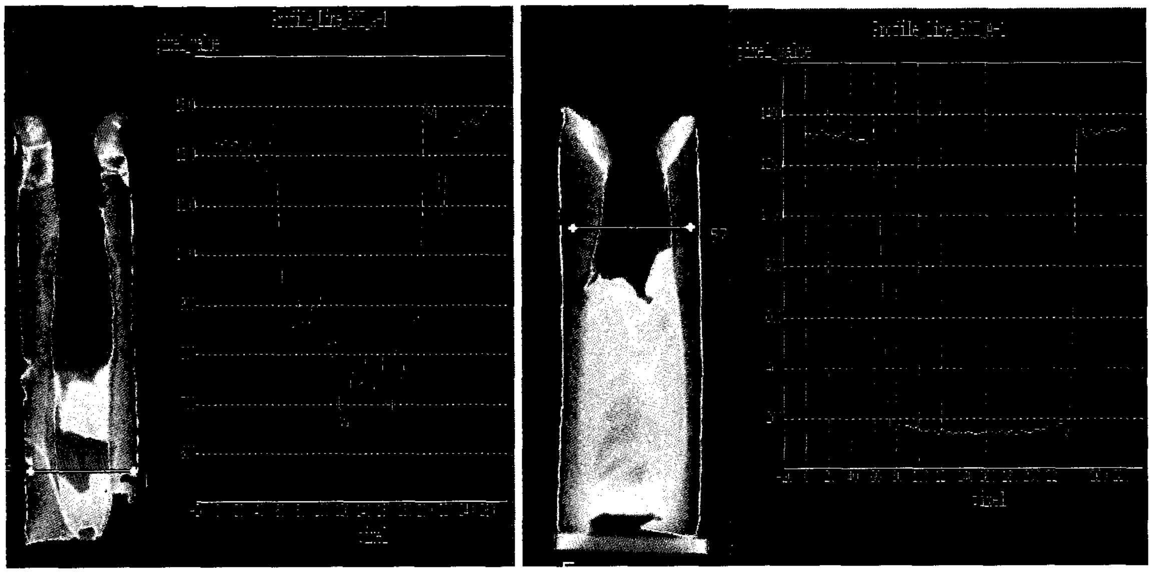

Figure 4-54: CT images of Silica Well Sorted sand packs prepared for thin sections. Slot sizes: 0.965 mm (0.038 in) and 0.711 mm (0.028 in)

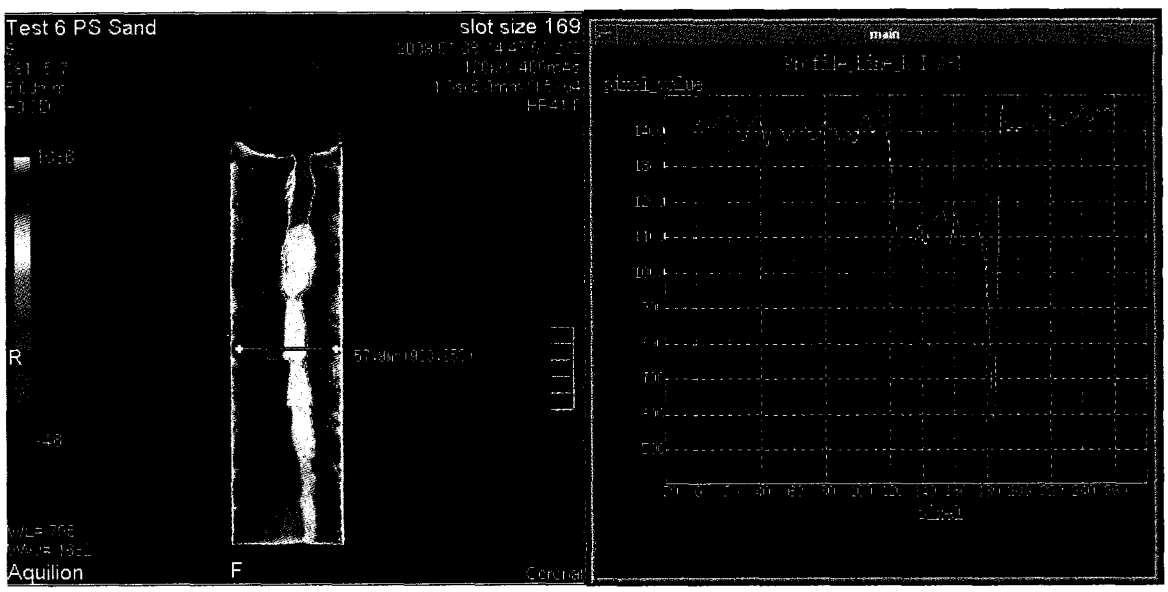

Figure 4-55: CT images of a Silica Poorly Sorted sand pack prepared for thin sections. Slot size 4.06 mm (0.169 in)

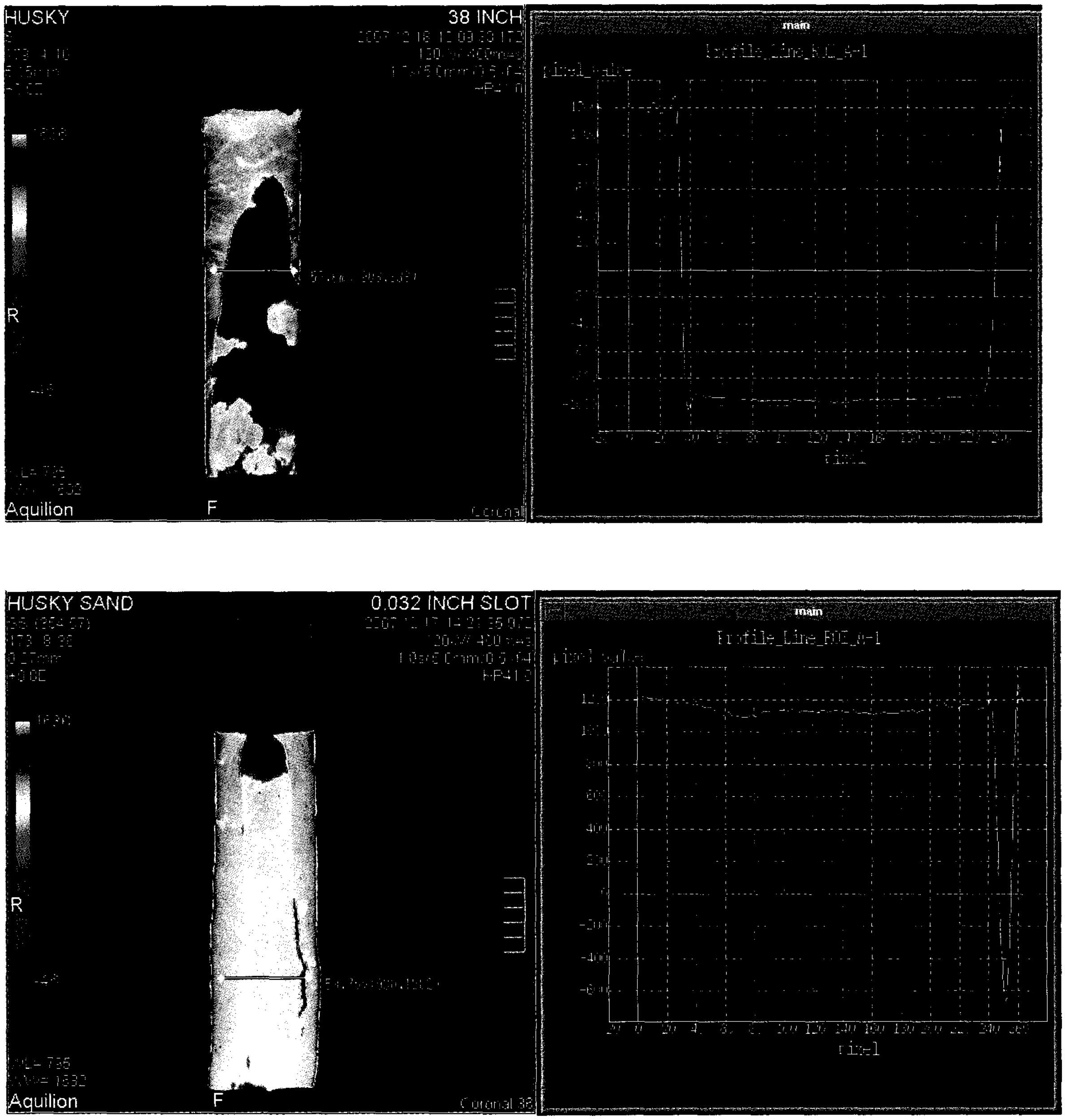

Figure 4-56: CT images of Husky sand cores prepared for thin sections. Slot sizes: 0.965 mm (0.038 in) in the upper sand pack and 0.813 mm (0.032 in) in the lower sand pack

5 Conclusions

In this thesis, the results of a comprehensive experimental program focused on the investigation of the flow of oil and sand in the vicinity of a heavy oil horizontal well under cold production are presented. The purpose of this research was to examine the possibility of controlled sand production, "sand on demand", for horizontal wells. Specifically, the effects of slot size, confining stress, fluid velocity and sand grain sorting on sand production under conditions representative of those in field applications have been investigated. The following conclusions were drawn from the research.

- From preliminary experiments on sand production with air-saturated packs, the coarsest fraction of the sand had the largest impact on sand production. Based on the observations from these experiments, two correlations were obtained between the parameter $SW/D_{99.9}$ and the sand production behaviour that allowed minimum and maximum slot width sizes to be estimated for controlled sand production.

- For the sand production experiments that form the core of the thesis, experiments using water-wet sand packs under confining stress saturated with heavy oil, the performance of the correlations was mixed. For a well-sorted sand, the results of the experiments with heavy oil were consistent with the correlation. However, with sands that were not as well-sorted, the results of the sand production experiments were not consistent with the predictions of the correlation. This suggests that the effect of the relationship between the slot width and grain size distribution on sand production is more complex than that indicated by a correlation simply between the very largest sand grains and the slot width. Evidently, the shape of the grain size distribution also has an important effect on sand production.

- From the results of the sand production experiments with heavy oil, operation-completion graphs were generated for two of the sands used in the study: a well-sorted sand, and a poorly-sorted sand. The operation-completion graphs show the influence of velocity and slot size on sand production. For the well-sorted sand, three well defined zones were identified:

- ❖ Zone where sand production did not occur;
- ❖ Zone where sand production was continuous and massive;
- ❖ Zone where sand production could be initiated, but was intermittent – within this zone, a delicate equilibrium existed between intermittent sand production, i.e. "sand production on demand", and continuing (and massive) sand production;

- The operation-completion graph generated for the well-sorted sand indicates that, for the control and management of sand production in these sands, the focus should be on slot sizes that are at the lower end of the interval defined by the correlation obtained from the preliminary air experiments.

- Flow rates are clearly a key factor in managing sand production through slots. As the slot width is increased, the critical pressure gradient (flow rate) required to initiate sand production decreases.

- The operation-completion graph for the poorly sorted sand did not yield characteristic sand production zones that were as well defined as in the case of the well-sorted sand. Nevertheless four zones indicative of different sand production behaviours could be identified. The transition between these zones were not nearly as sharp as in the case of the well-sorted sand:

  - ❖ Zone where sand production did not occur;
  - ❖ Zone where continuous and massive sand production was likely to occur;
  - ❖ Transition zone between the two zones described above where sand production behaviour is less certain. This transition zone could be sub-divided in two regions: in a lower zone (smaller pressure gradient or flow rate), it was unlikely that sand production could be initiated; in an upper zone (larger pressure gradient or flow rate), there is a possibility that sand production could be continuous and massive, although this region was not explored in the sand production experiments with heavy oil. In the transition between these regions, sand production behaviour was

uncertain, as it too could not be explored in the sand production experiments with heavy oil. There is a possibility that the sand production behaviour in this region would be similar to that in the experiments with well-sorted sands; i.e. sand production might be initiated but would be intermittent.

- The results of the sand production experiments as expressed in the operation-completion graphs could be considered in the design of slotted liners for managing sand production in horizontal wells; as an example, since the critical pressure for the initiation of sand production decreases as the slot size increases, a distribution of slot sizes could be envisaged along the length of the horizontal well with a higher proportion of narrow slot sizes at the heel of the well (where the pressure gradient into the well would be highest) and a higher proportion of wider slot size at the toe (where the pressure gradient into the well would be lowest). This would allow a better opportunity for intermittent sand production to occur along the entire length of the well, rather than preferentially near the heel.

- Sand production behaviour is influenced strongly by a critical pressure gradient:

    - The critical pressure gradient for initiation of sand production is much lower for a well-sorted sand than for a poorly sorted sand;

    - The critical pressure gradient decreases as confining stress increases;

    - A sufficiently large pressure gradient leads to persistent sand production and growth of channels.

- The effect of sand production on the sand packs used in the experiments were confined to localized regions (channels) where there was a large permeability and porosity increase. Outside these regions no changes in permeability and or porosity were observed. This suggests that the localized regions affected by sand production need to continue to grow into the reservoir to maintain oil production rates.

- Continuing sand production at low sand cuts (less than 1.5%) could be achieved if the initial flow rates were low and later increased in small increments. With this operating strategy, there is an opportunity to transport the sand produced by heavy oil along a horizontal well while simultaneously generating regions (channels) with high permeability.

- The grain size distribution of the sand plays an important role in the formation of stable arches/bridges. A wide grain size distribution appears to be conducive to the formation of arches; it likely also promotes sand bridging.

- Sand production did not select for certain fractions of the sand; the grain size distribution of the produced sand in the experiments matched the grain size distribution of the sand packs.

- Sand strength played an important role in determining sand production behaviour:

    - For stronger sands, higher pressure gradients were required to cause sand failure and subsequent sand production.

    - Both friction angle and cohesive strength were significant factors in the relationship between sand production behaviour and sand strength; it appeared that the strength of the sand as defined by the shear stress at failure provided the most consistent correlation with sand production behaviour;

    - From the measurements of sand strength, sands with a higher uniformity coefficient (i.e. not as well-sorted) were stronger. This reinforces the observation from the sand production experiments that a sand with a wider grain size distribution would be more difficult to produce.

- The visualization experiments that were performed with a CT scanner demonstrated that channel growth could be controlled successfully (i.e. stopped/re-started) through changes in flow rate.

- The estimated pressure gradient at which sand failure occurred at the channel tip in the CT experiments, provoking channel growth, agreed remarkably well with the predicted critical pressure gradient for sand failure at the tip of a channel provided by the Bratli and Risnes [55] stability criterion.

In conclusion, the results obtained in this study indicate that sand production through slots can be controlled through a combination of correct selection of slot size and proper management of the flow rate. In addition, the sand production experiments suggest that in a field application with horizontal wells, there is a reasonable possibility that sufficient amounts of sand could be produced to generate high permeability channels growing outward from the well that would in turn enhance the oil production rate into the well.

6 Recommendations for Future Work

1. The impact of controlled sand production on the productivity (i.e. oil production rates) from horizontal wells should be investigated with the aid of a commercial reservoir simulator. An estimate of the size and shape of the disturbed zone generated by sand production, as well as the changes in permeability and porosity in the disturbed zone, could be obtained from the analyses of the sand production experiments presented in this thesis. These effects could be incorporated into field-scale simulations of fluid production resulting from controlled sand production into horizontal wells using learnings obtained from field-scale simulations of the cold production process in vertical wells. The results of this simulation study, together with the results of the experimental study presented in this thesis, could be used to identify a set of sand production strategies for enhancing primary production in horizontal wells. These operating strategies could be tested in field pilots, to develop improvements in the exploitation of heavy oil reservoirs using horizontal wells.

2. The effect of the sand grain size distribution on sand production though slots should be investigated further. Special attention should be given to the tails (larger fractions, finer fractions) of the size distribution, which have been identified as having the greatest influence on sand production.

3. Further investigations should be attempted to find a more appropriate correlation between the slot size and grain size distribution regarding sand production behaviour in the case of less well-sorted sands.

4. In order to try to distinguish between the mechanisms of arching and plugging/bridging in the slot in controlling sand production, experiments with undercut slots should be performed.

5. In order to examine the effects of slot interference on sand production behaviour and the development of high permeability channels growing outward from the slot(s), experiments with more than one slot should be performed.

6. The role of live heavy oil on sand production through slots in a horizontal well should be assessed through an experimental study.

7 References

1 CHUGH, S., BAKER, R., TELESFORD, A. and ZHANG, E., Mainstream Options for heavy oil: Part I-Cold Production; *Paper 97-99 presented at the 48th Annual Technical Meeting of the Petroleum Society in Calgary, Alberta Canada, 8-11 June 1997.*

2 NATIONAL ENERGY BOARD, Crude oil Production and Available Supply; *table from NEB website www.neb.gc.ca, April 2008.*

3 SAWATZKY, R.P., LILLICO, D.A., LONDON, M., TREMBLAY, B.R. and COATES, R.M., Tracking Cold Production Foot prints; *Paper 2002-086 presented at the Petroleum Society's Canadian International Petroleum Conference 2002, Calgary, Alberta, Canada, 11 –13 June 2002.*

4 MCCAFFREY, W. and BOWMAN, R., Recent Successes in Primary Bitumen Production; *Paper presented at 8th Annual Heavy Oil and Oil Sands Technical Symposium, 14 March 1991.*

5 LOUGHEAD, D. and SALTUKLAROGLU, M., Lloydminster Heavy Oil Production. Why So Unusual?; *Ninth Annual Heavy Oil and Oil Sands Technical Symposium, Calgary, Canada, 11 March 1992.*

6 HUANG, W., MARCUM B., CHASE, M.R. and YU, C., Cold Production of Heavy Oil from Horizontal Wells in the Frog Lake Field; *SPE Reservoir Evaluation & Engineering, pp. 551-555, December 1998.*

7 METWALLY, M. and SOLANKI, S., Heavy Oil Reservoir Mechanisms, Lindbergh and Frog Lake Fields, Alberta. Part I: Field Observation and Reservoir Simulation; *Paper 95-63 presented at the 46th Annual Technical Meeting of the Petroleum Society of CIM, Banff, Alberta, Canada, 14-17 May 1995.*

8 SMITH, G., Fluid Flow and Sand Production in Heavy–Oil Reservoirs Under Solution-Gas Drive; *SPE Production Engineering, Vol. 3, No. 2, pp. 169-180, May 1998.*

9 SQUIRES, A., Inter-Well Tracer Results and Gel Blocking Program; *Paper presented at the 10th Annual Heavy Oil and Oil Sands Technical Symposium, 9 March 1993.*

10 YEUNG, K., Cold Flow Production of Crude Bitumen at the Burnt Lake Project, Northeastern Alberta; *Paper presented at the 1995 UNITAR Intl. Conference on Heavy and Tar Sands, Houston, 12-17 February 1995.*

11 TREMBLAY, B. SEDGWICK, G. and FORSHNER, K., Imaging of Sand Production in a Horizontal Sand Pack by X-Ray Computed Tomography; *SPE Formation Evaluation, pp. 94-98, June 1996.*

12 TREMBLAY, B. SEDGWICK, G. and FORSHNER, K., Simulation of Cold Production in Heavy-Oil Reservoirs: Wormhole Dynamics; *SPE Reservoir Engineering, pp. 110-111, 7 May 1997.*

13 TREMBLAY, B. SEDGWICK, G. and FORSHNER, K., Modelling of Sand Production from Wells on Primary Recovery; *The Journal of Canadian Petroleum Technology, Vol. 37, No. 3, March 1998.*

14 TREMBLAY, B. SEDGWICK, G. and VU, D., CT Imaging of Wormhole Growth under Solution Gas Drive; *SPE Reservoir Eval. & and Eng., Vol. 2, No. 1, February 1999.*

15 TREMBLAY, B. and OLDAKOWSKI, K., Wormhole Growth and Interaction in a Large Sand Pack; *Journal of Petroleum Science and Engineering, Vol. 34, pp. 13-34, 2002.*

16 VAZIRI, H.H., PHILLIPS, R. and HURLEY, S., Physical Modelling of Sand Production; *paper No. 323, Int. J. Rock Mech. & Min. Sci., Vol. 34, pp. 3-4, 1997.*

17 WONG, R.C.K., Sand Production in Oil Sand Under Heavy Oil Foamy Flow; *The Journal of Canadian Petroleum Technology, Vol. 42, No. 3, March 2003.*

18 WAN, R.G., WANG, J. and LIO, Y. N., Prediction of Volumetric Sand Production Using a Coupled Geomechanics-Hydrodynamic Erosion Model; *CIPC paper 2003-200 presented at the Petroleum Society's Canadian International Petroleum Conference 2003, Calgary, Alberta, Canada, 10 – 12 June 2003.*

19 YUAN, J-Y, TREMBLAY, B., and BABCHIN, A., A Wormhole Network Model of Cold Production in Heavy Oil; *SPE paper 54097 presented at the SPE Intl. Thermal Operations and Heavy Oil Symposium, Bakersfield, California, 17-19 February 1999.*

20 DENBINA, E.S., BAKER, R.O., GEGUNDE, G.G., KLESKEN, A.J., and SODERO, S.F., Modelling Cold Production for Heavy Oil Reservoirs; *The Journal of Canadian Petroleum Technology, Vol. 40, No. 3, March 2001.*

21 WANG, Y. and YUAN, J-Y., Cold Production and Wormhole Propagation in Poorly Consolidated Reservoirs; *UNITAR Paper 1998-041 presented at the 7th UNITAR Conference in Beijing, 1998.*

22 WANG, Y. and CHEN, C., Improved Production and Sand (Cold) Production in Conventional and Heavy Oil Reservoirs-A Field Case and Simulation; *SPE paper 57290 presented at the SPE Asian Pacific Improved Oil Recovery Conference, Kuala-Lumpur, Malaysia, 25-28 October 1999.*

23 COOMBE, D., TREMBLAY, B., TRAN, D. and MA, H., Coupled Hydro-Geomechanical Modelling of the Cold Production Process; *SPE paper 69719 presented at the SPE International Thermal Operations and Heavy Oil Symposium. Porlamar, Margarita Island, Venezuela, 12-14 March 2001.*

24 DUSSEAULT, M.B., GEILIKMAN, M. and SPANOS, T., Mechanism of Massive Sand Production in Heavy Oils; *Paper presented at the 7th UNITAR Conference, Beijing, China, 1998.*

25 MEZA, B., Experimental Investigation of Sand Production into a Horizontal Well Slot; *MSc Thesis, School of Mining and Petroleum Engineering, University of Alberta, Fall 2001.*

26 TREMBLAY, B., SEDGWICK, G. and VU, D., A Review of Cold Production in Heavy Oil Reservoirs; *Paper 2008 presented at the 10th European Symposium on Improved Oil Recovery, Brighton, UK, 18-20 August 1999.*

27 DUSSEAULT, M., Cold Production and Enhanced Oil Recovery, *Journal of Canadian Petroleum Technology, Vol. 32, No. 9, pp. 16-18, November 1993.*

28 TREMBLAY, B., SEDGWICK, G. and FORSHNER, K., Simulation of Cold Production in Heavy Oil Reservoirs: Wormhole Dynamics; *SPE Paper 35387 presented at 10th Symposium on Improved Oil Recovery, Tulsa OK, 21-24 April 1996.*

29 LEBEL, J.P., Performance Implications of Various Reservoir Access Geometries; *Document presented at the Eleventh Annual Heavy Oil & Oil Sands Technical Symposium "Challenges and Innovations", 1994.*

30 CHARLEZ, A., *Rock Mechanics, Petroleum Applications, Vol. 2, Editions Technip, Paris, 1997.*

31 HU, C., LIU, X., WANG, J., SONG, Z., FAN, Z. and YANG, F., Cold Production of Thin-Bedded Heavy Oil Reservoir in Henan Oilfield; *SPE Paper 50885 presented at the SPE International Conference and Exhibition, Beijing, China, 2-6 November 1998.*

32 MAINI, B., Foamy Oil Flow in Heavy Oil Production; *The Journal of Canadian Petroleum Technology, Vol. 35, No. 6, pp. 21-24, June 1996.*

33 KRAUS, W., MCCAFFREY, W. and BOYD, G., Pseudo-Bubble Point Model for Foamy Oils; *Paper No. CIM 93-45 presented at the Annual Technical Meeting of the Petroleum Society of CIM, Calgary, Canada, 9-12 May, 1993.*

34 SHENG, J., HAYES, R., MAINI, B. and TORTIKE, W., A Proposed Dynamic Model for Foamy Oil Properties; *SPE Paper 30253 presented at the International Heavy Oil Symposium, Calgary, Alberta, Canada, 19-21 June 1995.*

35 MAINI, B., SARMA, H. and GEORGE, A., Significance of Foamy-Oil Behaviour in Primary Production of Heavy Oils; *The Journal of Canadian Petroleum Technology, Vol. 32, No. 9, pp. 50-54, November 1993.*

36 BAYON, Y.M., COATES, R.M., LILLICO, D.A., CORDELIER, P.R. and SAWATZKY, R.P., Application and Comparison of Two Models of Foamy Oil Behaviour of Long Core Depletion Experiments; *Paper SPE/Petroleum Society of CIM/CHOA 78961 presented at the 2002 SPE International Thermal Operations and Heavy Oil Symposium and International Horizontal Well Technology Conference held in Calgary, Alberta, Canada, 4 –7 November 2002.*

37 KAMP, A.M., HENY, C., ANDARCIA, L., LAGO, M. and RODRIGUEZ, A., Experimental Investigation of Foamy Oil Solution Gas Drive; *SPE Paper 69725 presented at the 2001 SPE International Thermal Operations and Heavy Oil Symposium held in Porlamar, Margarita Island, Venezuela, 12-14 March 2001.*

38 ECONOMIDES, E. and FERNANDEZ, B., Global Experiences and Practice for Cold Production of Moderate and Heavy Oil; *SPE paper 58773 presented at the 2000 SPE International Symposium on Formation Damage Control. Lafayette, Louisiana, 23-24 February 2000.*

39 ISLAM, M.R. and GEORGE, A.E., Sand Control in Horizontal Wells in Heavy Oil Reservoir; *SPE paper 18789 presented at the SPE California Regional Meeting, Bakersfield, California, 5-7 April 1989.*

40 TOMA, P, TREMBLAY, B., HARRIS, P. and KORPANY, G., Experimental Investigation for Reducing the Risk of Sand Inflow in Slotted Horizontal Wells; *Paper 94-PET-2 presented at the Energy-Sources Technology Conference and Exhibition, New Orleans, Louisiana, 23-27 January 1994.*

41 MEZA, B, TREMBLAY, B. and DOAN, Q., Mechanisms of Sand Production Through Horizontal Well Slots in Primary Production; *Journal of Canadian Petroleum Technology, Vol. 42, No. 10, pp. 36-46, October 2003.*

42 MEZA, B, TREMBLAY, B. and DOAN, Q., Visualization of Sand Structures Surrounding a Horizontal Well Slot During Cold Production; *SPE/Petroleum Society of CIM/CHOA paper 79025 presented at SPE International Thermal Operations and Heavy Oil Symposium and International Horizontal Well Technology Conference held in Calgary, Alberta, Canada, 4–7 November 2002.*

43 VONDE, T.R., Specialized Pumping Techniques Applied to a Very Low Gravity. Sand-Laden Crude-Cat Canyon Field, California; *Journal of Petroleum Technology, pp. 1951-1957, September 1982.*

44 TREMBLAY, B. SEDGWICK, G. and VU, D., CT Imaging of Sand Production in a Horizontal Sand Pack Using Live Oil; *Paper 98-78 presented at the 49th Annual Technical Meeting of the Petroleum Society in Calgary, Alberta, Canada, 8-10 June 1998.*

45 KANTZAS, A. and BROOK, G., Preliminary Laboratory Evaluation of Cold and Post-Cold Production Methods for Heavy Oil Reservoirs; *CIPC Paper 2002-079 presented at the Petroleum Society's Canadian International Petroleum Conference 2002, Calgary, Alberta, Canada, 11–13 June 2002.*

46 WANG, Y. and CHEN, C., Simulating Cold Heavy-Oil Production with Sand by Reservoir-Wormhole Model; *Paper 2002-170 presented at the Petroleum Society's Canadian International Petroleum Conference 2002, Calgary, Alberta, Canada, 11–13 June 2002.*

47 FJÆR, E., HOLT, R., HORSRUD, P., RAAEN, A., and RISNES, R., *Petroleum Related Rock Mechanics, Elsevier Science Publishers B.V., Netherlands, 1992.*

48 CHALATURNYK, R., WAGG, B. and DUSSEAULT, M.B., The Mechanisms of Solids Production in Unconsolidated Heavy-Oil Reservoirs; *SPE paper 23780 presented at the SPE Intl. Symposium on Formation Damage Control, Lafayette, Louisiana, 26-27 February 1992.*

49 PENBERTHY, W.L. and SHAUGHNESSY, C.M., *Sand Control, SPE Series on Special Topics, Vol. 1, Fourth Edition 2002.*

50 GEILIKMAN, M., DUSSEAULT, M. and DULLIEN, F., Fluid Production Enhancement by Exploiting Sand Production; *SPE/DOE 27797 paper presented at the SPE/DOE Ninth Symposium on Improved Oil Recovery, Tulsa OK, 17-20 April 1994.*

51 MCCORMACK, M.E., Effective Sand Control – Some AOSTRA Experience; *Paper presented at the 42nd Petroleum Mechanical Engineering Workshop and Conference, Calgary, Canada, 21-23 September 1986.*

52 VAZIRI, H., BARREE, B., XIAO, Y., PALMER, I. and KUTAS, M., What is the Magic of Water in Producing Sand; *Paper presented at the SPE Annual Technical Conference and Exhibition, San Antonio, Texas, 29 September-2 October 2002.*

53 HALL, C. and HARRISBERGER, W., Stability of Sand Arches: A Key to Sand Control; *Journal of Petroleum Technology, pp. 821-829, July 1970.*

54 TIPPIE, D. and KOHLHAAS, C., Effect of Flow Rate on Stability of Unconsolidated Producing Sands; *SPE Preprint No. 4533 presented at the 48th Annual Fall Meeting, Las Vegas, Nevada, 30 September-3 October 1973.*

55 BRATLI, R., and RISNES, R., Stability and Failure of Sand Arches; *Society of Petroleum Engineers Journal, pp. 236-248, April 1981.*

56 SAWATZKY, R., LILLICO, D.A., VILCSAK, G., and TREMBLAY, B., Initiation of Sand Production in the Cold Production Process; *Paper CIM 96-25 presented at the Petroleum Society of CIM 47th Annual Technical Meeting, Calgary, Alberta, Canada, 10–12 June 1996.*

57 MORITA, N., WHIRFILL, D.L., MASSIE, I. and KNUDSEN, T.W., Realistic Sand Production Prediction: Numerical Approach; *SPE Production Engineering, pp. 15-24, February 1989.*

58 YIM, K., DUSSEAULT, M.B. and ZHANG, L., Experimental Study of Sand Production Processes Near an Orifice; *Paper presented at the Eurock'94: Rock Mechanics in Petroleum Engineering SPE/ISRM International Conference, Delft, Netherlands, pp. 339-346, 29-31 August 1994.*

59 MCCORMACK, M.E., Mechanisms of Sand Retainment by Wire-Wrapped Screens; *Preprint No. 56 presented at the 4th UNITER/UNDP Conference on Heavy Crude and Tar Sands. Edmonton, Alberta, 7-12 August 1988.*

60 COBERLY, C.J., Selection of Screen Opening for Unconsolidated Sands; *API Drilling and Production Practice, 1937.*

61 SELBY, R. and FAROUQ ALI, S.M., *CIM Preprint No. 87-38-55 presented at the 38th Annual Technical Meeting of the Petroleum Society of CIM. Calgary, Alberta, 7-10 June 1987.*

62 RISNES, R., BRATLI, R. and HORSRUD, P., Sand Stresses Around a Wellbore; *Society of Petroleum Engineers Journal, pp. 883-898, December 1982.*

63 CLEARY, M., MELVAN, J., and KOHLHAAS, C., The Effect of Confining Stress and Fluid Properties on Arch Stability in Unconsolidated Sands; *SPE Preprint No. 8426 presented at the 54th Annual Fall Meeting and Exhibition of the Society of Petroleum Engineers of AIME, Las Vegas, Nevada, 23-26 September 1979.*

64 MILLER, W.G., Sand Flow Mechanisms at Well Casing Perforations; *MSc Thesis, Department of Civil Engineering. University of Alberta, Fall 1994.*

65 MELVAN, J., The Effect of Overburden Stress on the Formation and Stability of Arches in Unconsolidate Sands; *MSc Thesis, Colorado School of Mines University, May 1978.*

66 DURRETT, J.L., GOLBIN, W., MURRAY, J.W. and TIGHE, R.E., Seeking a Solution to Sand Control; *Journal of Petroleum Technology, pp. 1664-1672, December, 1977.*

67 STEIN, N., ODEH, A., and JONES, L., Estimating Maximum Sand-Free Production Rates from Friable Sands for Different Well Completion Geometries; *Journal of Petroleum Technology, pp. 1156-1158, October 1974.*

68 VAZIRI, H.H., Mechanics of Fluid and Sand Production from Oil Sand Reservoirs; *CIM Preprint No. 86-37-75 presented at the 37th Annual Technical Meeting, Calgary, Alberta, 8-11 June 1986.*

69 BOONE, T.J., SMITH, R.J. and GALWAY, R., Sand Packing Liner Completions in Heavy Oil Reservoirs; *Paper presented at the Sixth One Day Conference on Horizontal Well Technology, Calgary, Alberta, 12 November 1997.*

70 YUAN, Y., ABAQUS Simulation on Near Well Bore Stresses and Deformation in Heavy Oil Reservoirs in Response to Rapid Pressure Drawdown; *Report submitted to Alberta Research Council, 22 November, 2000.*

71 BENNET, C., GILCHRIST, J.M., PITONI, E., BURTON, R.C., HODGE, R.M., TRONCOSO, J., ALI, S.A., DICKERSON, R., PRICE-SMITH, C. and PARLAR, M., Design Methodology for Selection of Horizontal Open-Hole Sand Control Completions Supported by Field Case Histories; *SPE Preprint No. 65140 presented at the 2000 SPE European Petroleum Conference, Paris, France, 24-25 October 2000.*

72 ÀRPÀD, K., *Handbook of Soil Mechanics, Elsevier Scientific Publishing Company, Chapter 2, Budapest, 1974.*

73 LAMBE, T.W. and WHITMAN, R. V., *Series in Soil Engineering: Soil Mechanics, Edited by T. William Lambe and Robert V. Whitman, Chapter 4.*

74 AMERICAN SOCIETY FOR TESTING AND MATERIALS, Standard Test Method for Particle-Size Analysis of Soils; *Designation D 442-63, pp. 10-16, (Reapproved 1990).*

75 TERZAGHI, K. and PECK, R. B., *Soil Mechanics in Engineering Practice, John Wiley and Sons, Inc. Chicago, p. 729, 1967.*

76 FOLK, R., *Petrology of Sedimentary Rocks, Hemphill Publishing Company, Austin, Texas, p. 183, 1974.*

77 AMERICAN SOCIETY FOR TESTING MATERIALS, Standard Test Method for Rubber Chemicals-Density; *Designation D 1817-96, pp. 346-347, (Reapproved 10 January 1996).*

78 PRYOR, W. A., *Grain Shape* in Procedures in Sedimentology; *Robert E. Carver Editor. Georgia, USA.*

79 POWERS, M., A New Roundness Scale for Sedimentary Particles; *Journal of Sedimentary Petrology, Vol. 23, No. 2, pp. 117-119, June 1953.*

80 ZHAN J., RAI, C.S., and SONDERGELD, C.H., Mechanical Strength of Reservoir Materials: Key Information for Sand Prediction; *SPE Reservoir Evaluation & Engineering, Vol. 3, No. 2, pp. 127-131, April 2000.*

81 TREMBLAY, B., OLDAKOWSKI, K. and SETTARI, A., Geomechanical Properties of Oil Sands at Low Effective Stress; *Paper 97-07 presented at the 48th Annual Technical Meeting of the Petroleum Society, Calgary, Alberta, Canada, 8-11 June 1997.*

82 HEAD, K.H., Manual of Soil Laboratory Testing. Volume 2: Permeability, Shear Strength and Compressibility Test; *Pentech Press, London, 1988.*

83 HEAD, K.H., Manual of Soil Laboratory Testing. Volume 3: Permeability, Shear Strength and Compressibility Test; *Pentech Press, London, 1988.*

84 Determination of the Shear Strength Parameters of Soil by the Triaxial Test; *DIN 18137-2 Deutsche norm, December 1990.*

85 CAMERON, S., *Personal communication, 21 May 2008.*

86 HARR, M.E., Groundwater and Seepage; *Dover Publications, Inc., New York, 1991.*

87 DULLIEN, F.A., Single Phase Flow Through Porous Media and Pore Structure; *Chemical Engineering Journal, Vol. 10, pp. 1-34, 1975.*

88 BIRD, R.B., STEWART, W.E. and LIGHTFOOT, E., *Transport Phenomena, John Wiley & Sons, Inc. USA, 1976.*

89 TREMBLAY, B. and OLDAKOWSKI, K., Modelling of Sand Transport through Wormholes; *AACI Report 9899-6, December 1998.*

90 GEILIKMAN, M.B. and DUSSEAULT, M.B., Fluid Rate Enhancement from Massive Sand Production in Heavy Oil Reservoirs; *Journal of Petroleum Science and Engineering, Vol. 17, pp. 5-18, 1997.*

91 TREMBLAY, B., Modelling of Sand Transport Through Wormholes; *The Journal of Canadian Petroleum Technology, Vol. 44, No. 4, April 2005.*

92 AKIN, S. and KOVSCEK, A.R., Computed Tomography in Petroleum Engineering Research; In: MEES, F., SWENNEN, R., VAN GEET, M. & JACOBS, P. (eds) *Applications of X-ray Computed Tomography in the Geosciences, Geological Society, London Special Publications, Vol. 215, pp. 23-38.*

93 BUSHBERG, J.T., SEIBERT, J.A., LEIDHOLDT E.M., and BOONE, J.M., The Essential Physics of Medical Imaging; *Second Edition by Lippincott Williams & Wilkins, Philadelphia, PA, USA, 2002.*

A Appendix I: Experimental Part

A.1 Solids Density Measurement: based on ASTM method designation D1817-96

In this method, a Weld's specific gravity bottle (picnometer) is used. A picnometer is a vessel used for determining exact volumes of materials. First, the total volume of the picnometer is calculated. This is performed by weighing the vessel empty and dry, and again when it is completely filled with water. Then, knowing the density of the water (ρ_w) and using Equation A-1 the volume of the picnometer is calculated. Secondly, to find out the sand density, the sand is weighed into the clean and dry picnometer. Water is added. The picnometer is placed in a vacuum desiccator for a certain period of time to remove all the air bubbles. The picnometer is then "topped" up, placed in a water bath for 15 minutes at the desired temperature, capped, and reweighed. The sand density is determined by using Equation A-2. More details regarding the test are given in the ASTM method D1817-96 [76].

The major change that was made to this method was the use of 1-Butanol as the filling solvent instead of water when the sand densities were calculated. The use of 1-butanol reduces the volume of air trapped in the sample. The density of the 1-butanol was measured at ARC laboratories using a PAAR densimeter.

The densities (ρ_s) of the sand were calculated using the following equations:

$$V_{Pic} = V_B = \frac{m_{Butanol}}{\rho_{Butanol}} = \frac{m_{Pic+Butanol} - m_{Pic}}{\rho_{Butanol}} = \frac{K}{\rho_{Butanol}} \quad \text{A-1}$$

$$\rho_s = \frac{m_s}{V_S} = \frac{m_s}{V_p - V_B'} = \frac{S * \rho_{butanol}}{K-(G-P)} \quad \text{A-2}$$

where:

V_{Pic} = volume of picnometer (cm^3)
V_B = volume of butanol (cm^3)
$m_{Butanol}$ = mass of butanol (g)
$\rho_{Butanol}$ = butanol density (g/cm^3)

m_{Pic} = mass of picnometer (g)
$m_{Pic+butanol}$ = [mass of picnometer+butanol] (g)
K= mass of butanol = [$m_{Pic+butanol}$ - m_{Pic}] (g)
m_s = mass of sand (g)
V_S = volume of sand (cm^3)
$V_B^{'}$= volume of butanol in the mix sand + butanol (cm^3) = $(G-P)/\rho_{Butanol}$
G= [mass of picnometer + sand + butanol] (g)= $m_{Pic + Sand + Butanol}$
P= [mass of picnometer + sand] (g)
S = [mass of picnometer + sand - mass of picnometer] (g) = P- m_{Pic}

Three densities should be measured per sand. The average of the three measurements was taken as the density of the material.

Sand densities were used in the porosity calculations as well as in the calculations of the volume of the sand produced.

A.2 Calculation of porosity in the pack

The porosity of the pack was calculated knowing the mass of the sand, its density and the total volume of the pack. This volume was calculated from the dimensions of the vessel and the total height of the sand in the cell.

The vessel was composed of a cylindrical section as shown in Figure 3.17. An example of a porosity calculation for Test 6, Silica Poorly Sorted sand pack is given below:

$$V_S = \frac{m_S}{\rho_S} = \frac{15650.3g}{2.6339g/cm^3} = 5942cm^3 \quad \text{A-3}$$

$$V_T = \pi r^2 L = 3.1416 * 95.06cm^2 * 29.88cm = 8923cm^3 \quad \text{A-4}$$

$$PV = V_T - V_S = (8923 - 5942)cm^3 = 2982cm^3 \quad \text{A-5}$$

$$\phi = \frac{PV}{V_T} = \frac{2982cm^3}{8923cm^3} = 0.334 \quad \text{A-6}$$

where:

V_S = sand volume	m_s = mass of sand	ρ_s = sand density
V_T = Total volume	r = radius of the cylinder	L = length of the sand pack
PV = Pore volume	ϕ = porosity	

Table A-1: Sand density calculations

T_{room} (°C) 22

$\rho_{butanol}$ (22 °C) (g/cc) 0.8058

Sand	Test #	m_{pic}	$m_{pic+butanol}$	m_{pic}	m_{s+p}	G	ρ (g/cc)	σ	%Desv
Glass Beads	1	34.8012	59.6386	34.8012	59.9431	76.5721	2.4735		-0.007
	2	34.5957	57.7075	34.5957	58.8516	74.0106	2.4630		0.416
	3	34.5987	57.7075	34.5987	55.0568	71.4921	2.4756		-0.093
	4	34.8012	59.6386	34.8012	54.7031	73.0628	2.4811		-0.315
	Average						2.4733	0.0044	
Husky	1	34.8032	59.6458	34.8032	46.9191	68.0351	2.6255		-0.179
	2	33.7394	56.5624	33.7394	58.0573	73.3788	2.6179		0.113
	3	30.9274	53.4893	30.9274	40.5050	60.1138	2.6191		0.066
	Average						2.6208	0.0029	
Silica sand	1	33.4538	57.9522	33.4534	49.2965	69.0362	2.6358		-0.0725
	2	33.4535	57.9512	33.4539	49.7824	69.3759	2.6360		-0.0790
	3	34.5602	57.1893	34.5602	50.6297	68.4212	2.6299		0.1515
	Average						2.6339	0.0016	

m_{pic} = mass of picnometer

m_{s+p} = mass of picnometer +sand

$S = m_{s+p} - m_{pic}$

P = mass of picnometer +sand = m_{s+p}

K = $mass_{picnometer+butanol}$ - m_{pic}

G = $mass_{picnometer + sand + butanol}$

A.3 Consolidation process

This procedure consists of an increase in the confining pressure in steps until a maximum of 6895 kPa (1000 psi) is reached. Then the pressure is decreased to atmospheric pressure in the same number of steps. During the process the change in volume of the confining fluid is recorded. The cycle is usually repeated three times. The consolidation process is stopped when the increase in volume change between consecutives cycles is small. During the last cycle, the pressure is decreased to the working pressure. A new porosity value is obtained after the procedure is applied to the pack. The confining pressure is kept constant at the value desired for the experiment.

The following equations were used to calculate the new porosity during the consolidation process:

$$e = \frac{PV}{V_S} \qquad \text{A-7}$$

where e is the void ratio and is define as the ratio of void volume (Pore Volume = PV) to solid volume (V_s). During the consolidation process the void ratio will vary by:

$$e = \frac{PV_i - \Delta V}{V_s} \qquad \text{A-8}$$

where PV_i is initial pore volume, ΔV is the net reduction in initial pore volume to the end of consolidation.

The new porosity is found using the following relationship between void ratio and porosity:

$$\phi = \frac{e}{1 + e} \qquad \text{A-9}$$

The volume changes in the experiments have been corrected taking into consideration the added volume due to the compressibility of the system (V_{sys}) and the initial volume (V_i)

needed to go from vacuum to the initial confining stress, usually between 100 to 200 kPa Thus:

$$\Delta V_{corr} = \Delta V - V_i - V_{sys} \quad \text{A-10}$$

$$V_{sys} = 0.0064(cc / kPa)\sigma' + 1.389cc \quad \text{A-11}$$

where σ' = effective stress, σ_c = total confining stress and p= pore pressure. The equation for the effective stress is given by:

$$\sigma' = \sigma_c - p \quad \text{A-12}$$

This process was performed before the pack was saturated. At this point the sand pack was open to atmosphere; therefore the pore pressure was assumed to be zero.

After the consolidation process the new porosity can be found at any confining stress using the trendlines obtained at the end of the process (see Figure A-1 and Figure A-2).

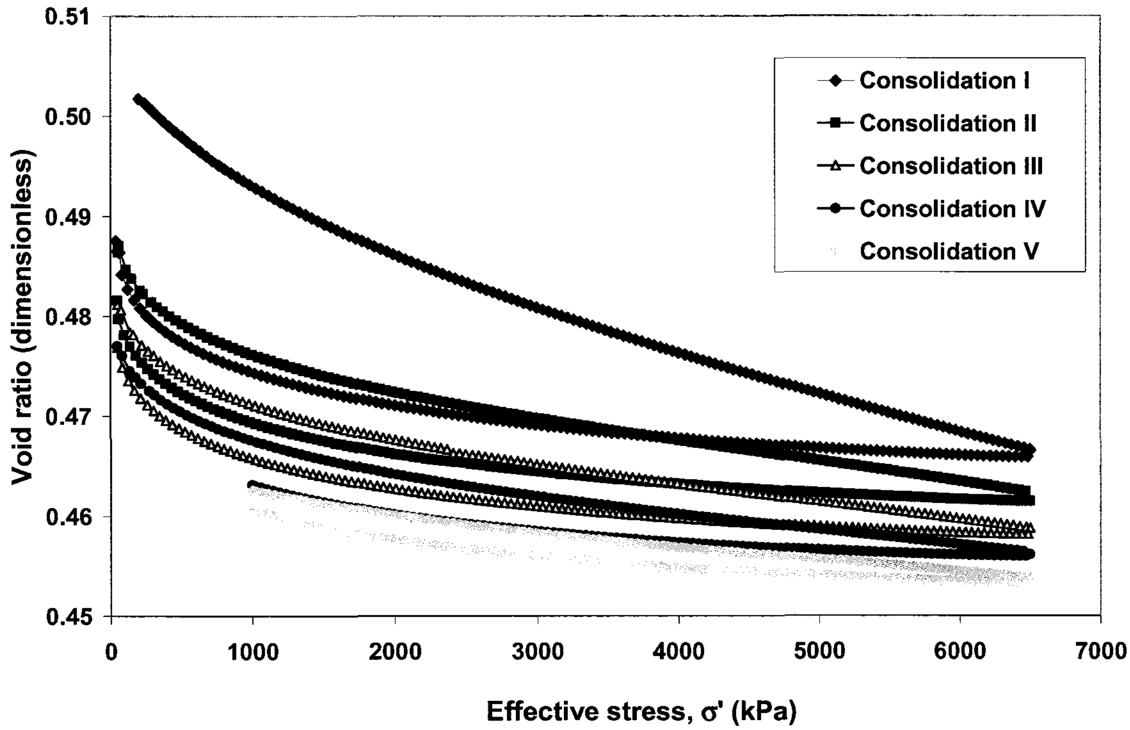

Figure A-1: Consolidations curves for Test 6. Silica Poorly Sorted sand

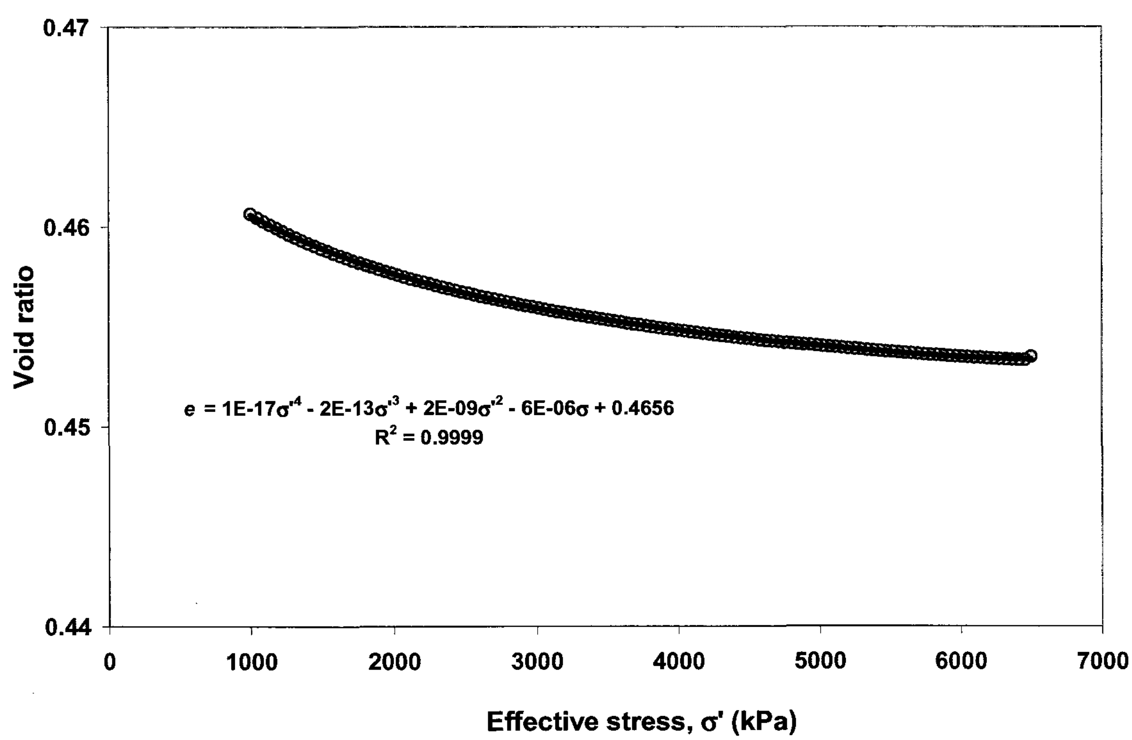

Figure A-2: Consolidation curve trendline for Test 6. Silica Poorly Sorted sand

A.4 Compressibility Tests

A.4.1 Procedure

1. Once the pack was saturated with water, the outlet valve was closed.
2. Water was injected at a constant rate.
3. Some time was allowed for readings to stabilize.

Pressure readings were taken by the data acquisition system during the test; the injected water volume was obtained from the Quizix pump software.

A.4.2 Calculations

For low gas saturation, the total compressibility of the air and water within the sand pack may be written as:

$$c_T = S_W c_W + S_g c_g \tag{A-13}$$

where: c_T = the total compressibility
S_W = the oil saturation
c_W = the oil compressibility
S_g = the gas saturtation
c_g = the gas compressibility

From the definition of isothermal compressibility, the gas compressibility is given by:

$$c_g = -\frac{1}{V}\frac{\partial V}{\partial p}\bigg|_T \tag{A-14}$$

Since the tests were performed at pressures close to atmospheric, the ideal gas equation can be used:

$$V = \frac{nRT}{p} \tag{A-15}$$

where: V = gas volume
n = number of moles
R= universal gas constant
T = temperature
p = pressure

The partial derivative of the previous expression with respect to p is:

$$\frac{\partial V}{\partial p} = -\frac{nRT}{p^2} \qquad \text{A-16}$$

Substituting A-15 and A-16 in A-14 we obtain for the compressibility of the gas:

$$c_g = \frac{1}{p} \qquad \text{A-17}$$

Therefore from A-14, assuming that the water compressibility can be neglected; we can calculate the volume of air present in the pack using A-17 for the gas compressibility as follows:

$$V = -p\frac{\Delta V}{\Delta p} \qquad \text{A-18}$$

A sample calculation from taking the data from Test 6 is given below:

<u>Compressibility Test III:</u>

Pump Initial Reading (V_i) = 8779.14 cm^3
Pump Final Reading (V_f) = 8790.66 cm^3
Initial Pressure @ Port 1 (p_{1i}) = 2.64 kPa
Final Pressure @ Port 1 (p_{1f}) = 157 kPa
Sand Pack Pore Volume (PV) = 2742 cm^3

$$\Delta V_{waterinjected} = -\Delta V_{gascompressed}$$
$$\Delta V_{waterinjected} = V_f - V_i = (8790.66 - 8779.14)cm^3 = 11.52cm^3$$
$$\Delta p = p_{1f} - p_{1i} = (157.00 - 2.64)kPa = 154.36kPa$$

Therefore the gas volume @ 2.64 kPa (initial pressure) was:

$$V_{@2.64kPa} = -(157.00 + 101.325)kPa\frac{-11.52cm^3}{154.36`kPa} = 19.28cm^3$$

The volume of gas in the pack at atmospheric pressure can be found using Boyle's law:

$$V_{@atm} = \frac{V_{@p_{1f}}p_{1f}}{p_{atm}} \qquad \text{A-19}$$

Therefore substituting values in A-19:

$$V_{@\,atm} = \frac{19.28cm^3 * (2.64 + 101.325)kPa}{101.325kPa} = 19.78cm^3$$

The percentage of air in the pack taking the PV calculated in Appendix A-3 is:

$$V_{air}(\%) = \frac{V_{@\,atm}}{PV} = \frac{19.78cm^3}{2742cm^3} * 100 = 0.72$$

Amounts of air in the pack less than 1 % were considered acceptable.

A.5 Material Balance Equation Derivation

The sand production rate will be calculated by using a mass balance equation. The incremental produced slurry is equal to the corresponding incremental changes inside the cell and the incremental mass of oil injected during the same time interval.

In this equation any injected quantity is positive (+), any produced quantity is negative (-). Thus the mass balance can be written as:

For the oil:

$$dm_{oi} + dm_{ot} + dm_{op} = 0 \quad \text{A-20}$$

For the sand:

$$dm_{st} + dm_{sp} = 0 \quad \text{A-21}$$

where the changes during a time interval dt are:

dm_{oi}: incremental mass of oil injected

dm_{ot}: incremental mass of oil in the cell

dm_{op}: incremental mass of oil produced

dm_{st}: incremental mass of sand in the cell

dm_{sp}: incremental mass of sand produced

From the conservation of mass for the sand:

$$dm_{st} + dm_{sp} = 0 \Rightarrow dm_{st} = -dm_{sp} \quad \text{A-22}$$

Similarly, from the conservation of mass for the oil:

$$dm_{oi} + dm_{ot} + dm_{op} = 0 \Rightarrow dm_{ot} = -dm_{op} - dm_{oi} \qquad \text{A-23}$$

In addition, the volume of the cell is fixed and equal to the sum of the volumes of oil and sand within the cell:

$$V_s + V_o = V_{cell} \qquad \text{A-24}$$

Since the volume of the cell does not change, the sum of the changes inside the cell in sand volume and oil volume must equal zero.

$$dV_{st} + dV_{ot} = 0 \Rightarrow -dV_{ot} = dV_{st} \qquad \text{A-25}$$

The incremental mass can be converted to the incremental volume from the definition of density:

$$\rho = \frac{dm}{dV} \qquad \text{A-26}$$

Therefore equation A-22 becomes:

$$dV_{st} = -dV_{sp} \qquad \text{A-27}$$

since the density of the sand does not change.

Substituting A-25 into A-27:

$$dV_{ot} = dV_{sp} \qquad \text{A-28}$$

Again, using the fixed density of oil to convert the expression A-23 to an equivalent expression for incremental volume, we have:

$$dV_{ot} = -(dV_{op} + dV_{oi}) \qquad \text{A-29}$$

Replacing dV_{ot} in A-28 by expression A-29 yields an expression relating the volume of oil injected to the produced oil and sand.

$$dV_{oi} = -(dV_{sp} + dV_{op}) \qquad \text{A-30}$$

On the other hand:

$$dm_{slurry} = dm_{op} + dm_{sp} = dV_{op}\rho_o + dV_{sp}\rho_s \qquad \text{A-31}$$

where dm_{slurry} is the incremental mass of slurry produced at a time incremental dt.

Expressions A-30 and A-31 form a system of two equations with two unknowns dV_{op} and dV_{sp}. Substituting dV_{op} from equation A-30 into equation A-31 yields:

$$dm_{slurry} = (-dV_{sp} - dV_{oi})\rho_o + dV_{sp}\rho_s \qquad \text{A-32}$$

From expression A-32:

$$dV_{sp} = \frac{dm_{slurry} + dV_{oi}\rho_o}{\rho_s - \rho_o} \qquad \text{A-33}$$

Since the flow rate will be constant over short time intervals the volume of oil injected is given by:

$$dV_{oi} = Q_{oi}dt \qquad \text{A-34}$$

where Q_{oi} is the volumetric flow rate of oil injected and dt is the time interval.

Therefore:

$$dV_{sp} = \frac{dm_{slurry} + Q_{oi}dt\rho_o}{\rho_s - \rho_o} \qquad \text{A-35}$$

This equation can be converted from volume to mass using the definition of density in A-26. The result is:

$$dm_{sp} = \frac{(dm_{slurry} + Q_{oi}dt\rho_o)\rho_s}{\rho_s - \rho_o} \qquad \text{A-36}$$

Thus, the sand production rate Q_{sp} over any time interval dt can be represented as:

$$Q_{sp} = \frac{dm_{sp}}{dt} = \frac{(dm_{slurry} + Q_{oi}dt\rho_o)\rho_s}{(\rho_s - \rho_o)dt} \qquad \text{A-37}$$

B Appendix II: Results

B.1 Sand Under Confining Stress Graphs

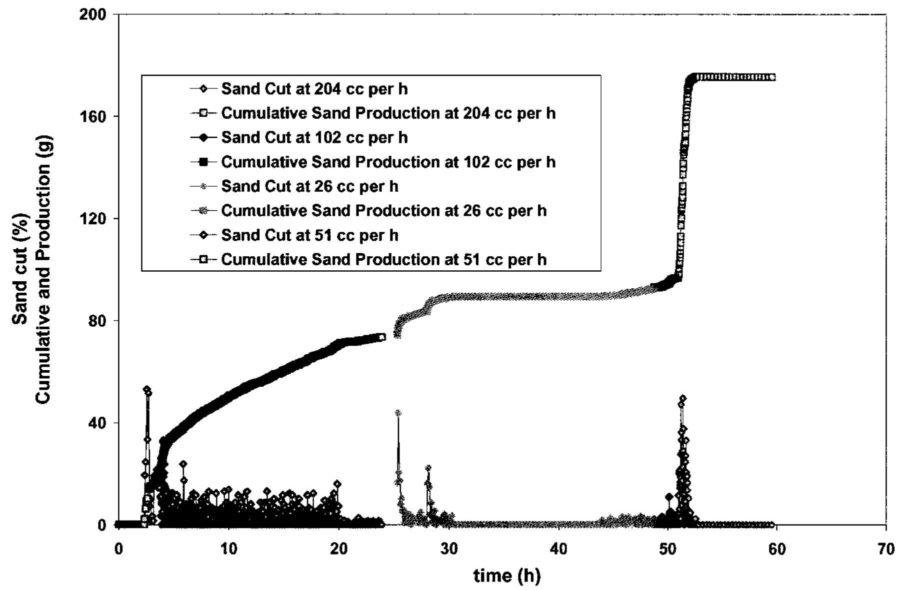

Figure B-1: Sand cut and cumulative sand production vs. time for experiment # 1. Sand: Silica Well Sorted. Slot size: 0.711 mm (0.028 in). σ_c: 519 kPa

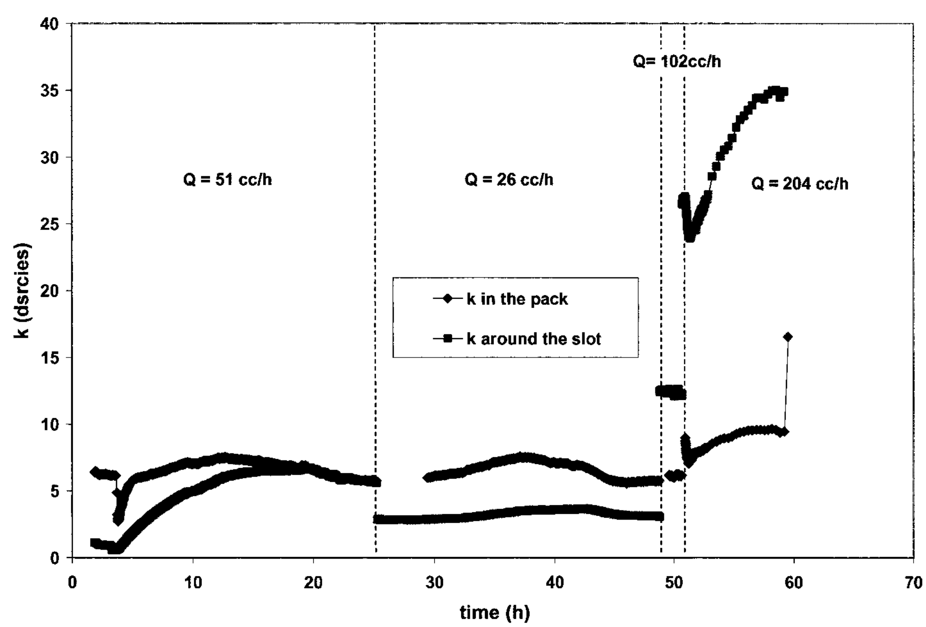

Figure B-2: Permeability inside pack and around the slot vs. time for experiment # 1. Sand: Silica Well Sorted. Slot size: 0.711 mm (0.028 in). σ_c: 519 kPa

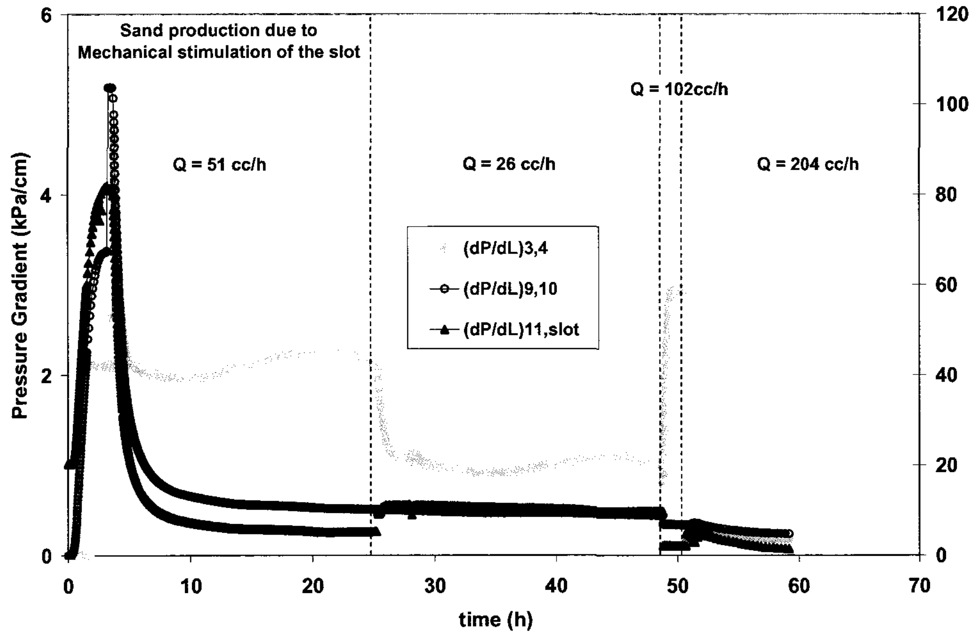

Figure B-3: Pressure Gradient vs. time for experiment # 1. Sand: Silica Well Sorted. Slot size: 0.711 mm (0.028 in). σ_c: 519 kPa

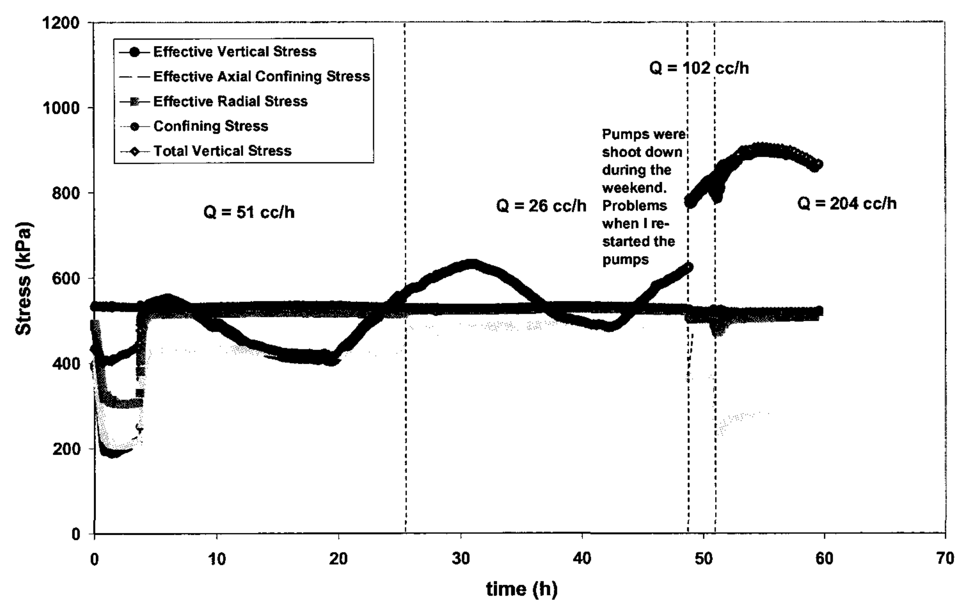

Figure B-4: Stress distribution in the sand pack as a function of time for experiment # 1. Sand: Silica Well Sorted. Slot Size: 0.711 mm (0.028 in). σ_c: 519 kPa

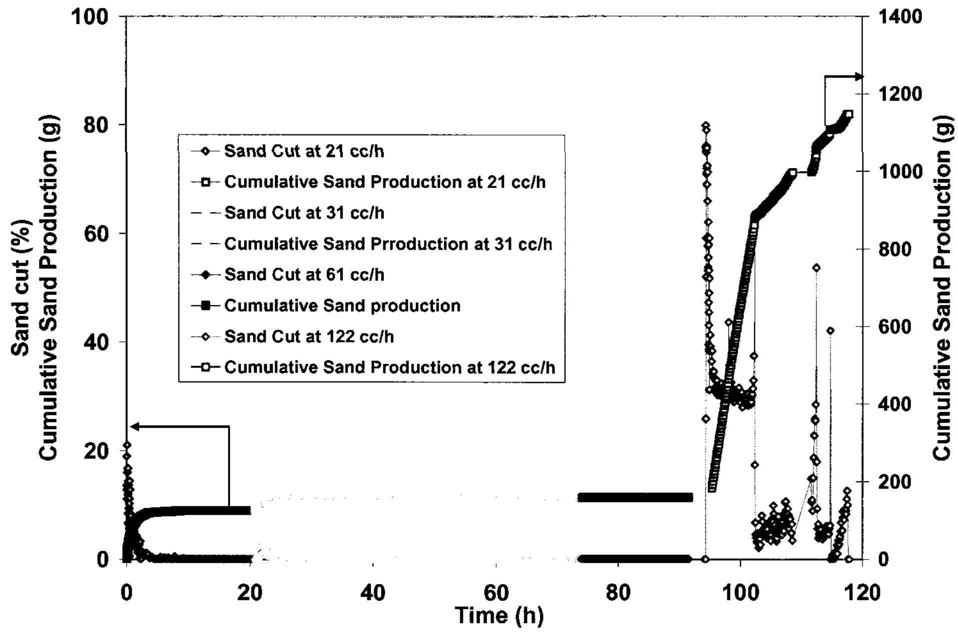

Figure B-5: Sand cut and cumulative sand production vs. time for experiment # 2. Sand: Silica Well Sorted. Slot size: 0.813 (0.032 in). σ_c: 531 kPa

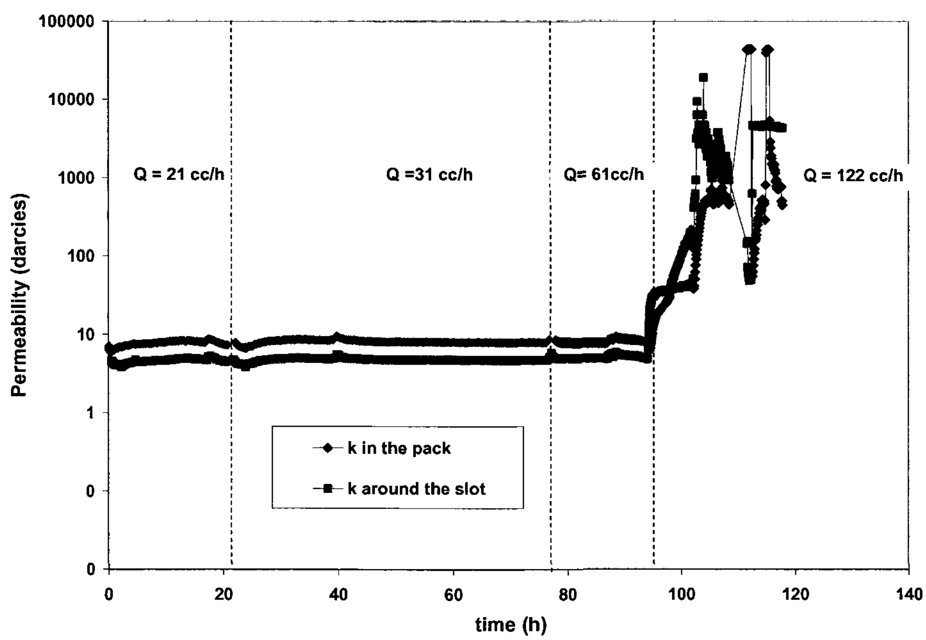

Figure B-6: Permeability inside pack and around the slot vs. time for experiment # 2. Sand: Silica Well Sorted. Slot size: 0.813 (0.032 in). σ_c: 531 kPa

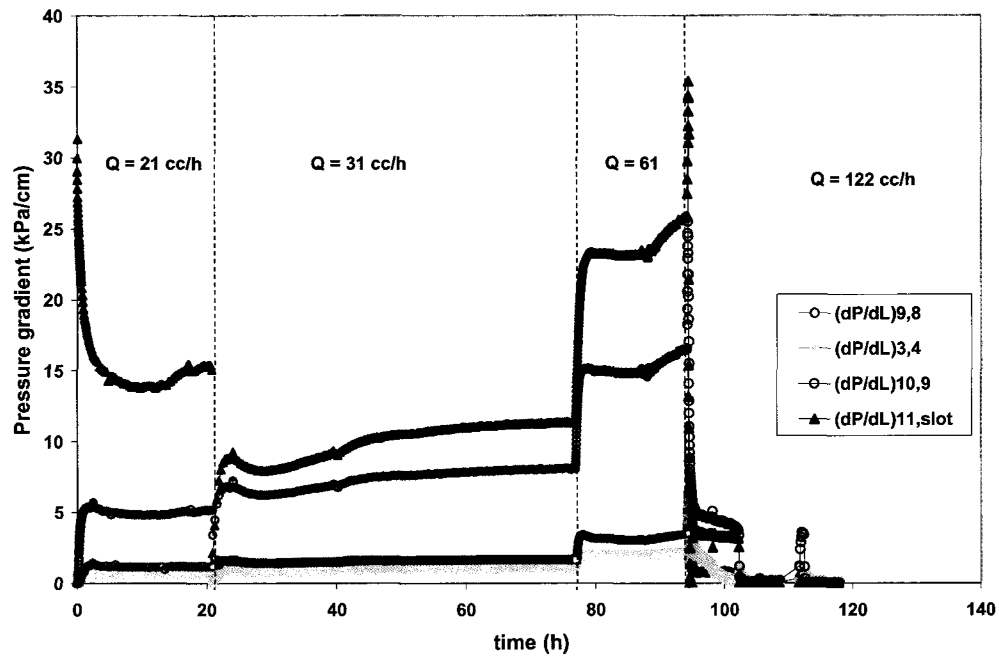

Figure B-7: Pressure Gradient vs. time for experiment # 2. Sand: Silica Well Sorted. Slot size: 0.813 (0.032 in). σ_c: 531 kPa

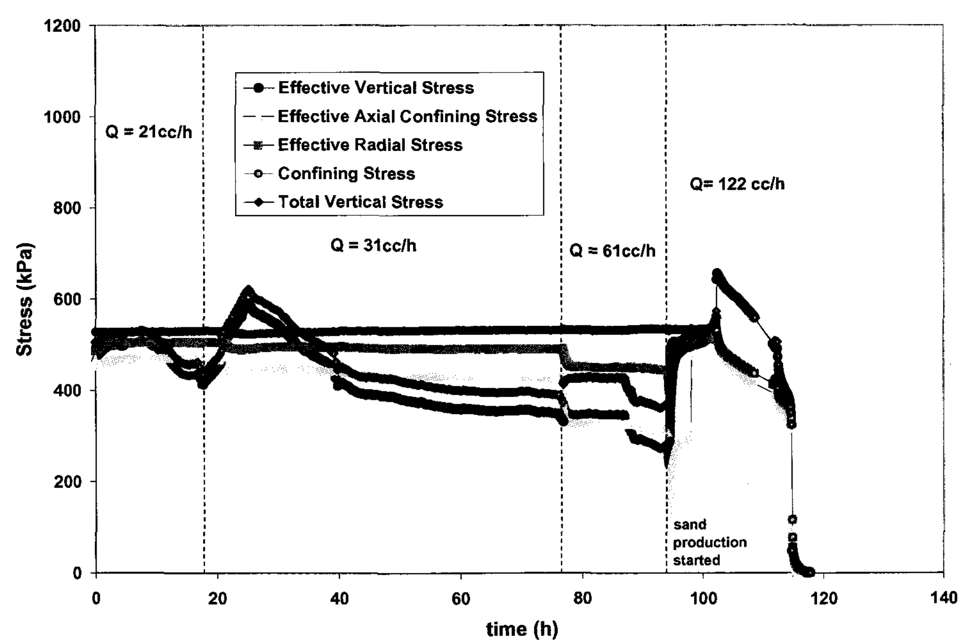

Figure B-8: Stress distribution in the sand pack vs. time for experiment # 2. Sand: Silica Well Sorted. Slot Size: 0.813 (0.032 in). σ_c: 531 kPa

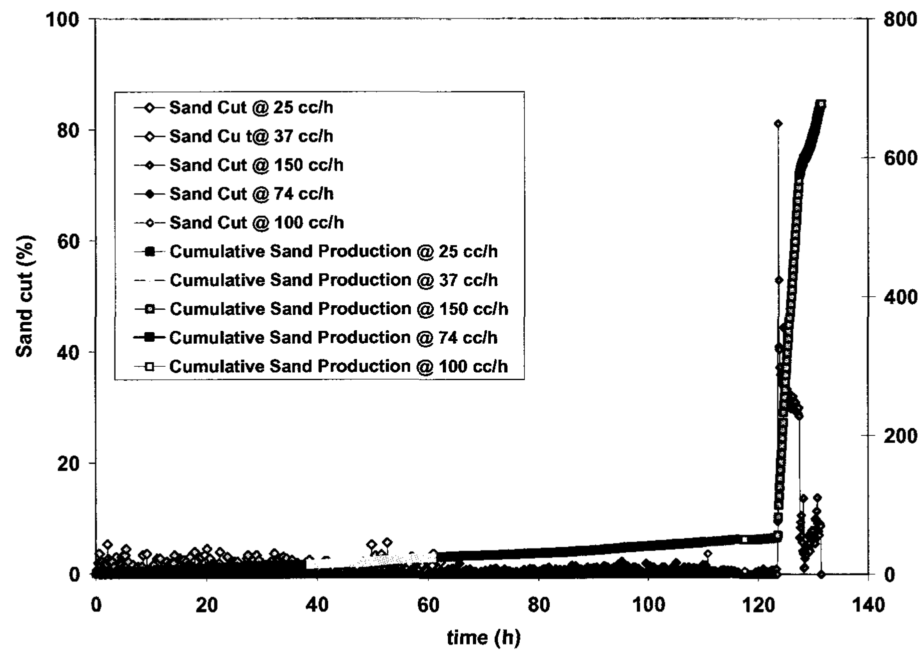

Figure B-9: Sand cut and cumulative sand production vs. time for experiment # 3. Sand: Silica Well Sorted. Slot size: 1.016 mm (0.040 in). σ_c: 982 kPa

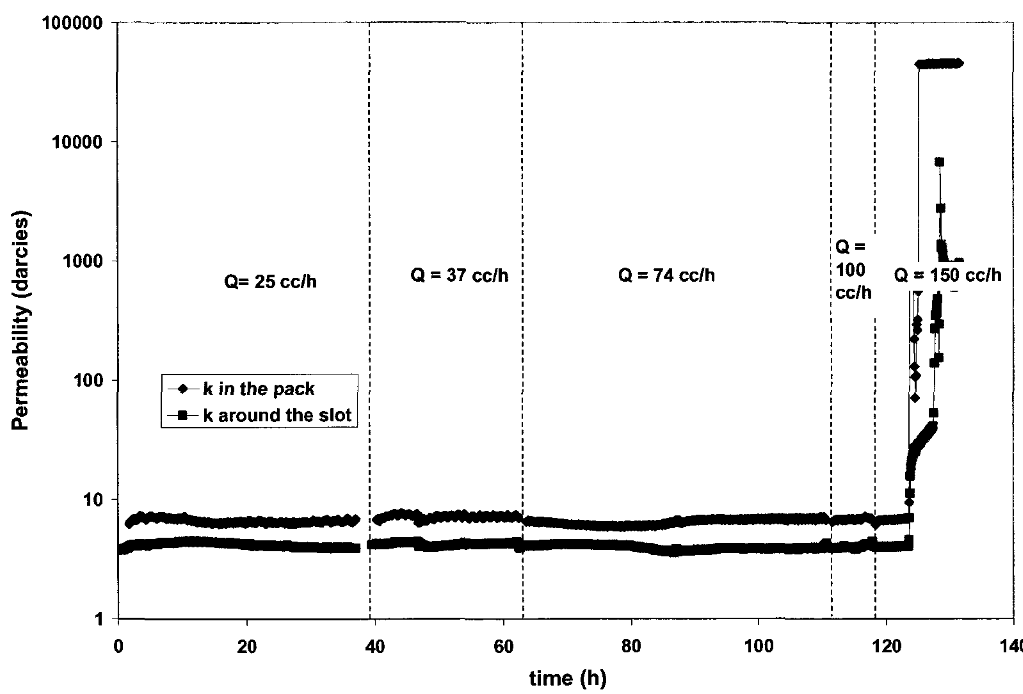

Figure B-10: Permeability inside pack and around the slot vs. time for experiment # 3. Sand: Silica Well Sorted. Slot size: 1.016 mm (0.040 in). σ_c: 982 kPa

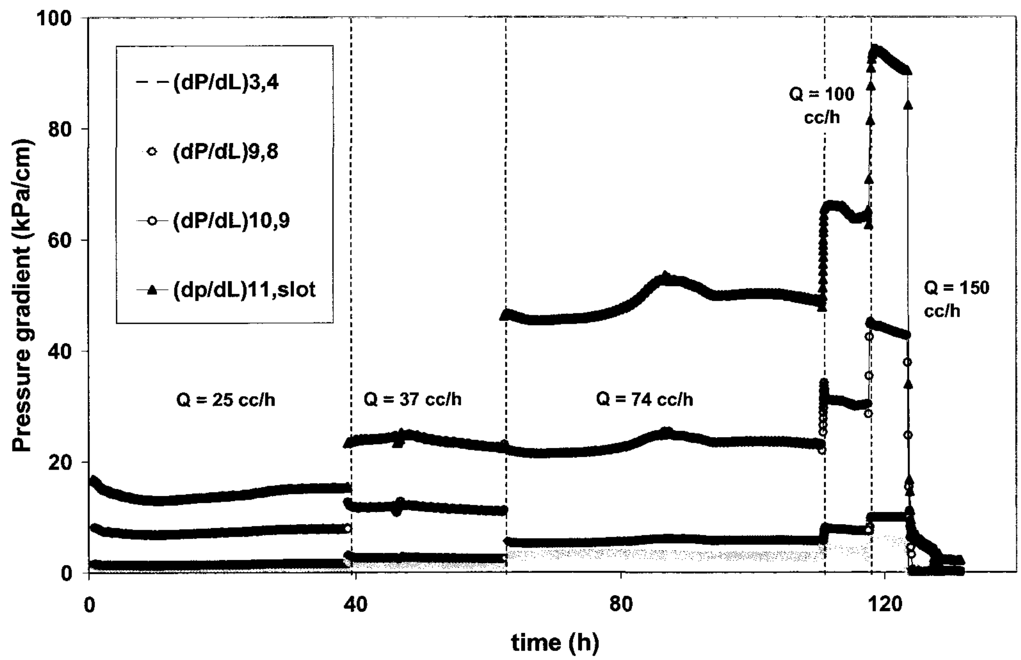

Figure B-11: Pressure Gradient vs. time for experiment # 3. Sand: Silica Well Sorted. Slot size: 1.016 mm (0.040 in). σ_c: 982 kPa

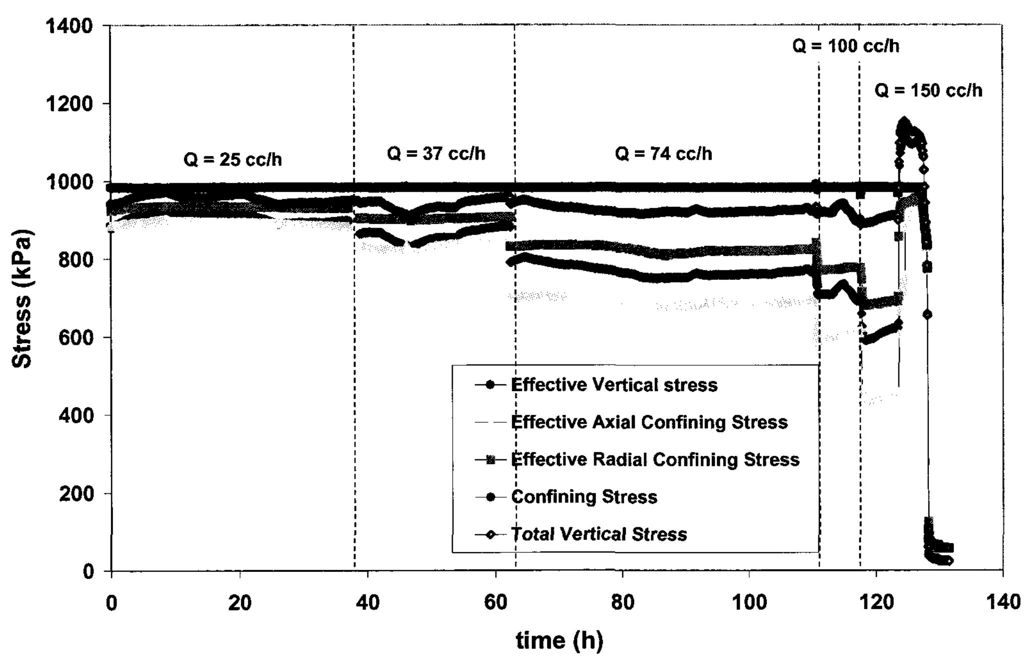

Figure B-12: Stress distribution in the sand pack as a function of time for experiment # 3. Sand: Silica Well Sorted. Slot Size: 1.016 mm (0.040 in). σ_c: 982 kPa

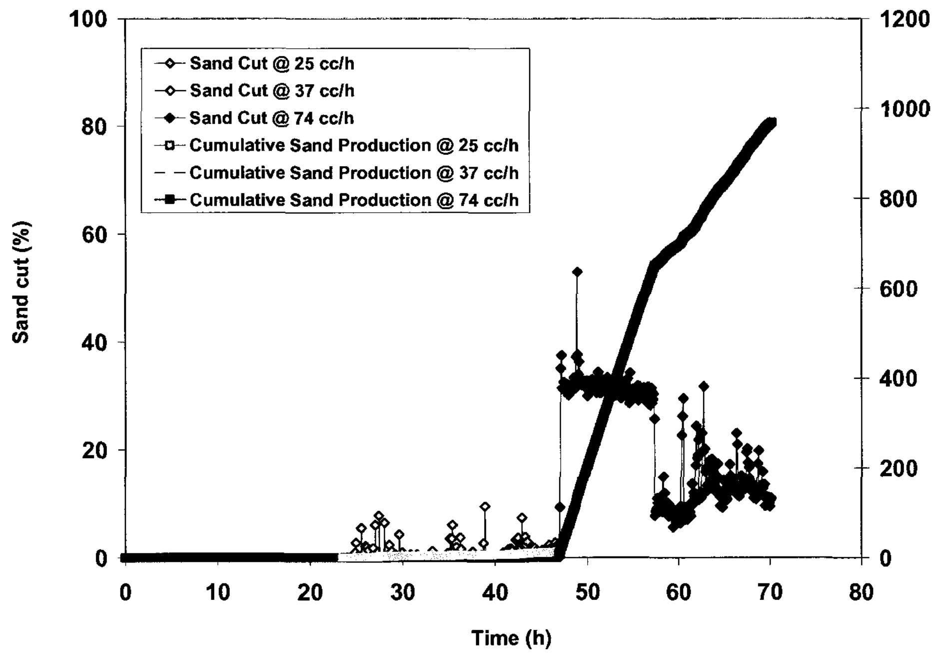

Figure B-13: Sand cut and cumulative sand production as a function of time for experiment # 4. Sand: Silica Well Sorted. Slot size: 1.016 mm (0.040 in). σ_c: 513 kPa

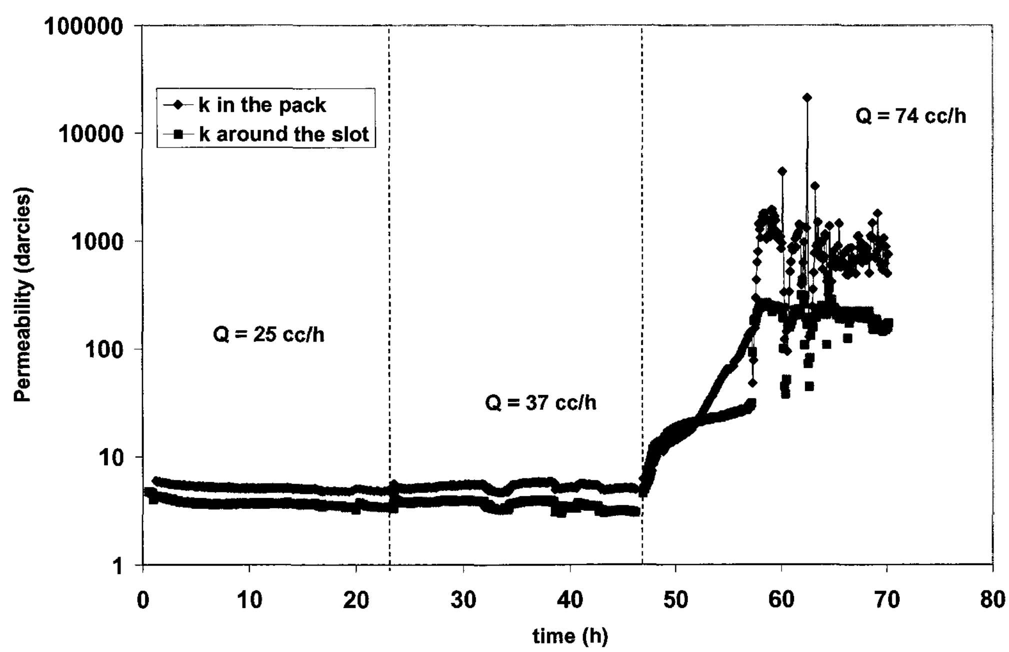

Figure B-14: Permeability inside pack and around the slot vs. time for experiment # 4. Sand: Silica Well Sorted. Slot size: 1.016 mm (0.040 in). σ_c: 513 kPa

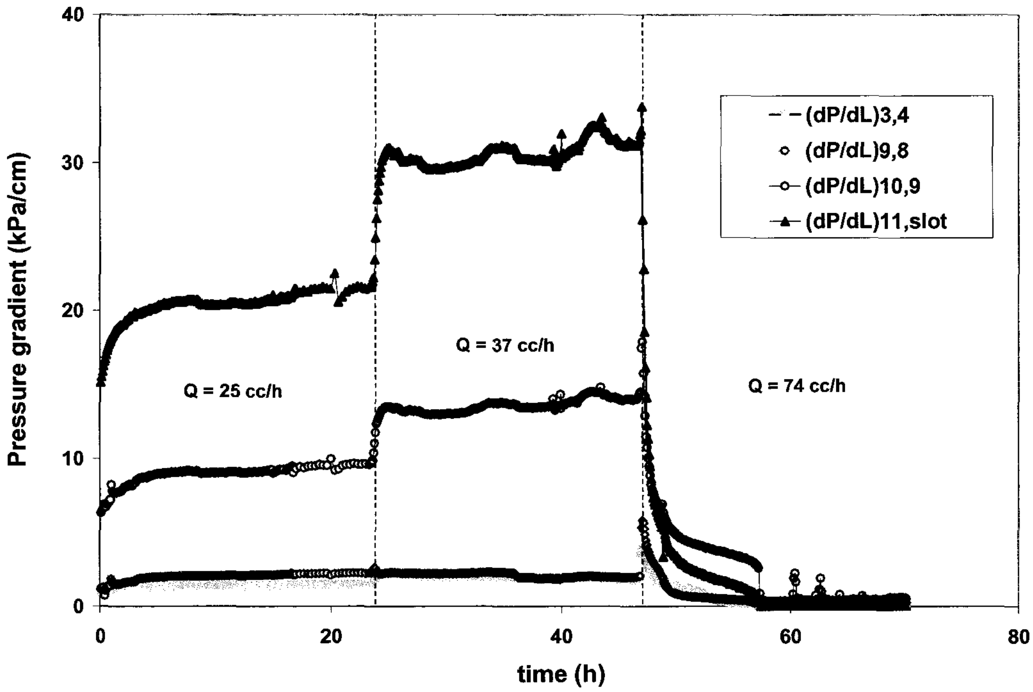

Figure B-15: Pressure Gradient vs. time for experiment # 4. Sand: Silica Well Sorted. Slot size: 1.016 mm (0.040 in). σ_c: 513 kPa

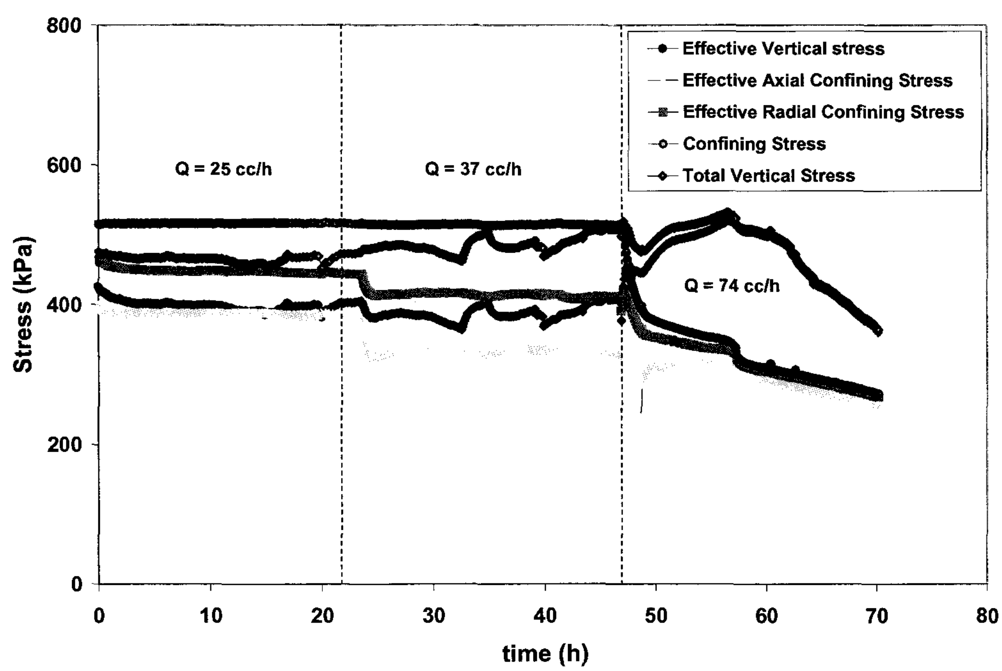

Figure B-16: Stress distribution in the sand pack as a function of time for experiment # 4. Sand: Silica Well Sorted. Slot Size: 1.016 mm (0.040 in). σ_c: 513 kPa

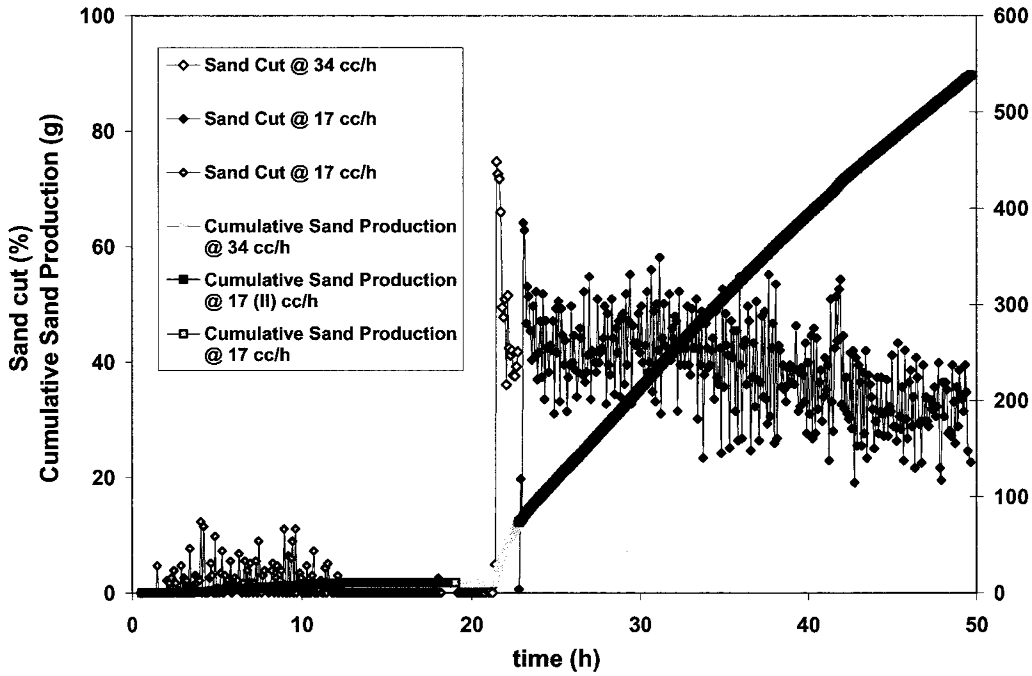

Figure B-17: Sand cut and cumulative sand production as a function of time for experiment # 5. Sand: Silica Well Sorted. Slot size: 1.422 mm (0.056 in). σ_c: 506 kPa

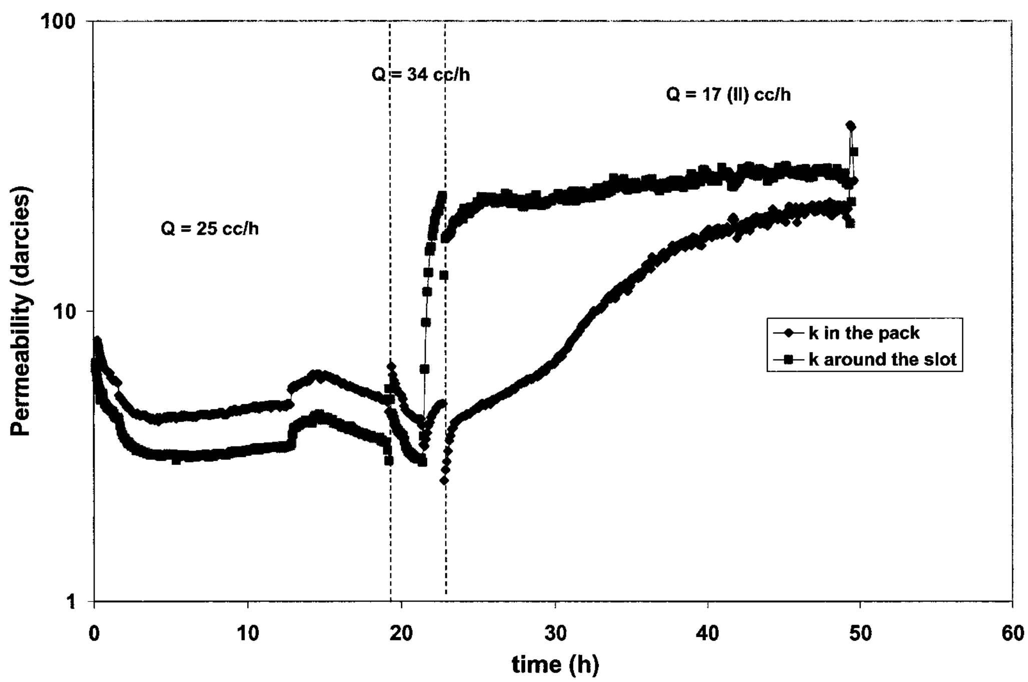

Figure B-18: Permeability inside pack and around the slot vs. time for experiment # 5. Sand: Silica Well Sorted. Slot size: 1.422 mm (0.056 in). σ_c: 506kPa

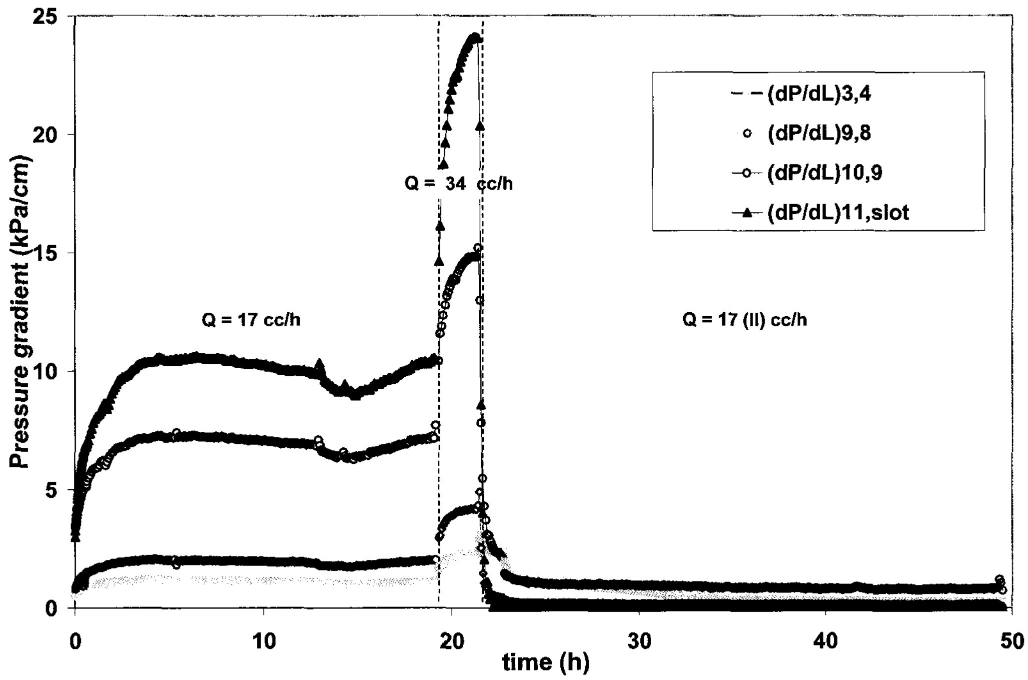

Figure B-19: Pressure Gradient vs. time for experiment # 5. Sand: Silica Well Sorted. Slot size: 1.422 mm (0.056 in). σ_c: 506 kPa

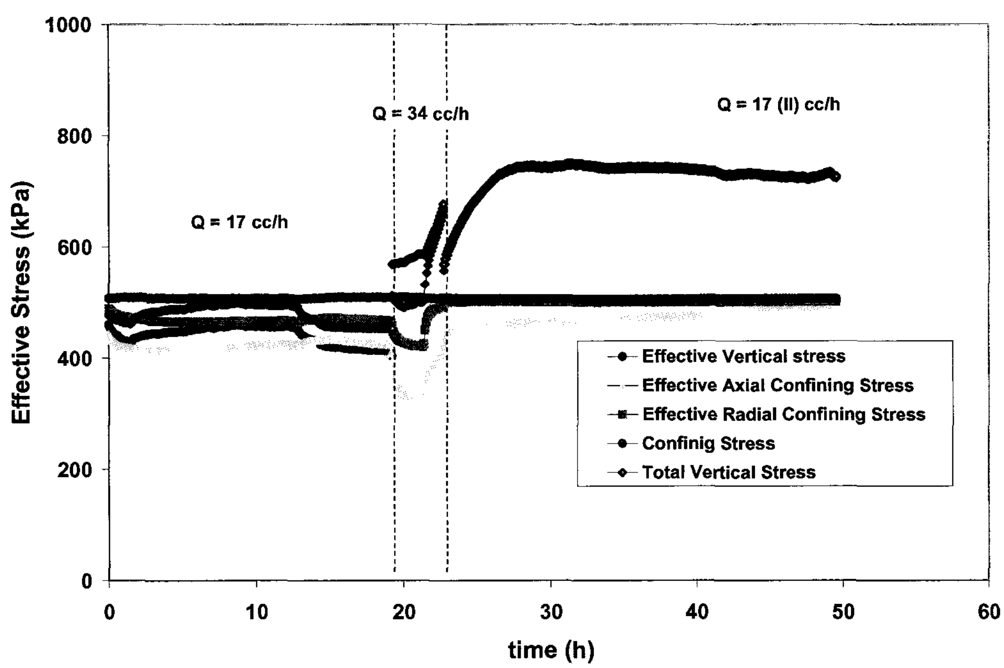

Figure B-20: Stress distribution in the sand pack as a function of time for experiment # 5. Sand: Silica Well Sorted. Slot Size: 1.422 mm (0.056 in). σ_c: 506 kPa

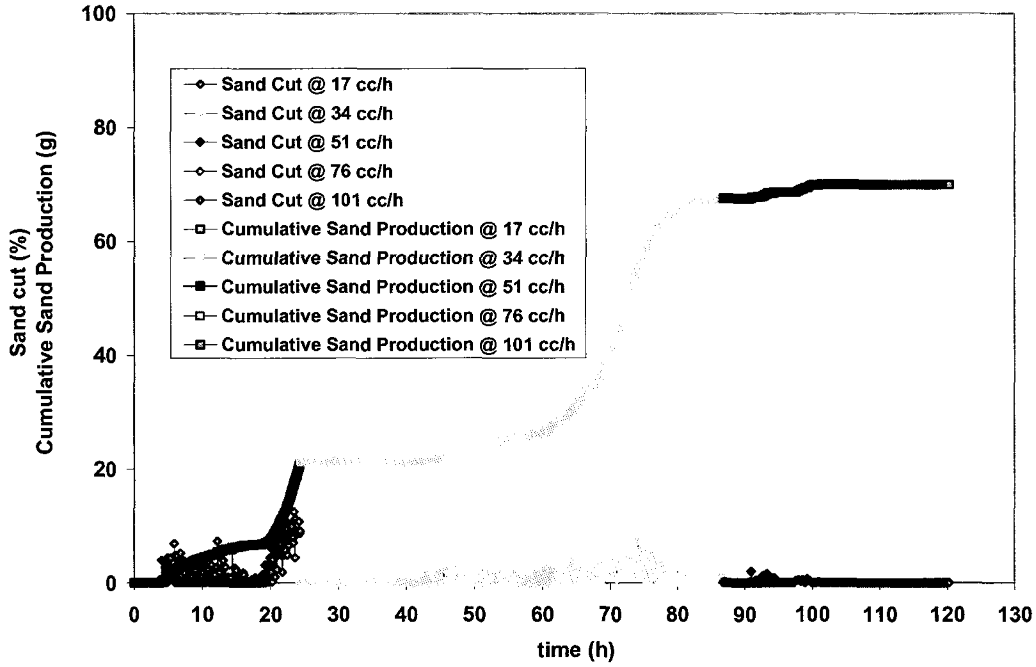

Figure B-21: Sand cut and cumulative sand production as a function of time for experiment # 6. Sand: Poorly Sorted. Slot size: 1.422 mm (0.056 in). σ_c: 2472 kPa

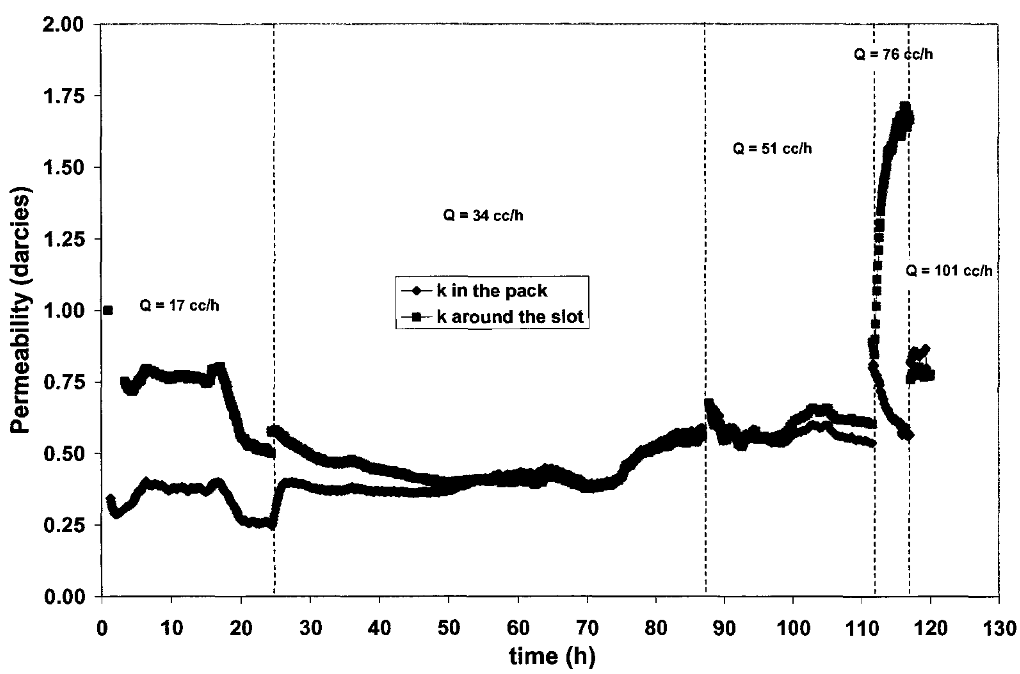

Figure B-22: Permeability inside pack and around the slot vs. time for experiment # 6. Sand: Poorly Sorted. Slot size: 1.422 mm (0.056 in). σ_c: 2472 kPa

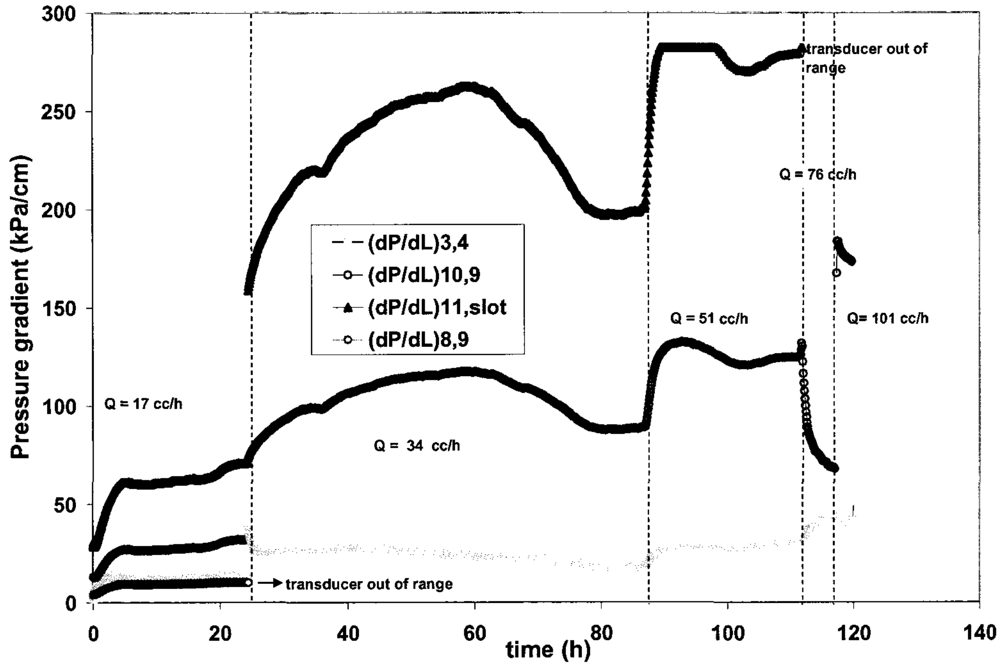

Figure B-23: Pressure Gradient vs. time for experiment # 6. Sand: Poorly Sorted. Slot size: 1.422 mm (0.056 in). σ_c: 2472 kPa

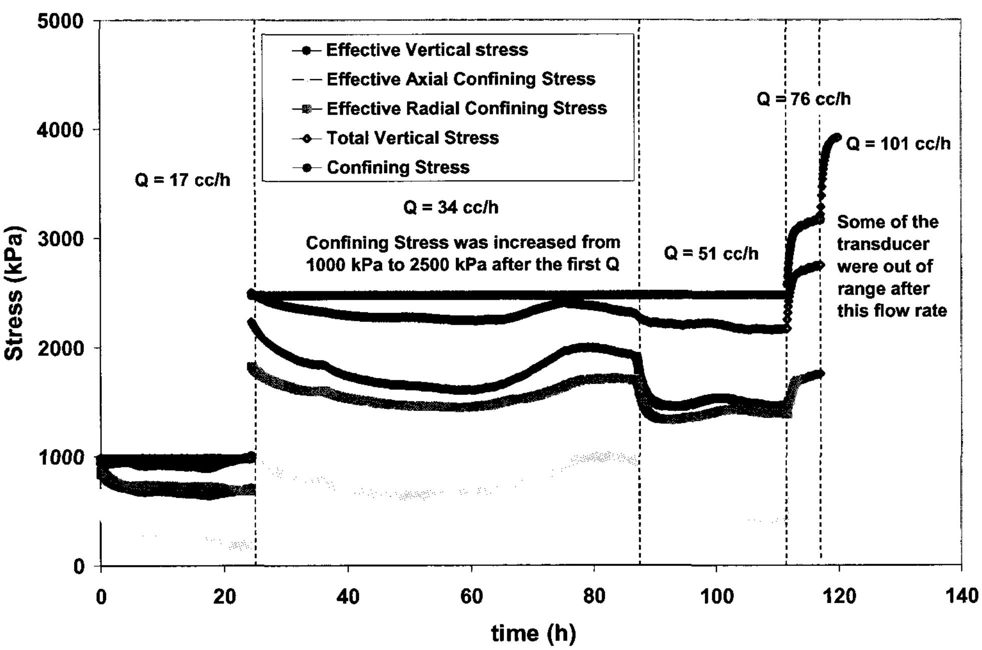

Figure B-24: Stress distribution in the sand pack as a function of time for experiment # 6. Sand: Poorly Sorted. Slot size: 1.422 mm (0.056 in). σ_c: 2472 kPa

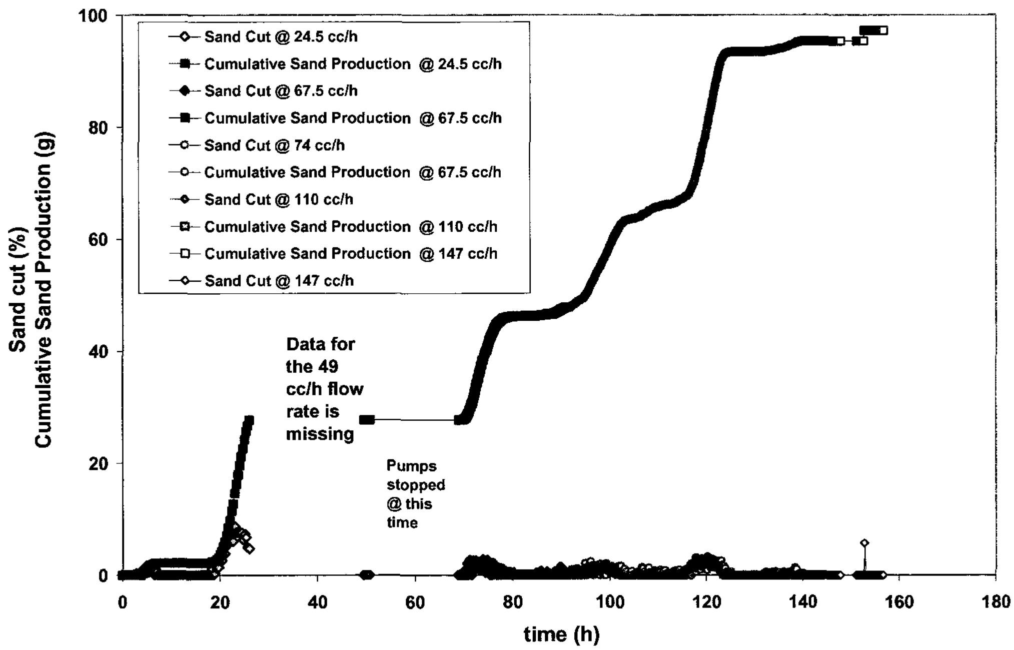

Figure B-25: Sand cut and cumulative sand production as a function of time for experiment # 7. Sand: Poorly Sorted. Slot size: 1.981 mm (0.078 in). σ_c: 2471 kPa

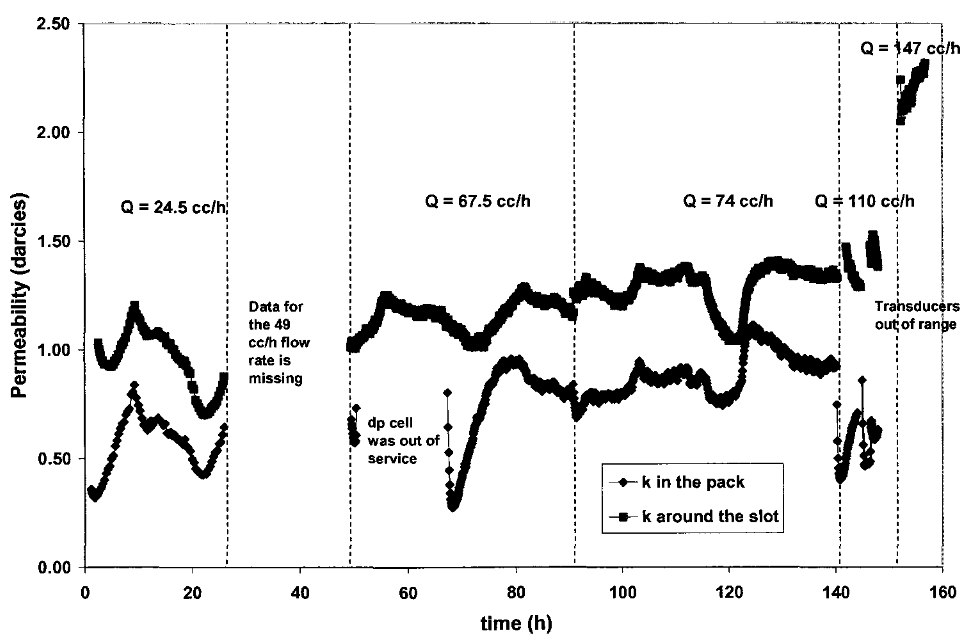

Figure B-26: Permeability inside pack and around the slot vs. time for experiment # 7. Sand: Poorly Sorted. Slot size: 1.981 mm (0.078 in). σ_c: 2471 kPa

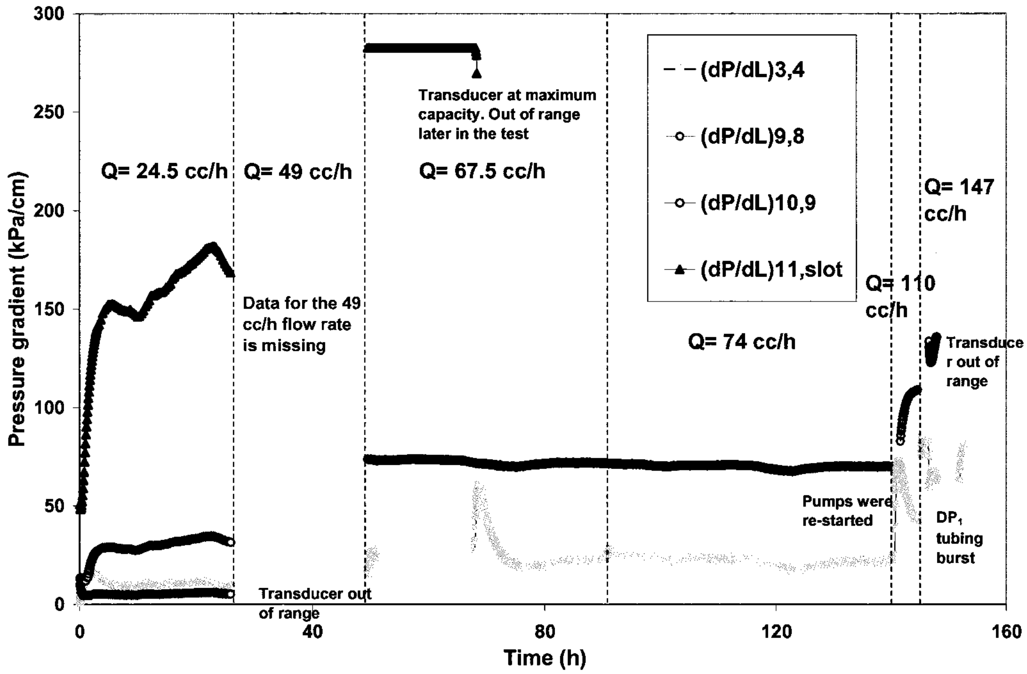

Figure B-27: Pressure Gradient vs. time for experiment # 7. Sand: Poorly Sorted. Slot size: 1.981 mm (0.078 in). σ_c: 2471 kPa

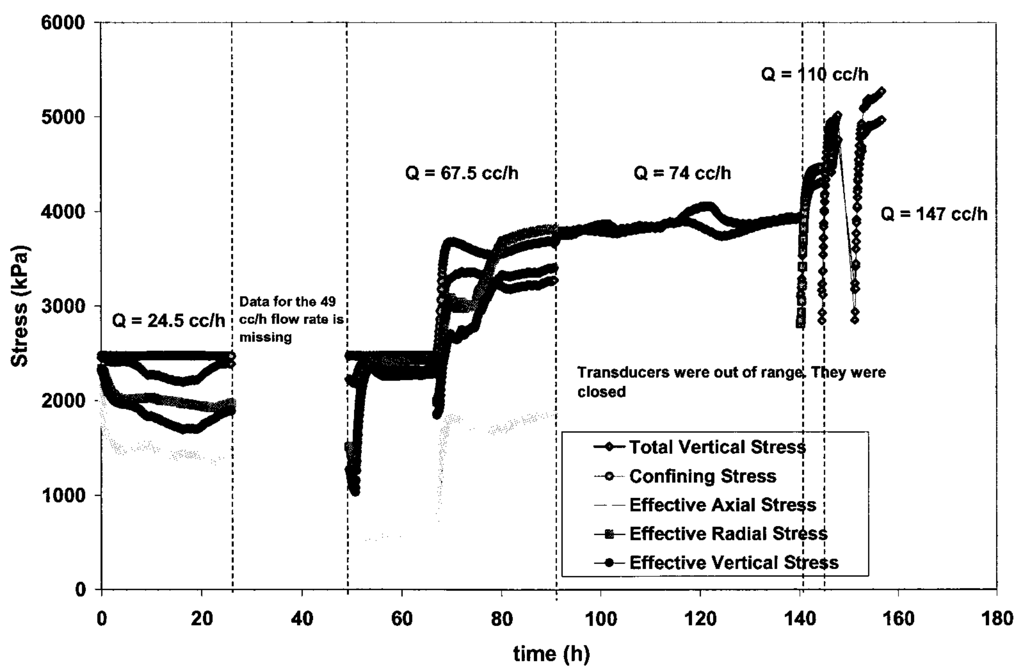

Figure B-28: Stress distribution in the sand pack as a function of time for experiment # 7. Sand: Poorly Sorted. Slot Size: 1.981 mm (0.078 in). σ_c: 2471 kPa

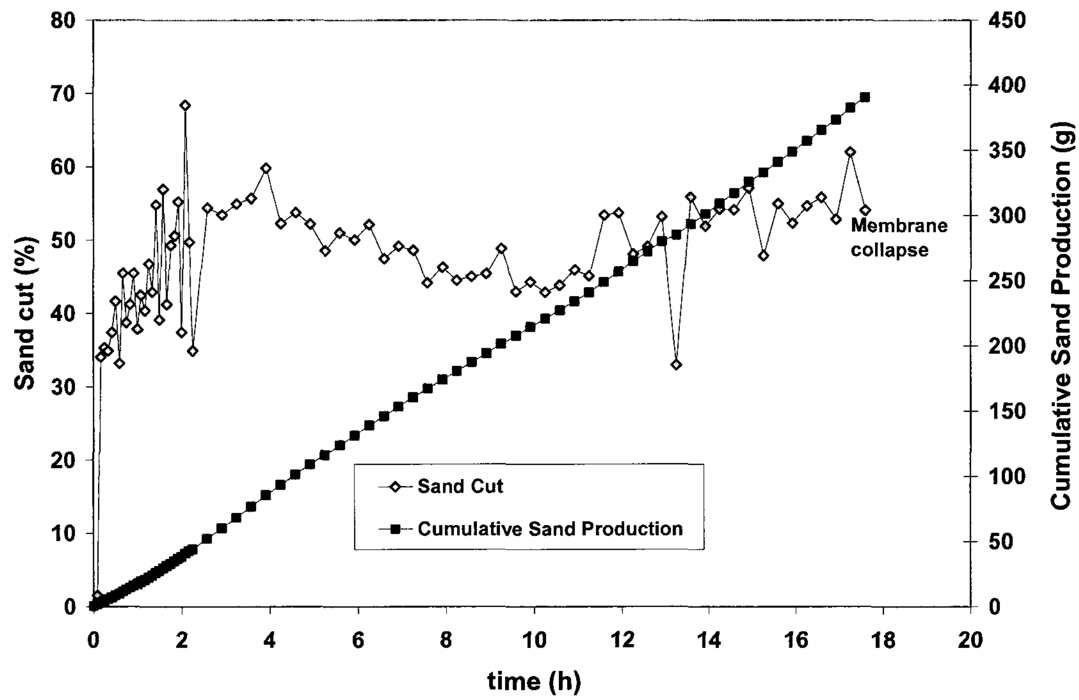

Figure B-29: Sand cut and cumulative sand production as a function of time for experiment # 8. Sand: Silica Well Sorted. Slot size: 1.422 mm (0.056 in). σ_c: 2469 kPa

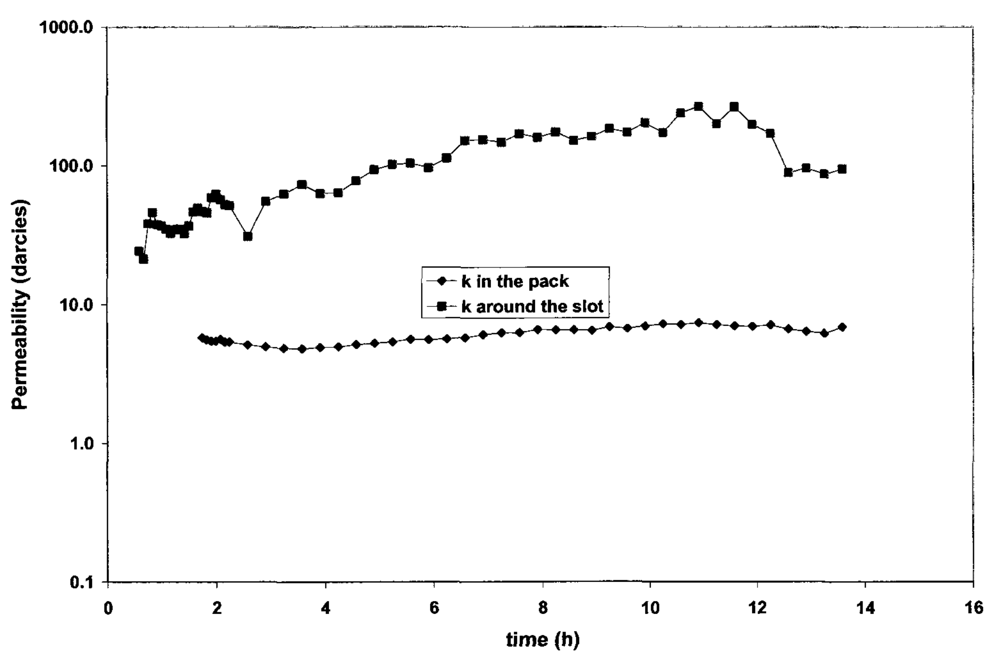

Figure B-30: Permeability inside pack and around the slot vs. time for experiment # 8. Sand: Silica Well Sorted. Slot size: 1.422 mm (0.056 in). σ_c: 2469 kPa

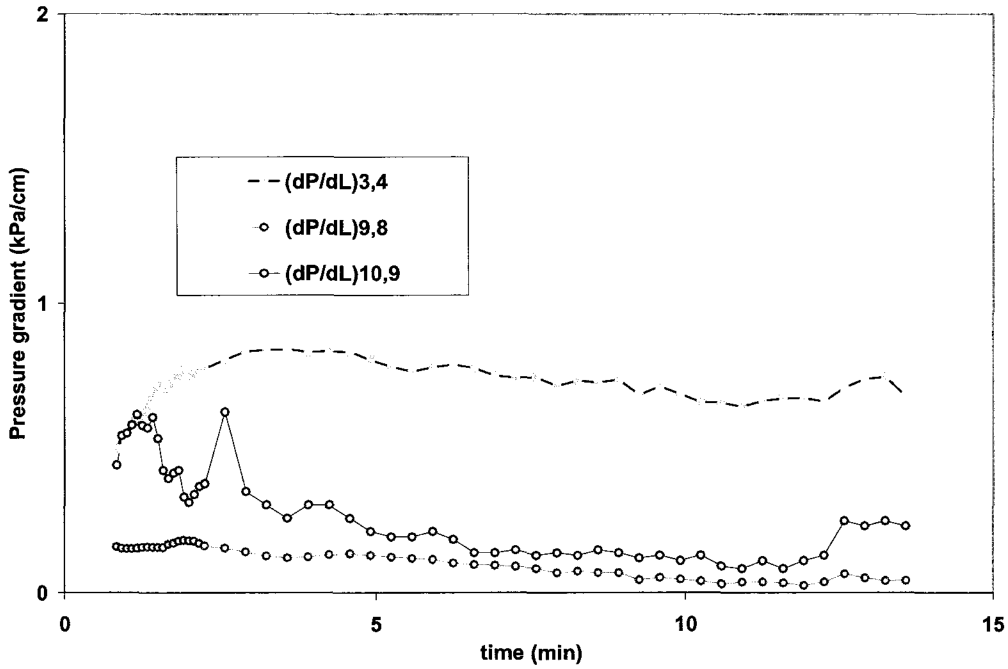

Figure B-31: Pressure Gradient vs. time for experiment # 8. Sand: Silica Well Sorted. Slot size: 1.422 mm (0.056 in). σ_c: 2469 kPa

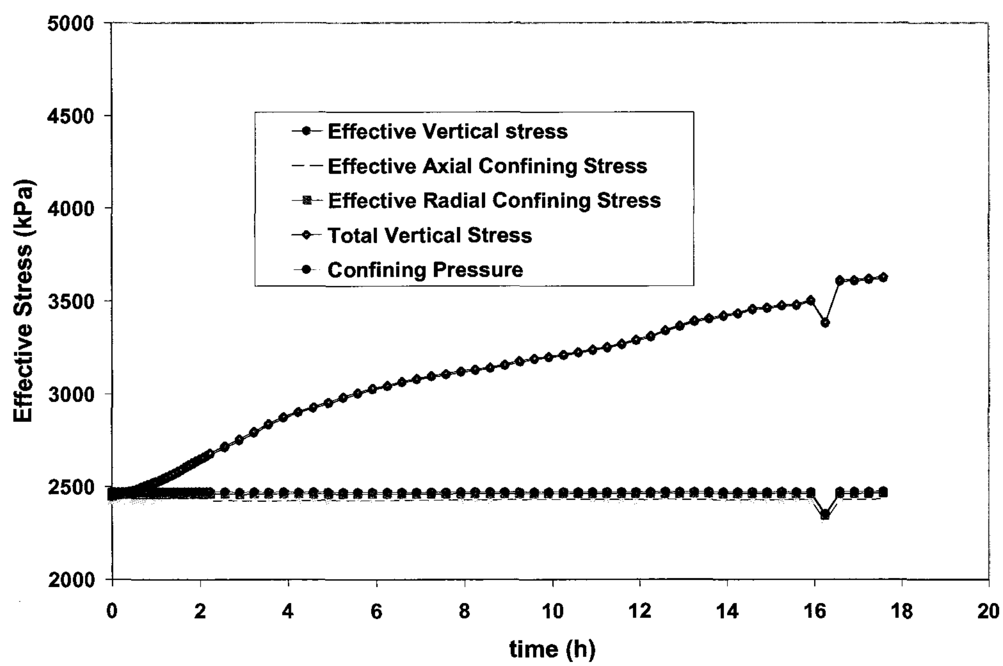

Figure B-32: Stress distribution in the sand pack as a function of time for experiment # 8. Sand: Silica Well Sorted. Slot Size: 1.422 mm (0.056 in). σ_c: 2469 kPa

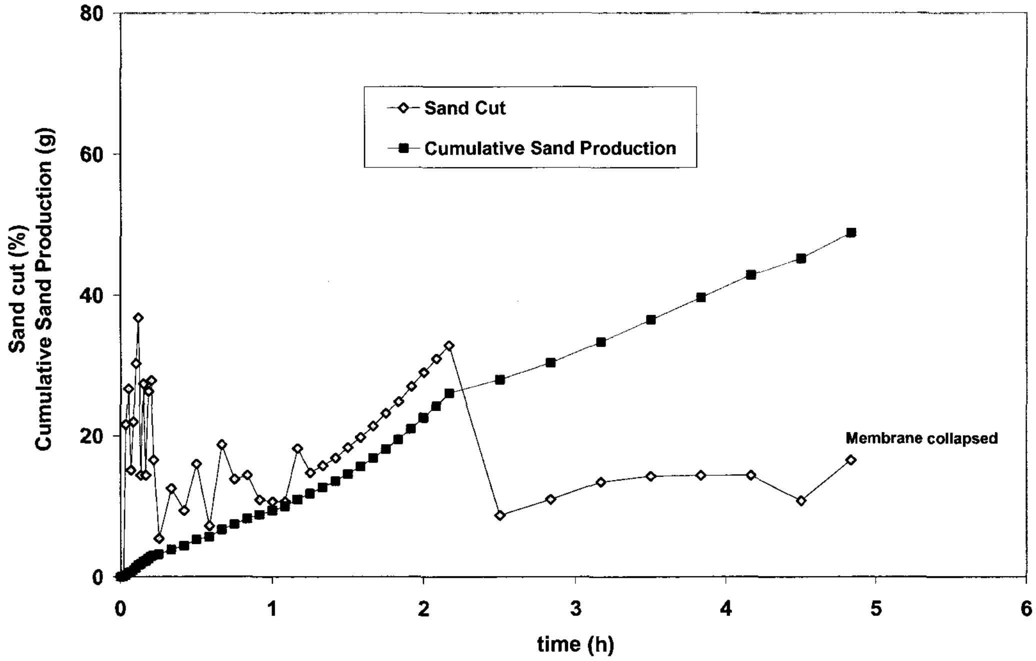

Figure B-33: Sand cut and cumulative sand production as a function of time for experiment # 9. Sand: Silica Well Sorted. Slot size: 1.016 mm (0.040 in). σ_c: 2472 kPa

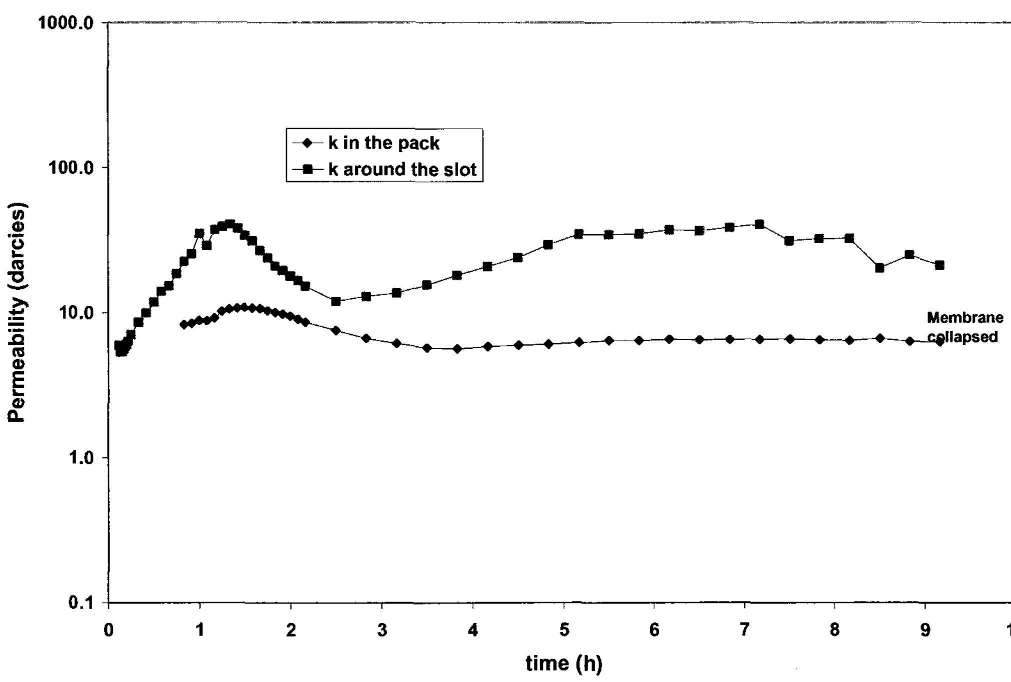

Figure B-34: Permeability inside pack and around the slot vs. time for experiment # 9. Sand: Silica Well Sorted. Slot size: 1.016 mm (0.040 in). σ_c: 2472 kPa

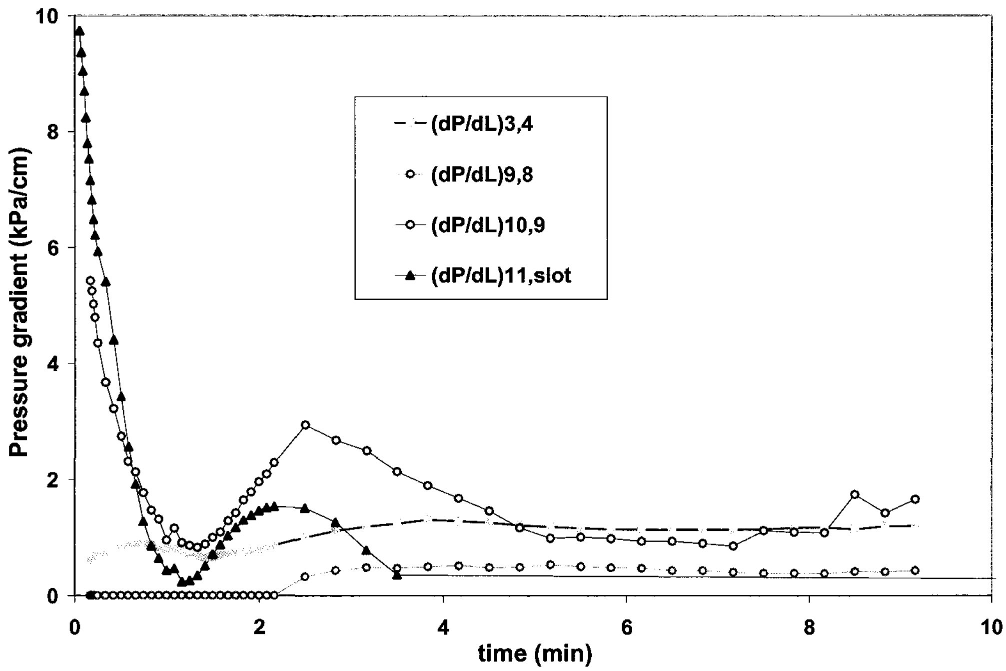

Figure B-35: Pressure Gradient vs. time for experiment # 9. Sand: Silica Well Sorted. Slot size: 1.016 mm (0.040 in). σ_c: 2472 kPa

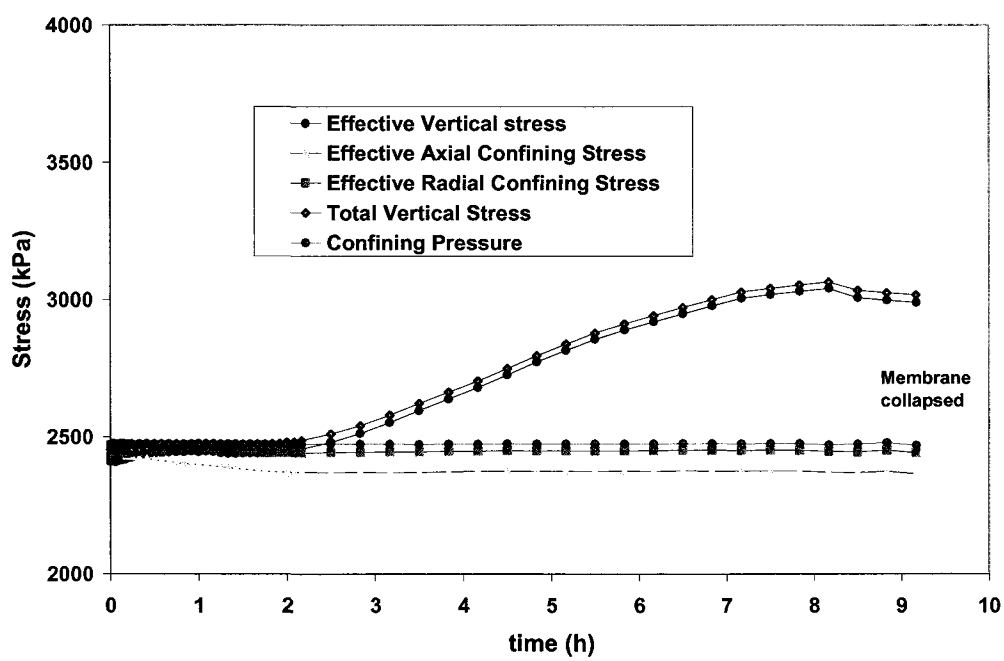

Figure B-36: Stress distribution in the sand pack as a function of time for experiment # 9. Sand: Silica Well Sorted. Slot Size: 1.016 mm (0.040 in). σ_c: 2472 kPa

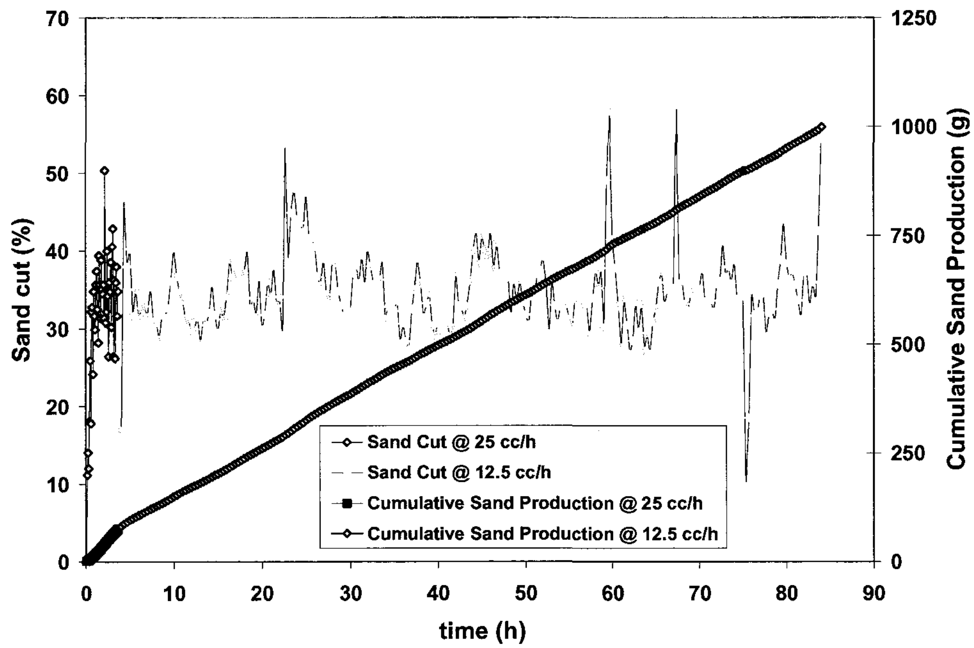

Figure B-37: Sand cut and cumulative sand production as a function of time for experiment # 10. Sand: Silica Well Sorted. Slot size: 0.711 mm (0.028 in). σ_c: 733 kPa

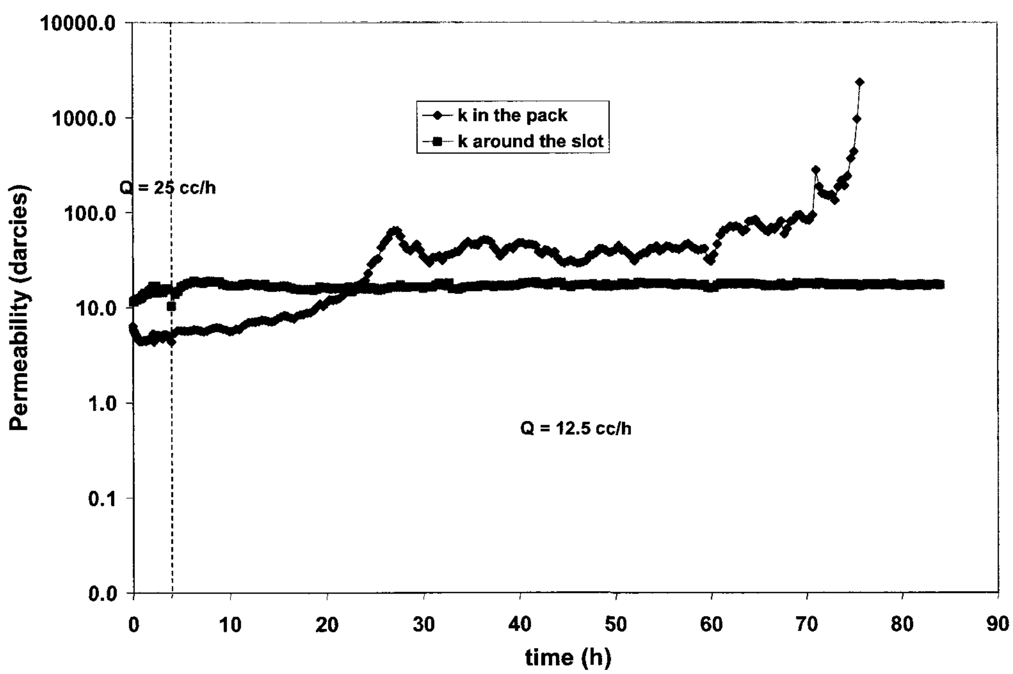

Figure B-38: Permeability inside pack and around the slot vs. time for experiment # 10. Sand: Silica Well Sorted. Slot size: 0.711 mm (0.028 in). σ_c: 733 kPa

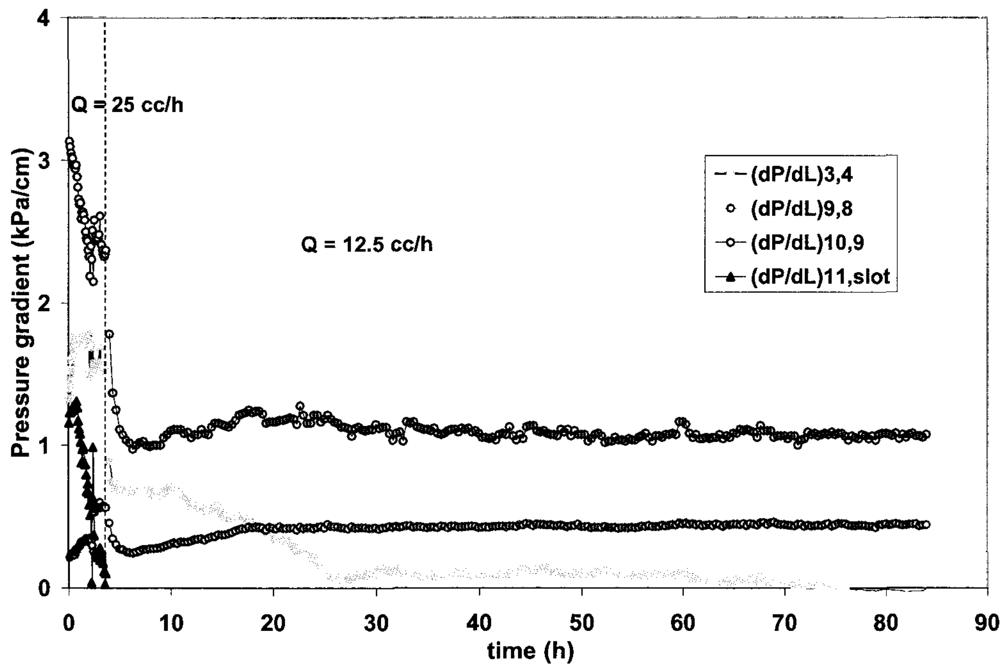

Figure B-39: Pressure Gradient vs. time for experiment # 10. Sand: Silica Well Sorted. Slot size: 0.711 mm (0.028 in). σ_c: 733 kPa

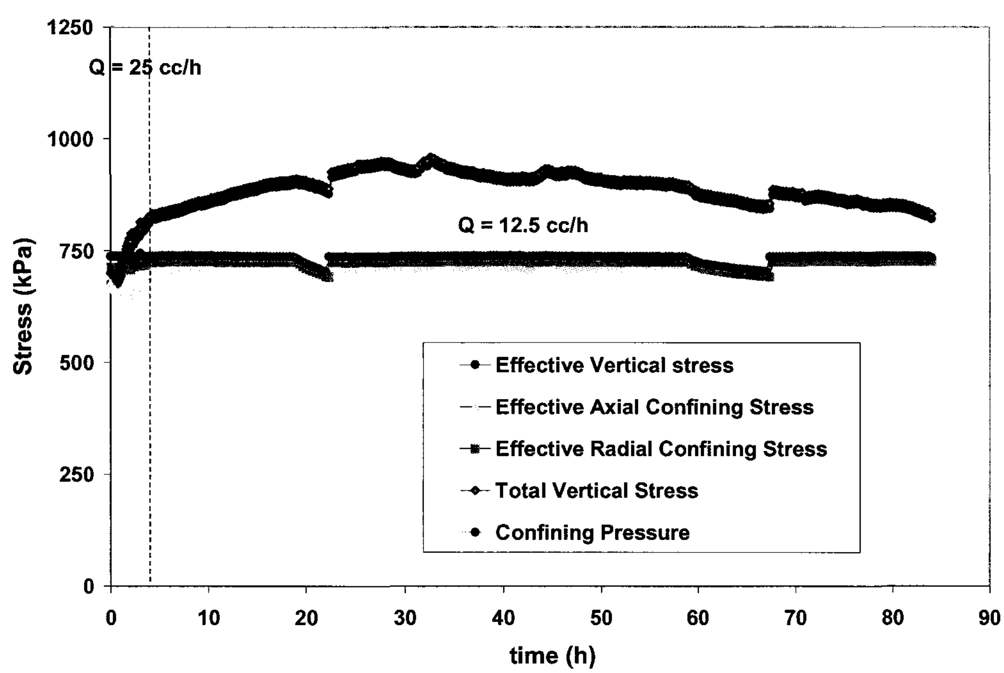

Figure B-40: Stress distribution in the sand pack as a function of time for experiment # 10. Sand: Silica Well Sorted. Slot Size: 0.711 mm (0.028 in). σ_c: 733 kPa

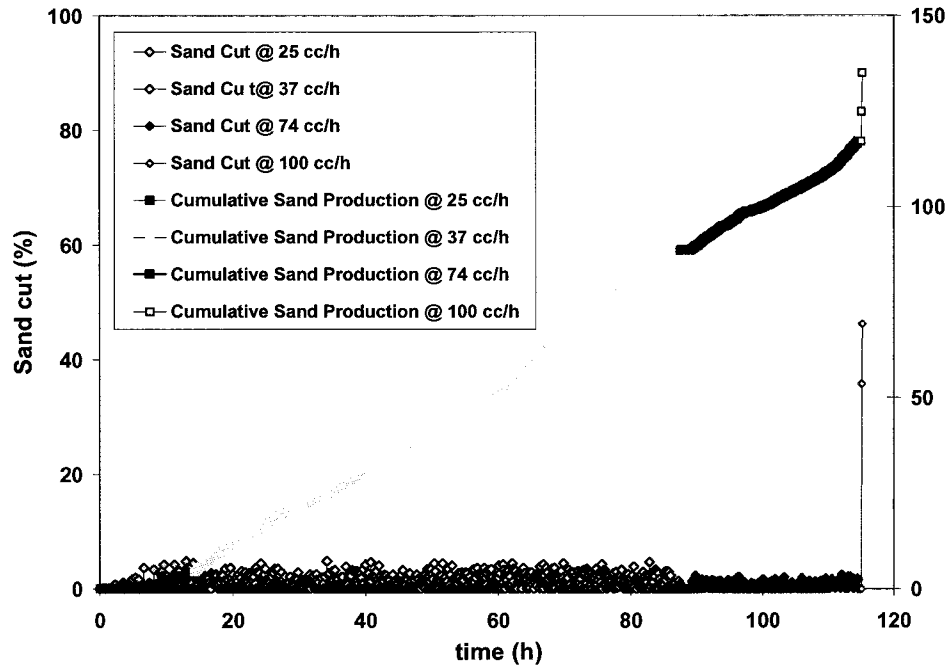

Figure B-41: Sand cut and cumulative sand production as a function of time for experiment # 11. Sand: Silica Well Sorted. Slot size: 0.813 mm (0.032 in). σ_c: 157 kPa

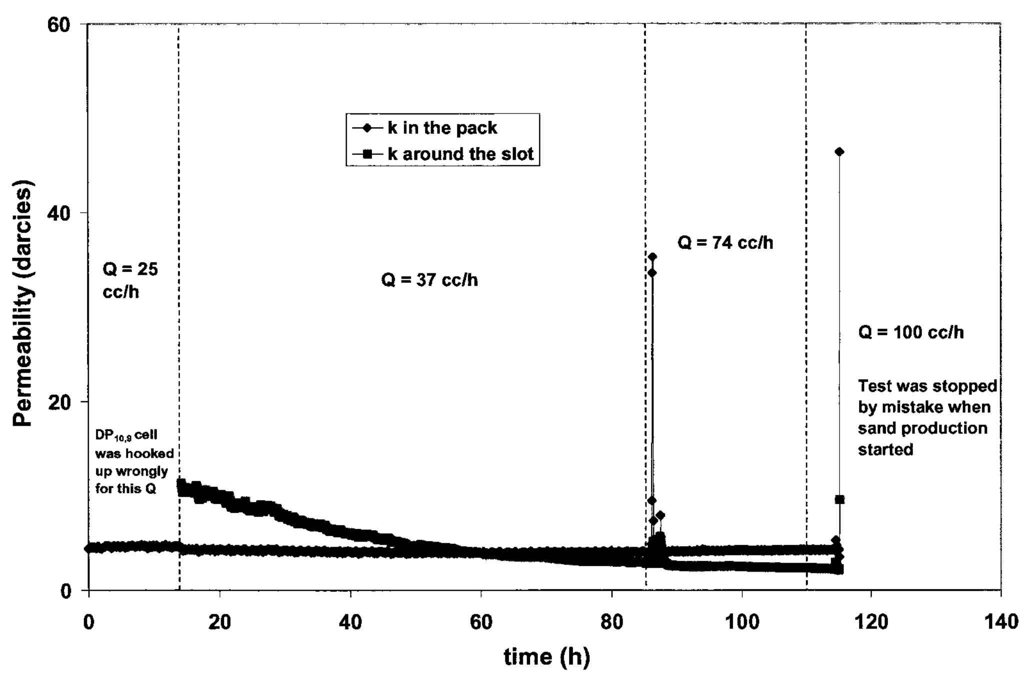

Figure B-42: Permeability inside pack and around the slot vs. time for experiment # 11. Sand: Silica Well Sorted. Slot size: 0.813 mm (0.032 in). σ_c: 157 kPa

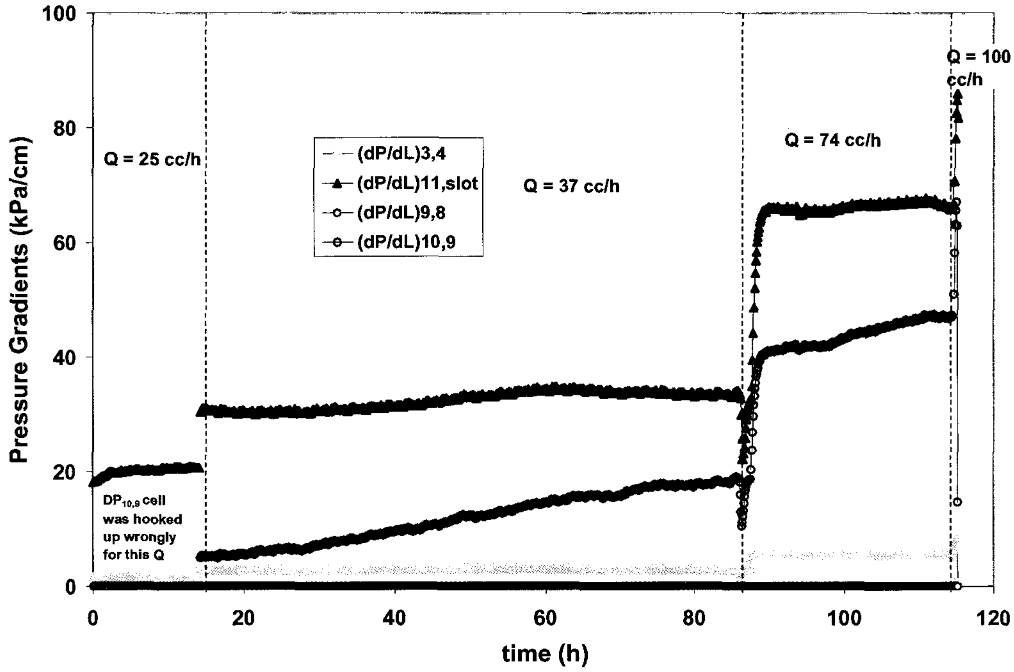

Figure B-43: Pressure Gradient vs. time for experiment # 11. Sand: Silica Well Sorted. Slot size: 0.813 mm (0.032 in). σ_c: 157 kPa

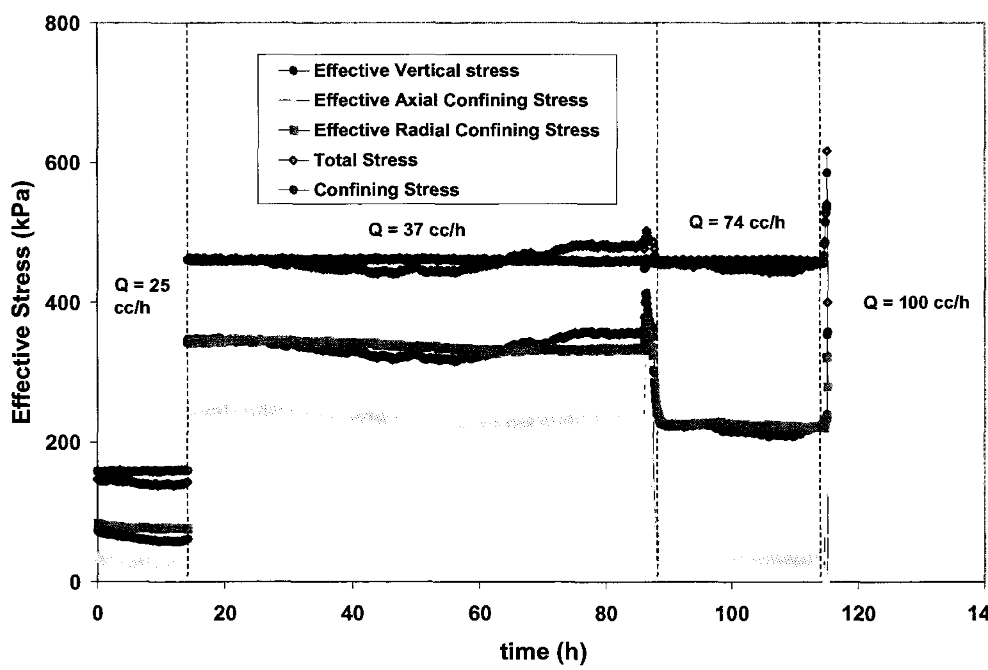

Figure B-44: Stress distribution in the sand pack as a function of time for experiment # 11. Sand: Silica Well Sorted. Slot Size: 0.813 mm (0.032 in). σ_c: 157 kPa

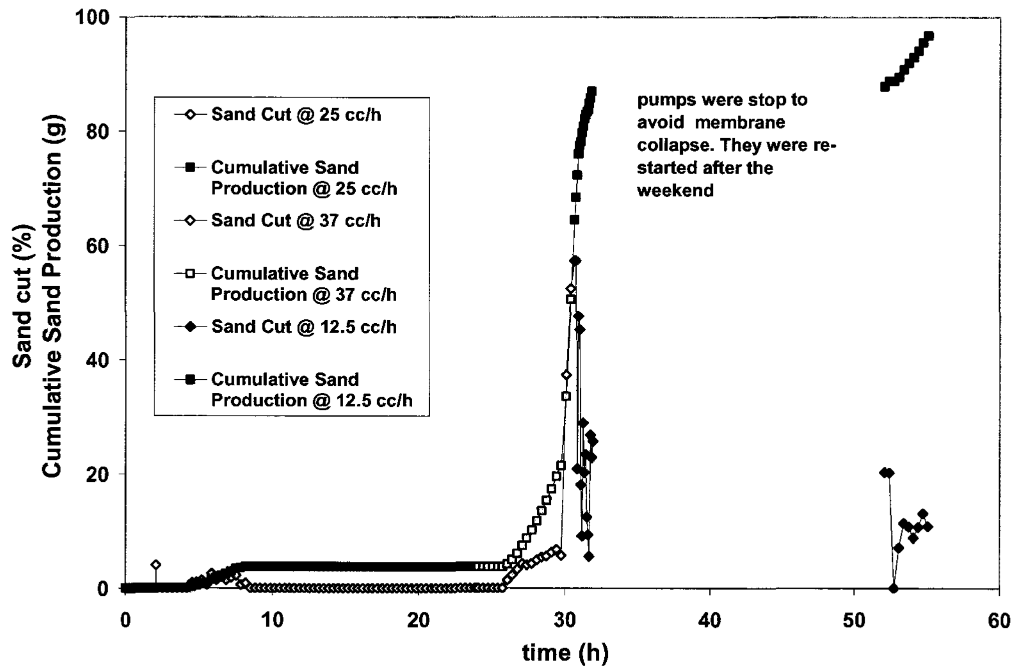

Figure B-45: Sand cut and cumulative sand production as a function of time for experiment # 12. Sand: Silica Well Sorted. Slot size: 1.016 mm (0.040 in). σ_c: 150 kPa

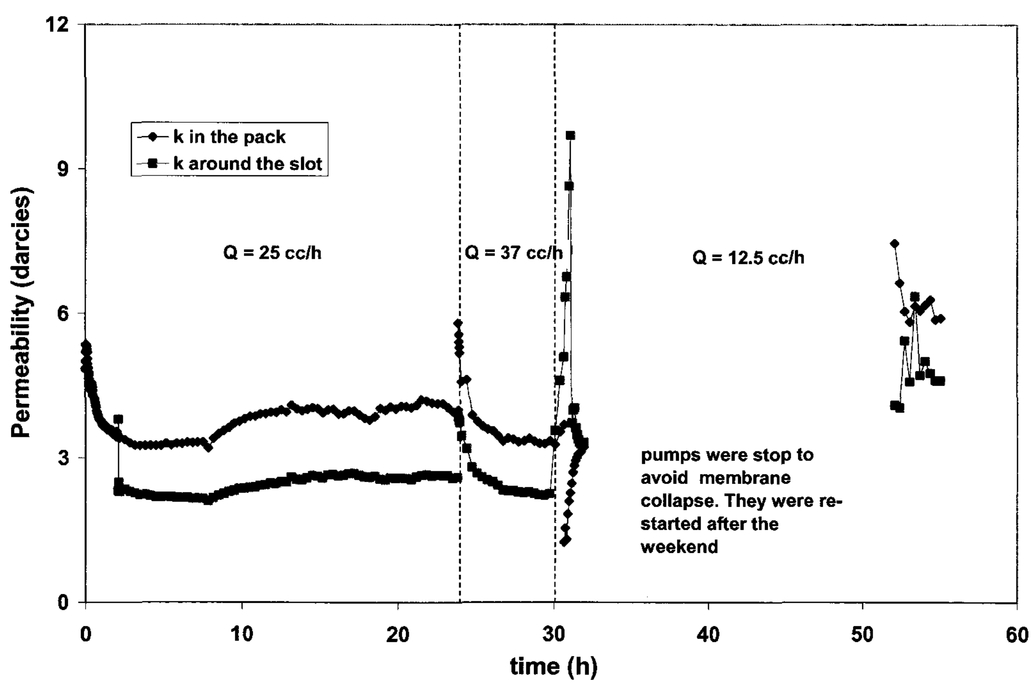

Figure B-46: Permeability inside pack and around the slot vs. time for experiment # 12. Sand: Silica Well Sorted. Slot size: 1.016 mm (0.040 in). σ_c: 150 kPa

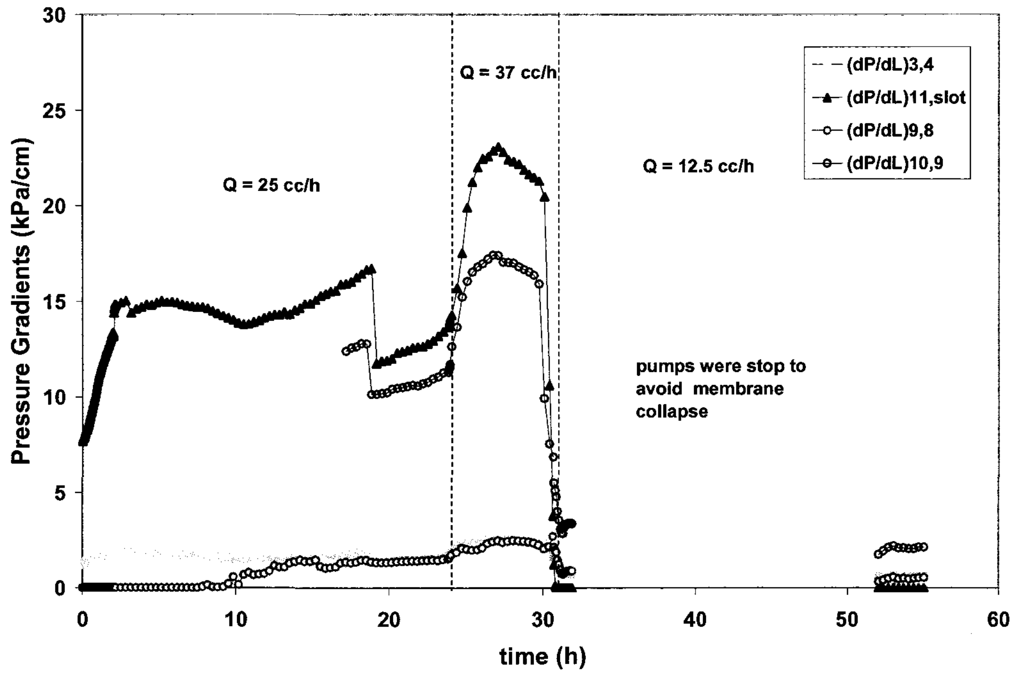

Figure B-47: Pressure Gradient vs. time for experiment # 12. Sand: Silica Well Sorted. Slot size: 1.016 mm (0.040 in). σ_c: 150 kPa

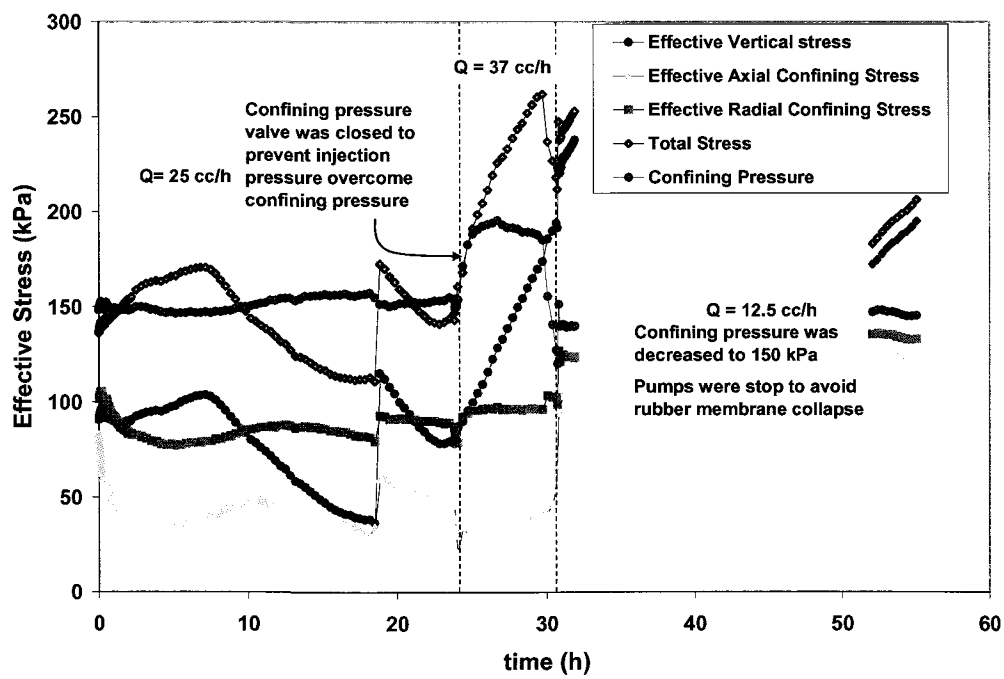

Figure B-48: Stress distribution in the sand pack as a function of time for experiment # 12. Sand: Silica Well Sorted. Slot Size: 1.016 mm (0.040 in). σ_c: 150 kPa

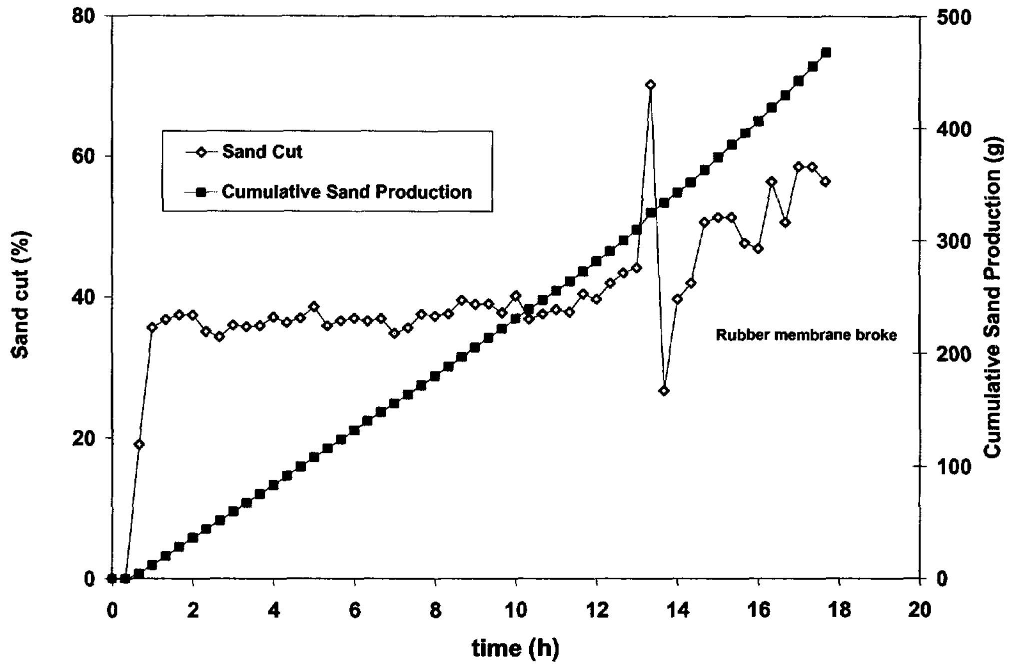

Figure B-49: Sand cut and cumulative sand production as a function of time for experiment # 13. Sand: Silica Well Sorted. Slot size: 1.016 mm (0.040 in). σ_c: 1000 kPa

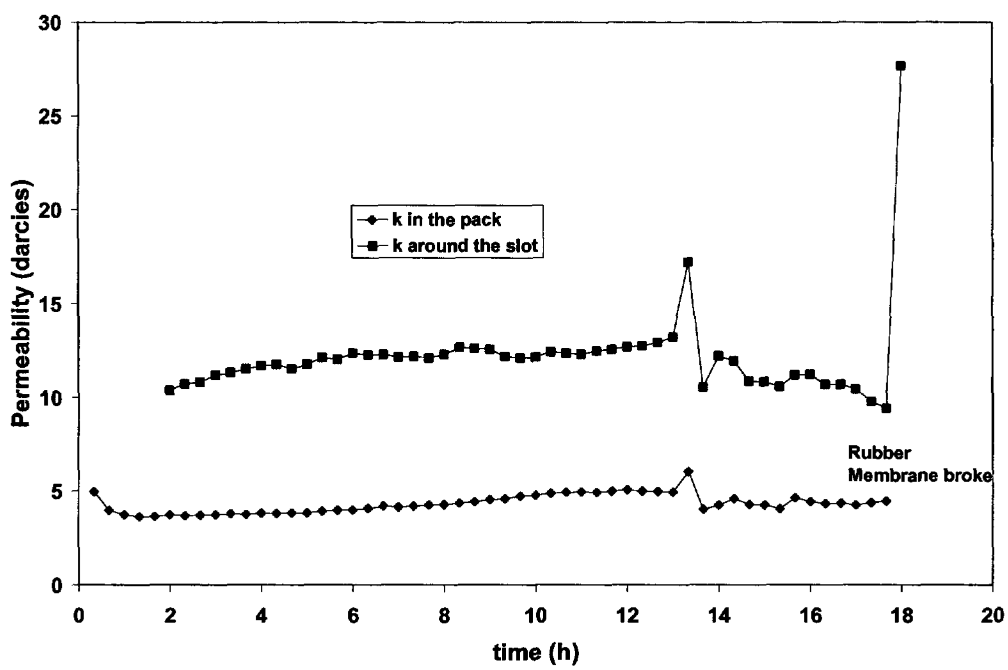

Figure B-50: Permeability inside pack and around the slot vs. time for experiment # 13. Sand: Silica Well Sorted. Slot size: 1.016 mm (0.040 in). σ_c: 1000 kPa

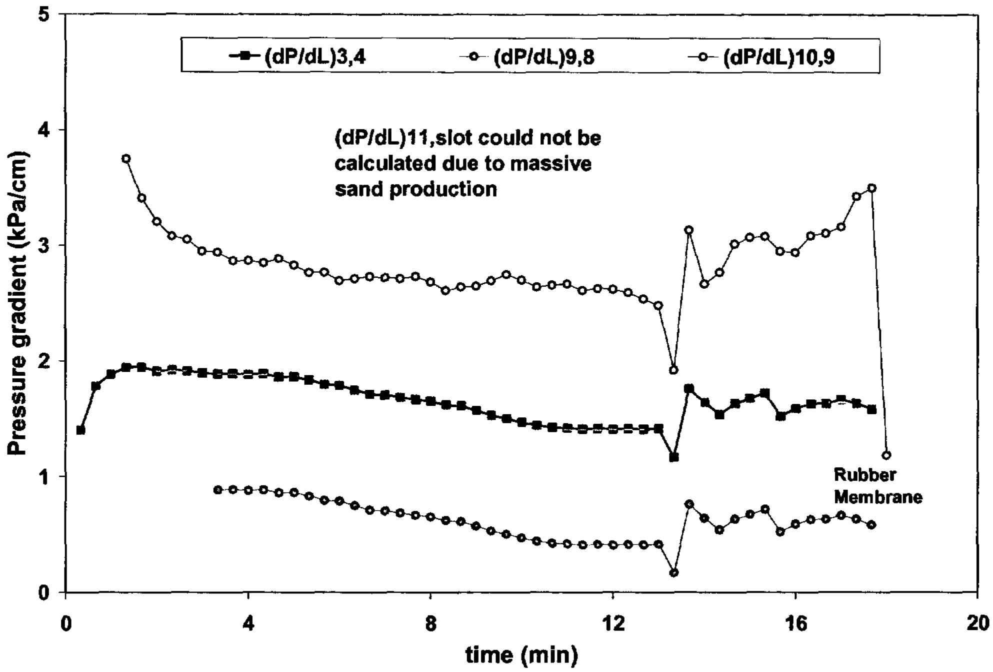

Figure B-51: Pressure Gradient vs. time for experiment # 13. Sand: Silica Well Sorted. Slot size: 1.016 mm (0.040 in). σ_c: 1000 kPa

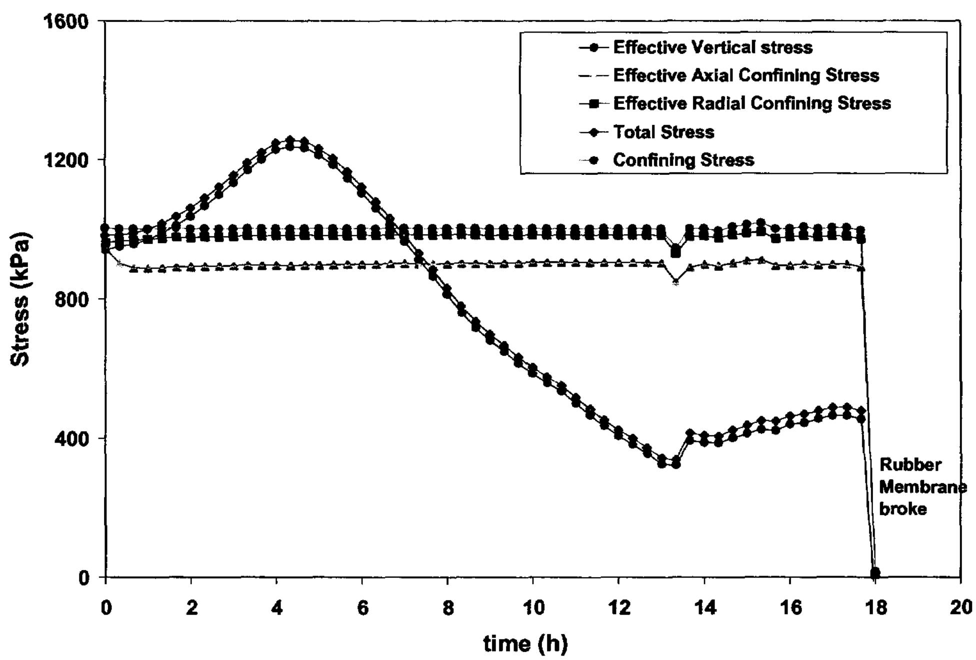

Figure B-52: Stress distribution in the sand pack as a function of time for experiment # 13. Sand: Silica Well Sorted. Slot Size: 1.016 mm (0.040 in). σ_c: 1000 kPa

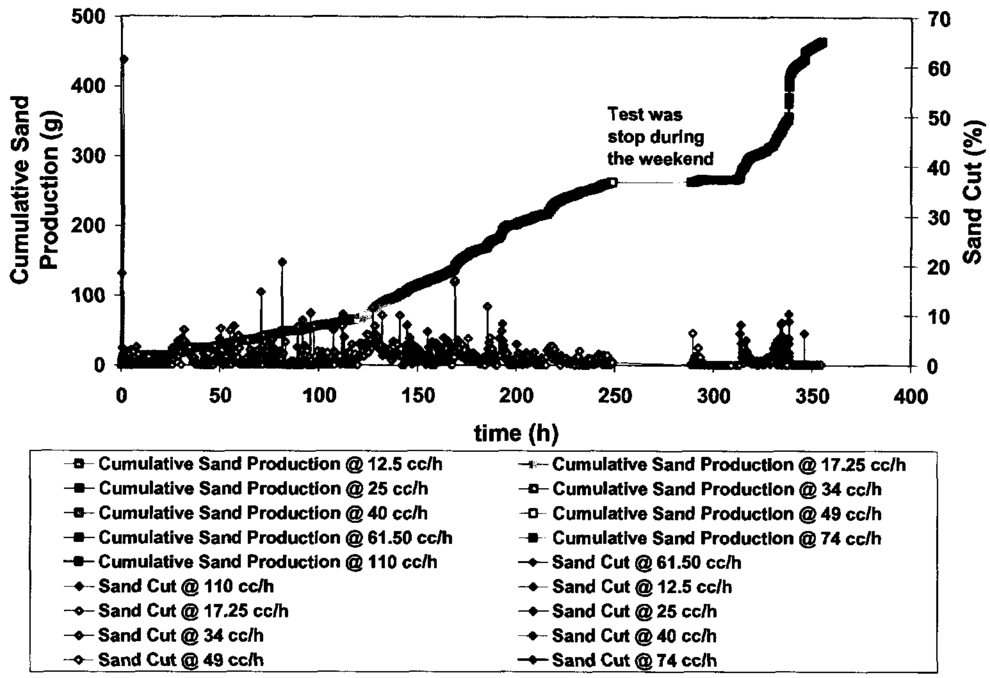

Figure B-53: Sand cut and cumulative sand production as a function of time for experiment # 14. Sand: Poorly Sorted. Slot size: 5.944 mm (0.234 in). σ_c: 2495 kPa

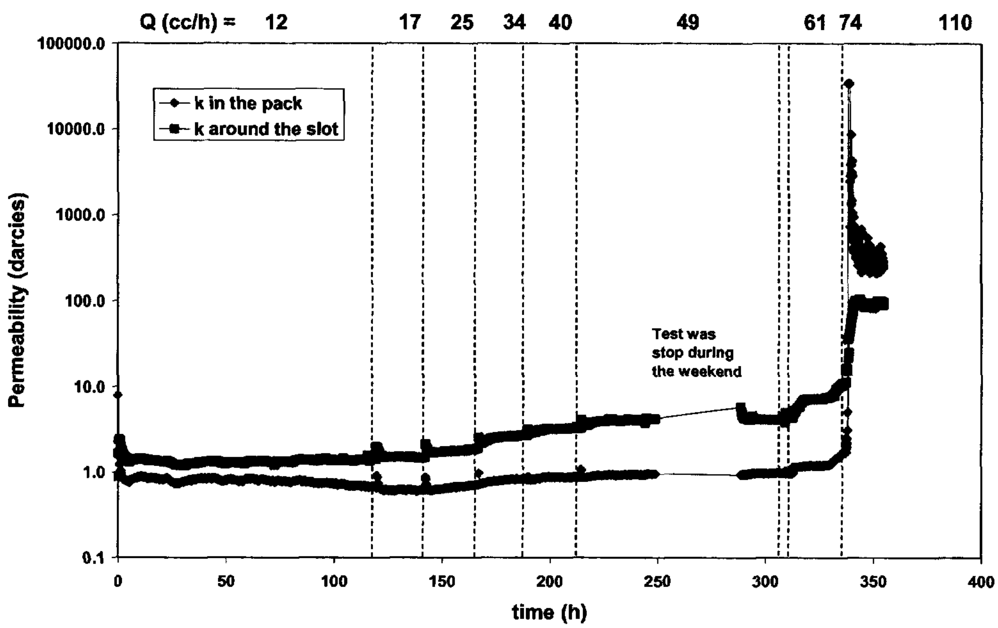

Figure B-54: Permeability inside pack and around the slot vs. time for experiment # 14. Sand: Silica Well Sorted. Slot size: 5.944 mm (0.234 in). σ_c: 2495 kPa

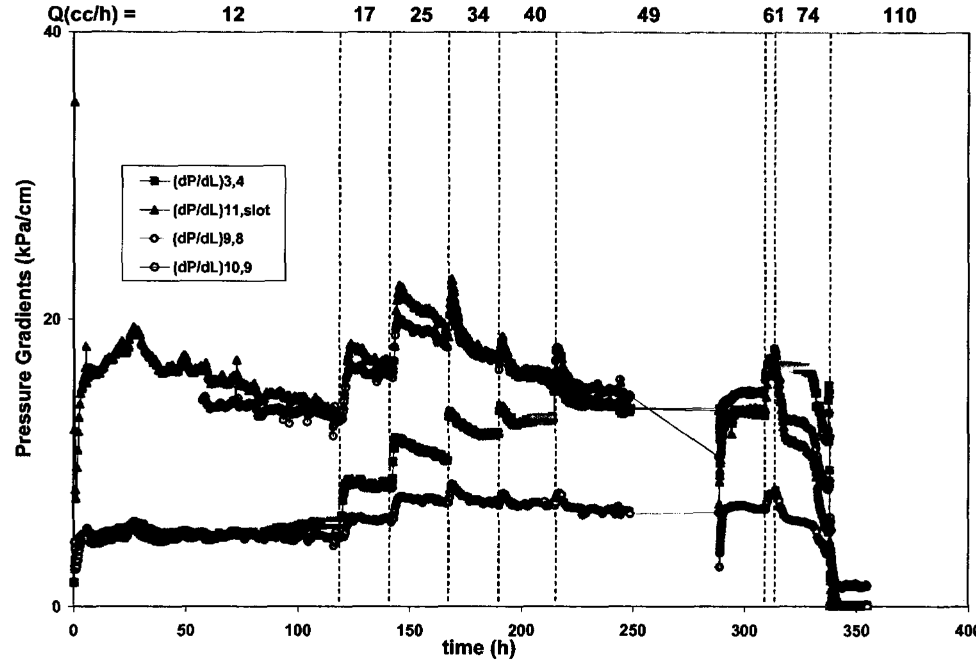

Figure B-55: Pressure Gradient vs. time for experiment # 14. Sand: Silica Well Sorted. Slot size: 5.944 mm (0.234in). σ_c: 2495 kPa

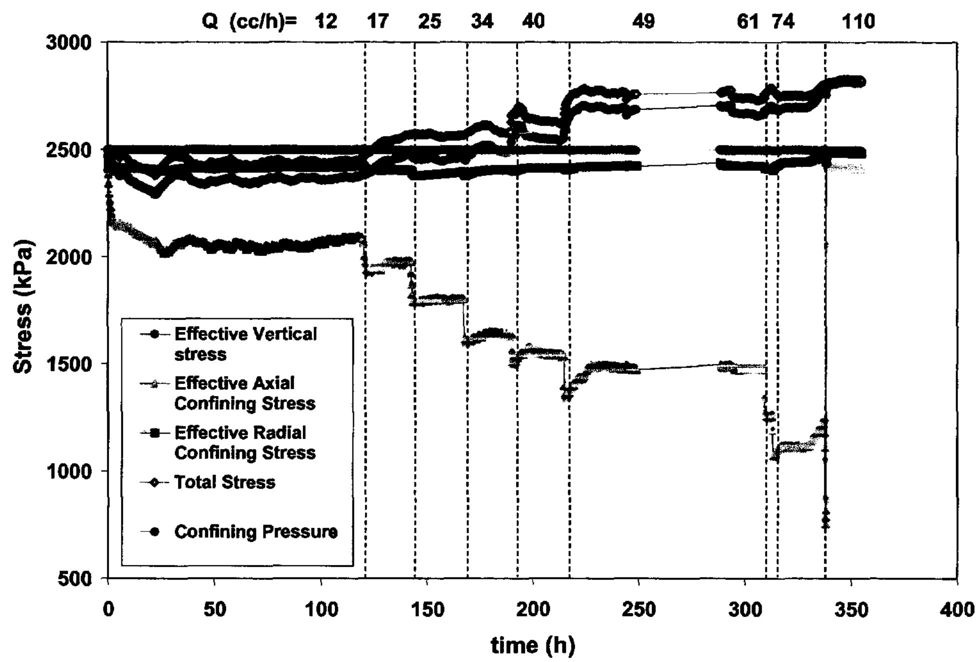

Figure B-56: Stress distribution in the sand pack as a function of time for experiment # 14. Sand: Silica Well Sorted. Slot Size: 5.944 mm (0.234 in). σ_c: 2495 kPa

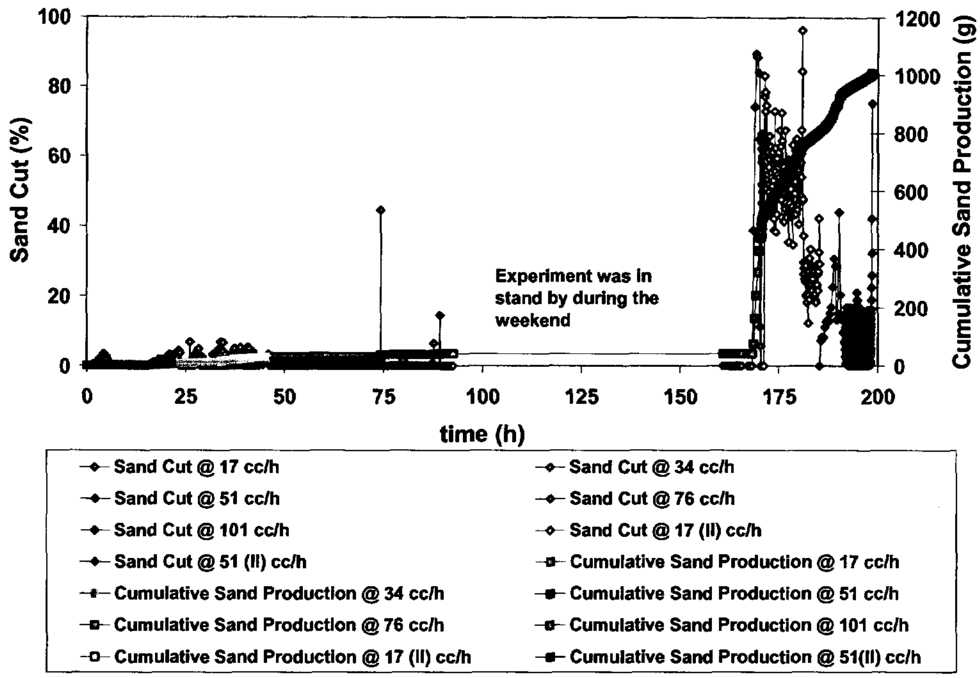

Figure B-57: Sand cut and cumulative sand production vs. time for experiment # 15. Sand: Silica No Large Fractions. Slot size: 1.422 mm (0.056 in). σ_c: 2495 kPa

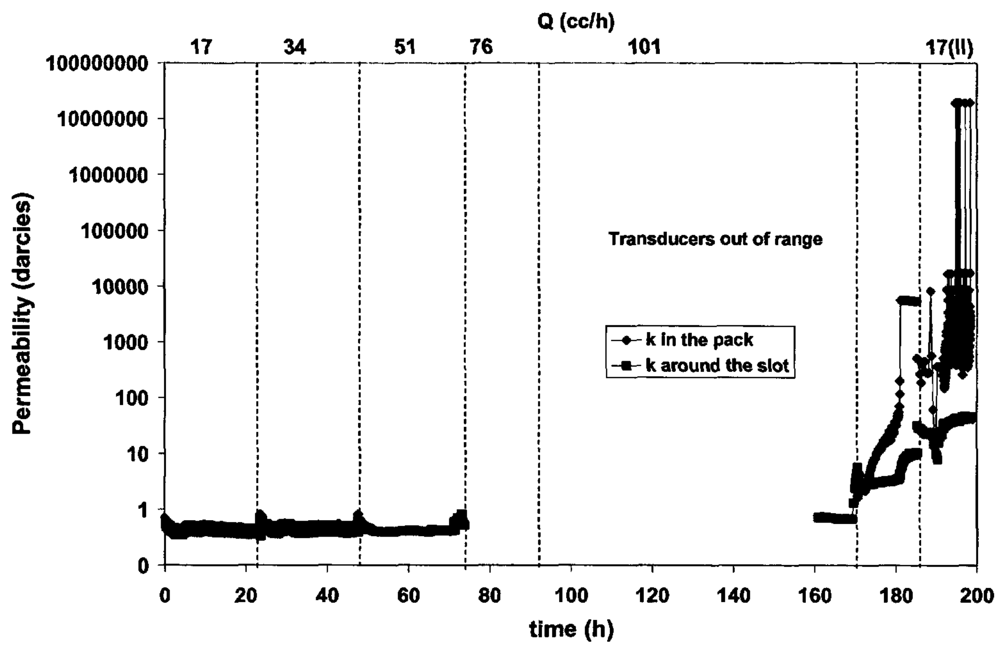

Figure B-58: Permeability inside pack and around the slot vs. time for experiment # 15. Sand: Silica No Large Fractions. Slot size: 1.422 mm (0.056 in). σ_c: 2495 kPa

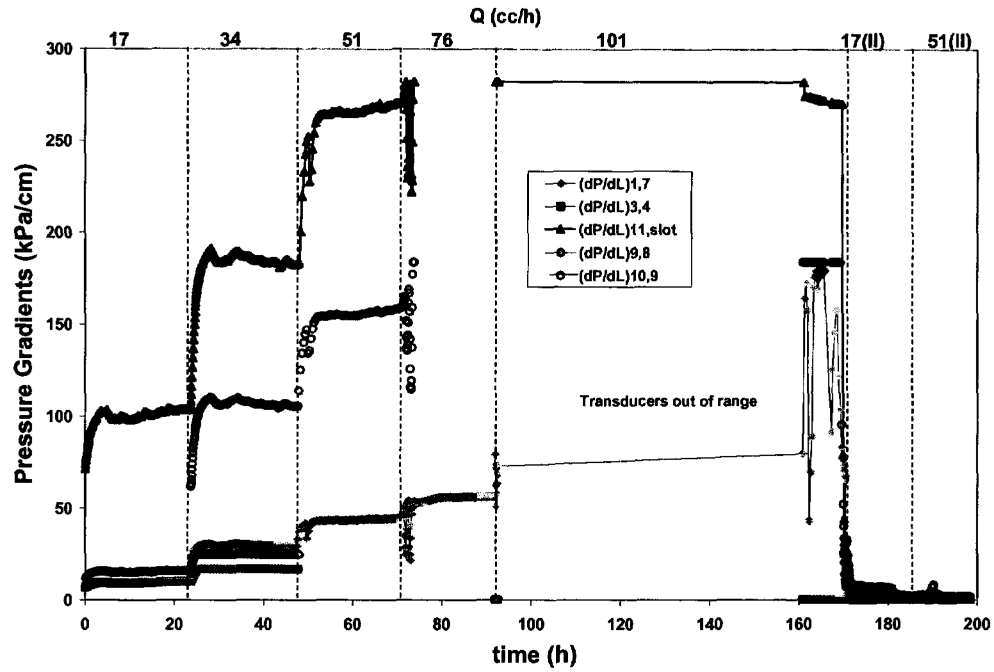

Figure B-59: Pressure Gradient vs. time for experiment # 15. Sand: Silica No Large Fractions. Slot size: 1.422 mm (0.056 in). σ_c: 2495 kPa

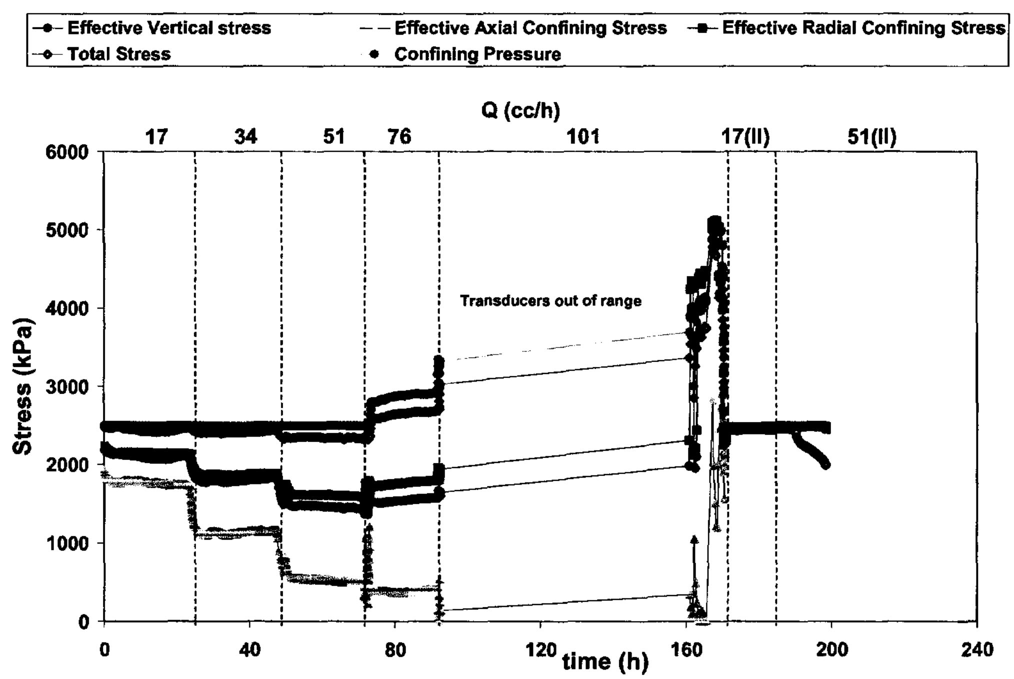

Figure B-60: Stress distribution in the sand pack as a function of time for experiment # 15. Sand: Silica No Large Fractions. Slot Size: 1.422 mm (0.056 in). σ_c: 2495 kPa

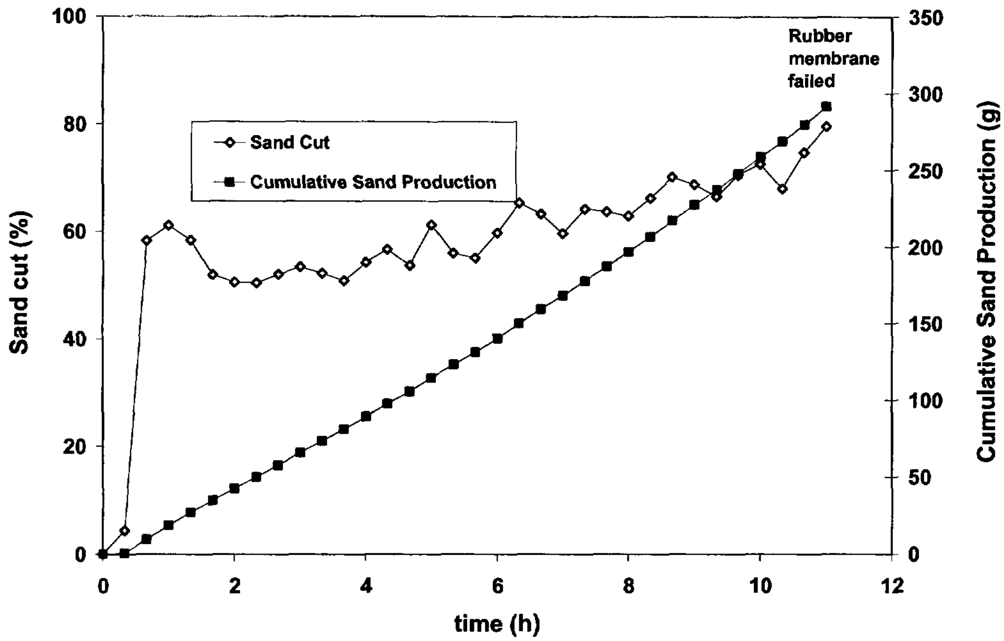

Figure B-61: Sand cut and cumulative sand production as a function of time for experiment # 16. Sand: Silica No Fines. Slot size: 1.422 mm (0.056 in). σ_c: 2493 kPa

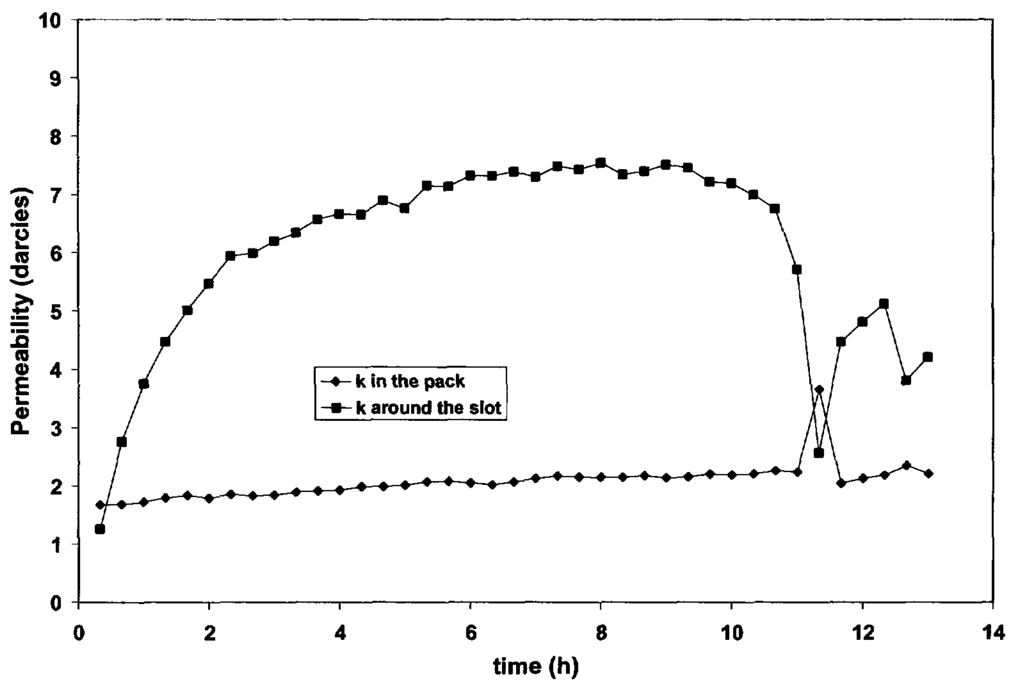

Figure B-62: Permeability inside pack and around the slot vs. time for experiment # 16. Sand: Silica No Fines. Slot size: 1.422 mm (0.056 in). σ_c: 2493 kPa

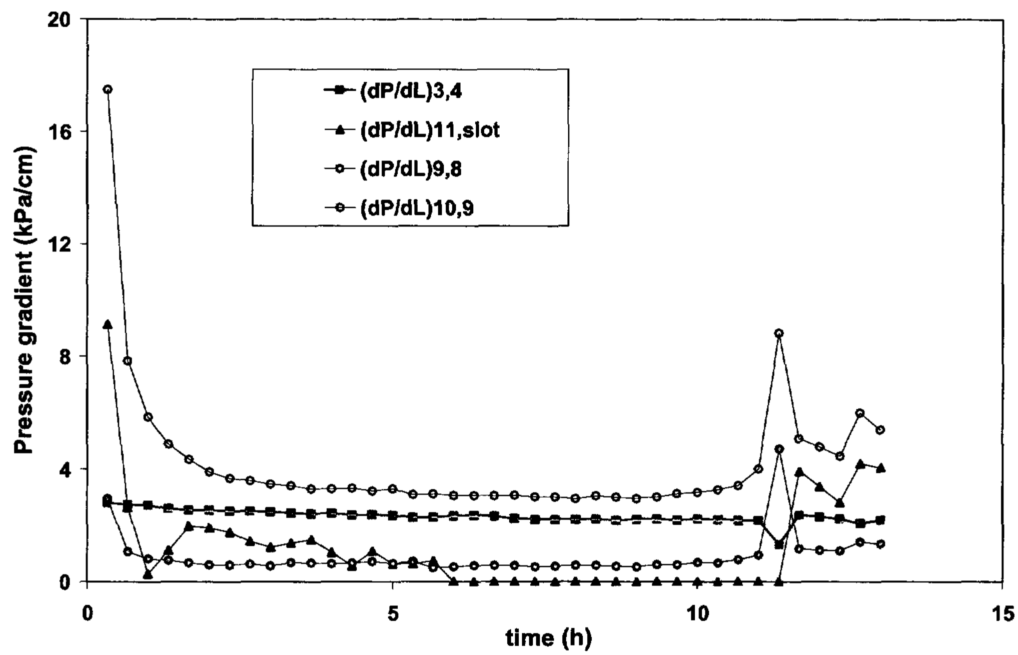

Figure B-63: Pressure Gradient vs. time for experiment # 16. Sand: Silica No Fines. Slot size: 1.422 mm (0.056 in). σ_c: 2493 kPa

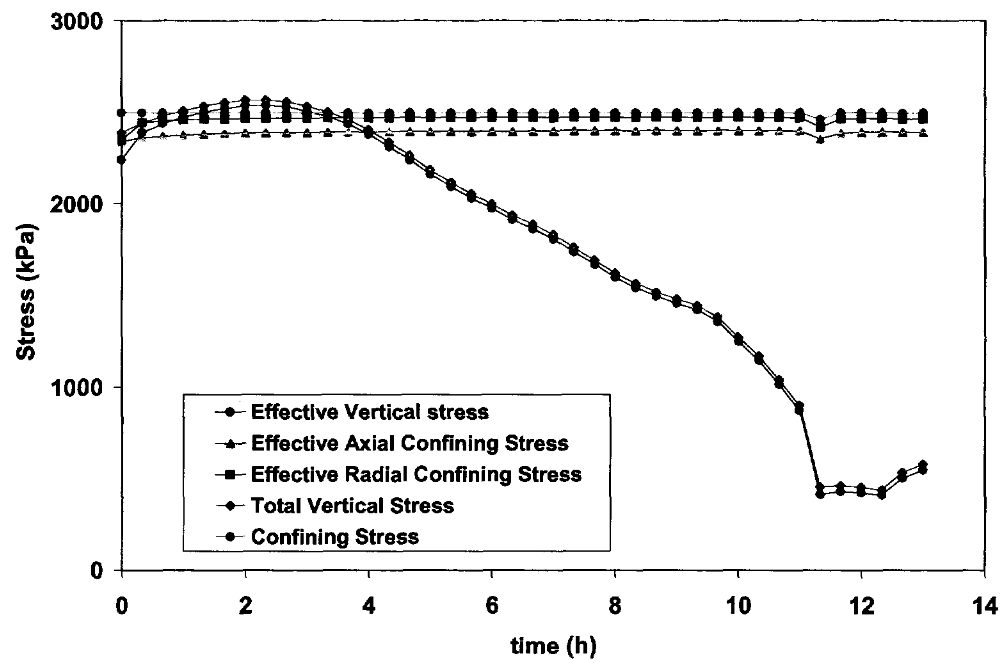

Figure B-64: Stress distribution in the sand pack as a function of time for experiment # 16. Sand: Silica No Fines. Slot Size: 1.422 mm (0.056 in). σ_c: 2493 kPa

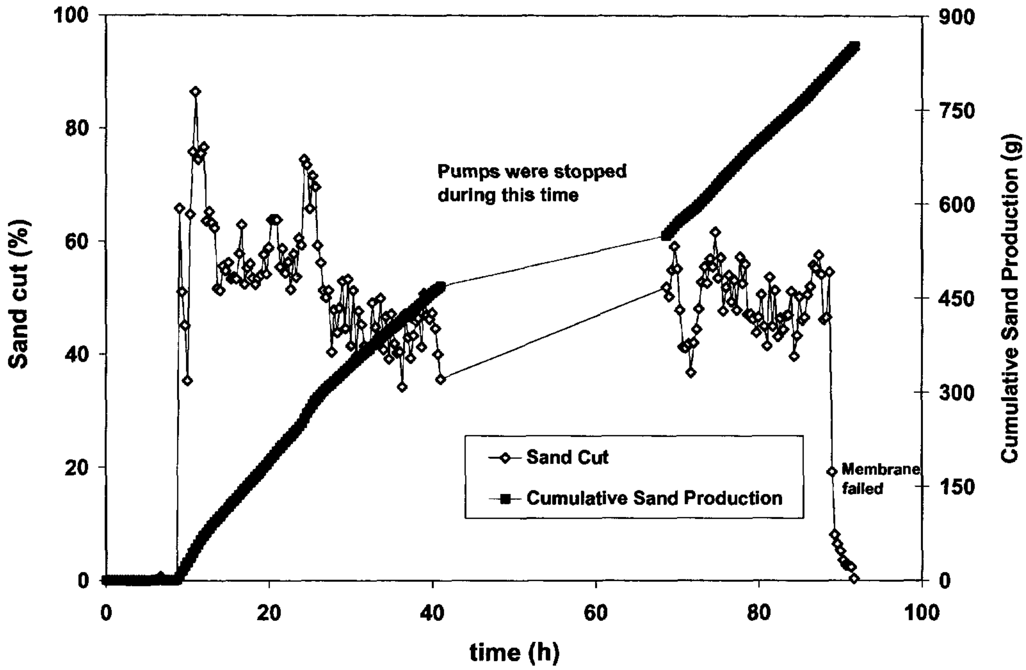

Figure B-65: Sand cut and cumulative sand production as a function of time for experiment # 17. Sand: Husky Sand. Slot size: 1.422 mm (0.056 in). σ_c: 507 kPa

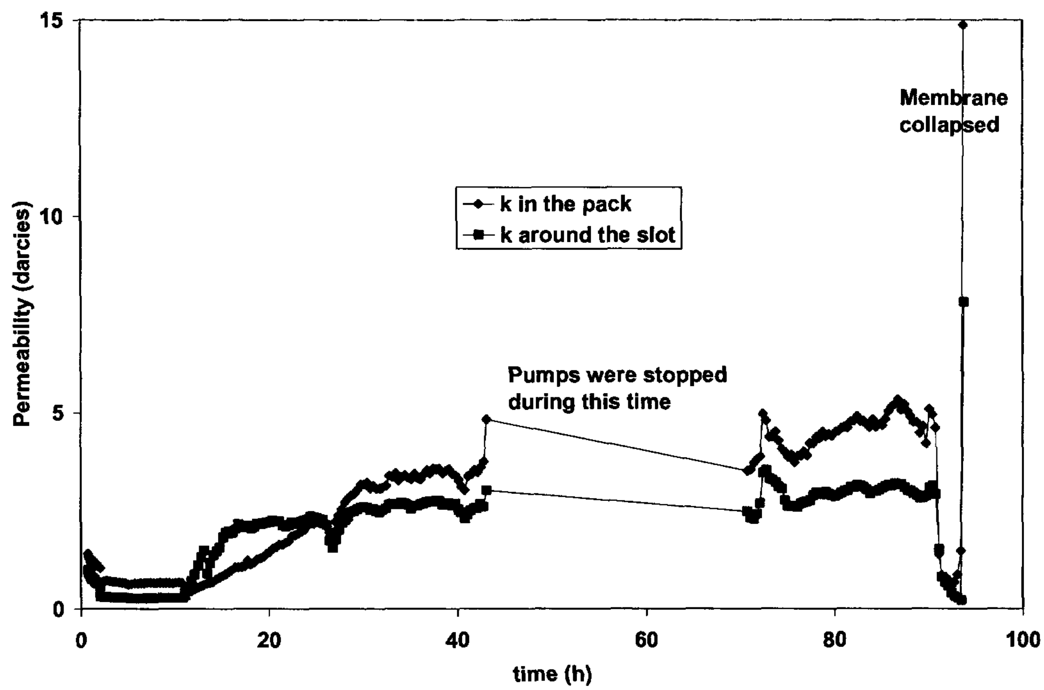

Figure B-66: Permeability inside pack and around the slot vs. time for experiment # 17. Sand: Husky Sand. Slot size: 1.422 mm (0.056 in). σ_c: 507 kPa

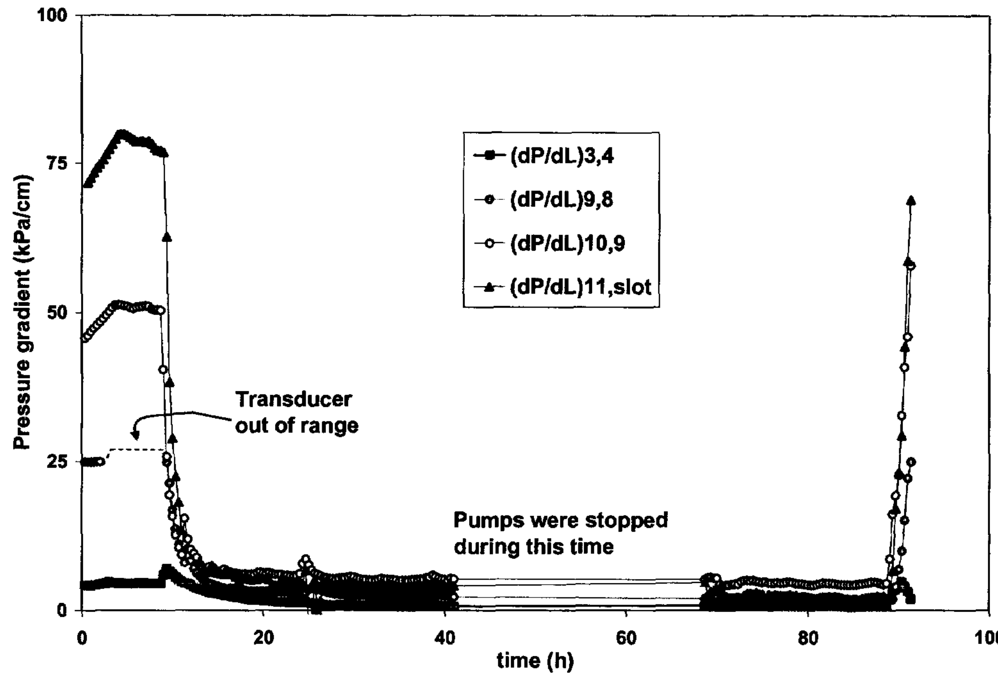

Figure B-67: Pressure Gradient vs. time for experiment # 17. Sand: Husky Sand. Slot size: 1.422 mm (0.056 in). σ_c: 507 kPa

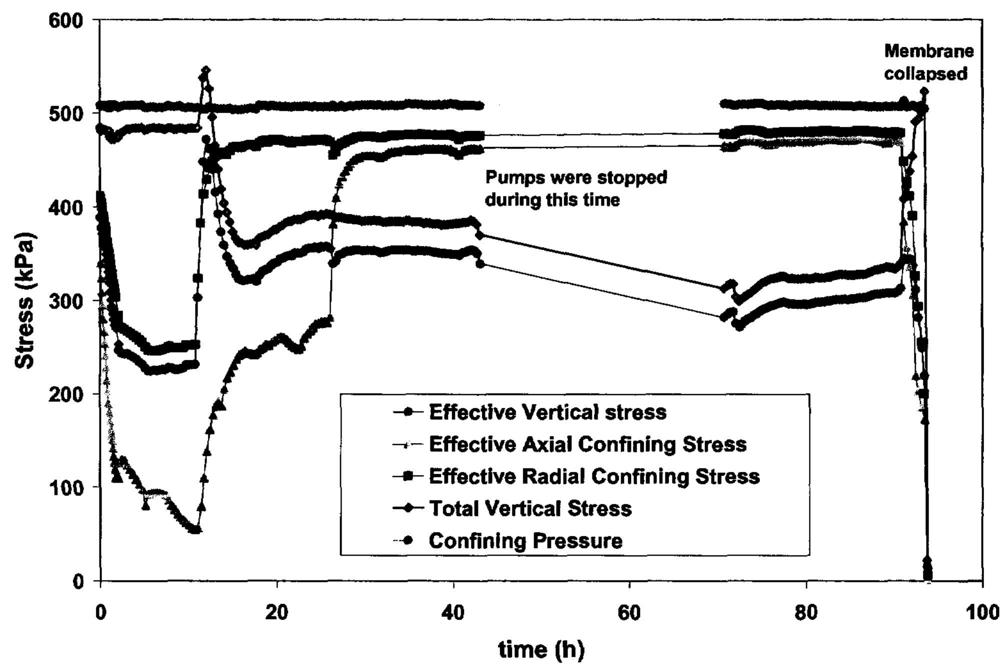

Figure B-68: Stress distribution in the sand pack as a function of time for experiment # 17. Sand: Husky Sand. Slot Size: 1.422 mm (0.056 in). σ_c: 507 kPa

B.2 Sand Strength Experiments Graphs

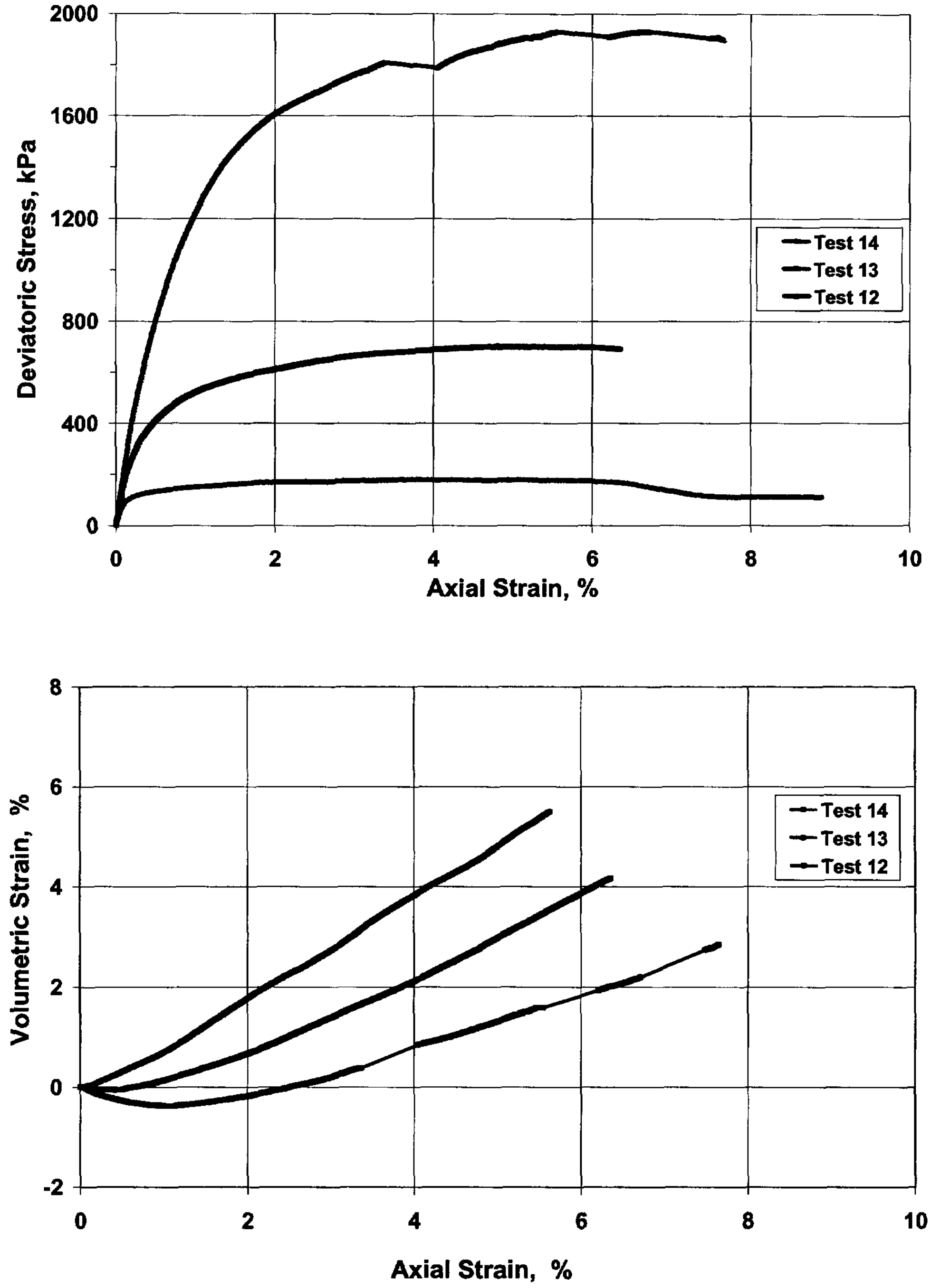

Figure B-69: Deviatoric stress and volumetric strain vs. axial strain for the Well Sorted sand.

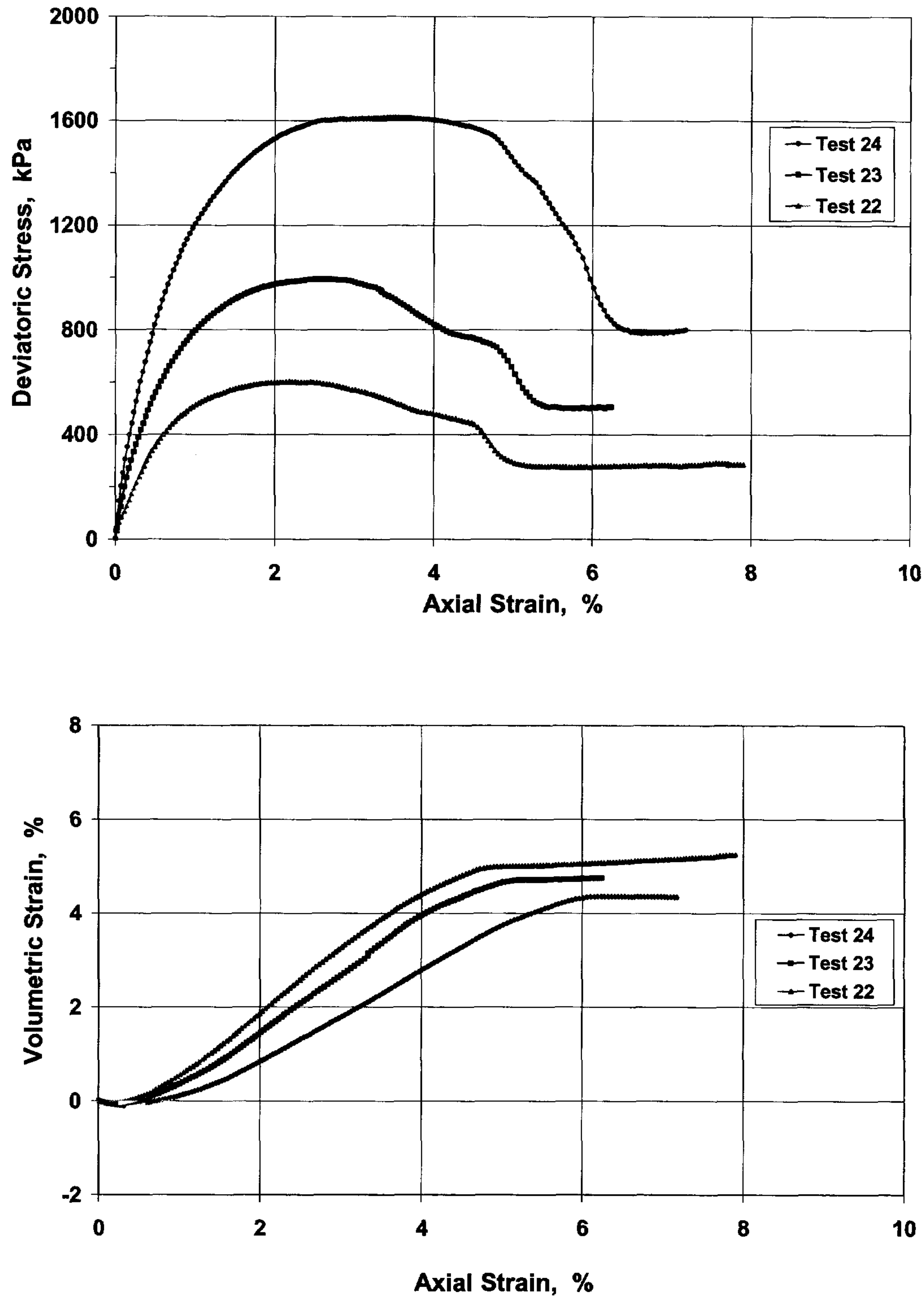

Figure B-70. Deviatoric stress and volumetric strain vs. axial strain for the Silica No Large Fractions sand.

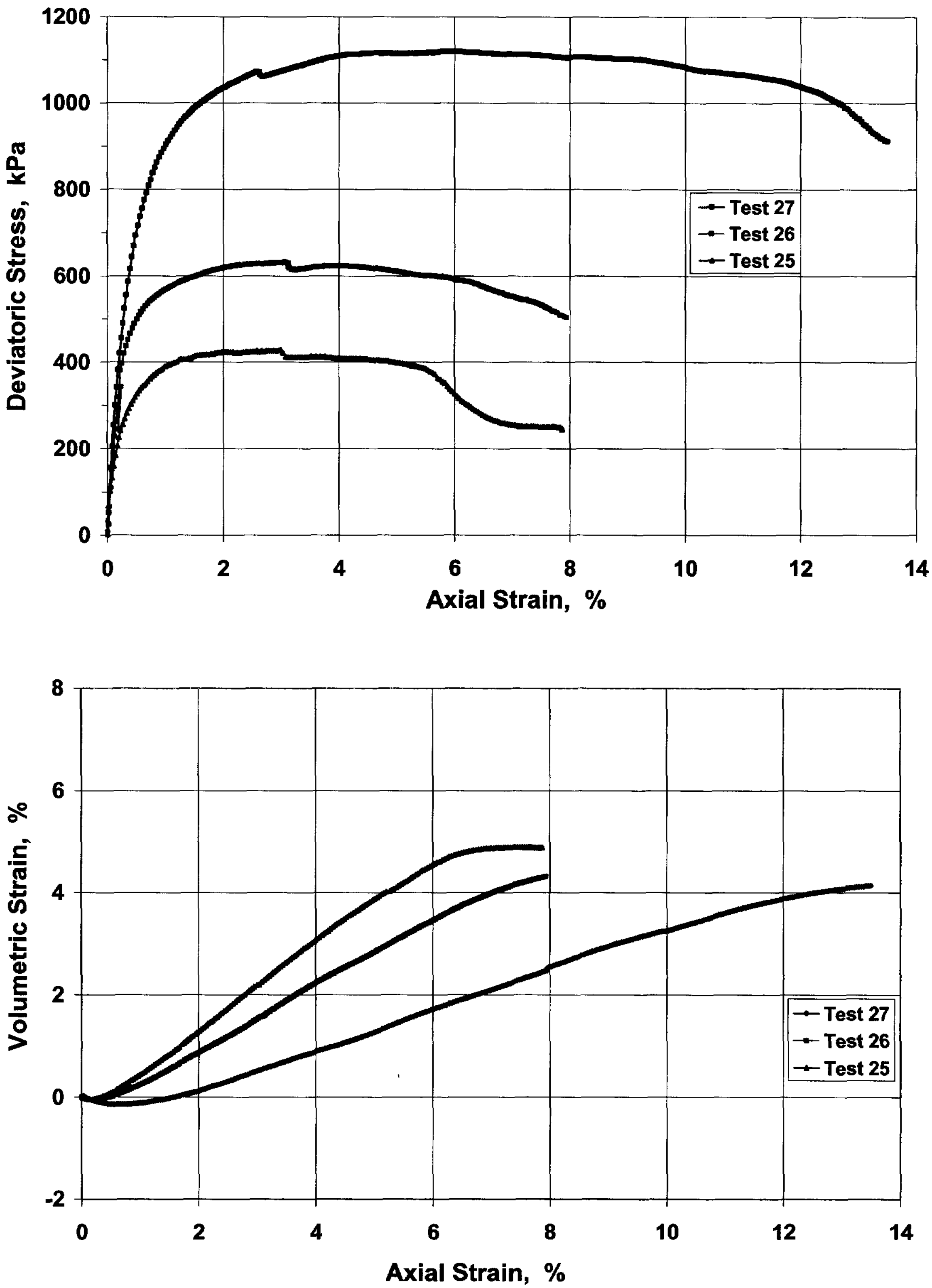

Figure B-71. Deviatoric stress and volumetric strain vs. axial strain for the Silica No Fines sand.

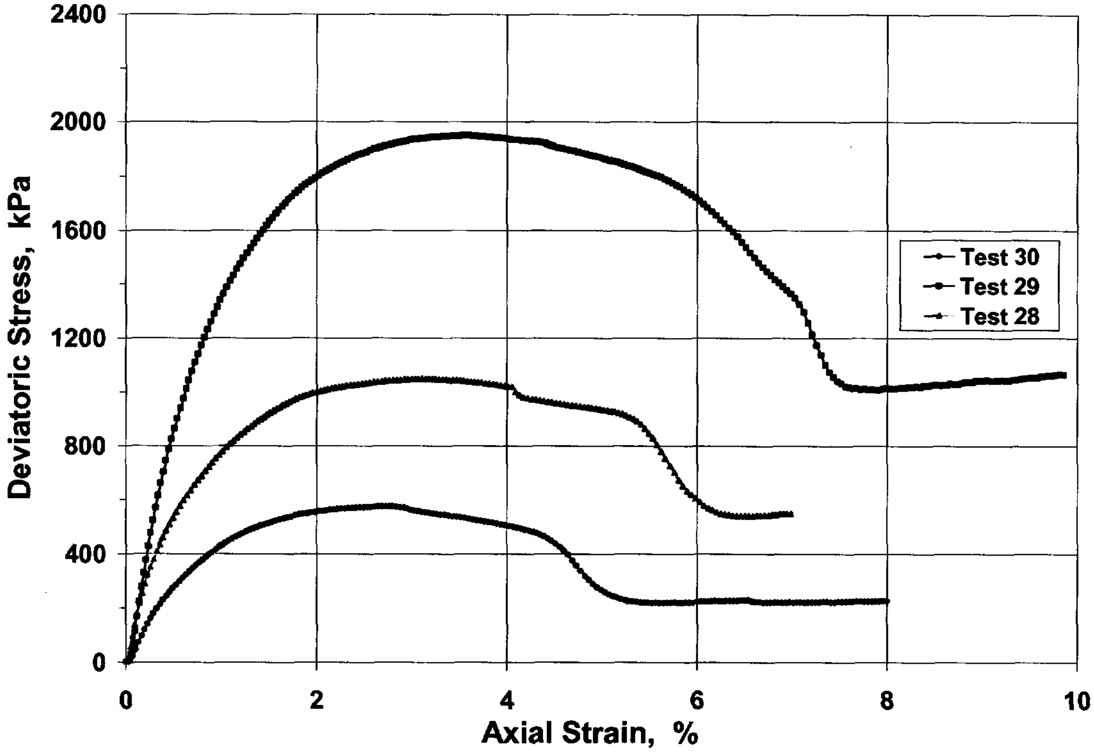

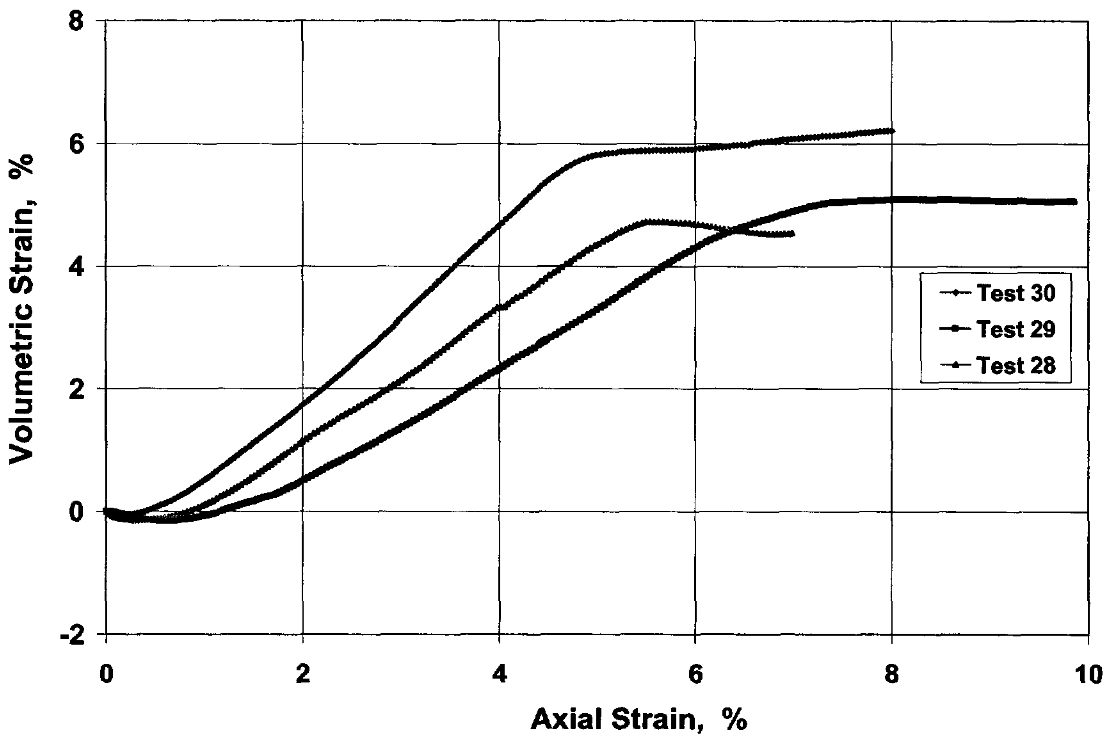

Figure B-72. Deviatoric stress and volumetric strain vs. axial strain for the Poorly Sorted sand.

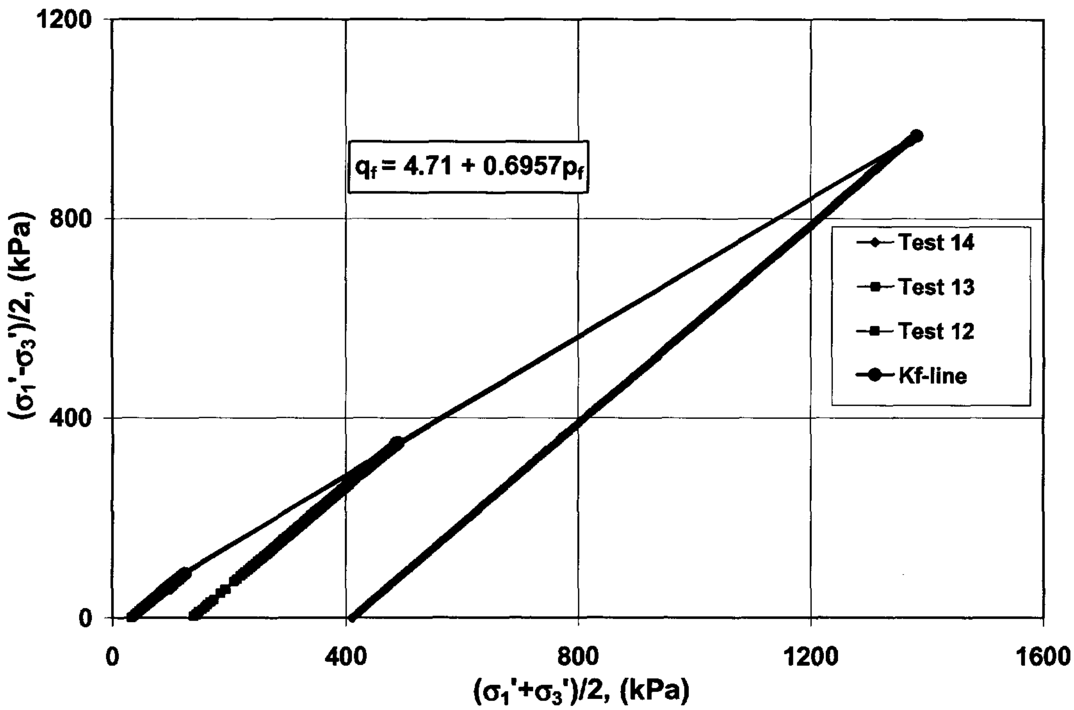

Figure B-73. Stress path and Kf-line for the Well Sorted sand

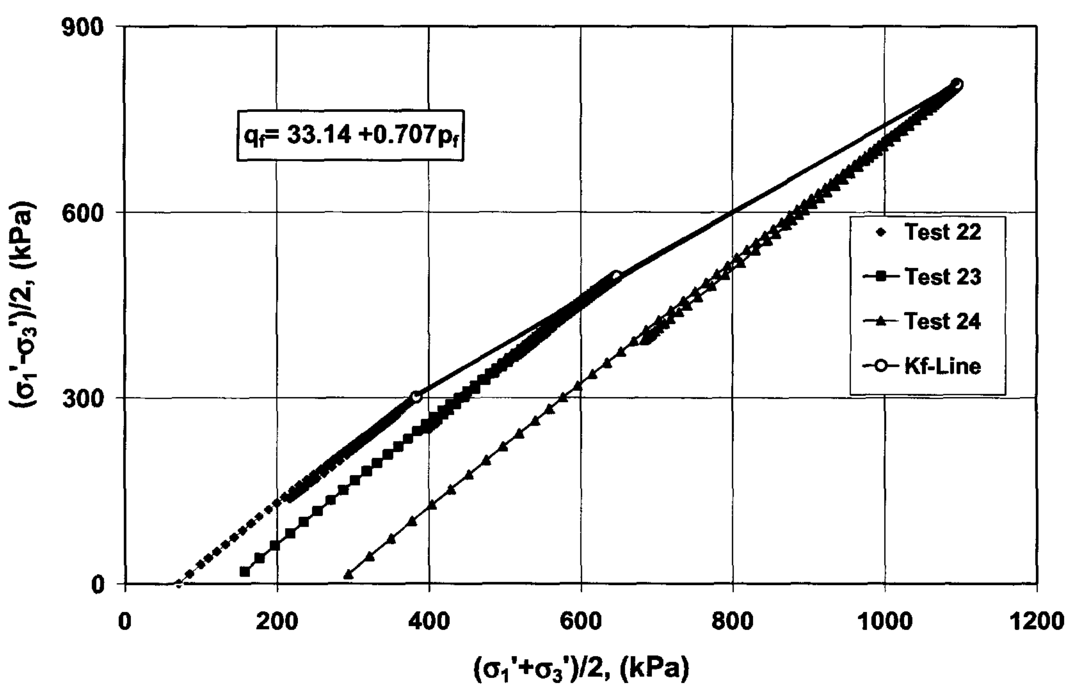

Figure B-74. Stress path and Kf-line for the Silica No Large Fractions sand

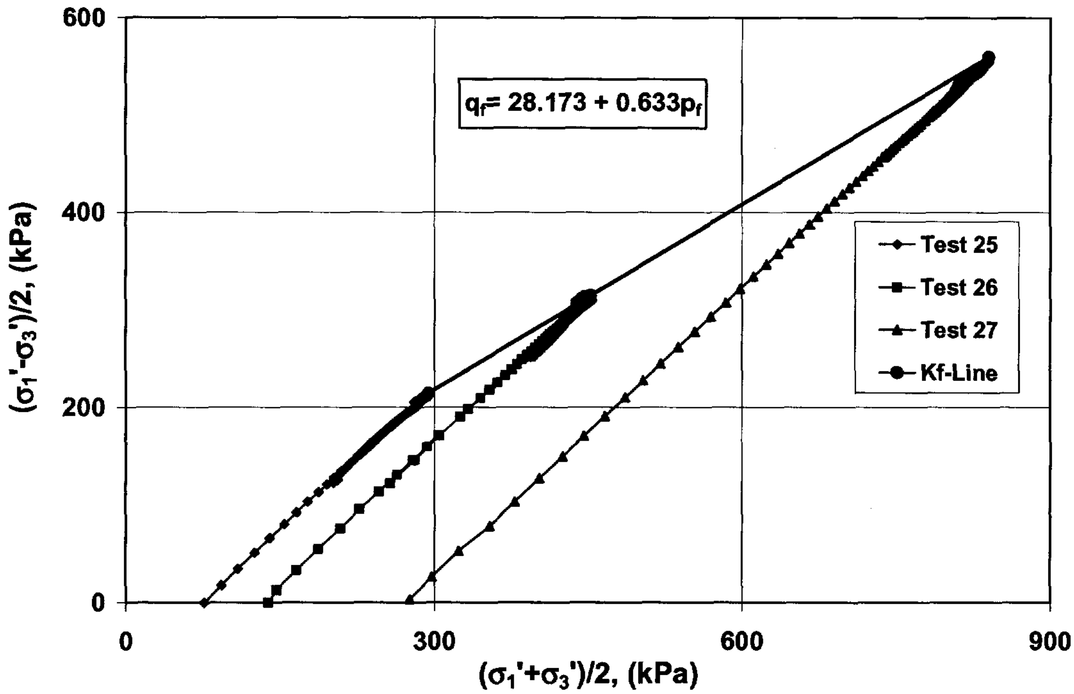

Figure B-75. Stress path and Kf-line for the Silica No Fines sand

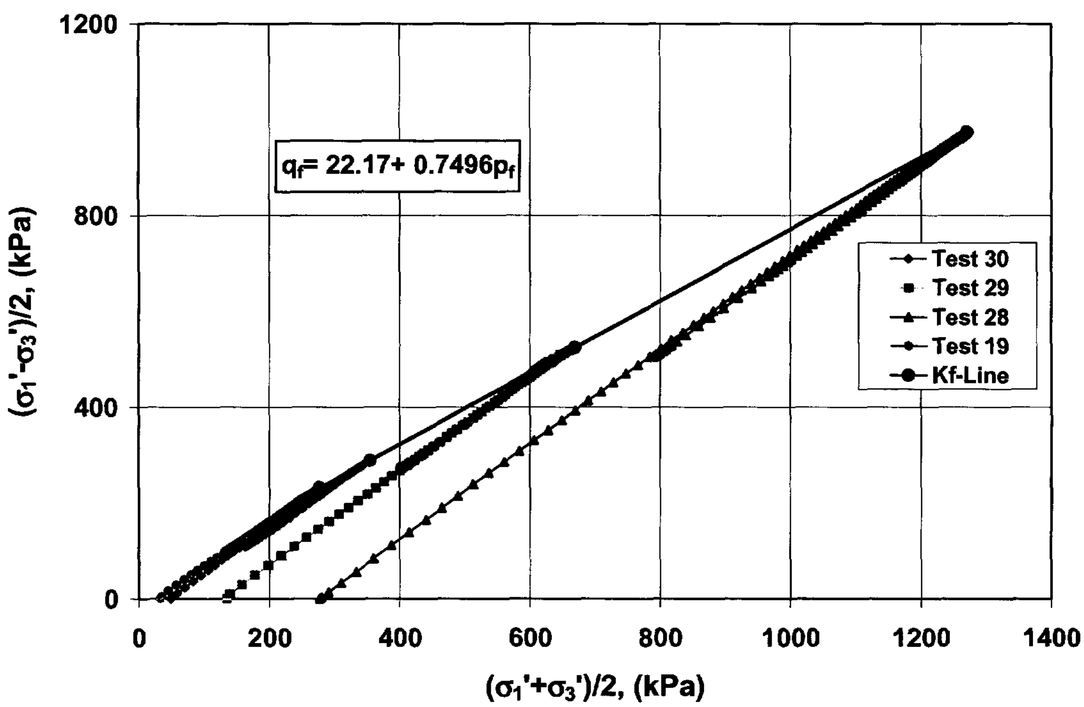

Figure B-76. Stress path and Kf-line for the Poorly Sorted sand

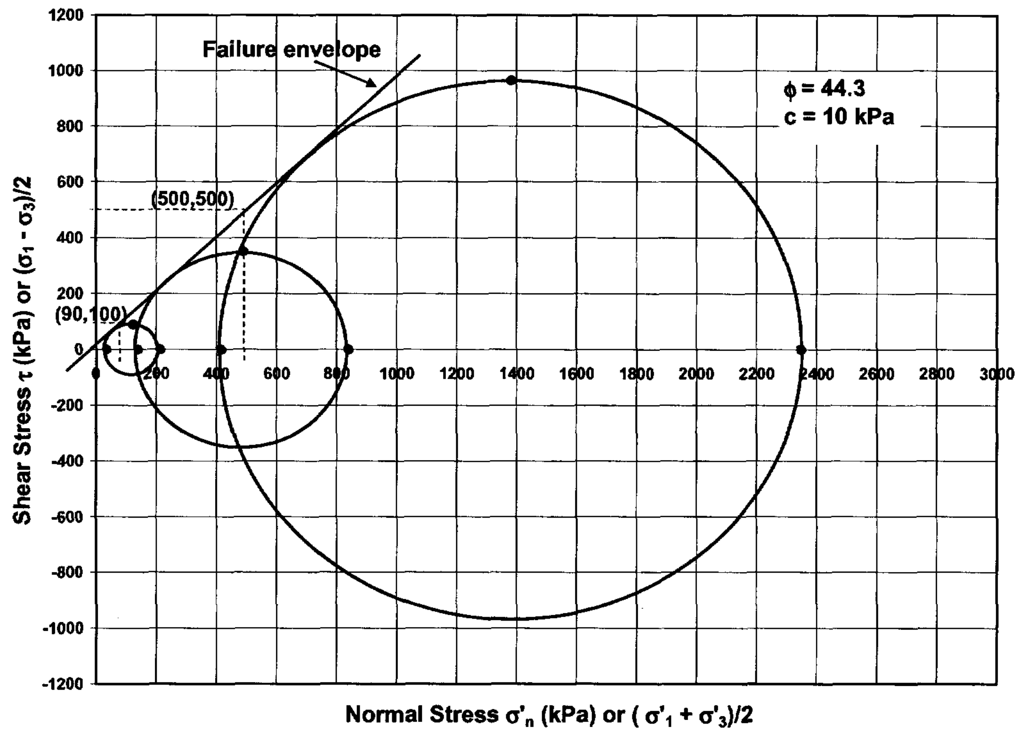

Figure B-77. Mohr circles, failure envelope and strength parameters for the Well Sorted sand

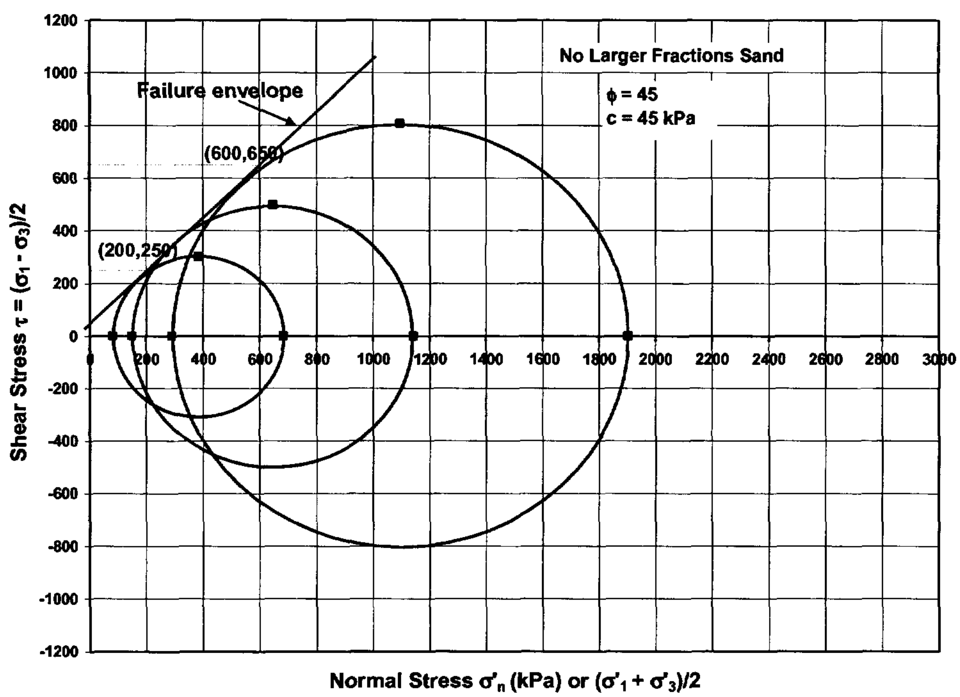

Figure B-78. Mohr circles, failure envelope and strength parameters for the Silica No Large Fractions sand

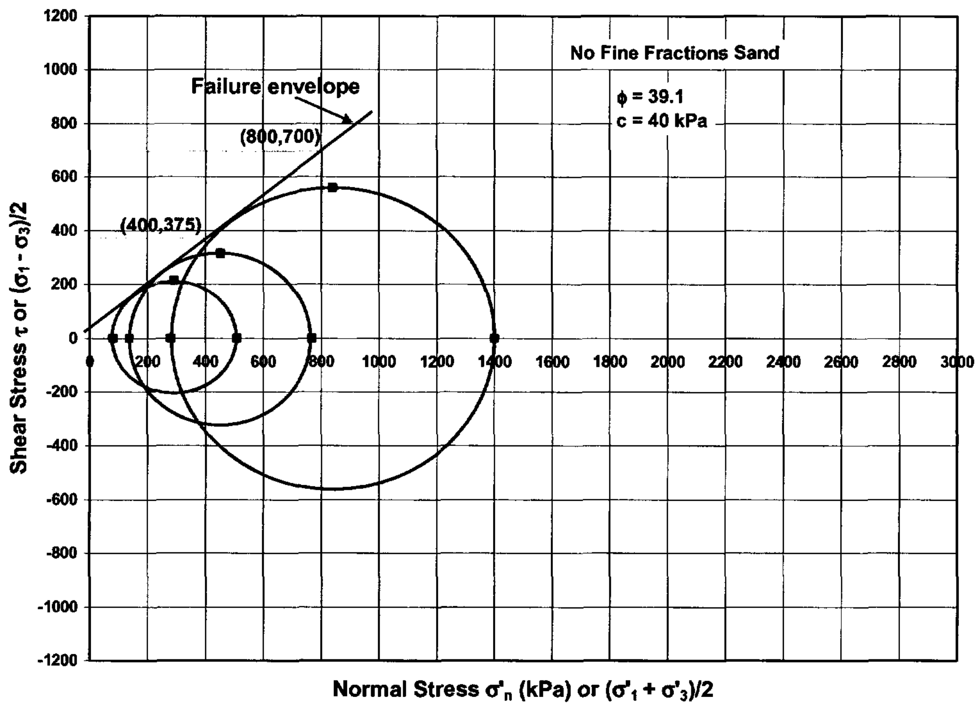

Figure B-79 Mohr circles, failure envelope and strength parameters for the Silica No Fines sand

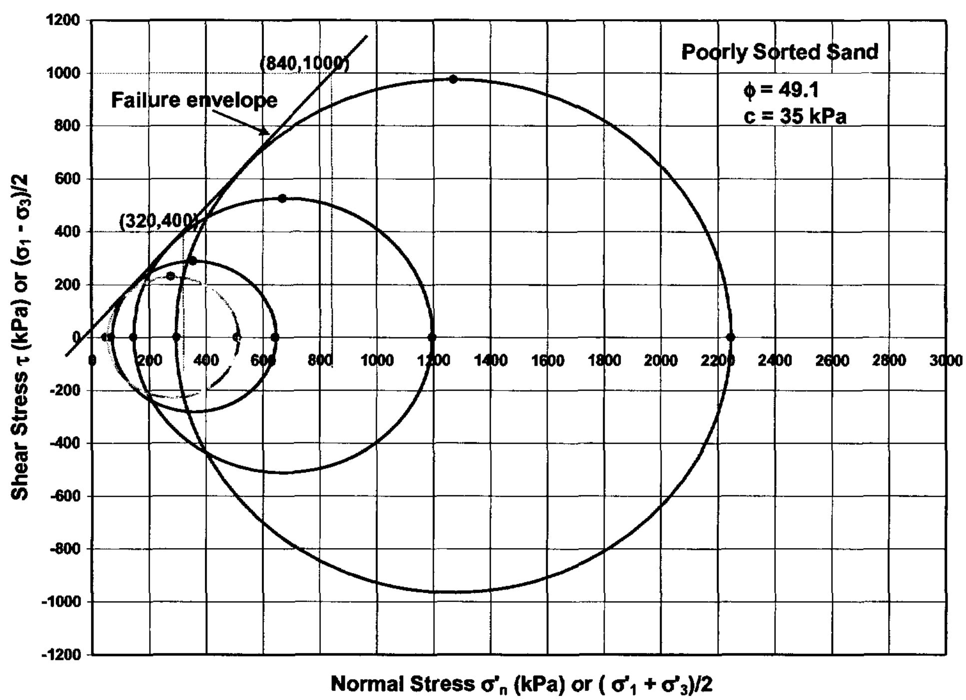

Figure B-80 Mohr circles, failure envelope and strength parameters for the Poorly Sorted sand.